TOWARDS "MACROMOLECULAR" ELECTRONICS: PHOTOCHEMICAL AND ELECTRICAL PROPERTIES OF π-CONJUGATED POLY(3-ALKYLTHIOPHENES)

by

Mohamed S. A. Abdou

M.Sc. , Cairo University, Egypt, 1989

A THESIS SUBMITTED IN PARTIAL FULFILLMENT

OF THE REQUIREMENT FOR THE DEGREE OF

DOCTOR OF PHILOSOPHY

in the Department

of

Chemistry

Simon Fraser University

December 1994

APPROVAL

Name: Mohamed Saied Awad Abdou
Degree: Doctor of Philosophy
Title of Thesis: Towards "Macromolecular" Electronics: Photochemical and Electrical Properties of π-Conjugated Poly(3-alkylthiophenes)

Examining Committee:
Chairman: Dr. D. Sen

Dr. S. Holdcroft
Senior Supervisor

Dr. R. H. Hill

Dr. E. J. Wells

Dr. J. R. Dahn
Internal Examiner
Professor,
Department of Physics,
Simon Fraser University

Dr. F. Wudl
External Examiner
Professor,
Department of Chemistry,
University of California- Santa Barbara

Date of approval: Dec. 13, 1994

PARTIAL COPYRIGHT LICENSE

I hereby grant to Simon Fraser University the right to lend my thesis, project or extended essay (the title of which is shown below) to users of the Simon Fraser University Library, and to make partial or single copies only for such users or in response to a request from the library of any other university, or other educational institution, on its own behalf or for one of its users. I further agree that permission for multiple copying of this work for scholarly purposes may be granted by me or the Dean of Graduate Studies. It is understood that copying or publication of this work for financial gain shall not be allowed without my written permission.

Title of Thesis/Project/Extended Essay:

Towards "Macromolecular" Electronics:
Photochemical and Electrical Properties
of π-Conjugated Poly(3-alkylthiophenes)

Author:

(signature)

Mohamed Akhtar

(name)

12/13/94

(date)

ABSTRACT

This work investigates the photochemical and electrical properties of π-conjugated poly(3-alkylthiophenes), (P3ATs), at different levels of doping. The study is prompted by the growing interest in organic macromolecular materials and their potential applications in microelectronics, optoelectronics, and photonics.

Thin films of poly(3-hexylthiophene), (P3HT), a solution processable analog of intractable polythiophene, were deposited on various substrates and their photochemical and photolithographic properties were investigated. P3HT undergoes two main photochemical reactions: photobleaching and photooxidation. The former is largely the product of photosensitization, and reaction of, singlet oxygen with thiophene moieties. Photooxidation occurs via free-radical chain reactions which are initiated by photolysis of residual iron impurities used in polymerization of the material. While chain scission is the main photooxidation reaction in polymer solutions, photooxidation leads to crosslinking and insolubilization of polymers in the solid state. Conventional photolithography, and laser, direct-write microlithography proved useful for designing P3AT macromolecular wires with high resolution. Unfortunately, the doped, conducting form of the materials suffers from a poor long-term stability. Thus, a study of their doping-dedoping behavior was undertaken.

A new de-doping process was discovered. The process is photolytic in nature and plays a major role in the degradation of conductivity of a number of conducting polymers. The mechanism of this process is discussed in terms of photoreduction of the dopant with subsequent electron transfer to the doped polymer. New strategies for improving the stability of conducting polymers were

also investigated. Conducting polymers doped with $AuCl_3$ were found to possess superior stability over conventional dopants.

The electrical properties of P3AT semiconductors were investigated using Metal-Insulator-Semiconductor structures (MIS). The nature of impurities in P3ATs prepared via oxidative coupling using ferric chloride was found to be octahedral Fe (III) complexes. These were found to contribute to the origin of charge carriers in the material. Tailoring the electrical properties of macromolecular P3AT semiconductors using their photo-oxidative chemistry was also demonstrated.

Oxygen was found to play a pivotal role in the photochemical and electronic properties of the material. Molecular oxygen was found to form a reversible charge transfer complex (CTC) with poly(3-alkylthiophenes). The concentration and diffusion coefficient of oxygen in the material were determined using the time-lag technique. Thermodynamic parameters associated with the CTC were determined using the Benesi-Hildebrand equation. The effect of the CTC on the photochemical and electronic properties of P3ATs was evaluated.

To Ola, Hossam, and Muhannad.

ACKNOWLEDGMENTS

I would like to express my sincere gratitude to my senior supervisor Dr. Steven Holdcroft for giving me the opportunity to carry out interesting research, and for his invaluable guidance and constructive criticism of my work and in the preparation of this manuscript. I would also like to thank Dr. Ross. H. Hill and Dr. Edward J. Wells for useful discussions.

Thanks are also due to Drs. Z. Xie, D. Sharma, J. Dahn, and F. Orfino for assistance in some of the experimental work.

Thanks also to the members of the research group for friendship and useful discussions.

Thanks also to E. Plettner and J. Shipley for proofreading of this manuscript.

I wish to thank Dr. Steven Holdcroft and Simon Fraser University for financial assistance.

TABLE OF CONTENTS

LIST OF TABLES

LIST OF FIGURES

LIST OF ABBREVIATIONS

A	Absorbance
AA	Atomic Absorption spectroscopy
AES	Auger electron spectroscopy
Al	Aluminum
asym	Asymmetric
BP^{2+}	Bipolarons
C_i	Insulator capacitance (Farade, F)
C_{ox},	Capacitance of oxide layer (F)
C_S	Capacitance of semiconductor
CTC	Charge transfer complexes
C-V	Capacitance-voltage
D	Diffusion coefficient (cm^2s^{-1})
D_g^i	Interface gel dose (einstein/cm^2)
$D_g^{0.5}$	Resist Sensitivity (einstein/cm^2)
def.	Deformation
DSC	Differential scanning calorimetry
e	Electron charge ($1.6x10^{-19}$ C)
E	Electric fields (V)
EA_A	Electron affinity of an acceptor
E_b	Binding energy of charged bipolarons to the counter ions (eV)
E_c	Conduction band energy (eV)
E_{CTC}	Energy of the charge-transfer transition (eV or nm)
E_F	Fermi level energy (eV)
E_{Fi}	Intrinsic Fermi level energy (eV)

E_g	Band gap energy (eV)
$E^{o'}$	Formal potential (eV)
E_V	Valence band energy (eV)
$E^A_{1/2}$	Half wave potentials of an acceptor (eV)
$E^D_{1/2}$	Half wave potentials of a donor (eV)
EPR	Electron paramagnetic resonance spectroscopy
ESCA	Electron spectroscopy for chemical analysis
ESR	Electron spin resonance spectroscopy
F	Faraday constant (96487 C mol^{-1})
FTIR	Fourier Transfor infra-red spectroscopy
g	Electron free spin g-factor
GC	Gas chromatography
GCMS	Gas chromatography-Mass spectrometry
GPC	Gel permeation chromatography
$h\nu$	Photon energy (eV or nm)
HH	Head-Head dyad configuration
HT	Head-Tail dyad configuration
I_{bk}	Bulk current (A)
I_{ds}	Drain currant (A)
I_0	Radiation flux (Einstein cm^{-2} s^{-1})
I_p	Primary ion current density (A/cm^2)
IP_D	Ionization potential of a donor (eV)
I-V	Current-voltage
ITO	Indium-Tin oxide glass
k	Rate constant
kT	Thermal energy (0.026 eV at 298 K)
l	Film thickness (cm)

L	Channel length (cm)
M	Atomic mass number of elements
M_n	Number average molecular weight
M_w	Weight average molecular weight
MIS	Metal-Insulator-Semiconductor
MISFETs	Metal-Insulator-Semiconductor Field Effect Transistors
MISDs	Metal-Insulator-Semiconductor Diodes
MWD	Molecular weight distribution
m	Concentration of chromophores ($mol.L^{-1}$)
n	Number of free charge carrier per unit volume (cm^{-3})
N_a	Number of ionized impurities (majority carrier concentration, cm^{-3})
N_c	Density of states at the conduction band ($cm^{-3}\ eV^{-1}$)
N_A	Avogardro number ($6.023x10^{23}$ molecules/mole)
NMR	Nuclear Magnetic Resonance Spectroscopy
OD	Optical density
P	Permeability coefficient (cm^2s^{-1})
$P^{+\bullet}$	Polaron
$\overline{P}_n$	Number average degree of polymerization
p_O	Fracture density per unit radiation dose
PA	Polyacetylene
PANI	Poly(aniline)
PFu	Poly(furan)
PITN	Poly(isothianaphthalene)
PPP	Poly(p-phenylene)
PPS	Poly(phenylene sulfide)
PPV	Poly(p-phenylene vinylene)
PPy	Poly(pyrrole)

PT	Poly(thiophene)
P3ATs	Poly(3-alkylthiophenes)
P3BuT	Poly(3-butylthiophene)
P3HT	Poly(3-hexylthiophene)
P3HT-A	Polymer containing 3.2 wt% iron
P3HT-B	Polymer containing 1.3 wt% iron
P3HT-C	Polymer containing 0.05 wt% iron
P3OT	Poly(3-octyllthiophene)
q	Crosslinking density
q_0	Crosslinking density per unit radiation dose
r	radiation dose (einstein cm^{-2})
s	Average number of chain scission
S	Sol fraction
s_P	Spacing between the probes (four point-probe technique)
S_y	Sputtering yield (atom/ion)
SCE	Saturated calomel electrode
sh	Shoulder
Si	Silicon
str.	Stretching
sym.	Symmetric
TF-MISFETs	Thin Film- Metal-Insulator-Semiconductor Field Effect Transistors
Tg	Glass transition temperature (^oC)
T_m	Melting point (^oC)
$t_{1/2}$	Half-life time of a reaction
U_B	Coulomb energy (eV)
UV-vis-NIR	Untra-violet-visible-Near infra-red
V	Applied voltage (V)

V_{ds}	Drain voltage (V)
V_f	Flat band potential (V)
V_{gs}	Gate voltage (V)
V_{th}	Threshold voltage (V)
vib.	Vibration
VRH	Variable-range-hopping
W	Channel width (cm)
x_D	Mole Fraction of a donor
XPS	X-ray photoelectron spectroscopy
z	Sputtering rate of elements (nm/s)
γ_n	Resist contrast
ε	Molar extinction coefficient (L^{-1}.mol.cm^{-1})
ε_o	Dielectric constants of insulator
ϕ_b	Contact potential (V)
ϕ	Work function (eV)
ϕ_s	Spectrometer work function (eV)
Φ_s	Quantum yield of chain scission
Φ_x	Quantum yield of crosslinking
δ	Isomer shift (mm s^{-1})
Δ	Quadrupole splitting (mm s^{-1})
ΔE^o	Difference in the standard electrochemical potentials (V)
ΔG^o	Standard free energy change (kcal/mol)
ΔH^o	Standard heat of formation (or binding energy)(cal deg^{-1} $mole^{-1}$)
ΔS^o	Standard entropy change (kcal/mol)
χ	Electron affinity (eV)
λ_{max}	wavelength of maximum absorption (nm)
μ	Carrier mobility (cm^2. V^{-1} s^{-1})

μ_{EFF}	Effective carrier mobility ($cm^2. V^{-1} s^{-1}$)
ρ	Density (g/cm^3)
σ	Conductivity ($\Omega^{-1}cm^{-1}$)
1-D	One dimension
3-D	Three-dimension

Chapter I: GENERAL INTRODUCTION

I.1 Introduction

Advances in the miniaturization of electronic components have led to improvements in the speed and performance of electronic devices. Current Si-circuit technology is based on circuit elements that have linewidths of 0.5 μm (5000 Å). Future requirements for nanoscale system designs are, however, in conflict with the progress in reducing the size of Si based components since miniaturization in Si devices is expected to come to a limit of a few hundred Å. Below these dimensions semiconductor devices may not operate properly because depletion layers, which are the potential barriers between the different regions of the device, will not be effective and electron (hole) tunneling will occur.[1] In addition, as the device density increases the number of processing steps become greater, resulting in a lowering of device yield and raising of the processing costs. A continuing search for alternative materials that fit the future requirements for complex structures is therefore necessary.

The term macromolecular electronics refers to the possible future use of macromolecules as electronic circuit elements such as macromolecular wires and macromolecular transistors.[2] The basic concepts of macromolecular electronics are completely different from conventional Si electronics since the notion of miniaturization is replaced by *assemblage*. The dimensions of macromolecules can be controlled by the nature and number of the building monomer units covering the range from a few Å, which is the typical size of oligomers, to a few nanometers, the size of a polymer chain. Consequently, a molecular integrated circuit is an assembly of preformed molecular components of dimensions in the nanoscale range. The other important feature of macromolecular components is that their properties are open to manipulation by common techniques of organic and polymer chemistry.

Macromolecular electronics will use materials in which the molecules retain their separate identity. As a result, the properties of such materials depend on structure, arrangements, and interactions of the constituting molecules (Figure I.1).

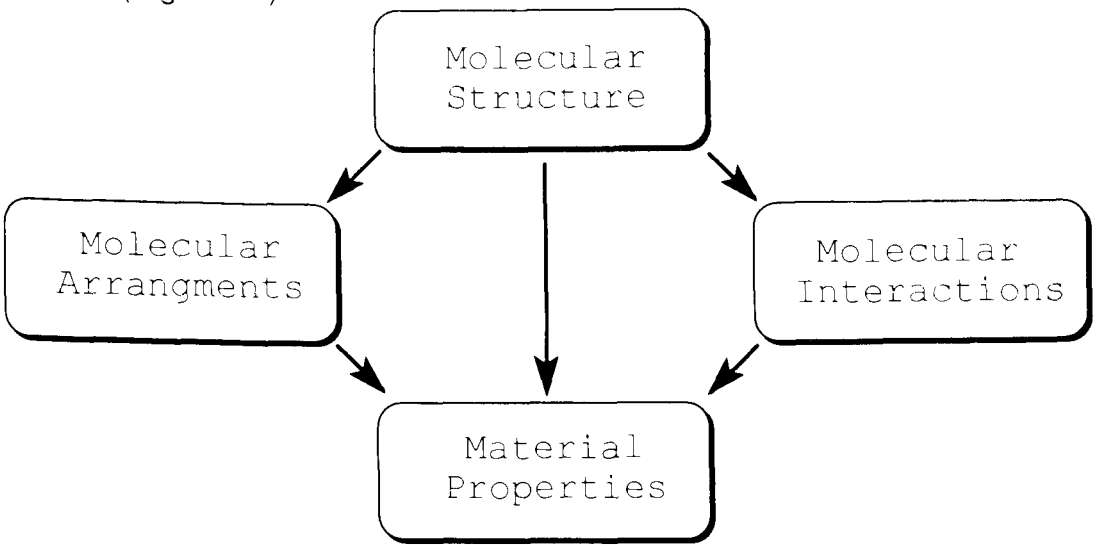

Figure I.1: Elements of Macromolecular Materials

The field of macromolecular electronics is interdisciplinary: it ranges from Chemistry through Solid-state Physics and Materials Science to Solid-state Electronics (Figure I.2).

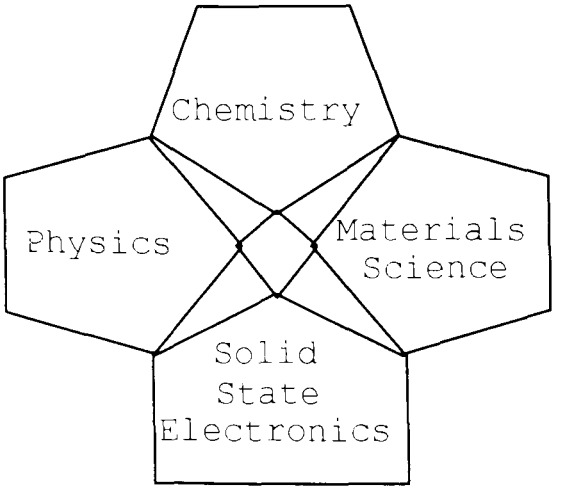

Figure I.2: Disciplines within Macromolecular Electronics

Development of materials with properties that meet the requirements of molecular and macromolecular electronics is quite a challenging task. Chemists can be considered to work towards this goal from the atom "up". Building and arranging of atoms in a controlled fashion "one atom at a time" should in principle provide a powerful method of tailoring materials to predesigned purposes. π-Conjugated polymers are believed to be a suitable material for macromolecular electroincs.

I.2 Macromolecular Semiconductors

π-Conjugated polymers are particularly promising for macromolecular electronics. The polymers possess delocalized electronic structures that can accommodate charge carrying species e.g. electrons and holes. The band gap energies of these polymers are in the range of 1.0 to 3.5 eV. This energy is important in determining the intrinsic properties of the material, since it specifies the energy required to excite an electron from the valence band to conduction band. In addition, conjugated polymers are quasi-one dimensional and their molecular dimensions can be designed and synthesized in a controlled fashion. π-Conjugated polymers are thus the molecular analogs of inorganic semiconductors i.e. "macromolecular semiconductors".

While the history of inorganic semiconductors is a long one extending over more than a century, studies of the electronic properties of organic semiconducting polymers may be traced back to the early 60's. A brief historical note on these two materials is presented below.

Inorganic semiconductors. The first feature used to distinguish this class of electrical conductors from metals and other poor conductors was their negative temperature coefficient of resistance, i.e. their resistance generally falls as the temperature is raised while that of metals rises.[3] Michael Faraday (1833) was the first to notice this effect when studying the electrical properties of silver sulfide.[4] In 1873, forty years later, two important advances were made. The phenomenon of rectification was observed by F. Braun using substances such as lead sulfide and iron pyrites.[5] Photoconductivity of selenium was noticed by W. Smith.[6] Other substances were soon found to show similar effects, e.g. metallic sulfides, oxides, and the element silicon. After this, a great deal of work was carried out and a class of substances, called "semiconductors" with these properties began to emerge. A review of the early work and problems of identifying semiconductors has been given by B. Gudden (1924).[7]

In the early 30's, the chemistry of semiconductors was studied.[8] These studies led to the identification of two distinct types of semiconductors: defect (p-type) and excess (n-type) semiconductors. The other importance of this work was the demonstration of the vital role of impurities in determining the properties of semiconductors.

Increased interest in these materials was aroused in the 1930's largely due to the stimulus of technological applications. The first important application were rectifiers which were introduced by Grondahl and Geiger in 1927.[9] The transistor was invented by Bardeen and Brattain, and Shockley and Pearson in 1948.[10,11]

Organic Semiconducting Polymers

(i) Early Era. Natural organic polymers including wood, fur, leather, wool, cotton and silk were not structurally analyzed until early 1920 when modern methods of chemical and physical analysis became available.[12] In 1940 a new chemistry involved in the synthesis of organic polymers was established.

Organic polymers capable of conducting electricity by a purely electronic process are rather new (1960). The concept of π-conjugation as a necessary requirement for conduction in polymers was obvious for early work.[13-17] Polyconjugated systems, as they were first called, were prepared by pyrolysis of organic polymers.[18-20] Thus, high temperature pyrolysis of synthetic organic polymers such as poly(vinylidine chloride) and polyacrylonitrile was used to prepare polyvinylenes. These polyconjugated polymers showed semiconducting properties. The conductivity (σ) and band gap energy (E_g) of the material were 10^{-7} $\Omega^{-1}cm^{-1}$ and ~1.7 eV, respectively. The concentration of impurities resulting from the preparation technique was ~10^{18} spins/gram (g = 1.981-2.001), as determined using electron spin resonance spectroscopy (ESR).[21-25]

This synthetic technique was later replaced by more rational organic chemistry. Thus, polyacetylenes have been prepared with Ziegler catalysts at reaction temperatures of -70 to 80 ^{o}C.[26] The structure was characterized by infra-red spectroscopy and x-ray diffraction. The amorphous polymer was found to have E_g in the order of 0.83 eV while E_g of the crystalline materials was 0.46 eV. Conductivities as high as 10^{-4} $\Omega^{-1}cm^{-1}$ have been reported.[27]

In contrast to polyacetylene, polyphenylenes were found to have high thermal stability. A number of polyphenylenes was synthesized by various techniques. Thus, dihalogenated benzenes were polymerized using sodium or copper as a catalyst.[28,29] Organomagensium compounds have also been used.[30] Direct polymerization of benzene, on the other hand, has been

accomplished by heating benzene with transition metal halides such as ferric chloride.[31] The electrical properties of the polymer were found to be $\sigma = 10^{-11}$ $\Omega^{-1}cm^{-1}$, E_g = 0.9-1.7 eV, and [impurity] = 10^{18}-10^{19} spin/gram (g=2.00).

The third member of polyconjugated systems, initially studied, was polypyrrole. This polymer was made by pyrolysis of iodopyrrole at 120 ^{o}C. The resulting polymers were reported to contain a considerable amount of iodine as shown by ESR measurements. The material was found to possess conductivity as high as 10^{-1} $\Omega^{-1}cm^{-1}$ which was attributed to the presence of polypyrrole-iodine charge transfer complexes.[32-33] It has also been shown that the iodine-containing polymers exhibit an extrinsic *p*-type behavior which was attributed tentatively to the removal of π electrons by the chemisorbed iodine.

(ii) Modern Era. Increased interest in conjugated organic polymers was initiated in the mid-1970s, after the discovery of Shirakawa (1973)[34] and Ito (1974)[35,36] that polyacetylene (PA) could be prepared as films having metallic luster in contrast to PA polymer powder prepared earlier by Hatano (1961).[26] This was followed, in 1977, by the novelty that the conductivity of PA could be increased by doping it with various donor or acceptor species to yield p-type or n-type semiconductors.[37-43] The conductivity of doped PA, during this period, was reported to be 10^3 $\Omega^{-1}cm^{-1}$. By 1987, Naarmann and Theophilou had developed a new synthetic route for preparation of free standing films of PA.[44] When stretch oriented and doped with iodine it possesses conductivities in excess of 10^5 $\Omega^{-1}cm^{-1}$.

Since the discovery of doped PA, a number of other organic polymers and their derivatives have been synthesized and evaluated as conductors and semiconductors. Although the list is extensive, they all belong to three main classes:

I. Polyenes: PA (discussed above),

II. Polyaromatics: polymers containing phenyl groups in the main chain with or without heteroatoms along the polymer backbone. These include poly(p-phenylene) (PPP), poly(p-phenylene vinylene) (PPV), poly(phenylene sulfide) (PPS), and poly(aniline) (PANI). The electrical characteristics of PPP were first studied by Ivory (1979),[45] and Shacklette (1979),[46] PPV by Wnek (1979),[47] PPS by Rabolt (1980)[48] and Chance (1980),[49] and PANI by Diaz (1980).[50]

III. Polyheterocycles: these are polyheteroaromatics with a heteroatom in the ring structure. The main members of this class are poly(thiophene) (PT), poly(pyrrole), (PPy), poly(furan), (PFu), and poly(isothianaphthene), (PITN). Thin films of PPy were prepared electrochemically by Diaz (1979)[51]. PT powder was prepared by Yamamoto (1980) using Grignard polycondensation[52]. Thin films of PT and PFu were prepared electrochemically by Garnier (1982)[53]. PITN was prepared by Wudl in 1985.[54] The latter has an exceptionally small band gap energy (~1 eV), the smallest known for conducting polymers. The chemical structures of the above polymers are shown in Figure I.3.

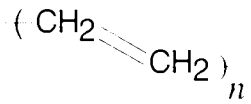

Poly(acetylene)

PPP

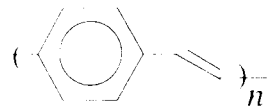

PPV

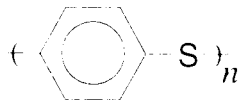

PPS

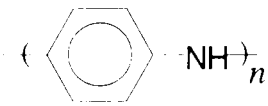

PANi

Polyaromatics

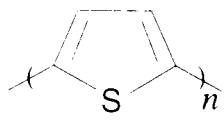

PT

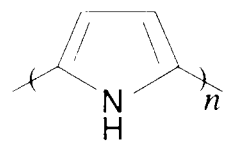

PPy

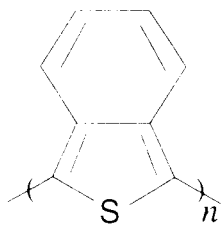

PITN

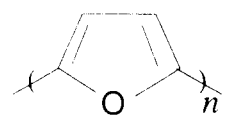

PFu

Polyhetreroaromatics

Figure I.3: Chemical structure of common conjugated polymers

I.3 Properties of Macromolecular Semiconductors

Because of electronic delocalization, π-conjugated polymers can have the properties of semiconductors and metals. They are semiconductors in the "neutral" form and have interesting electrical and optical properties. These polymers can also be processed to change electrical characteristics from semiconductor-like (*conductivity* ~ 10^{-7} *S* cm^{-1}); to highly conducting metal-like (*conductivity* 10^{5} *S* cm^{-1}) materials. The physical attributes of conjugated polymers are discussed in more detail in the following sections. Special emphasis will be directed to poly(3-alkylthiophenes) (P3ATs), which are the macromolecular materials employed in this study.

I.3.1 Semiconducting Properties

I.3.1.1 Chromism (Thermo-, Solvato- and Electro-)

Reversible color changes associated with variation in conformation or oxidation state of materials is referred to as "chromism".[55-57] P3ATs, and conjugated polymers in general, exhibit electro-, thermo-, and solvato-chromisms due to the strong interaction between the electronic structure and polymer chain conformation.

The thermochromic effect is a thermally-induced change in color.[56] It is usually reversible in a certain temperature range depending on the thermal stability of the material. The mechanism of this process is attributed to variations in the conformation of the polymer backbone associated with a change in temperature as a result of thermally induced disorder in the alkyl side-chains. This effect has been studied by UV-vis, IR, and Ultraviolet photoelectron spectroscopy and modeled theoretically by the Valence-Effective Hamiltonian method.[58,59]

Solvatochromism is a characteristic property of conjugated polymer solutions due to changes in solvent parameters. This effect has been observed in P3ATs when a non-solvent, such as methanol, is added to a polymer solution in a good solvent, e.g. chloroform. It can also be observed by changing the temperature of the polymer solution.[55]

Electrochromism originates from color changes accompanying electro-oxidation-reduction reactions. It is a common phenomenon to P3ATs, and conjugated polymers in general. The color change of the material is due to creation of localized electronic states in the band gap upon electrooxidation/reduction.[60] The time for color switching is ~10-300 ms with cycle-life up to 10^5 charging/discharging cycles.[61]

I.3.1.2 Optical Properties

The optical properties of conjugated polymers are important in establishing an understanding of the electronic structure of the material. It is also fundamental to the study of photochemistry, photoconductivity, and non-linear optical processes.

Photo-excitation of semiconductors, with light of energy greater than E_g, results in the formation of electron-hole pairs. In conjugated polymers, such as P3ATs, the neutral excited state is called a polaron-exciton because of its tendency for self-trapping and confinement along the polymer chain (Figure I.4).[62] Within the exciton, chain relaxation causes the creation of localized electronic states in the band gap in a similar fashion to that of polaron and bipolaron generation. These states are singly occupied and the singlet configuration is shown in Figure I.4. The transition from the upper to lower level is dipole-allowed. It is a radiative recombination which provides fluorescence. In the solid state, the efficiency of fluorescence is very low (~10^{-3}) indicating that

there are efficient non-radiative decay processes.[63] The non-radiative decay channels include: (i) charge separation through interchain electron transfer yielding polarons and bipolarons which may act as deactivation centers as evidenced by voltage- and doping-modulated luminescence,[64,65] (ii) non-radiative decay at structural and impurity defects, (iii) quenching by oxygen, or (iv) intersystem crossing to low-lying triplet states which may give rise to long-lived emissions such as phosphorescence.

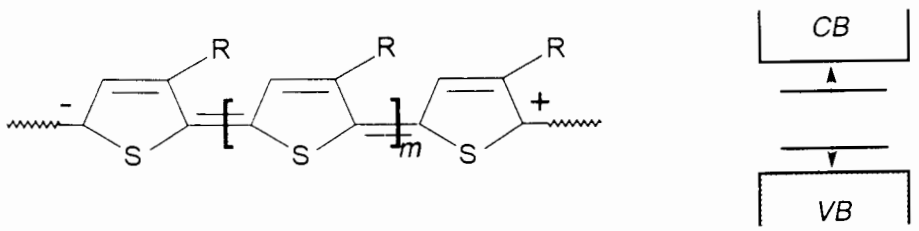

Figure I.4: Molecular and band structure of excitons

Phosphorescence and delayed fluorescence from P3ATs have recently been observed.[66,67] These emissions can only be detected when the polymer is excited at 250 nm which corresponds to a much higher energy than the interband transition (500 nm in solid films). Thus, the mechanism by which the triplet state is populated may involve an upper excited-state transfer.

In addition to the photoluminescent properties, photoexcitation can also lead to interesting photoconduction properties if excitation is carried out in the presence of an electric field. In this case separation of charge carriers is favored over charge recombination. π-Conjugated polymers are good candidates as photoconductors. Thus, P3ATs exhibit interesting photoconduction properties.[68] Light-induced charge carriers have been studied using ITO/P3AT/Al sandwich structures. The efficiency of photoconduction was found to be dependent on atmosphere, temperature and electric fields. Oxygen was found to have a sensitizing effect which increases the photoconduction efficiency.

Photoexcitation may also modify the chemical and physical properties of the materials. These photochemical changes form the basis for light-induced processing techniques such as photolithography which is the subject of *Chapter III*.

I.3.1.3 Electronic Properties[69]

π-Conjugated polymers are characterized by their semiconducting properties in the neutral form. They are all classified as medium- to wide-gap semiconductors due to their large band gap energies (E_g ~1.0-3.5 eV). Conjugated polymers are usually p-type semiconductors because of their relatively low ionization potentials (~ 5 eV). The neutral polymers possess conductivities in the range of 10^{-9} - 10^{-6} Ω^{-1} cm^{-1}. The charge carrier mobility, as determined using metal-insulator-semiconductor structures, is typically 10^{-6} - 10^{-5} $cm^2V^{-1}s^{-1}$.

The nature of charge carriers in macromolecular organic semiconductors is different from conventional inorganic semiconductors. In macromolecular semiconductors, the presence of charges causes a lattice distortion due to strong electron-phonon couplings. The charge is localized over a small segment of the polymer (~4-6 monomer units) and takes the form of polaron-like entities (charge plus lattice distortion). These polarons are mobile and are responsible for the relatively high conductivity of the material. The presence of polaronic charge carriers also leads to the generation of localized electronic states in the band gap.

The origin of charge carriers in conjugated polymers in the "neutral" form is still open to question, as is electronic transport. These are the subject of *Chapter V* of this thesis.

I.3.2 Metallic Properties

The electrical properties of conjugated polymers can be controlled by a simple redox chemistry, a process termed "Doping" (Scheme I.1).[37] This process leads to an increase in the charge carrier concentration, and consequently, doped conjugated polymers, "conducting polymers", are good conductors (σ = 10-10^4 $\Omega^{-1}cm^{-1}$). Doping can be achieved by various chemical, electrochemical, and photochemical techniques.

$$\textit{n-type doping} \xleftarrow[\textit{reduction}]{+e^-} P \xrightarrow[\textit{oxidation}]{-e^-} \textit{p-type doping}$$

Scheme I.1

The generation of charge carriers by doping of conjugated polymers is very different from that of inorganic semiconductors. Crystalline inorganic semiconductors have a rigid, three dimensional lattice structure and a conductivity that is related to free electrons or holes.[70] In contrast, conducting polymers are quasi-one dimensional and their conductivities are discussed in terms of the polaron-bipolaron models.[71]

Conductivity of conjugated polymers increases with increasing the doping level of the material. Figure I.5 shows the typical variation in conductivity with doping. It is characterized by three main regimes: low, moderate, and high as represented by regions I, II, and III. In the low doping regime, the conductivity increases gradually with doping level due to the conductivity percolation phenomenon of the material i.e. conductive regions separated by semiconducting domains. In contrast, at moderate doping levels the conductivity undergoes a dramatic increase with doping which can be rationalized in terms of reduction of the barrier energy between the conductive regions. If the doping

level increases beyond this point, the effect of charge scattering opposes the process of charge transport thereby compensating for the increase in charge carrier concentration. Consequently, conductivity of the polymer in region III reaches a steady state value independent of the doping level.

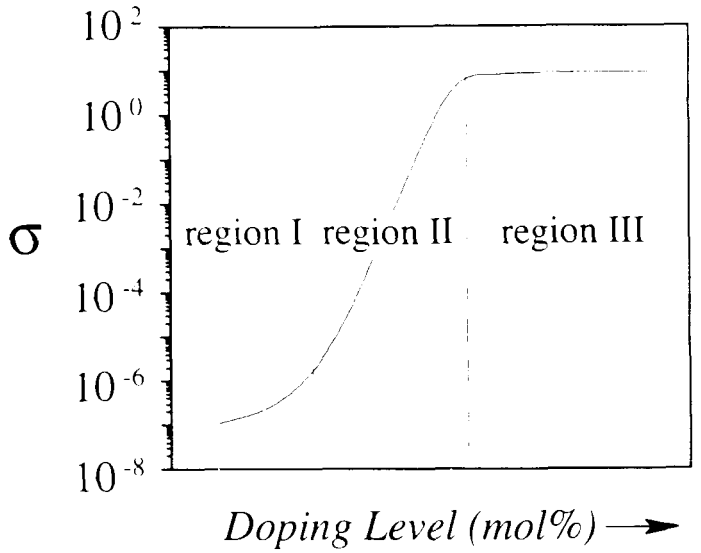

Figure I.5: Conductivity-doping level relationships

The conductivity of the material is highly dependent on regiochemistry of the polymer. Thus, the maximum conductivity of P3ATs possessing regio-*irregular* structures is 10^{-4} Ω^{-1} cm^{-1}, when heavily doped.[72] In contrast, regio-*regular* P3ATs possess conductivities in excess of $2x10^{3}$ Ω^{-1} cm^{-1}.[73] The nature of the dopant (counter ion) has essentially little effect on conductivity of the materials but does play a major role in determining stability of the polymers in the doped form.[74] Thus, polymers doped with nitrosomium tetrafluoroborate are unstable under ambient conditions and undergo a rapid dedoping process (re-reduction) as evidenced by a loss of the conductivity in a matter of several minutes. By contrast, when $FeCl_3$ is used as a dopant the degradation of

conductivity occurs over a period of several hours. Insights into this problem are discussed in *Chapter IV*.

I.4 Technological Innovations

Some of the proposed applications of macromolecular semiconductors include molecular electronics, electro-optics, opto-electronics, and microelectronics, e.g. molecular wires,[75,76] molecular switches,[77] nano-transistors,[78] light emitting diodes,[79] solar cells,[80] solid-state and microelectrochemical transistors,[81,82] capacitors,[83] sensors,[84] batteries,[85] drug-delivery systems,[86] electrochromic displays,[87] and electromagnetic interference shielding.[88]

I.5 Aim of the Work

As part of the search for alternative materials to conventional inorganic semiconductors, macromolecular organic semiconductors are particularly promising. The molecular dimensions can be controlled over a wide range depending on the number of the building monomer units. Macromolecular semiconductors can be processed to have properties of semiconductors and metals and can be tailored by common organic and polymer chemistry. There are, however, certain fundamental challenges that need to be addressed and overcome before the realization of all organic macromolecular electronics. These challenges form the core of this thesis and encompass

1. Study of the photochemistry of π-conjugated Poly(3-alkylthiophenes) (P3ATs) with the aim of designing macromolecular wires.
2. Study of the doping-dedoping behavior of the macromolecular P3AT wires with the goal of devising new strategies for improving the stability of the conducting form of the material.

3. Study of the origin of charge carriers in macromolecular P3AT semiconductors, transport properties, and the factors controlling the performance of P3AT-based transistors.

I.6 Thesis Structure

This thesis is concerned with the photochemical and electrical properties of π-conjugated poly(3-alkylthiophenes). These properties collectively determine the fundamental requirements of molecular semiconductors and thus the foundations for designing macromolecular electronics. The thesis is divided into two main parts, namely; Macromolecular Wires which encompasses Chapters III and IV, and Macromolecular Transistors which is the focus of Chapters V and VI (Figure I.6).

Chapter II is concerned with the techniques of preparation and characterization. Chapter III describes the feasibility of processing macromolecular P3AT semiconductors using microlithography. Chapter IV highlights plausible mechanisms of degradation of conductivity of the material in the oxidized (doped) form and provides possible solutions to the problem. Insights into the origin of charge carriers in molecular semiconductors, and factors controlling the mechanism of charge transport are presented in Chapter V. The last Chapter is concerned with the role of molecular oxygen on the optical and electronic properties of the materials.

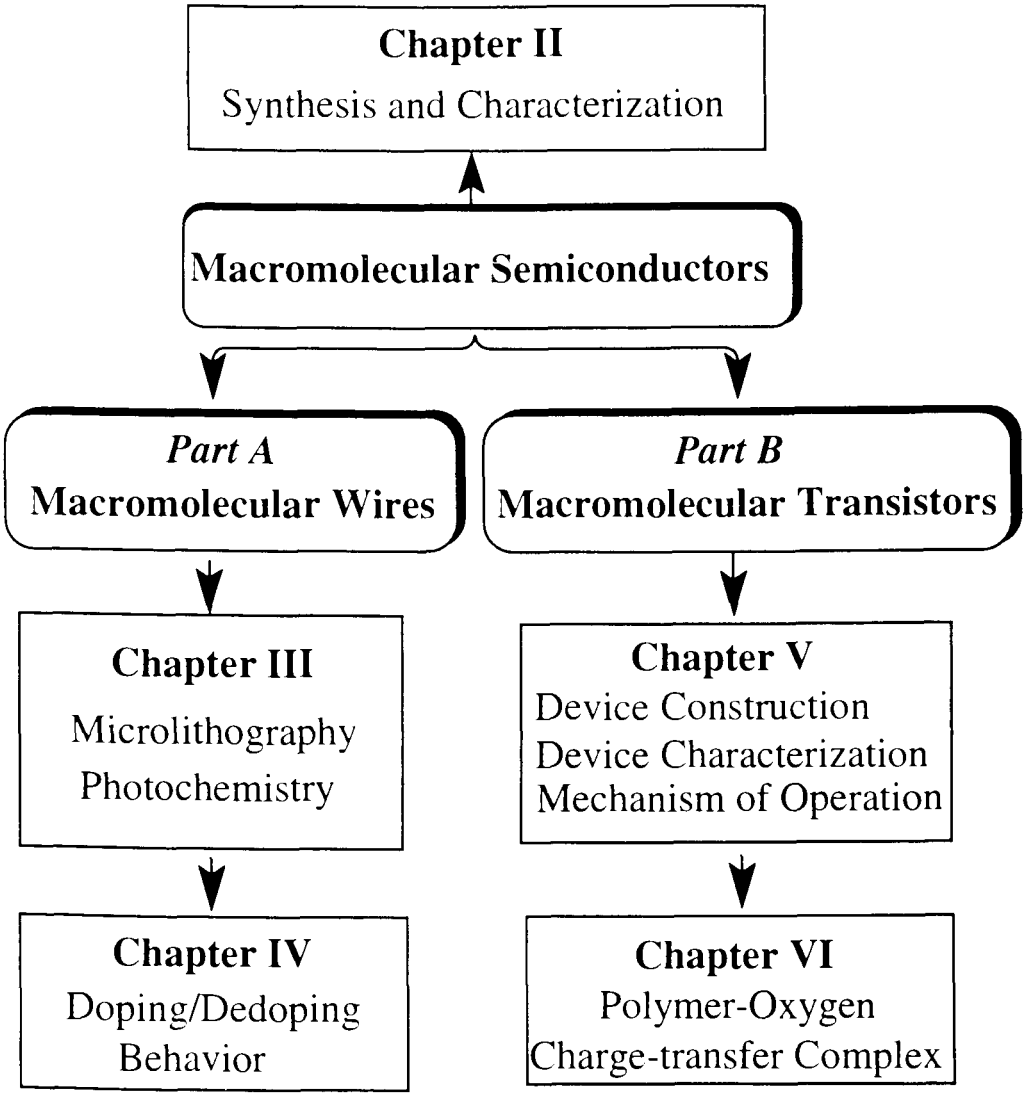

Figure I.6: Thesis structure

Chapter II: π-CONJUGATED POLY(3-ALKYLTHIOPHENES): SYNTHESIS AND CHARACTERIZATION

II.1 Introduction

Polythiophene (PT) is an insoluble, non-moldable material. It has been chemically synthesized using organomagnesium chemistry,[52] while thin, solid polymer films have been prepared by electrochemical polymerization.[53] Intractability of the material has been a major obstacle in processing and structural characterization of the material and has impeded efforts for improving the properties of PT in particular and conjugated polymers in general.

Recent advances, particularly in polythiophene chemistry, have provided solutions to this problem.[89,90] Substitution of thiophene at the 3-position with long alkyl chains (longer than *n-butyl*) yields soluble and melt processable polymers (Figure II.1). The side chains decrease the relatively strong interchain interaction of the polymer and thus render it soluble in common organic solvents.

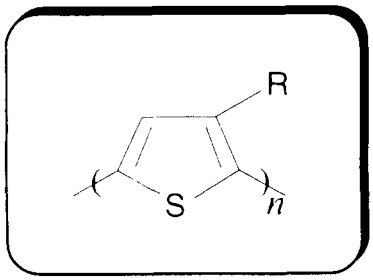

R = Hexyl

Figure II.1: Chemical structure of P3ATs

The aim of this Chapter is to present the methods of preparation and the important chemical and physical characteristics of poly(3-alkylthiophenes). Although well documented, it was important to repeat the synthesis and characterization in order to understand the different properties of the material and be able to control and improve them according to the purpose of study. One of the main problems of organic semiconducting polymers, in general, is impurities. Control of the nature and concentration of impurities in poly(3-alkylthiophene) semiconductors is the focus of this Chapter.

II.2 Experimental

II.2.1 Synthesis

Monomer. 3-Hexylthiophene monomers were synthesized by coupling the Grignard reagent of 1-bromohexane (Aldrich) with 3-bromothiophene using [1,3-bis-(1,3-diphenylphosphino)propane] nickel(II)chloride ($Ni(dppp)_2Cl_2$) as catalyst.[91]

Polymer. Poly(3-hexylthiophene)(P3HT) was prepared by three main methods, namely; electrochemical polymerization, Grignard polycondensation, and oxidative coupling using transition metal halides such as $FeCl_3$.

(I) Oxidative coupling: Polymerization of the monomer was achieved by mixing a solution of 3-hexylthiophene in chloroform with a chloroform solution of anhydrous ferric chloride in a molar ratio of 1:4.[90] The mixture was stirred for 24 h. The solid product was filtered, washed successively with NH_4OH (28%), water, and acidified methanol. The crude polymer was dissolved in hot dichloromethane and insoluble products were removed by filtration. Low molecular weight products were removed by fractional precipitation. The polymer was purified by soxhlet extraction and extensive washing with ammonia. The precipitate was dried under reduced pressure at 50°C.

(II) Grignard route: 3-Hexylthiophene (7.8 g, 46 mmol) and 12.2 g (48 mmol) of I_2 (BDH Chemicals Ltd.) were added to a mixture comprising 18 ml chloroform, 3 ml concentrated HNO_3, and 3 ml H_2O.[52] The mixture was refluxed for 16 hours. The product (2,5-diiodo-3-hexylthiophene) was purified through a silica gel column using hexane (71% yield, purity, >99%). ^1H NMR (400 MHz, $CDCl_3$), δ_{ppm}: 6.89 (1H, s), 2.50 (2H, t), 1.53 (2H, m), 1.4-0.8 (9H, m). Magnesium metal (0.29 g, 12 mmol) was allowed to react with 4.2 g (10 mmol) of 2,5-diiodo-3-hexylthiophene in ether and the polymerization initiated by $Ni(dppp)_2Cl_2$. After 24 hours the reaction was quenched with $MeOH/H_2O$. The

reaction mixture was poured into 5% HCl in methanol to precipitate the polymer. The polymer was purified by repeated reprecipitation.

(III) Electropolymerization:[53,92] P3HT was prepared by electrochemical polymerization of 3-hexylthiophene in acetonitrile. The polymerization vessel was a one-compartment cell equipped with an indium/tin oxide glass (ITO) anode and a platinum cathode. The polymerization was carried out at 20°C at a constant current density of 2 mA/cm^2 under nitrogen atmosphere. Tetra butylammonium perchlorate was used as electrolyte (0.2 M). The concentration of the monomer was 0.1 M. Neutral films were obtained by reversing the polarity of the electrodes after deposition. The polymer films were further reduced with NH_4OH (28%) for 24 hours, washed successively with acidified methanol, water and then dried.

II.2.2. Iron Impurities

The iron content in polymers prepared by oxidative coupling were controlled by the following procedures. The solid product was filtered, washed successively with NH_4OH (28%), water and finally with acidified methanol. The crude polymer was dissolved in hot dichloromethane and insoluble products were removed by filtration. Low molecular weight products were removed by fractional precipitation. The precipitate was filtered and dried under reduced pressure at 50°C (**P3HT-A**). A fraction of the sample was purified further by soxhlet extraction using methanol (2 days) and acetone (5 days) (**P3HT-B**). Subsequently, a fraction of this polymer was purified even further by treating a solution of the polymer in $CHCl_3$ with NH_4OH (28%). The polymer was precipitated, washed to chloride-free waste and dried as described above (**P3HT-C**). By this route three polymers samples containing various levels of iron impurities were obtained.

Atomic Absorption. Iron content was determined by standard acid digestion procedures followed by atomic absorption analysis. Dissolution of iron and breakdown of the organic materials was achieved by digesting 50 mg of polymer with 10 ml of concentrated sulfuric and nitric acids (50 vol%).[93] Stock solutions of iron were prepared by dissolving 0.250 g of iron (Baker Chemicals) in 250 ml nitric acid (~5 ml) and distilled water. Standard iron solutions (25 ml) containing 2, 4, 8, 12, 16 and 20 ppm iron were prepared by appropriate dilution with 0.1 HCl. A 2483 Å lamp was used. Atomic absorption measurements were performed using a Perkin-Elmer 1100B AA spectrophotometer.

Mössbauer. The identity of the iron impurities was determined using Mössbauer spectroscopy. Mössbauer spectra were recorded by using a constant-acceleration Harwell Instruments spectrometer (200 series) with the ^{57}Co/Rh source (New England Nuclear). The source and absorbers were immersed in liquid nitrogen in a Harwell Instruments Dewar. The 35.5 KeV Mössbauer γ-ray was monitored through the 6 KeV escape peak in a Xe/CO_2 proportional counter. The spectra were accumulated in a Nuclear Data 66 analyzer as 256-channel spectra and were subsequently computer-fitted to Lorentzians using the N.D. 66 as a computer terminal for transmitting data to and for computation on, the University IBM 4341 main-frame computer. Absorbers, containing ca. 80 mg of polymer sample, were mounted in Teflon holders. The cross-sectional area of the sample was 2 cm^2. The isomer shifts are quoted with respect to iron metal as a reference. Mössbauer measurements were carried out with the help of Dr. D. Sharma.

Elemental Analysis. Elemental analysis of polymers prepared by oxidative coupling and their residual iron impurities were carried out by Microanalyical Laboratories, Vancouver.

II.2.3 Polymer Characterization

GPC.[94] When polymers are prepared, a mixture of molecular sizes is usually obtained. The properties of a polymer sample depends on the average size of the molecules present. There are a number of ways by which such an average can be calculated, and different methods of averaging yield different results.

Methods based on counting the molecules in a given mass of material afford the number average molecular weight, M_n, which is defined by the following expression

$$M_n = \frac{\sum N_i M_i}{\sum N_i} \qquad \text{(II.1)}$$

M_i is the molar mass of the molecular species i, and N_i is the number of molecules of i in the sample. Other methods measure quantities proportional to the mass of molecules. In this case, the weight average molecular weight, M_W, is obtained. M_W is defined as follows

$$M_W = \frac{\sum N_i M_i^2}{\sum N_i M_i} \qquad \text{(II.2)}$$

Gel permeation chromatography (GPC) is an important technique in determining molecular mass (M_W and M_n) of synthesized polymers. GPC is a size exclusion method for molecular weight measurements in which separation is accomplished on a chromatographic column packed with a porous material that separates the polymer molecules according to size.

Molecular weight distribution curves of polymers were determined by size exclusion chromatography using 10^5, 10^4 and 10^3 Å μ-Styragel columns at 25°C. Polymers were eluted with tetrahydrofuran (THF, BDH-HPLC grade) and detected using a UV-vis spectrophotometer (Waters Model 486). Data were acquired, stored, and analyzed on a personal computer using a custom made software. Polystyrene standards (Polymers Labs.) of molecular weights ranging from 233 000 to 750 were used for calibrating GPC columns for hydrodynamic volume versus elution volume. The polystyrene (PS) calibration curve was converted to a poly(3-hexylthiophene) (P3HT)-based calibration according to equation II.3 and using the Mark-Houwink constants determined by Holdcroft:[95] $K_{P3HT} = 2.28 \times 10^{-3}$ cm^3/g, $a_{P3HT} = 0.96$, $K_{PS} = 1.29 \times 10^{-2}$ cm^3/g and $a_{PS} = 0.713$.

$$\log M_{P3HT} = \left(\frac{1}{1+a_{P3HT}}\right)\log\frac{K_{PS}}{K_{P3HT}} + \frac{1+a_{PS}}{1+a_{P3HT}}\log M_{PS} \qquad \text{(II.3)}$$

FTIR. Infrared spectra were recorded on a Bomem Michelson FTIR (120 series). The polymer samples were prepared by solvent evaporation in the form of thin polymer films on KBr discs

UV-vis-NIR. UV-vis-NIR spectra were recorded on various spectrophotometers: Perkin Elmer Lambda 3A, Cary E1 (Varian) and Cary 17 (Varian Instruments) . Measurements were conducted at 25°C. Thin polymer films were prepared by spin coating of polymer solutions onto quartz slides. Polymer solutions were prepared in chloroform.

NMR. ^{1}H and ^{13}C NMR were obtained using a 400-MHz and 100.6 MHz Bruker AMX400. $CDCl_3$ was used as a solvent for the polymer.

X-ray Diffraction. X-ray experiments were performed with a Siemens D-5000 diffractometer with a Cu Kα source and graphite monochromator. The samples had a thickness of 0.5-1.0 μm and a geometry of 2x2 cm^2. X-ray diffraction measurements were carried out with the help of Dr. J. R. Dahn, Department of Physics, Simon Fraser University.

DSC. Differential scanning calorimetry (DSC) is an important analytical technique for determining the thermal properties of polymers.[96] It is a power-compensation method in which the difference in temperature between the polymer sample and an inert reference derives the differential power necessary to keep the sample temperature identical to that of the reference. This adjustment provides a varying electrical signal equivalent to the varying thermal behavior of the sample. Glass transition (T_g), melting, crystallization, and thermal decomposition temperatures can be determined using DSC.

DSC measurements were performed using a Perkin-Elmer DSC7 calorimeter. The temperature was scanned over 380 °C starting from -30 °C with a heating rate of 5.0 °C/min. The polymer sample was cast by solvent evaporation directly onto the Al sample holder. An empty holder was used as a reference.

II.3 Results and Discussion

III.3.1 Polymer Synthesis

Oxidative Coupling. This method is based on the use of a Lewis acid such as $FeCl_3$ to initiate the polymerization reaction.[90] This reaction is believed to proceed via radical mechanism according to Scheme II.1.[97] This mechanism has been proposed by Österholm et. al. based on quantum chemical calculations, regiochemistry of the polymer, and the fact that HCl was one of the reaction products. This method produces polymers of controlled molecular weight (M_w) up to 250 000, with a relative high degree of stereoregularity for P3ATs.[98] The resulting polymers contain residual iron salts. Control of the concentration of the iron impurities was achieved using repeated reprecipitation.

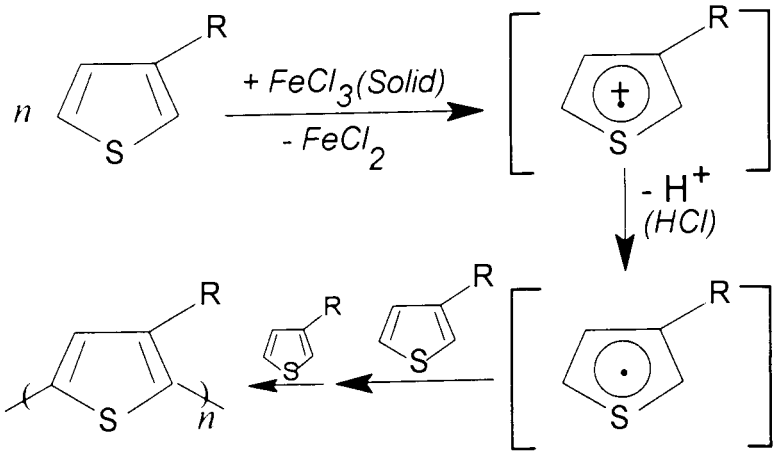

Scheme II.1

Grignard Polycondensation: Metal catalyzed coupling between RMgX and R'X forms the basis of this technique. Thus, 3-hexylthiophene was polymerized using nickel catalyzed Grignard coupling of 2,5-dihalothiophene monomers according to Scheme II.2.[52]

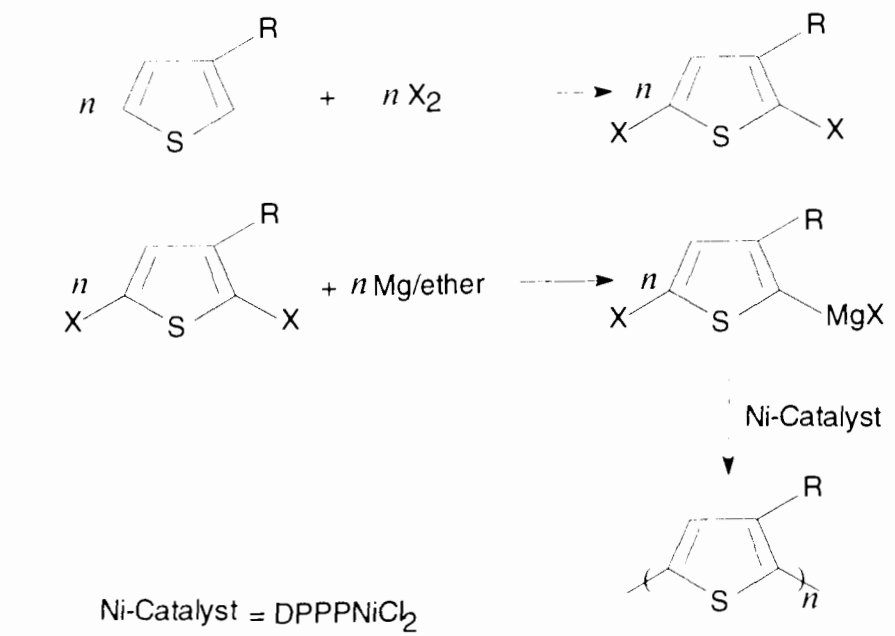

Ni-Catalyst = $DPPPNiCl_2$

(1,3-Bis(diphenylphosphino)propane nickel(II) chloride)

Scheme II.2

Grignard polycondensation is a versatile synthetic method for controlling the stereoregularity of the polymer.[99] It has recently been shown that a careful control of the polymerization conditions could lead to regioregular P3ATs possessing ~98% head-tail dyad configurations.[100] The main disadvantages of the technique are lower molecular weights (M_w ~ 5,000-20,000) and high concentrations of residual impurities (e.g. iodide ~10^{18} *atoms* cm^{-3}).[101]

Electrochemical Polymerization: In this technique, electric current is used to initiate the polymerization process.[53,92] Polymerization can be carried out by either electro-oxidation or electro-reduction based on the chemical nature of the monomer. Thus, thiophene-nickel complexes (2-bromo-5-thienyl)triphenylnickel bromide) were polymerized by electro-reduction[102] while electro-oxidation was used to polymerize uncomplexed thiophenes.[92] The mechanism of electropolymerization of thiophene has been extensively investigation.[103] Electrooxidative polymerization is believed to proceed via electrophilic aromatic substitution reaction of radical cation intermediates with neutral monomers according to Scheme II.3.[104] Electrochemical polymerization is known to produce high purity polymers, but the main disadvantage of this technique is the fact that it can result in polymers with substantial chemical defects (α,α & α,β couplings) and very wide molecular weight distributions.[105] The polymerization yields are limited by the area of the electrode on which the polymer is deposited.

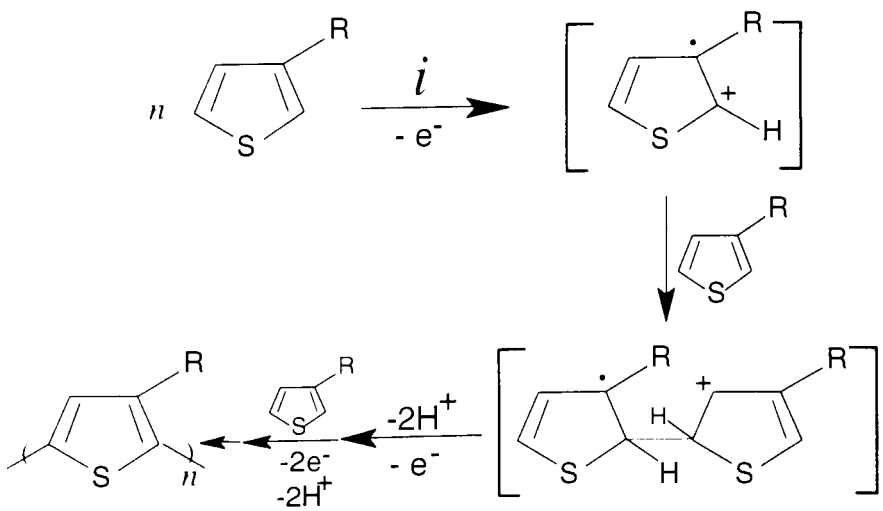

Scheme II.3

II.3.2 Impurity Characterization

P3ATs prepared by oxidative coupling using $FeCl_3$ were used in most studies of this thesis. This synthetic technique leads to incorporation into the polymer of a relatively large amount of iron salts according to [90]

$$n\,(3HT) + 4n\,FeCl_3 \longrightarrow (P3HT)^{2n+} \cdot 2nFeCl_4^- + 2n\,FeCl_2 \qquad (II.4)$$

The polymer is prepared in the oxidized form and requires reduction to the neutral, soluble form for polymer processing. Ammonia solutions were used to carry out the reduction according to reaction II.5.[106]

$$3\,(P3HT)^{2+} + 8\,NH_3 \xrightarrow{H_2O} 3\,P3HT + N_2 + 6\,NH_4^+ \qquad (II.5)$$

As described in the experimental section, purification of the polymer was performed to varying degrees so as to produce three samples of polymer containing different levels of impurity. This ensures that the polymer's structure and molecular weight are identical and variations in properties of the material originate only from the difference in impurity concentration. Atomic absorption spectroscopic analysis indicated the concentrations of residual iron were 0.05 wt% (P3HT-C), 1.3 wt% (P3HT-B), and 3.2 wt% iron (P3HT-A). Elemental analysis determined that the molar ratio of Fe:Cl was 1:1 for each polymer. Mössbauer spectroscopy was performed to provide further information on the nature of the iron impurities. Figure II.2 shows the Mössbauer spectra of P3HT-C. The isomer shift, δ, and the quadrupole splitting, Δ, of the neutral polymer are 0.26 and 0.32 mm s^{-1} respectively; indicative of an iron(III) octahedral complex.[107] P3HT-A and P3HT-B provided similar Mössbauer spectra, confirming the common nature of the iron complex in each of the samples.

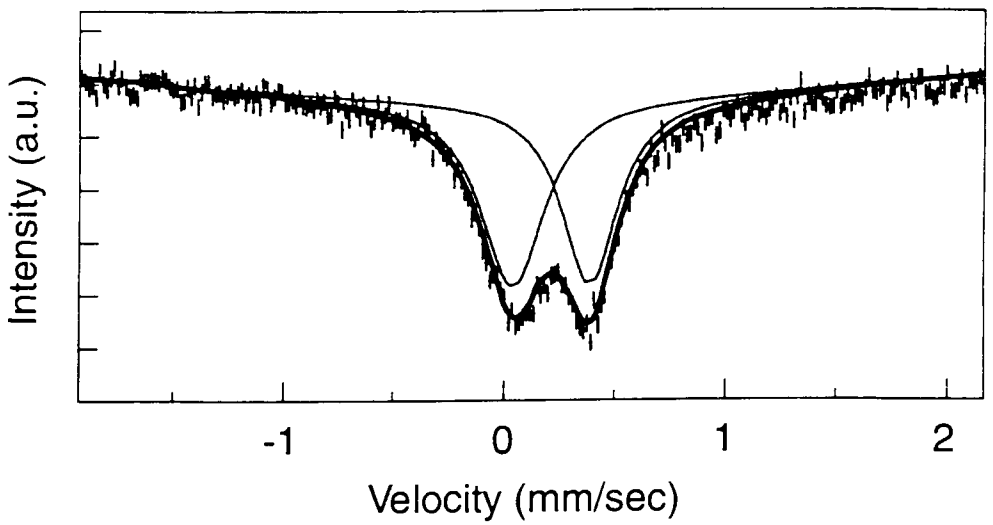

Figure II.2: Mössbauer Spectrum of P3HT-C in the neutral form (Fe content = 0.05 wt%) (298 K)

FTIR studies of neutralized P3HT reveal the absence of characteristic NH_4^+ absorptions (3310,3100 & 1080 cm^{-1}),[108] indicating that NH_4^+ is not a constituent of either the iron complex or the polymer. FTIR of the polymer yields a broad absorption at 3500 cm^{-1} which is assigned to -OH groups. The intensity of the absorption is dependent on the concentration of iron impurities indicating that OH groups are associated with the octahedral iron(III) complex and not the polymer.

Mössbauer spectroscopy indicates an octahedral complex so that additional molecules must be coordinated to Fe^{3+}. These are most likely H_2O molecules. FTIR analyses indeed supports the presence of OH functionality although they cannot be specifically assigned to the Fe(III) complex. The possibility exists that the complex is coordinated to the polymer backbone.[109,110] Two main sites are available for coordination: π (η^5) coordination and S-bonded (η^1).

II.3.3 Characterization of P3ATs

Molecular Weight. It has been shown by Holdcroft that M_n of P3HT determined by GPC using polystyrene standards is ~2 times greater than that determined by ebulliometry, which is known to give absolute number average molecular weight independent of the hydrodynamic volume.[95] This was attributed to the different hydrodynamic volumes acquired by the two polymers in THF (the standard solvent for GPC), assuming same molecular weights.[95,111,112] Due to the extended π-conjugation along the backbone, the polymer chains are stiff and thus acquire larger hydrodynamic volumes.

Figure II.3 represents the GPC trace of P3HT prepared by oxidative coupling using $FeCl_3$. The molecular weight of the material can be controlled to by the polymerization period. Thus, increasing the polymerization time from 3 h (trace II) to 24 h (trace I) leads to a ~5 fold increase in M_n of the polymer. M_n values of P3HT prepared by oxidative coupling, Grignard coupling, and electropolymerization methods were reported in Table II.1.

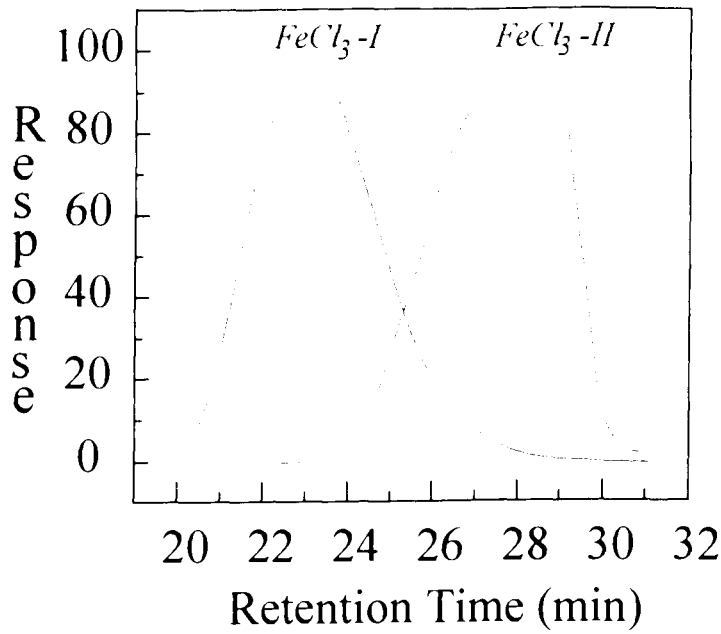

Figure II.3: GPC trace of P3HT prepared using $FeCl_3$

Table II.1: GPC data of P3HT

Polymerization Method	M_n#	MWD*
$FeCl_3$-I	41 000	3.1
$FeCl_3$-II	8 500	3.2
Grignard	10 000	4.6
Electrochem.	9 000	7.1

calculated according to equation II.3

*Molecular weight distribution (MWD = M_w/M_n)

FTIR Spectroscopy. Figure II.4 shows the IR spectra of thin P3HT films in the neutral form. Assignment of the various vibrational stretchings of P3HT were made according to the literature IR data of thiophene derivatives and thiophene oligomers.[113-118] Data are summarized in Table II.2.

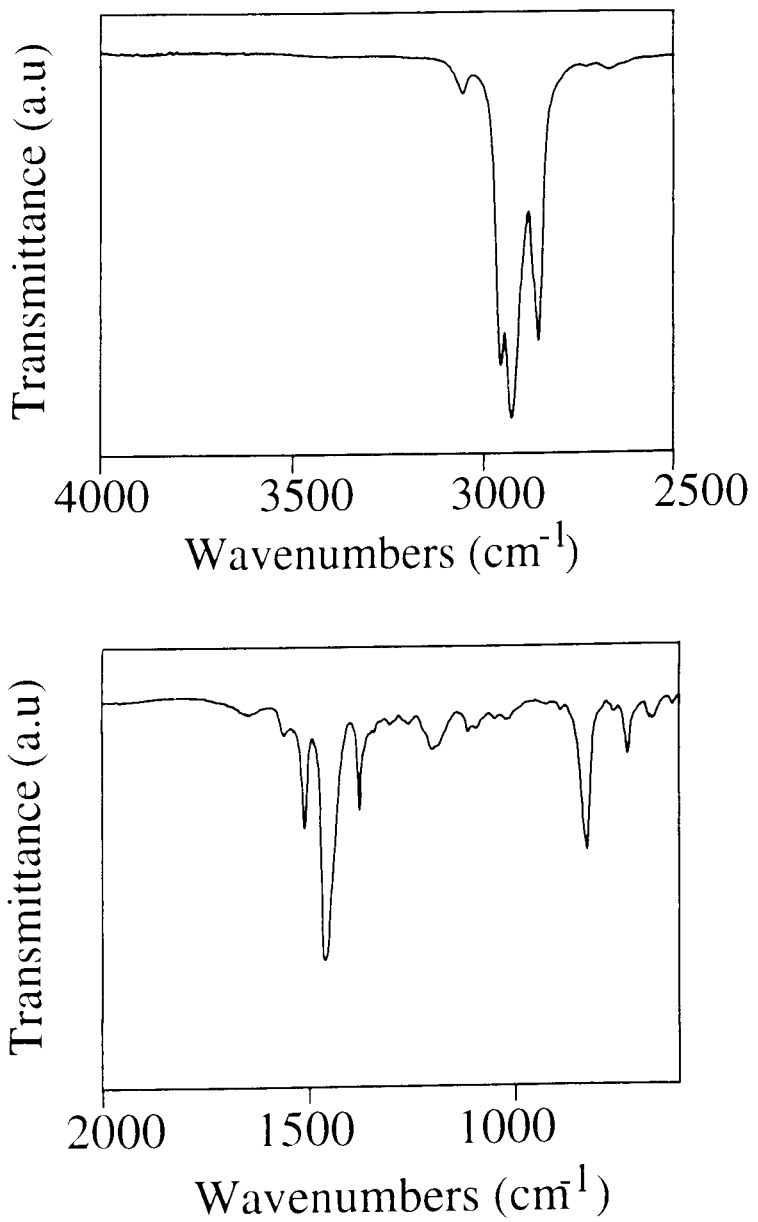

Figure II.4: FTIR spectra of P3HT-C (Fe content = 0.05 wt%)

Table II.2: FTIR data of P3HT [a]

cm^{-1}	assignment	cm^{-1}	assignment
3055	C-H str.(aromatic)	1377	methyl def.
2955	CH_3 asym. str.	1260	C-C inter-ring bond str.
2926	CH_2 in-phase vib.	1190-	wagging and twisting of
2870	CH_3 sym. str.	1155-	methylene groups.
2856	CH_2 out-of-phase vib.	1090	C-H in-plane bending of
1655	overtone of thiophene		thiophene ring.
	ring.	823	C-H out-of-plane
1560-	$C_2=C_3$&$C_4=C_5$ asym.		def. of thiophene ring.
1512	and sym. str. modes of	725	rocking mode of
1460-	thiophene ring.		methylene groups.

a) Films cast on KBr disks.

Nuclear Magnetic Resonance Spectroscopy. ^1H and ^{13}C NMR of P3HT-C (0.05 wt% iron) in solution are shown in Figures II.5. Analysis of the ^1H and ^{13}C chemical shifts were accomplished according to literature data.[119-121] Assignments for polymers prepared by $FeCl_3$ are summarized in Table II.3.

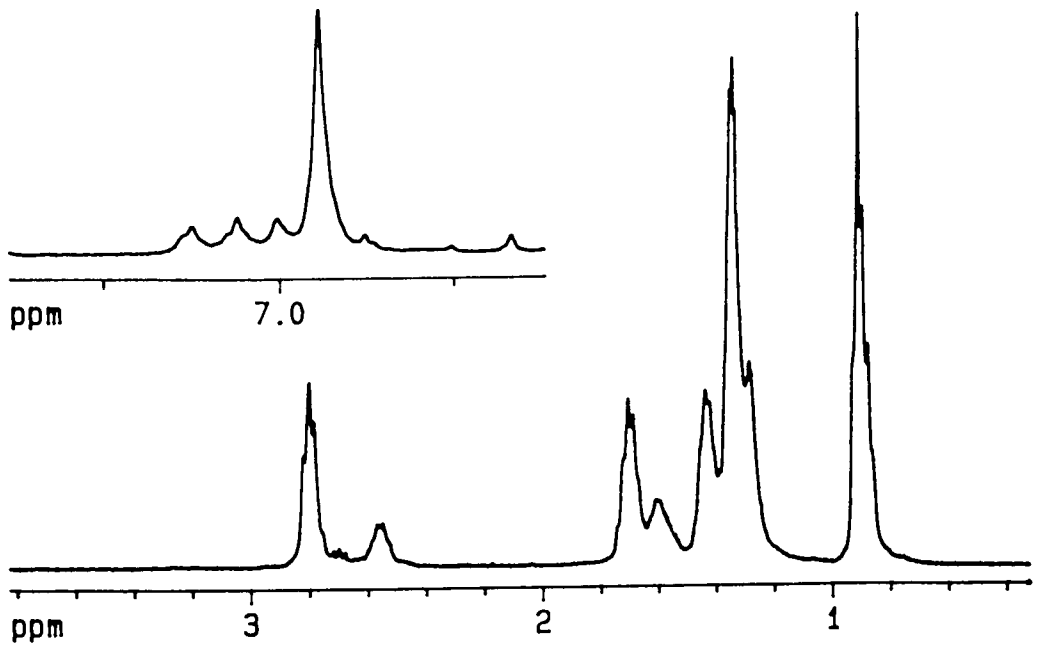

(A)

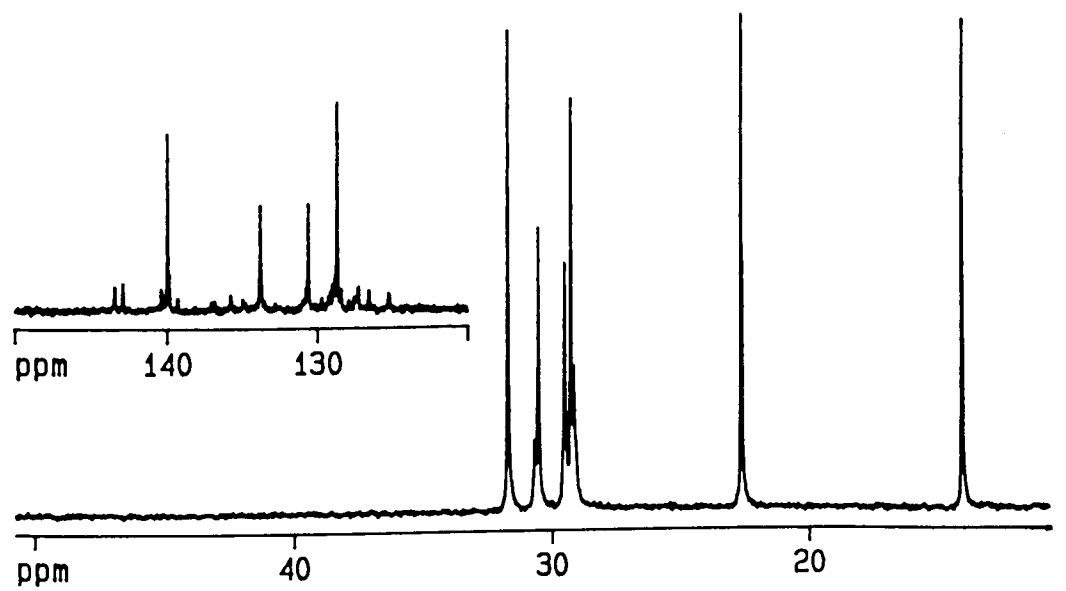

(B)

Figure II.5: ^{1}H and ^{13}C NMR spectra of P3HT-C (Fe content = 0.05 wt%)

Table II.3: NMR data of P3HT

^{1}H NMR		^{13}C NMR*	
Chemical Shift (ppm)		**Chemical Shift (ppm)**	
0.91	methyl protons.	14.06	methyl carbon.
1.2-1.8	ω,δ,γ and β methylene-	22.63	ω methylene carbon.
	protons.	29.24	γ and δ methylene-
2.56-2.79	α methylene protons.	29.48	carbons.
6.98 (major peak)	aromatic-	30.50	β-methylene carbon.
7.00,7.03,7.05	protons.	31.70	α-methylene carbon.
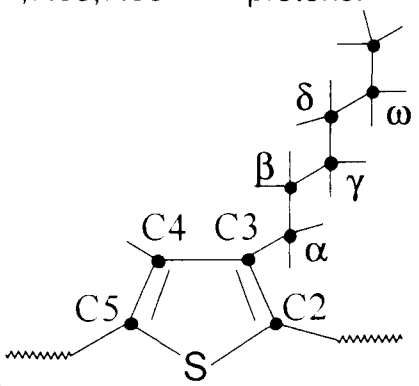		128.65	C4
		130.58	C2
		133.79	C5
		139.93	C3

* ^{13}C Chemical shifts of major resonances.

NMR is uniquely powerful for providing information concerning configuration and conformation of polymers.[122] It has been extensively used for studying regiochemistry of P3ATs.[119] The main elements of regiochemistry in P3ATs are thiophene dyad and triad configurations which are shown in Figure II.6. Thiophene triads are used to describe the configuration of the polymer based on NMR characteristics of β-proton (4-position) of the thiophene ring. Dyad configurations, on the other hand, are discussed in terms of the chemical shifts of the α-CH_2 of the alkyl side chains. Resonances in the spectral region 2-

3 ppm are due to the α-CH_2 and are assigned to HH (2.56 ppm) and HT (2.79 ppm) configurations, respectively.[99,119] The ratio of HT to HH configurations for P3ATs can be determined from the integrals of these two resonances. A value of 80:20 was determined for P3HT prepared using oxidative coupling. The resonances in the aromatic region 6.98, 7.00, 7.02, and 7.05 ppm are due to β-proton and are assigned to HT-HT, TT-HT, HT-HH, and TT-HH triad configurations.[99] These NMR analyses are consistent with NMR characterization of thiophene oligomers of tailored regioregularity.[123]

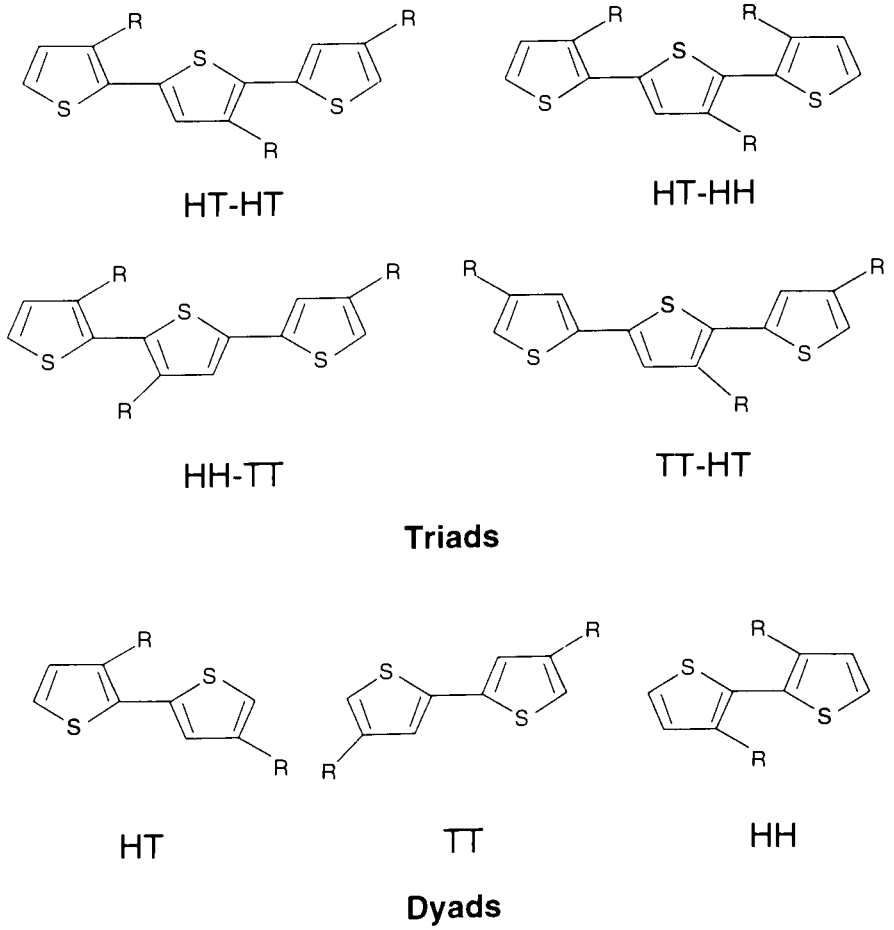

Figure II.6: Triad and dyad configurations of 3-alkylthiophenes

The ratios of HT-HH configurations of polymers prepared by $FeCl_3$, Grignard and electrochemical methods are reported in Table II.4.

Table II.4: Comparison of dyad ratios and λ_{max} (nm) of P3HT prepared by different methods.

Polymer	HT-HH ratio	λ_{max} (nm)	
		solid films	solutions
$FeCl_3$	80:20	500	440
Grignard	65:35	455	415
Electrochem.	75:25	485	430

Electronic Absorption Spectroscopy. The wavelength of maximum absorption (λ_{max}) of P3HT in solid films and in solutions prepared by $FeCl_3$, Grignard, and electrochemical methods are reported in Table II.4. The electronic absorption spectra of P3HT in thin films and in solutions are shown in Figure II.7.

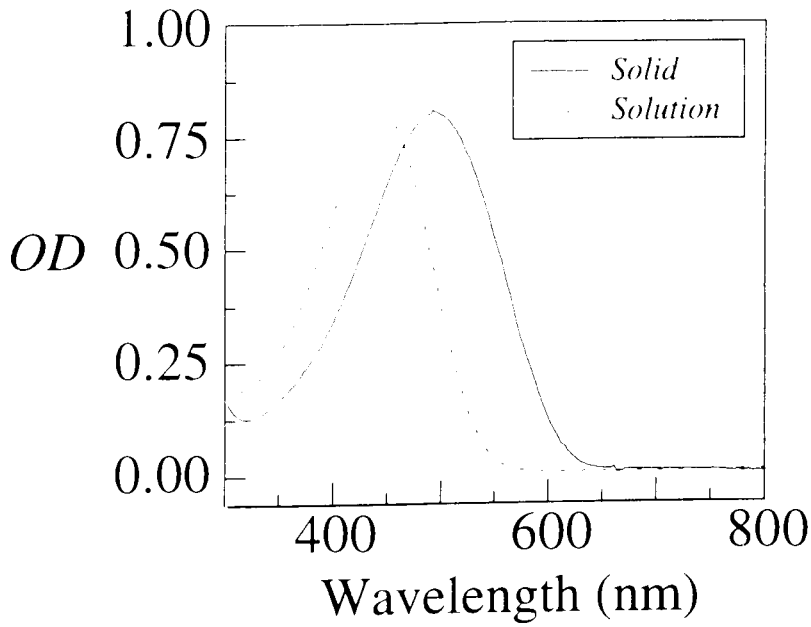

Figure II.7: UV-vis Spectra of P3HT prepared using $FeCl_3$

The neutral polymer films have a strong absorption band at 500 nm characteristic of the π–π^* interband transition.[124,125] This absorption band is blue shifted in solution. This blue shift has been attributed to changes in the conformation of the polymer chains.[124,125] The conformation of the polymer in solution is that of a coil with short effective conjugation length while the polymer in solid film has a rod-like structure with a higher degree of electronic delocalization. λ_{max} of the polymer in solid films and in solutions undergoes a red shift with increasing of the content of HT dyad configurations. The HT configurations enhance the coplanarity of the polymer backbone yielding P3ATs with longer effective conjugation length (coplanar polymer segment).

Optical spectroscopy has also been used in determination of optical band gap energy of semiconductors.[126] The band edge of optical absorption (onset of electronic transition) gives a reasonable estimate of the band gap energy (E_g) of π-conjugated polymers. The optical band gap energy of P3ATs is ~2.1 eV.

X-ray Diffraction. X-ray techniques are important in characterization of polymer morphology and molecular dimensions.[127] Figure II.8 shows the diffraction profile of a thin film of P3HT-C (~1 μm). The profile is characterized by a sharp reflection at a scattering angle of 5.4°, 10.8° and ~16.4° in addition to a weak, broad reflection at 22°. These reflections are indicative of a short range ordering in the material. P3HT, in the neutral form, is thus semicrystalline.

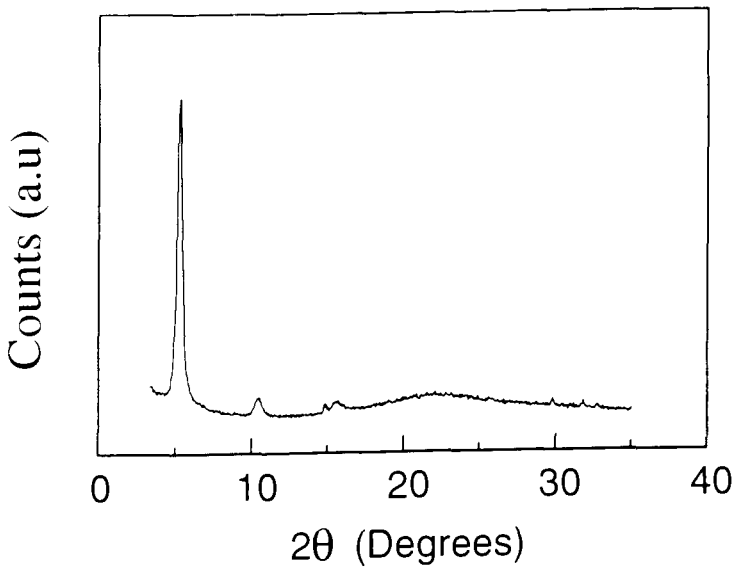

Figure II.8: X-ray diffraction profile of P3HT-C (Fe content = 0.05 wt%)

It has been shown by Heeger and Carlsen that diffraction profiles of P3ATs are typical of comb-shaped polymers.[128,129] These are indicative of a layer structure in which sheets of polymer are assembled into three dimensional structures by stacking the polymer backbone chains, one on top of the other, forming a lamellar structure with the alkyl side-chains acting as spacers between the stacks as shown in Figure II.9.

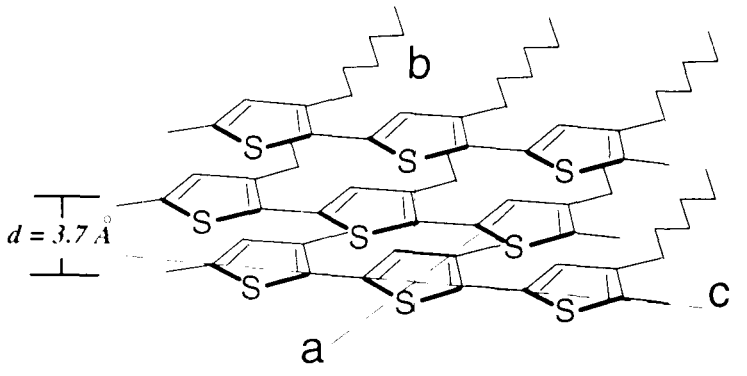

Figure II.9: Schematic diagram of the layer-structure of P3ATs. (d is the interchain distance)[129]

Thermal Analysis. Figure II.10 shows the DSC thermogram of P3HT-C under N_2. It is characterized by two endothermic transitions at 55 °C (temperature at mid-way of the first transition), and 170 °C (peak temperature). These transitions are assigned to T_g and T_m, respectively, which are consistent with dynamic mechanical analysis (DMA).[130,131] Crystallization of the alkyl side-chain is possible. Thus, P3ATs with long alkyl side-chains, e.g. poly(3-tetradecylthiophene) (C14), show exothermic, liquid crystalline transition (T_c) at 75 °C.[131] No such transitions were observed in the case of P3HT.

In addition to the non destructive thermal transitions, P3ATs undergo thermal decomposition in air at about 250 °C. In inert atmosphere, the polymer is thermally stable up to 350 °C. The mechanism of the thermal degradation

process is, however, unknown. Insights into the mechanism of this process are discussed in Chapter III.

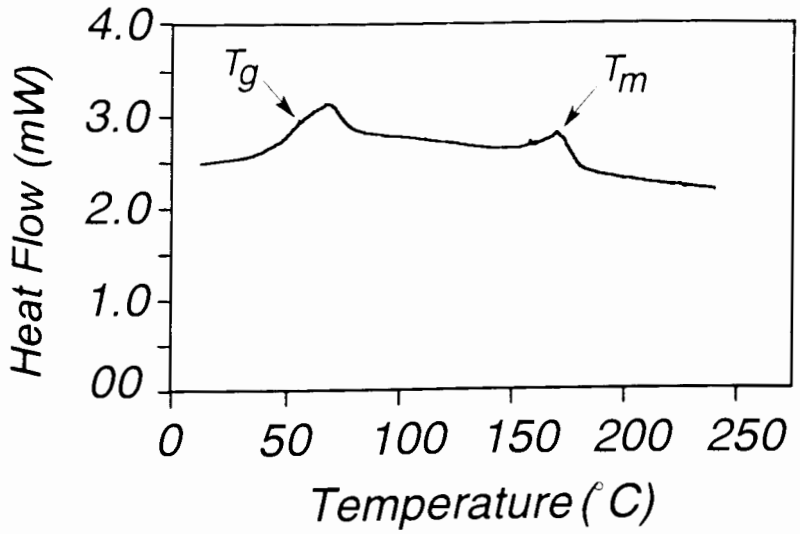

Figure II.10: DSC thermogram of P3HT-C (Fe content = 0.05 wt%)

II.4 Conclusion

The poly(3-alkylthiophenes) class of polymers is a versatile macromolecular material. Solution processability made structural characterization of the materials amenable using solid-state and solution techniques. The various preparation techniques provide a tool for controlling the length of the macromolecules (MW) and the nature of impurities in the material. They also enable a complete control of crystallinity and conformation of the polymer. Polymers prepared by oxidative coupling using $FeCl_3$ contain residual iron salts. These salts take the form of octahedral iron(III) complexes as shown by Mössbauer measurements. Repeated reprecipitation proved useful in controlling concentration of the residual iron impurities.

Chapter III: MICROLITHOGRAPHY AND PHOTOCHEMISTRY OF π-CONJUGATED POLY(3-ALKYLTHIOPHENES)

III.1 Introduction

π-Conjugated polymers might play an important role in macromolecular electronics. One of the fundamental challenges, however, is processing of the material in a controlled fashion. In general, three techniques have been used for designing three-dimensional macromolecular architectures, namely; lithography,[132] vapor deposition,[133] and self-assembly.[134] The revolution in conventional semiconductor microelectronics has been made possible, in part, by microlithigraphy, a process in which light, for example, is used to spatially direct the simultaneous formation of many electrical components. It is believed that the design and development of conjugated polymers for advanced microlithography are critical to the success of constructing macromolecular electronics.

Processing of poly(3-alkylthiophenes) was investigated using conventional photolithography and laser, direct-write microlithography. A detailed photochemical study was undertaken in order to understand the mechanisms of the photochemical reactions involved. This study was achieved by investigating the photochemistry of the polymer in the solid-state and in solution. The potential for constructing P3AT-based macromolecular wires was demonstrated. A brief discussion of the basic elements of microlithography and photochemistry of polymers is presented in the following section.

III.2 Microlithography

The word lithography is defined as " the art or process of putting designs on stone with a greasy material and producing a printed impression therefrom".[135] Today the terms *Micro-* and *Nano*-lithography are used to describe the lithographic process for fabricating micro- and nanometer-sized electronic devices.[132] Microlithography of polymers refers to a process which deposits a thin polymer film, using some radiation source, into a patterned form with a resolution, i.e. minimum linewidth, in the micro- and submicrometer domains. The resulting pattern is called a resist. This generic name "resist" was evolved as a description of the ability of the resist material to resist etchants. In traditional semiconductor devices, the resist does not play an *active role* in the electronic operation of the circuit. It is used only for pattern transfer into the underlying substrate and is usually removed after use. Conjugated polymer resists, however, are the polymeric semiconductor or conductor which might be an *integral component* of the device.

Resists are classified into four types according to the nature of the radiation source used in the process (Table III.1).[132,136] The corresponding lithographic processes are also listed in Table III.1.

Table III.1: Types of resist

Radiation Source	Resist Class	Lithographic Method
1. UV-vis	Photoresist	Photolithography
2. X-ray	X-ray resist	X-ray lithography
3. Electron beam	E-beam resist	E-beam lithography
4. Ion beam	I-beam resist	I-beam lithography

III.2.1 Photolithography[132,135,136]

The basic processes of photolithography are shown in Scheme III.1.

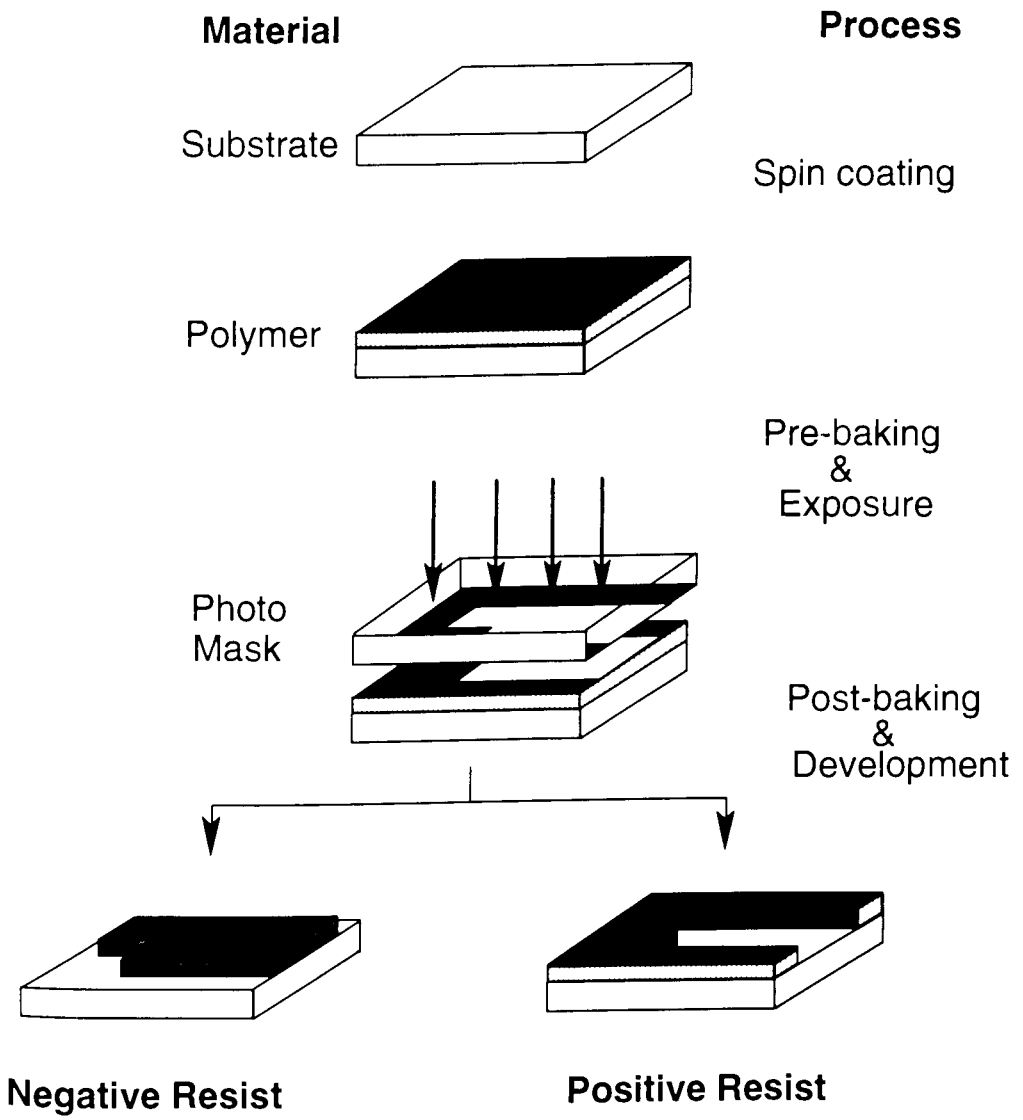

Scheme III.1

When the polymer resist is exposed certain chemical reactions take place in the exposed regions, resulting in a change in its solubility. Utilizing the solubility difference between the exposed and unexposed area, a pattern image can be developed using a developer. Three main photochemical processes govern the solubility of the polymer photoresists, these are crosslinking, chain scission, and chemical modification. For negative resists, crosslinking occurs predominantly in the exposed area resulting in decreased solubility. Chain scission results in an increase in the solubility of the exposed regions and form the basis for depositing positive-tone resists.[132,136] Chemical modification can either increase or decrease the solubility of photoresists depending on chemical structure of the products.

The basic components of a photolithographic equipment are a UV-vis light source, interference filters, an alignment system, a photomask, a substrate, and a photoresist material. The photomask usually consists of circuit patterns defined in a thin film (~1000 Å) of chromium deposited on a glass or quartz substrate. It is usually fabricated by E-beam lithography.

The exposure techniques used in photolithography are contact, proximity, and projection printings.[132] In contact printing, the photoresist and the photomask are in intimate contact and there is no gap between them. In proximity exposure, a gap (≥10 μm) is maintained between the resist and the mask. In projection printing, the image on the mask is projected onto the wafer with either a reflective or refractive optical system. Photomasks are usually expensive and impractical for designing composite circuits.

Laser, direct-write microlithography is a new technology developed, in part, at Simon Fraser University.[137] This system uses lasers as exposure sources and computer-controlled writing systems. There are a great number of advantages for this new laser technology. The most important advantage is the

fact that the photomask is replaced by computer-controlled mask information i.e. the mask information is controlled by software which can be programmed to provide any circuit pattern. The basic building components of the laser system are shown schematically in Figure III.1.

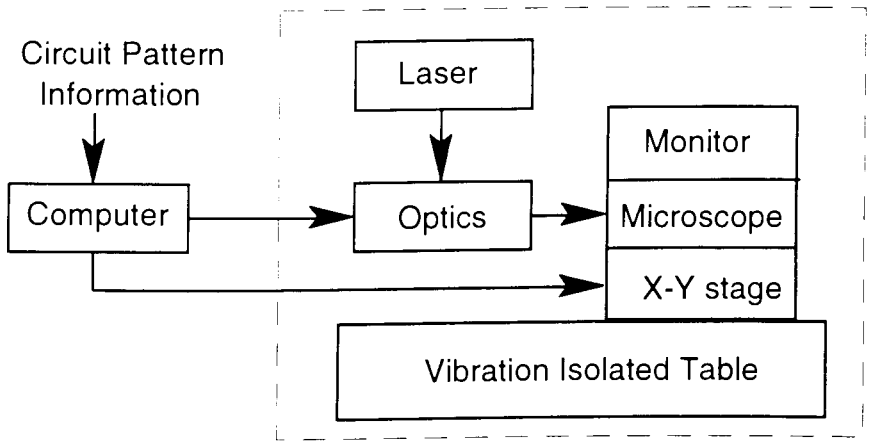

Figure III.1: Block-Diagram of Laser, direct-write System

III.2.2 Resist Performance

The performance of a resist depends on the intrinsic properties of the materials and on the processing parameters.[132,136] The important intrinsic properties of the polymer resists are chemical structure, molecular weight, molecular weight distribution (MWD), glass transition temperature (T_g), and adhesion properties. The processing parameters include resist film thickness, pre-bake and post-bake conditions, developer and development conditions, exposure dose, and the nature of the substrate onto which the resist film is deposited. The side of exposure is also an important factor for resist evaluation.

The photo-reactivity of the resist materials is expressed in terms of three main parameters, called lithographic parameters. These are interface gel dose (D_g^i or r_{gel}), sensitivity, and contrast (γ_n). For negative photoresists, D_g^i is

defined as the minimum radiation dose required to induce a reaction such that an insoluble gel (residue) of polymer remains after development. Sensitivity is signified by the exposure dose required to yield a particular response in the resist polymer after development. It is most commonly defined as the dose required to leave 50% of the original thickness and is represented by $D_g^{0.5}$. D_g^i and $D_g^{0.5}$, are illustrated in Figure III.2.

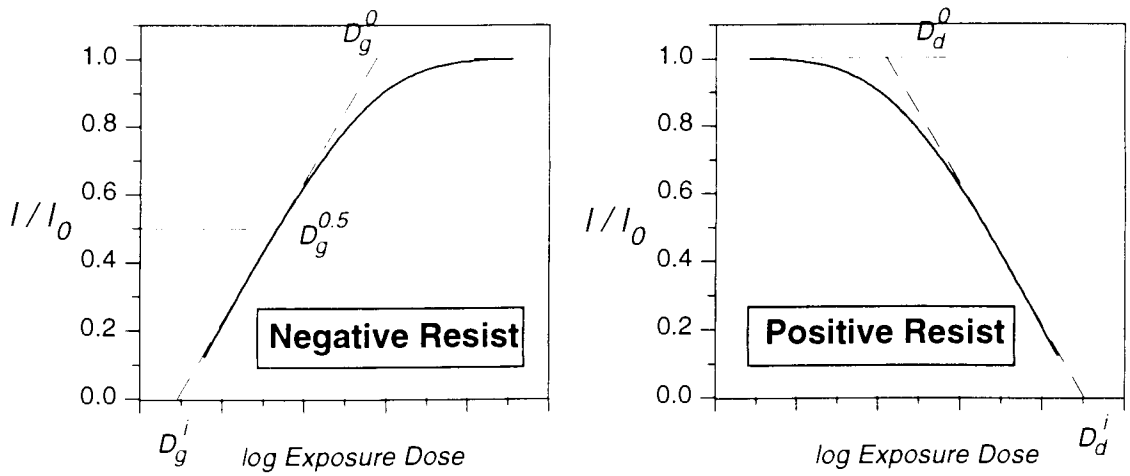

Figure III.2: Sensitivity curves of negative and positive resists

Plots shown in Figure III.2 are usually obtained by measuring the film thickness of the resist remaining after a series of exposures followed by a common development process. The normalized remaining film thickness (l/l_0) is plotted against the exposure dose. l_0 and l represent the original and remaining film thicknesses of the photoresist, respectively. The contrast of the photoresist , γ_n, is defined as the rate of insolubilization (or the rate of crosslinking) at a constant input energy. It is given by

$$\gamma_n = \frac{1}{\log D_g^0 - \log D_g^i} = \left[\log \frac{D_g^0}{D_g^i}\right]^{-1} \qquad \text{(III.1)}$$

where D_g^0 is the dose required to produce 100% gel formation of the original film. It is determined by extrapolation of the linear portion of the sensitivity plot to a dose value equivalent to 1.0 normalized film thickness.

Back-side exposure is required for resist evaluation. This is because when exposure is carried out from the back side, the lowest exposure dose that cause crosslinking will leave the insolubilized film attached to the substrate and meaningful results are thus obtained (Figure III.3)[136]

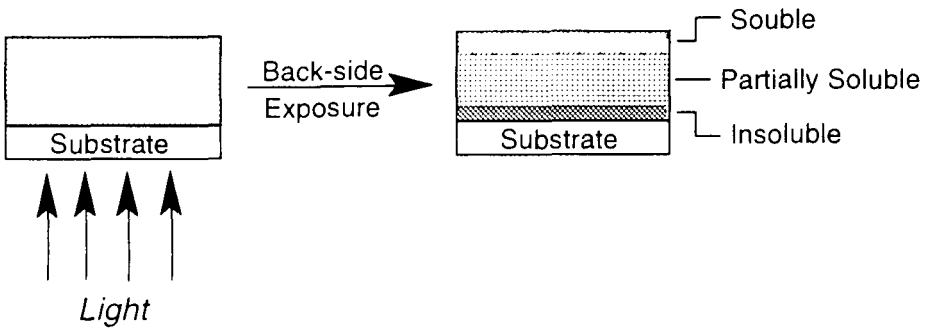

Figure III.3: Back-side exposure of polymer resist

In practice, however, *top-side* exposure is usually used. On opaque substrates, the resist should develop-off the substrate unless severely overexposed. Reflective substrates are useful in top-side exposure because the reflected radiation initiates crosslinking and insolubilization at the polymer/substrate and thus reduces the gel dose. A comparison of the different stages of insolubilization of negative resists using top-side and back-side exposures on various substrates is shown in Figure III.4.

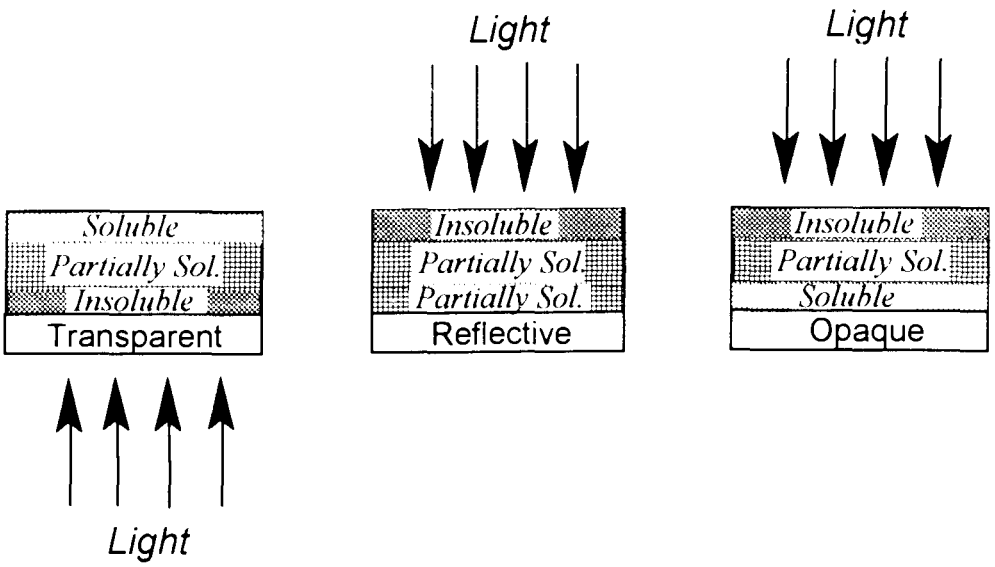

Figure III.4: Stages of insolubilization of negative resists.

Resolution (linewidth) of a lithographic resist is one of the critical processing parameters. It is a property that is difficult to quantify since many variables affect the size of the minimum features that can be resolved. It has been found that resolution is intimately related to the contrast of the resist. The higher the contrast, the higher the resolution. This is because resist materials with high contrast have a potential for producing steep sidewall images and therefore high resolution. Resolution is also related to wavelength of light. The potential for producing higher resolution (smaller features) increases with decrease of wavelength. As a consequence, developments of deep-UV and 193 nm laser lithography are currently in progress. It has the potential for producing submicron resolution and is the resist technology of the future.[138]

The basic aspects of positive photoresists are similar to those of negative resists. The main difference is enhanced dissolution in case of positive tone resists in contrast to insolubilization in negative resist lithography (Scheme III.1 and Figure III.2). D_d^i and D_d^0 represents the exposure dose of incipient and complete dissolution of the resist, respectively.

III.2.3 Quantum Yield-Gel Dose Relationships for Negative Resists[139-141]

For negative photoresists which function via photo-crosslinking reactions, quantum yield of cross-linking (gelation) is defined as[139-141]

$$\Phi_x = \frac{\#\ of\ crosslinks}{\#\ of\ quanta\ absorbed} \qquad \text{(III.2)}$$

If we define q as the crosslinking density which is the proportion of the main chain units crosslinked by a radiation dose r, then number of crosslinked units is given by

$$\#\ of\ crosslinked\ units = q\,N \qquad \text{(III.3)}$$

N is number of molecules per unit area and is given by

$$N = \frac{l\,\rho}{M_o} N_A \qquad \text{(III.4)}$$

where l and ρ are the thickness and density of the polymer, M_O is the molecular weight of the monomer units, and N_A is Avogadro's number. The number of crosslinks is given by

$$\#\ of\ crosslinks = \frac{N}{2} q = \frac{l\,\rho}{2\,M_o} q\,N_A \qquad \text{(III.5)}$$

since each crosslink involves the linking together of two units.

The number of photons absorbed is given by

$$\#\ of\ quanta\ absorbed = \varphi\ r\,N_A \qquad \text{(III.6)}$$

where φ is the fraction of incident radiation density r (Einstein.cm^{-2}) absorbed by the material (φ = 1-10^{-A}, where A is the optical density of the polymer film). Substituting equations III.5 and III.6 into III.2 yields quantum yield of crosslinking:

$$\Phi_x = \frac{l\,\rho\,q}{2\,M_o \varphi\ r} \qquad \text{(III.7)}$$

The gel dose (D_g^l or r_{gel}), as defined above, is the minimum exposure required for incipient gel formation. This corresponds to a crosslinking density, on average, of one crosslink per chain, which can be expressed quantitatively by the Stockmeyer's rule as[142]

$$q = \frac{M_0}{M_w} \qquad \text{(III.8)}$$

If we assume that crosslinks are formed uniformly throughout the depth of the polymer film, the gel dose, r_{gel}, is obtained by combining equations III.7 and III.8

$$r_{gel} \quad \frac{l\rho}{2 M_w \varphi \Phi_x} \qquad \text{(III.9)}$$

For optically thin polymer films, the fraction of light absorbed (φ) is adequately approximated by

$$\varphi = 2.303 A = 2.303 \varepsilon ml \qquad \text{(III.10)}$$

where ε is the extinction coefficient of the chromophore, and m is its molarity in the solid film. Equation III.9 now takes the form

$$r_{gel} \quad \frac{\rho}{2x2.303 M_w \varepsilon \ m \Phi_x} \qquad \text{(III.11)}$$

This is the fundamental equation of photolithography of polymers. It relates the quantum yield of crosslinking to experimentally measurable parameter namely, gel dose. It shows that r_{gel} depends on both the molecular weight and density of the polymer. r_{gel} is, however, independent of the polymer film thickness assuming optically thin films.

The efficiency of the overall reaction is defined as[140]

$$\Phi = \frac{\#of\ moles\ of\ product}{\#\ of\ moles\ of\ photon\ absorbed} \qquad \text{(III.12)}$$

It can be derived from the dependence of the rate of chemical conversion ($dx\ dt$) on exposure dose via the equation

$$\Phi = \frac{n_0}{I_0 \varphi} \frac{dx}{dt} \qquad \text{(III.13)}$$

where n_0 is the number of moles of chromophores in 1 cm^3 of the film, and I_0 is the radiation flux (Einstein $cm^{-2}\ s^{-1}$). Photochemical crosslinking involves *inter-* and *intra*molecular mechanisms. Insolubilization originates from intermolecular crosslinking mechanism which results in an increase in molecular weight of the polymer and leads to the formation of a three-dimensional network.

Intramolecular crosslinking does not affect the molecular weight and thus has no contribution in gel formation. Moreover, crosslinking is usually accompanied by main-chain scission. As a result, the efficiency of the overall reaction is usually greater than the quantum yield of gelation. These three reaction mechanisms lead to complications in the dynamics of the photochemical reaction and thus complex quantum yield expressions. The dynamics and quantum efficiencies of simultaneous crosslinking and chain scission reactions are discussed below.

III.2.4 Sol-Gel Properties[139,141,143]

In the above discussion it was assumed that crosslinking is the only process occurring during irradiation of thin solid polymer films. In fact, crosslinking of most polymers is accompanied, to some extent, by scission of the main chain (Figure III.5). The relative amounts of chain scission to crosslinking (sol-gel fractions) following irradiation determine the physical properties of the polymer and whether or not it is useful as a resist material.

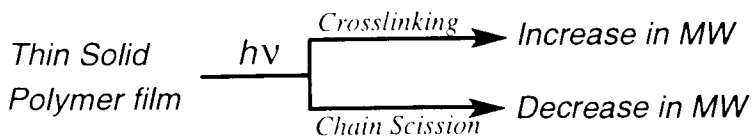

Figure III.5: Changes in molecular weight of polymers following irradiation

Most polymers, therefore, requires two parameters to describe their radiation behavior: a proportionality constant to relate the number of crosslinks to the radiation dose; and a chain scission parameter, measuring the number of main chain fractures produced per crosslinked unit formed.

Charlesby and Pinner have developed a theory for the simultaneous crosslinking and scission of polymers by radiation.[143] It is based on estimation

of changes in molecular weight (MW) and solubility of the polymer with irradiation. Crosslinking causes an increase in the average MW, while scission of the main chain results in a reduction in average MW. The solubility properties of the polymer will thus alter depending on the relative rates of the two processes. The theory also assumes that both crosslinking and scission occur at random and that both being proportional to the radiation dose.

For a polymer of an initially random molecular weight distribution, the change of the weight-average molecular weight, M_w, with irradiation dose, r, follows the expression

$$\frac{1}{M_w} = \frac{1}{M_{w0}} + \left[\frac{\Phi_s}{2} - 2\Phi_x\right] r \qquad \text{(III. 14)}$$

where Φ_s and Φ_x are the quantum yields of chain scission and crosslinking, respectively. This equation implies that gel formation will occur only if $4\Phi_x > \Phi_s$. If $\Phi_s = 4\Phi_x$, chain scission will compensate for crosslinking and the molecular weight (M_w) of the polymer will be independent of irradiation dose.

Solubility of the polymer (sol fraction, S) can be determined as a function of irradiation dose by solvent extraction. The solubility equation is given by [139,143]

$$S + S^{1/2} = \frac{p_o}{q_o} + \frac{1}{q_o \overline{P}_n} \frac{1}{r} \qquad \text{(III.15)}$$

p_o and q_o represent the fracture and crosslinking densities per unit radiation dose, and $\overline{P}_n$ is the number average degree of polymerization ($\overline{P}_n = M_n/M_o$). The term p_o/q_o gives the relative amounts of scission to crosslinking as a function of irradiation. There are two limiting values for p_o/q_o at infinite r. These are

1. $p_o/q_o \geq 2$

This yields value for S of 1 at infinite radiation dose which implies that the polymer will remain completely soluble, independent of the radiation dose.

2. $p_o/q_o < 2$

This implies that crosslinking is the dominant photochemical reaction. The dose of incipient gelation, r_{gel}, under this condition, will be governed by the relative amounts of p_o to q_o.

Changes of sol fraction of a polymer with irradiation dose are shown in Figure III.6.

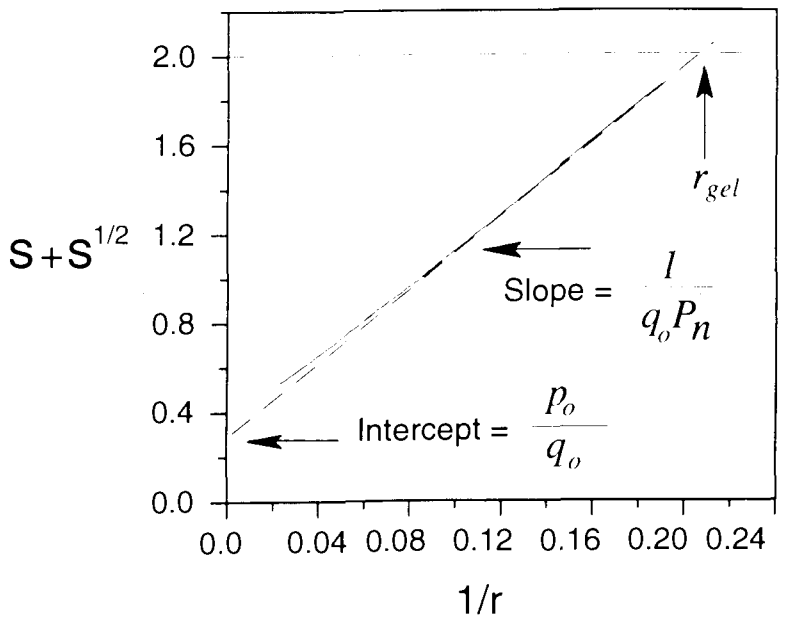

Figure III.6: Solubility curve of polymers following irradiation

The photochemical reactions occurring following light absorption thus determine the tone of resulting resist. The mechanisms of such reactions and factors controlling them is the subject of the following discussion.

III.3 Photochemistry of Polymers

The absorption of light by polymers produces noticeable physical and chemical changes. Photo-oxidation and photo-degradation are common photochemical reactions of conventional, saturated polymers. π-Conjugated

polymers differ from their saturated relatives (σ-bonded polymers) primarily in their possession of a main-chain with delocalized electronic structure. Excitation in this case no longer corresponds to antibonding σ^* levels which may give rise to bond cleavage but rather to excitation of the π-conjugated sequence (π^* levels). The validity of this assertion was not known prior to this study since virtually *nothing* was known about the photochemistry of polythiophenes, in particular, or π-conjugated polymers, in general.

The effect of light on polymer semiconductors also plays an important role in a number of specialized technical innovations. For example, photoconduction and generation of charge carriers by light are the principles behind designing optoelectronic devices.[68] Photoluminescence is being investigated with the goal of understanding the electroluminescent properties of conjugated polymers.[62,67] Photovoltaic effects are useful for the development of polymer solar cells as inexpensive alternatives to conventional solar cells.[80] The study of the photochemistry of π-conjugated polymers is thus necessary in order to understand the effect of light on these materials.

III.3.1 Light-Polymer Interactions

The Grotthus-Draper law states that "no photochemical reaction can occur unless a photon of light is absorbed".[144] The light absorption requires the presence of light absorbing species, i.e. chromophores. For polymers, there are two types of chromophores; intrinsic chromophores, such as functional groups; and extrinsic chromophores, such as impurities.

The principal laws governing the absorption of light by materials are Lambert's and Beer's laws.[145] The first of these states that "the proportion of light absorbed by a transparent medium is independent of the intensity of the incident light and that each successive layer of the medium absorbs an equal

fraction of the light passing through it". Mathematically this leads to the expression

$$log_{10}\left[\frac{I_0}{I}\right] = K\,l \qquad \text{(III.16)}$$

where I_0 and I are the intensity of the incident and transmitted light, respectively, l is thickness of the absorbing material (cm), and K is the Bunsen and Roscoe extinction coefficient (cm^{-1}). K is arbitrarily called the penetration depth of light and is defined as the distance over which the incident light attenuates e times.[146] This law, however, contains no *concentration* factor. Beer's law has dealt with the *concentration* variable. It states that "the amount of light absorbed is proportional to the number of molecules of absorbing substance through which the light passes". It is defined mathematically as

$$log_{10}\left[\frac{I_0}{I}\right] = \varepsilon\, m\, l \qquad \text{(III.17)}$$

where ε is the molar extinction coefficient ($L\ mol^{-1}cm^{-1}$), and m is the concentration of chromophores ($mol\ L^{-1}$). For convenience the term $log_{10}\,(I_0 / I)$ is usually replaced by absorbance, A.

Absorption of a photon promotes an electron from the ground state (P), which is singlet for nearly all organic compounds, to a higher energy singlet state ($^1P^*$). The lifetime of this state is in the order of $\sim 10^{-12}$-10^{-6} s. It undergoes various deactivation processes depending on the nature of the chromophore. The key photochemical and photophysical processes of polymers, in general, are shown in Figure III.7.[147,150] Radiative transition occurring between states of the same multiplicity (spin) is defined as fluorescence (Fl). This emission has a short lifetime and usually takes place from the excited singlet state ($^1P^*$). Phosphorescence (Ph) is a radiative emission from a transition between states of different multiplicity, e.g. $^3P^* \rightarrow P$ transition. Non-radiative transitions compete with both Fl and Ph. These are internal conversion (IC) and inter-system

crossing (*ISC*). *IC* is a rapid process (lifetime is ~10^{-12}-10^{-6} s) which occurs via vibronic coupling from an upper excited state to the lowest excited or ground state. *ISC* is a spin-forbidden radiationless transition (10^{-12}-10^{-4} s). It is the most important route through which triplet states are populated.

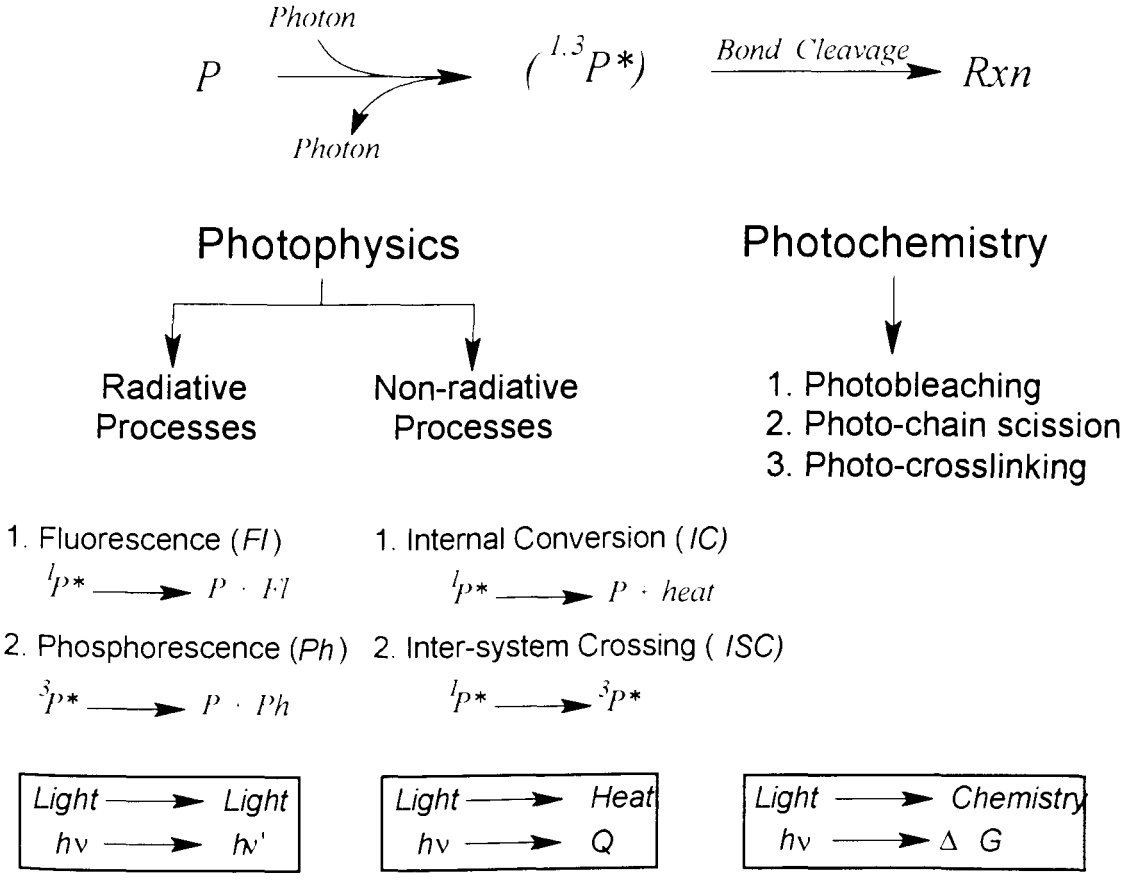

Figure III.7: Key photochemical processes in polymers

The triplet state is characterized by its long lifetime (~10^{-6}-10^{2} s) and the presence of two unpaired electrons. This state is thus more susceptible to chemical reactions (*Rxn*). For polymers, bond cleavage is usually homolytic in nature yielding pairs of free radicals.[147] Heterolytic bond cleavage has been observed in a few cases where the resulting ions are particularly stable. The

other important requirement for bond breaking is that energy of the incident photon, that is absorbed by the material, must be greater than the dissociation energy of the bond. The dissociation energies of typical chemical bonds found in most polymers are listed in Table III.2.[147]

Table III.2: Bond dissociation energies of some organic species

Bond Broken	Bond Dissociation Energy (kcal/mol)
C-H	105-82
RO-H	~102
R-OH	92-102
C-C	84-78
C-O	~76
ROO-H	~90
R-OOR	~50
RO-OH	~35

The nature of the photochemical reactions depends on several internal and external factors. Internal factors include the chemical nature of chromophores which determine the relative importance of the various photophysical and photochemical processes. External factors include wavelength of excitation, and irradiation conditions such as temperature and atmosphere. They also include the physical state of the material, i.e. solid state, solution, etc. One of the important external factors is the presence or absence of oxygen. Its effect on the photochemistry of π-conjugated polymers is discussed below.

III.3.2 Effect of Oxygen

Molecular oxygen plays an important role in the photochemistry of polymers both in the ground and excited states.[151,152] It has a relatively low formal potential, $E_{\prime\prime}^{\prime}$ = -0.82 V (versus saturated calomel electrode (SCE)),[153] and tends to form ground-state charge transfer complexes (CTC) with most organic compounds including alkanes, olefins and aromatic hydrocarbons.[154] The CTC plays a pivotal role in photodegradation of polymers. Its excitation may lead to the generation of singlet oxygen ($^1O_2$).[151]

Oxygen is also an efficient quencher of both singlet and triplet excited states (Schemes III.2 and III.3).[150,155]

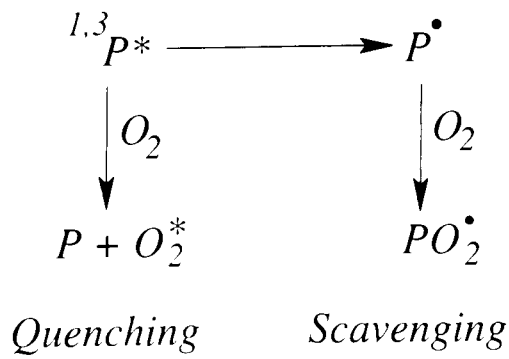

Scheme III. 2.

The interaction of O_2 with photoexcited species of aromatic hydrocarbons, e.g. anthracene, results in the formation of singlet oxygen ($^1O_2$) as shown in Scheme III.3. The formation of $^1O_2$ via the singlet state is thermodynamically feasible only if the singlet-triplet energy gap of the excited species ($\Delta E(^1P^*\text{-}^3P^*)$) is greater than 22.5 kcal/mol, which is the energy gap

between the ground state and the first excited singlet state of molecular oxygen ($^3\Sigma O_2 \longrightarrow {}^1\Delta_g O_2,\ \Delta E = 22.5\ kcal/mol$).[155] Energy transfer cannot, however, be a general requirement for the generation of $^1O_2$ i.e. singlet quenching does not necessarily yield singlet oxygen but can enhance intersystem crossing.[156] Formation of $^1O_2$ is often restricted to the triplet state annihilation processes (T-T annihilation) as shown in Scheme III.3.

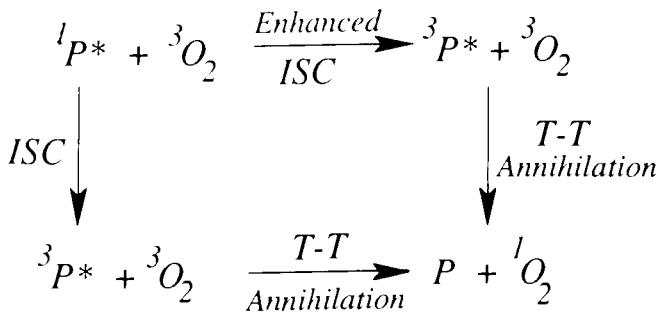

Scheme III.3

In solid polymers, singlet oxygen has a sufficiently long lifetime (20-50 μs) to react with polymers.[157] It also survives ~10^4 collisions with solid walls and more than 10^8 molecular collisions in the gas phase.[158] It is highly reactive and reacts with most unsaturated hydrocarbons. The characteristic reactions with aromatic compounds are dioxetane and endoperoxide.[152,156] Scheme III.4 shows reaction of $^1O_2$ with anthracene, for example.

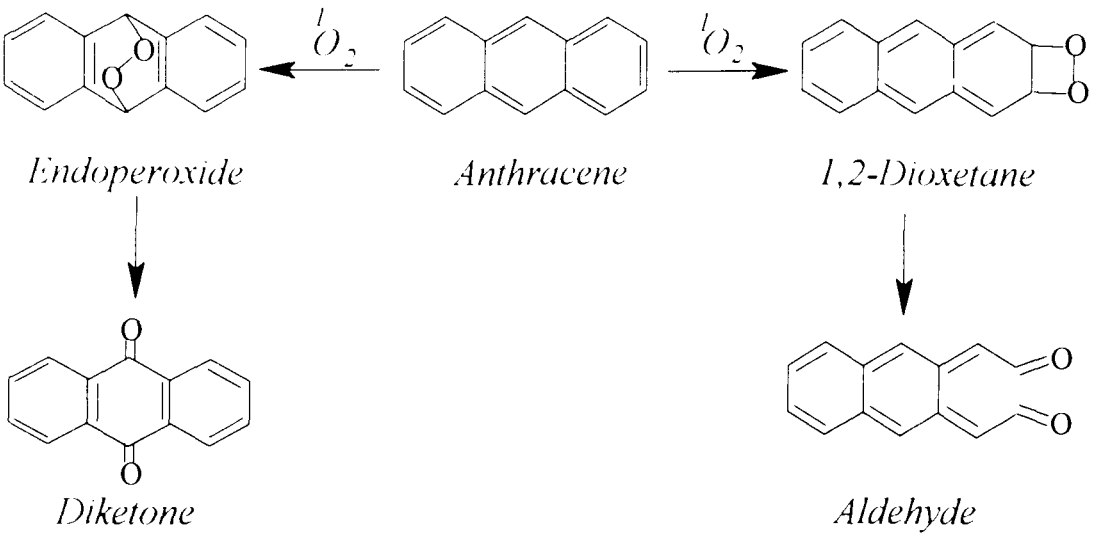

Scheme III.4

In contrast, olefins, which contain allylic hydrogen atoms, are oxidized with $^1O_2$ to peroxides according to Scheme III.5 (the *ene* reaction).[159]

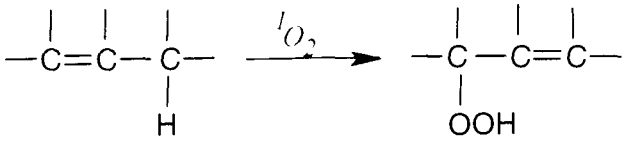

Scheme III.5

Direct reaction of singlet oxygen with saturated hydrocarbons is, however, improbable because the reaction is endothermic (Bond energies: R-H > R-OOH). Thus, no detectable amount of hydroperoxide was found after 51 hours of exposure of polypropylene to singlet oxygen.[160]

Oxygen is an efficient free radical scavenger (Scheme III.2).[161,162] It scavenges polymer radicals $R^{\bullet}$ to yield peroxy radicals $ROO^{\bullet}$ with very fast rates, ($k \sim 10^9$ L mol^{-1} s^{-1}), i.e. close to diffusion controlled processes ($k_{diff} = 10^{10}$ L mol^{-1} s^{-1}).[162] This species ($ROO^{\bullet}$) is believed to be the intermediate in the mechanism of free radical autoxidation of most hydrocarbons.[147-149]

III.3.3 Mechanisms of Photo-oxidation[147-149]

The process of photooxidation of polymers can be rationalized in terms of a free-radical chain reaction comprised of initiation, propagation, and termination.

Initiation. The mechanism of initiation of photooxidation of conventional polymers such as polyethylene, polyvinyl chloride, and polystyrene in the wavelength region >300 nm is complicated due to the fact that these polymers are transparent and have no allowed electronic transition in that wavelength region. Photoinitiation is not, therefore, an intrinsic property of the material. Possible photoinitiating chromophores are (a) extrinsic chromophores such as transition metal impurities incorporated in polymerization of the material, (b) peroxide and carbonyl groups created during polymerization or processing of the polymer.

Transition metal impurities usually absorb light in the UV-vis region and have high extinction coefficients (ε_{max} ~10^4 L mol^{-1} cm^{-1}). $Fe^{3+}.X^-$ ion pairs, for example, where X^- is halogen or hydroxyl ion, have broad electronic absorptions extending over a wide wavelength range (~250-450 nm).[163] $Fe^{3+}.X^-$ is known to undergo photoreduction to produce iron(II) and free radical $X^\bullet$ according to equation III.18

$$Fe^{3+}.X^- \xrightarrow{h\nu} [Fe^{2+}X^\bullet] \longrightarrow Fe^{2+} + X^\bullet \qquad \text{(III.18)}$$

The resulting radicals ($X^\bullet$) are very reactive and are capable of abstracting hydrogen from most hydrocarbons (RH) and thus initiate the photodegradation reactions (equation III.19).

$$RH + X^\bullet \longrightarrow R^\bullet + HX \qquad \text{(III.19)}$$

Reaction III.19 is thermodynamically feasible only if it is exothermic. That is H-X bond strength is greater than the R-H bond strength. The H-X bond strength, therefore, determines the abstracting power of the radical i.e. *radical selectivity*.[164] Thus, the chlorine atom is an unselective species that attacks aliphatic hydrocarbons in a rather indiscriminate manner since the bond energy of H-Cl is 102 kcal/mol. In contrast, the bromine atom (Bond energy H-Br = 86 kcal/mol) is a relatively discriminating species that selectively abstracts benzylic or allylic hydrogen atoms (Bond energy ~82 kcal/mol) over more strongly bound aliphatic hydrogen atoms (Bond energy ~95 kcal/mol).

Peroxides (ROOR or ROOH) are often introduced into the polymer during preparation or processing of the material. Thus, oxygen can be incorporated by a free-radical mechanism or thermal processing of the polymer e.g. annealing or preparation of polymer films by hot-pressing of the molten material to produce peroxy links. Peroxides and hydroperoxides absorb light in the region 300-360 nm (ε_{max} ~10-100 L mol^{-1} cm^{-1}).[165] Absorption of light causes cleavage of the O-O bond to give hydroxy ($^{\bullet}$OH) and alkoxy (RO$^{\bullet}$) radicals according to equation III.20.

$$ROOH \xrightarrow{h\nu} RO^{\bullet} + {}^{\bullet}OH \qquad \text{(III.20)}$$

The quantum yield of the photochemical decomposition of t-butylperoxide, for example, in solution at 313 nm is ~1.[165] The radical pairs are reactive enough to initiate the degradation reaction. R-O and O-H bonds are less labile to photo-decomposition since the dissociation energies of these bonds are ~50 and ~90 kcal/mol compared to 35 kcal/mol for O-O.

Propagation.[147,164] Alkoxy and hydroxy radicals produced by photolysis of hydroperoxides are both reactive species and can readily abstract hydrogen atoms from hydrocarbons (RH) (equation III.21)

$$RO^{\bullet} + RH \longrightarrow R^{\bullet} + ROH \qquad \text{(III.21)}$$

Generally, alkyl radicals are very reactive and form peroxy radicals in the presence of oxygen because of the biradical nature of the latter

$$R^{\bullet} + O_2 \longrightarrow ROO^{\bullet} \qquad \text{(III.22)}$$

The resulting radical, although fairly stable, can abstract hydrogen to complete the propagation process and regenerate R•.

$$ROO^{\bullet} + RH \longrightarrow ROOH + R^{\bullet} \qquad \text{(III.23)}$$

(O_2 regenerates $ROO^{\bullet}$)

The product of this propagation cycle is a hydroperoxide which can undergo further photolytic reactions.

Termination.[147,162] Termination of free-radical chain reactions occurs by several processes. The main bimolecular reaction mechanisms are

(i) Radical coupling. Conversion of alkyl radicals to nonradical species terminates the propagation reactions and leads to crosslinking of the polymer. The reactions, however, have to be sufficiently rapid (> 10^9 L mol^{-1} s^{-1}) to compete with the addition of oxygen (*cf.* equation III.22)

$$2R^{\bullet} \longrightarrow R\text{-}R \qquad \text{(III.24)}$$

Coupling of alkoxy (RO•) or peroxy radicals (ROO•) does not terminate the propagation process since the products are photochemically active and produce radicals upon further photolysis (*cf.*, equation III.20).

(ii) H-abstraction. Abstraction of a hydrogen atom by an alkoxy radical yields an alcohol according to

$$RO^{\bullet} + RH \longrightarrow ROH + R^{\bullet} \qquad \text{(III.25)}$$

(iii) β-scission. The alkoxy radical may undergo scission by the β-scission process to give carbonyl group.

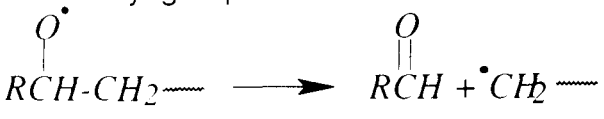

(III.26)

(iv) Coupling of hydroperoxides. The photochemical decomposition of hydrogen bonded hydroperoxide dimers results in crosslinking of the polymer through the formation of ether linkages (equation III.27).

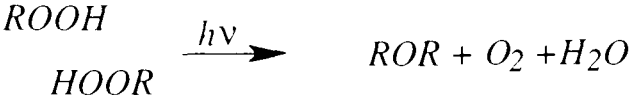

(III.27)

In summary, photooxidative degradation of conventional polymers can be described in terms of a free-radical chain mechanism involving hydroperoxides as the reactive intermediates and extrinsic chromophores as sensitizers (initiators).

III.4. A Survey on Microlithography and Photochemistry of π-Conjugated Polymers

Conjugated polymers have been important targets for processing due to the rapidly growing interest in constructing polymer-based microelectronics and optoelectronics. Photochemistry forms the basis of light-induced processing of materials namely photolithography. Photochemistry is also useful because many interesting innovations of π-conjugated polymers result from their interaction with, and response to, light.

Since this study was initiated in 1990 a number of reports on microlithography and photochemistry of π-conjugated polymers appeared. A summary of these recent reports is presented below. This survey covers most conjugated polymers and is structured according to the various types of polymers as classified in chapter I (*cf.* I.2).

Strategies used in processing π-conjugated polymers include

1. Radiation-induced doping/dedoping processes of polymers.
2. Light-directed polymerization, namely; photosensitized polymerization, photoelectrochemical polymerization, and photothermal-enhanced electrochemical polymerization.
3. In-situ polymerization on preformed catalyst patterns.
4. Photoelimination reactions.
5. Laser ablation.

I. Polyacetylene[166,167]

PA was the first conjugated organic polymer found to exhibit metallic conductivity when doped. However, intractability of the material continues to be an obstacle in processing it. Two main approaches have been adopted to solve this problem, namely; the precursor Durham route, and structure modification by addition of solubilizing side chains. Pattenring of PA was demonstrated using the soluble Durham precursor of PA. The strategy employed in the patterning process is shown schematically in Figure III.8. The soluble precursor was spun cast onto a substrate from acetone solution, and exposed through a photomask. This was followed by a heating process to eliminate hexafluoroxylene residues. Exposed regions undergo photobleaching and insolubilization reactions which form insulating patterns. Thermal treatment at ~150-200 ^{o}C was necessary to convert unexposed, insulating regions into PA. Conjugated polymer patterns are thus generated in an insulating film.

The mechanism of photobleaching was explained in terms of reactions of singlet oxygen with the polymer. The origin of singlet oxygen was not, however, discussed.

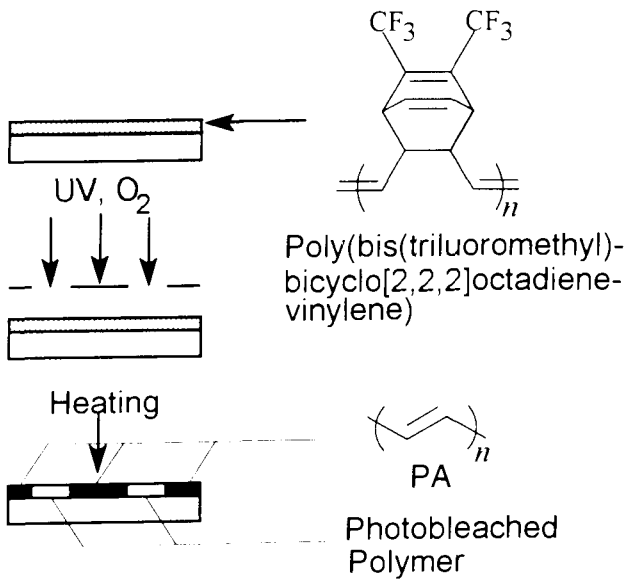

Figure III.8: Photoimaging of PA via the Durham precursor route

II. Polyaromatics

Microlithography of three members of this class has been investigated, namely; poly(p-phenylene sulfide) (PPS), poly(p-phenylene vinylene) (PPV), and polyaniline (PANI).

Poly(p-phenylene sulfide). Photoimaging of PPS has so far relied on photodoping the material.[168] The technique is based on the solubility difference created between exposed (photodoped) and unexposed (neutral) polymer, assuming the polymer is soluble in the neutral, undoped form. A soluble S-phenylated PPS derivative was employed in the study since the parent polymer is only soluble above 220 ^{o}C in solvents such as chloronaphthalene. The other important feature of these S-phenylated derivatives is that their chemical structures are similar to triaryl sulfonium salts, which are known photoacid generators. Under UV irradiation, these salts decompose to yield radical coupled products and a Brønsted acid according to Scheme III.6.[169]

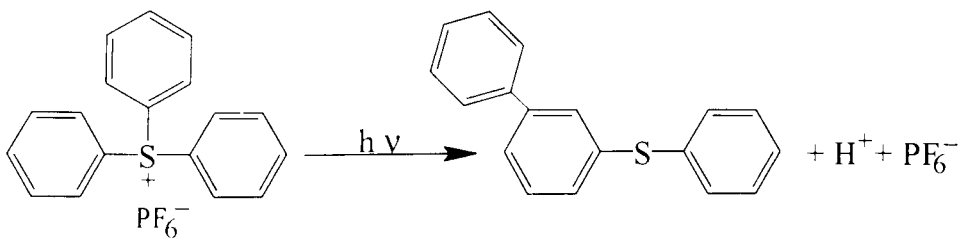

Triphenyl Sulfonium Salt *Photochemical Products*

Scheme III.6

The photogenerated acid is fairly reactive and dopes many π-conjugated polymers. S-phenylated PPS was found to undergo similar photochemistry and doping reactions. The material assumes a different solubility after photolysis. The photolyzed polymer is soluble in dimethyl sulfoxide whereas the pristine

polymer is soluble in acetone. Positive or negative resists was obtained by a proper choice of solvents following irradiation.

The photochemistry of PPS has been studied using several model compounds such as phenelyne sulfide oligomers and their halogenated derivatives.[170] It was found that the material undergo photodegradation when irradiated in air with a UV-vis light. The was assumed that the mechanism of photodegradation proceeds via homolytic cleavage of the C-S bond leading to thiophenoxy radicals. This supposition was supported by laser flash photolysis measurements which showed that the cleavage occurs mainly from the singlet state. The triplet state was readily quenched by oxygen so that C-S bond cleavage from the triplet states is inefficient. Quenching by oxygen was found to generate singlet oxygen which is a reactive oxidant of organic sulfides producing sulfoxides and sulfones.

Poly(p-phenylene vinylene). Laser-induced elimination reactions in polymer precursors have been employed in the microlithography of PPV.[171] Polymer precursors derived from 1,4-bis(tetrahydrothiophenium salts) of benzene and its 2,5-derivatives are soluble in organic solvents. Elimination converts the insulating, soluble precursor into the insoluble π-conjugated polymer (Scheme III.7). Dissolution of the unexposed regions thus generates conjugated polymer patterns.

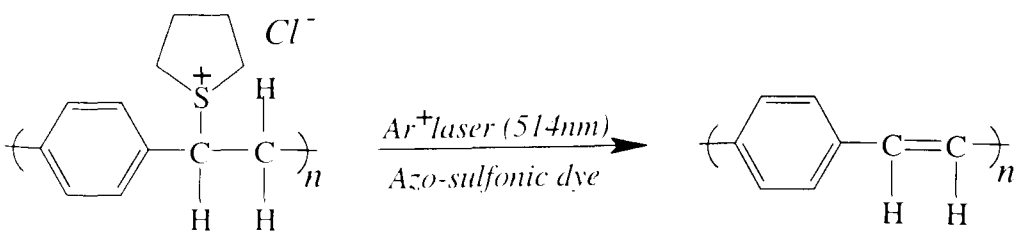

Souble PPV Precursor *Insouble, π–Conjugated PPV*

Scheme III.7

A 514 nm Ar^+ laser sourse was used for irradiation. Thin films formed from the polymer precursor are green in color and have very low absorption coefficients at 514 nm so that no elimination occurs upon direct photolysis even at exposure doses of ~350 W/cm^2. Photosensitizers, e.g. azo-sulfonic dye, were used to enhance the efficiency of elimination. No proof for complete elimination, however, was presented.

Photoimaging of the PPV precursor has also been attempted using 488 nm Ar^+ laser and 254 nm light where the polymer precursor is highly absorbing.[172,173] It was found that photoelimination did not convert the precursor to a fully conjugated polymer and that prolonged irradiation introduced new functional groups such as carbonyl and hydroxyl groups indicating thus photodegradation of the material.[172] The mechanism of photodegradation was not discussed.

The other obstacle in the photoimaging of the PPV precursor is the thermal instability of solutions of the polymer precursor. Elimination occurs at room temperature yielding polymer gels which lead to poor quality polymer films and difficulty in controlling film thicknesses.

Polyaniline. Microlithography of PANI has attracted most of the attention among members of this class because of its "relative" stability under ambient conditions and solution processability. Radiation-induced doping was applied for patterning of PANI using photoacid generators (PAGs) such as triphenyl sulfonium salts.[169,174] The generated acid is an effective dopant of the polymer and renders it insoluble. Pattern generation was achieved based on the differential solubility between doped and neutral regions. While a resolution of 0.5 μm was attained by UV irradiation, a higher resolution of 0.25 μm was

generated by E-beam lithography. The process is shown in Scheme III.8.[174,175]

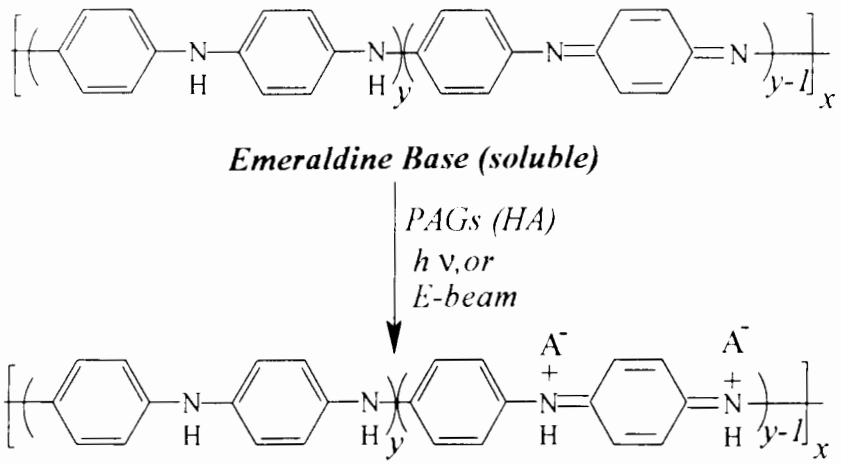

Scheme III.8

Photoimaging of doped PANI has been attempted.[176] In contrast to the above method, light in this case was used for reduction of doped polymer films containing semiconductor microparticulates. The basic principle of this process is depicted in Figure III.9.

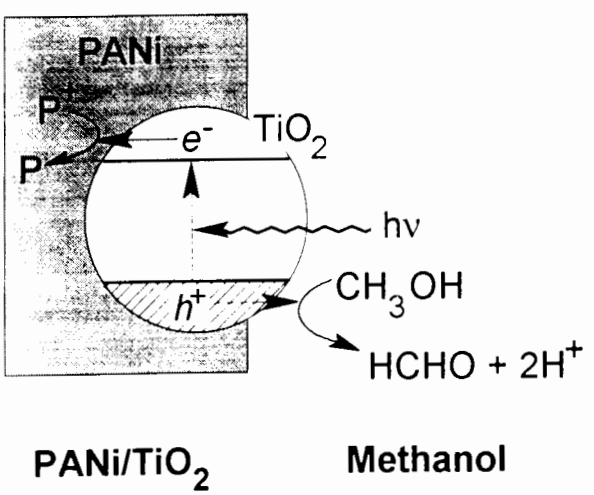

Figure III.9: Light-writing on PANI

Light-induced reduction of doped PANI is based on the use of a photosensitizer which has a conduction band energy (reduction potential) more negative than the formal electrochemical potential of PANI ($E^{O'}$ = -0.1 V SCE) and a valence band energy (oxidation potential) more positive than the $E^{O'}$ of the sacrificial reducing agent used for hole scavenging. This concept has been demonstrated using a wide band gap semiconductor such as TiO_2 (E_g = 3.5 eV) as a photosensitizer and methanol as a sacrificial reducing agent (E_o = ~-0.4 V SCE). Insulating patterns were generated by writing with light on doped PANI films.[177]

Deposition of PANI patterns have been achieved by laser-induced electropolymerization.[178] Aniline can be polymerized electrochemically at potentials more positive than +0.9 V SCE. Under laser irradiation, the electropolymerization potential is reduced to 0.65 V SCE thus allowing laser-directed electrodeposition of PANI on metal electrodes. Laser-induced thermal effects were proposed as the likely rationale for the shift in electropolymerization potential during irradiation.

Scanning electrochemical microscopy has also been used in deposition of high resolution PANI patterns.[179] The technique is based on direct electrochemical polymerization of aniline on preformed metal electrodes.

The photochemistry of PANI has been studied using various forms of PANI: leucoemeraldine (LEM, fully reduced (y=00), y is the doping level), emeraldine base (EMB, partially oxidized (y=0.5)), and emeraldine salt (EMS, partially oxidized (y=0.75)).[180] It was found that light causes degradation of the polymer. The extent of the reaction depends on the oxidation state of the material and wavelength of excitation. Thus, the rate decreases with an increase in the doping level of the polymer (LEM > EMB >EMS). The degradation was manifested by the formation of carbonyl groups following irradiation, as evidenced by both IR and X-ray photoelectron spectroscopy. This

was accompanied by a blue shift in the interband (π-π^*) transition indicating disruption the conjugated system along the polymer backbone.

III. Polyheterocycles

Polypyrrole. Photolithography of PPy was the first study conducted on microlithography of conjugated polymers, in general. Initial attempts involved photoelectrochemical polymerization of pyrrole on semiconductor electrodes.[181] The process is shown in Figure III.10.

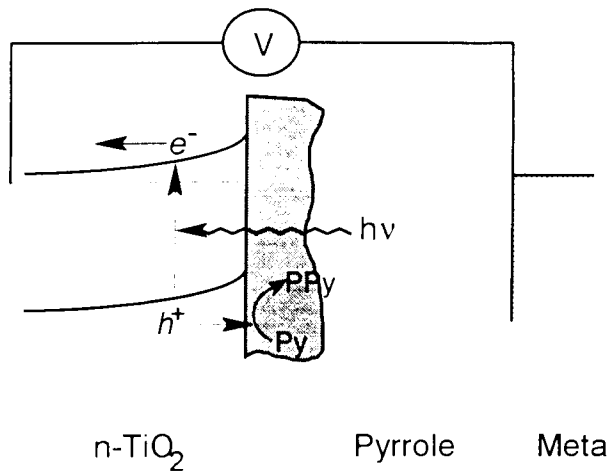

Figure III.10: Photoelectrochemical Polymerization of PPy

Irradiation of a semiconductor electrode with a photon of energy greater than the semiconductor band gap results in the generation of electron-hole pairs. If the hole is sufficiently oxidative, it will initiate polymerization of pyrrole. For pyrrole a bias of 0.5 V SCE was necessary to establish the initiation process on illuminated n-TiO_2 electrodes. This bias is lower than the potential required for the polymerization of pyrrole at metal electrodes (> 1.5 V SCE), leading to photselective deposition of PPy.

This technique suffers from several disadvantages: 1) It is a "wet" process and thus is incompatible with solid-state processing techniques, 2) The technique is limited to deposition of polymers to semiconductor surfaces, and 3) The resolution of the polymer patterns is limited by the diffusion length of photogenerated holes in the semiconductor.

The same authors have attempted deposition of PPy on insulating substrates.[182] Their method used photosensitized polymerization of pyrrole. Tris(2,2'-bipyridine) ruthenium(II)) ($Ru(bpy)_3^{2+}$) was used as a sensitizer and penta-amminechlorocobalt(II) ($[Co(NH_3)_5Cl]Cl$) as sacrificial oxidizing agent. Selective deposition of PPy on organic surfaces has been demonstrated using Nafion membranes substrates. The process is shown in Figure III.11.

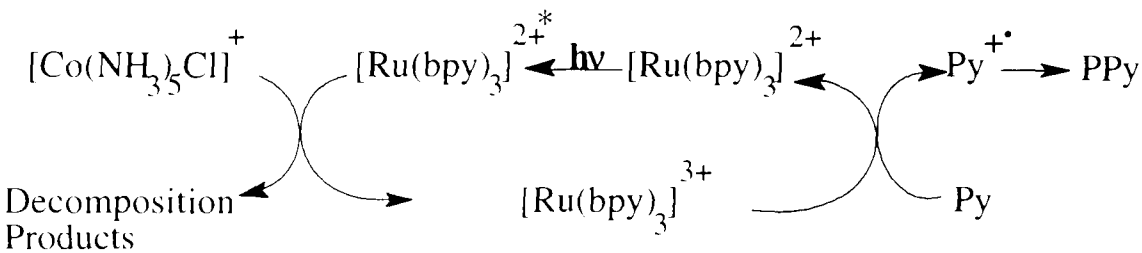

Figure III.11: Photosensitized polymerization of PPy

PPy patterns have also been achieved by *in-situ* chemical oxidation of pyrrole on preformed patterns of polymerization catalysts such as transition metal halides.[183] This concept was illustrated using copper and iron salts. Thus, copper salts, e.g. $CuCl_2$, patterns were generated by first patterning copper lithographically and then allowing it to react with a chlorine gas. In contrast, patterns of iron(III) salts were generated by photochemical reduction of iron(III) compounds enclosed in polyvinyl chloride films. The polymer patterns were obtained by in-situ polymerization of pyrrole vapor on the metal halide

patterns. In similar procedures, onium salts such as diphenyl iodonium salts have been employed to initiate the polymerization process. This in-situ polymerization technique suffers from poorly controlled polymerization kinetics due to inhomogenity of the catalyst and thus generation of ill-defined polymer patterns.

Laser ablation has also been used in microlithography of conjugated polymers.[184] Irradiation of thin polymer films through a mask with pulsed UV laser radiation ablates exposed areas, and renders pattern generation. This technique leads to damage of the polymer surrounding the irradiated spot producing patterns of low resolution.

Poly(3-alkylthiophenes). Recently, deep-UV and E-beam lithography have been used for imaging P3ATs. These methods entail using 1,2-bis(4-azido-2,3,5,6-tertrafluorobenzoate)(ATFB) as a crosslinking agent.[185,186] Irradiation of ATFB results in the formation of a nitrene intermediate which causes crosslinking of the polymer via a CH insertion mechanism (Scheme III.9). This technique was also used for modification of poly(3-alkylthiophenes) with a functionalized perfluorophenyl azide.[186]

The main drawback of this insertion technique is the incorporation of amino groups on the polymer. These groups might hinder doping of the material due to their highly reducing power.

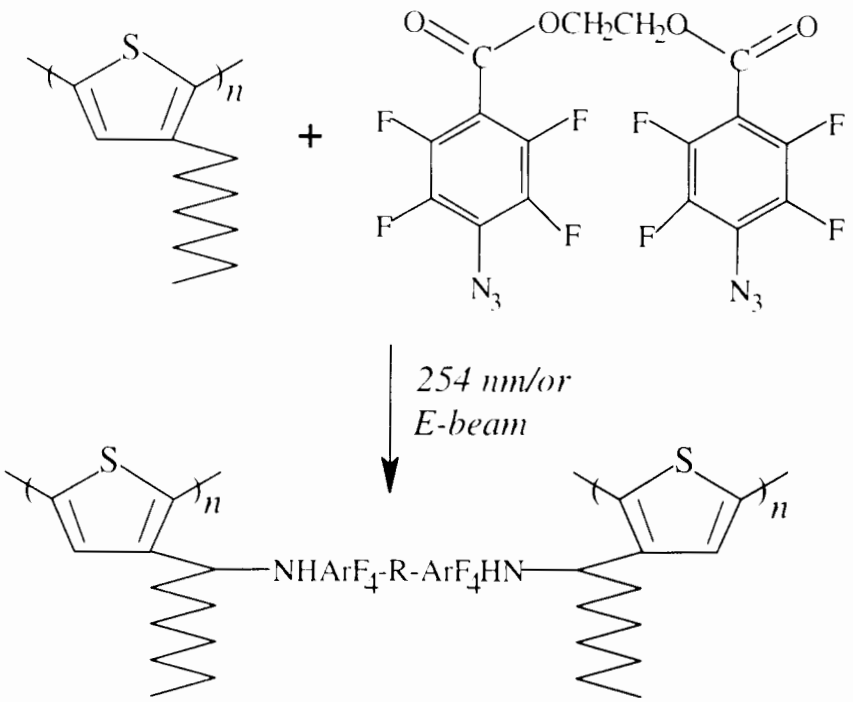

Scheme III.9

In summary, although significant efforts have been devoted to light-induced processing of π-conjugated polymers, the photochemistry of these polymers is still sparse. The survey also revealed that most of the studies were qualitative in nature and standard resist performance and characterizations are largely absent. Furthermore, the conductivity of the polymer patterns has been largely neglected.

III.5. Experimental

Polymer. Studies of this Chapter are based on P3HT prepared by oxidative coupling using $FeCl_3$ unless stated otherwise. The concentration of residual iron impurities was selected based on the type of study and is specified whenever necessary. Polymer solutions were prepared by dissolving an appropriate amount of solid polymer in toluene followed by filtration through a 0.2 μm filters in order to remove insoluble residues. Polymer films were prepared by two main techniques: spin casting and solvent evaporation. The thickness of the polymer films were measured using a profilometer (Tencor Instruments, Alpha-Step 200).

Extinction coefficient. The extinction coefficients of P3HT in the solid form and in solution were determined according to equation III.28

$$A = \varepsilon \, l \, m \qquad \text{(III.28)}$$

The concentration of the monomer in the solid film is 6.5 M, as calculated based on the polymer density (ρ=1.1 g/cc)[187] and molecular weight of the thienyl units. The extinction coefficient was determined from variations of absorbance with film thickness. In solution, ε was determined from variations of absorbance with concentration of the polymer solution.

Photolyses. The illumination source was a 150 W mercury lamp (Illumination Industries Ltd.). Irradiation was carried out using a 300 nm cut-off filter unless stated otherwise. For several experiments the wavelength of irradiation was selected using an appropriate 10 nm bandwidth interference filter or another cut-off filter. The temperature of the cell was kept constant at 25°C using a cooling block and a circulating water bath. Photolysis was performed in ambient air, unless otherwise stated. The intensity of incident light at 366 was

1.39 mW/cm^2 as measured by Radiaometer/Photometer IL 1350 (International light).

Sol fraction.[143] Thin films of polymer (100 nm) were spin-cast onto quartz slides from dilute solutions of the polymer in toluene (10 mg/ml). After drying, the polymer films were exposed through the quartz (*back-side exposure*). After irradiation, the soluble fraction was extracted by solvent development of the polymer films in 5 ml chloroform for 5 min. The sol fraction, S, was determined by measuring the optical density, OD, of soluble polymer fractions following irradiation and development. P3HT-B (1.3 wt% iron) (*cf.* II.3.2) was employed in this study.

Lithographic parameters.[136] Lithographic parameters were determined from gel dose curves constructed by plotting the residual thickness of the polymer image after solvent development as a function of the energy absorbed by the polymer.

Conventional photolithography. Films of polymer (30-0.05 μm) were spin-cast (1000-7000 rpm for 30 s) onto glass slides or silicon wafers from polymer solutions 10 and 20 mg/ml. Pre-baking of the polymer films was carried out at 120 ^{o}C in order to remove residual solvent. No post-baking was necessary. Relief images were formed in thin polymer films by irradiating through a photomask using contact printing. Polymeric patterns were observed upon development with chloroform. Scanning electron microscopy was used for inspection of polymer morphology. P3HT-B (1.3 wt% iron) was employed in this study.

Laser, direct-write microlithography. Thin films of polymer (0.16 μm) were spin-cast (5000 rpm for 30 seconds) onto glass slides or silicon wafers (bare Si, Al and SiO_2 coated wafers) from dilute solutions of the polymer dissolved in toluene (10 mg/ml) followed by pre-baking at 120 ^{o}C for 30 min. The laser, direct-write system was custom-built by the School of Engineering Science, Simon Fraser University and employs a helium-cadmium laser with a 442 nm output.[137] A 1 μm^2 laser spot was focused on the sample and patterns were generated by software-controlled motion of a X-Y translation stage which was transversed at a rate of 33 cm s^{-1}. The intensity of laser irradiation was 0.364 mW. Approximately 70% of the irradiation was absorbed by the polymer. Relief images were scanned four times, unless stated otherwise, giving an irradiation dose of 160 mJ cm^{-2}. The study was conducted in a clean room class 100. P3HT containing 1.3 wt% iron was employed in this study. The polymer possesses number average molecular weight, M_n, and molecular weight distribution, MWD, of 26,000 and 2.1, respectively.

Solution photochemistry. Polymer solutions were 1 mg/ml in concentration and the solvent was $CHCl_3$ unless otherwise stated. The optical density 435 nm was ~1.0 at. Solutions containing 7 mg/ml and 35 mg/ml in $CDCl_3$ were used for ^{1}H and ^{13}C NMR spectroscopy, respectively. For NMR measurements, irradiation was carried out under an oxygen atmosphere using a quartz cell fitted with a condenser to prevent loss of solvent and maintain a constant concentration. Samples (1.0 ml) were extracted periodically for NMR measurements. The absorption spectrum of the polymer solution was monitored with irradiation time. FTIR spectra of photolyzed polymers were recorded as thin polymer films cast onto KBr pellets. Photochain scission was

determined periodically by extracting a 50 μl aliquots for GPC analysis. The average number of chain scission, s, was calculated from[188,189]

$$s = \frac{M_n}{M_{n0}} - 1 \qquad \text{(III.29)}$$

where M_{n0} and M_n are the initial and final number-average molecular weights. P3HT-C was used in all spectroscopic analyses. P3HT-A and P3HT-B were used for comparison of rates of chain scission.

Generation of singlet oxygen. Singlet oxygen was generated chemically using hypochlorite/ hydrogen peroxide system according to Scheme III.10.[190-192]

$$OCl^- + H_2O_2 \longrightarrow HOCl + {}^{\cdot}O_2H$$
$$HOCl + {}^{\cdot}O_2H \longrightarrow HOOCl + OH^-$$
$$HOOCl + OH^- \longrightarrow H_2O + {}^{\cdot}OOCl$$
$${}^{\cdot}OOCl \longrightarrow {}^1O_2 + Cl^-$$

Scheme III.10

The experimental setup is depicted in Figure III.12. To a cold freshly prepared solution of hypochlorite a cold hydrogen peroxide solution is added. The rate of singlet oxygen generation is controlled by the rate of addition. The resulting gas is passed through a cold finger at -70°C (dry ice/acetone) to remove water vapor then through a trap at -150°C (liquid N_2/isopentane path) to remove any traces of chlorine gas. Pure singlet oxygen was bubbled through the test solution.

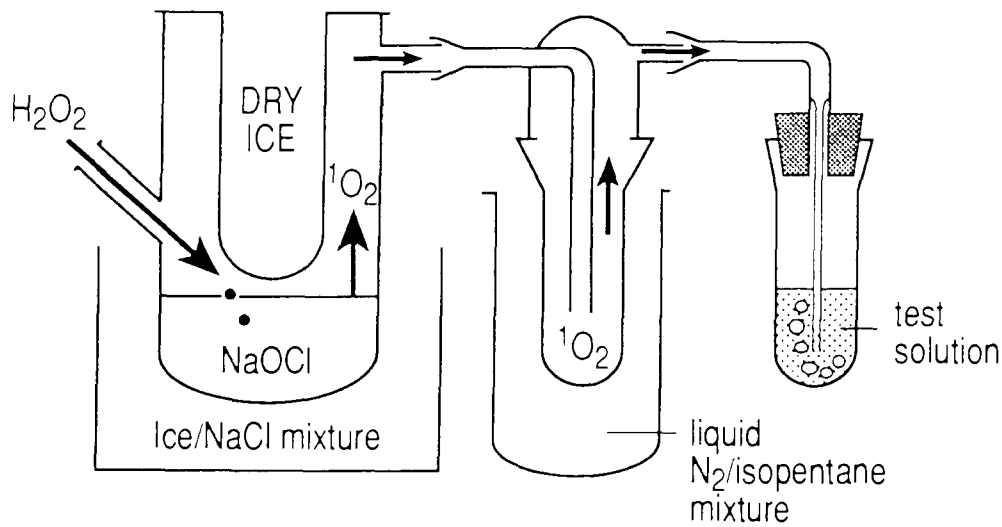

Figure III.12: Experimental setup for the chemical generation of singlet oxygen.

The generation of singlet oxygen was confirmed using anthracene as a trap. Anthracene undergoes 1,4-cycloaddition with singlet oxygen to give anthracene endoperoxide. Thermolysis yields the anthraquinone. Conversion of anthracene into anthraquinone was followed by GC. The product, anthraquinone, was identified by GCMS (208 m/e); UV (324, 273, 261(sh) 252 nm in $CHCl_3$) and IR spectroscopy (1675, 1595, 1355, 1320, 1305, 1285, and 690 cm^{-1}).[193,194]

Thermolysis of *t*-butyl peroxide in the presence of P3HT. 15 ml of benzene solution of P3HT-C (1mg/ml) and *t*-butyl peroxide were refluxed vigorously at a temperature of 160 °C under an atmosphere of oxygen for 45 h.. The initiator concentration was maintained at ~0.1 M by periodic additions of the reagent. Samples of the polymer were extracted at intervals to monitor the change in optical density and the degree of chain scission.

III.6 Results and Discussion

III.6.1 Sol-Gel Properties of Poly(3-hexylthiophene)

Figure III.13 shows the solubility plot of P3HT following irradiation at 435 nm under ambient conditions. This curve was constructed by plotting the soluble fraction $S+S^{1/2}$ of P3HT films as a function of the energy absorbed by the polymer ($1/r$) according to equation III.15.

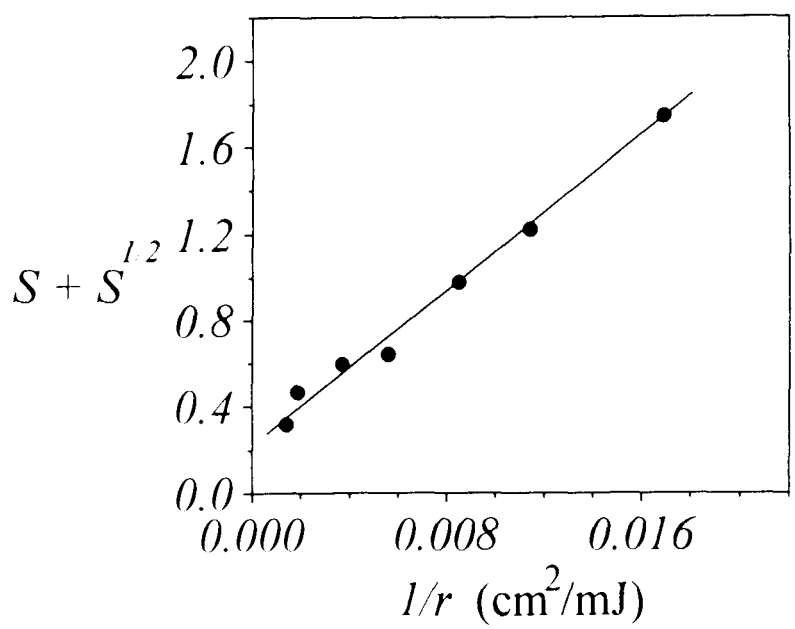

Figure III.13: Solubility curve of P3HT following irradiation at 435 nm

The intercept of the linear plot at infinite r gives the relative amounts of scission to crosslinking, p_0/q_0. A value of 0.23 was calculated for p_0/q_0. This value indicates that thin films of P3HT undergo simultaneous crosslinking and chain scission. The crosslinking density, q_0, is ~ 4.5 times greater than the fracture density, p_0, so that crosslinking of P3HT is the predominant photochemical reaction. P3HT is therefore a negative-type photoresist and the material can be processed by virtue of its photochemical crosslinking. The energy required for

incipient gelation, r_{gel}, of P3HT, calculated from extrapolation of the linear plot to a sol fraction $S+S^{1/2} = 2$, is 49 mJ.cm^{-2} or 1.78x10^{-7} einstein.cm^{-2}. Accordingly, the quantum yield of crosslinking, Φ_X, at 435 nm was calculated to be 2.37x10^{-3} mol einstein^{-1}. From the ratio of p_0/q_0, the quantum yield of main-chain scission, Φ_S, was estimated to be 5.45x10^{-4} mol einstein^{-1}. Main-chain scission was supported by the decrease in MW of the extracted polymer following irradiation.

The lithographic parameters of P3HT at 435 nm were determined from its sensitivity curve (Figure III.14).

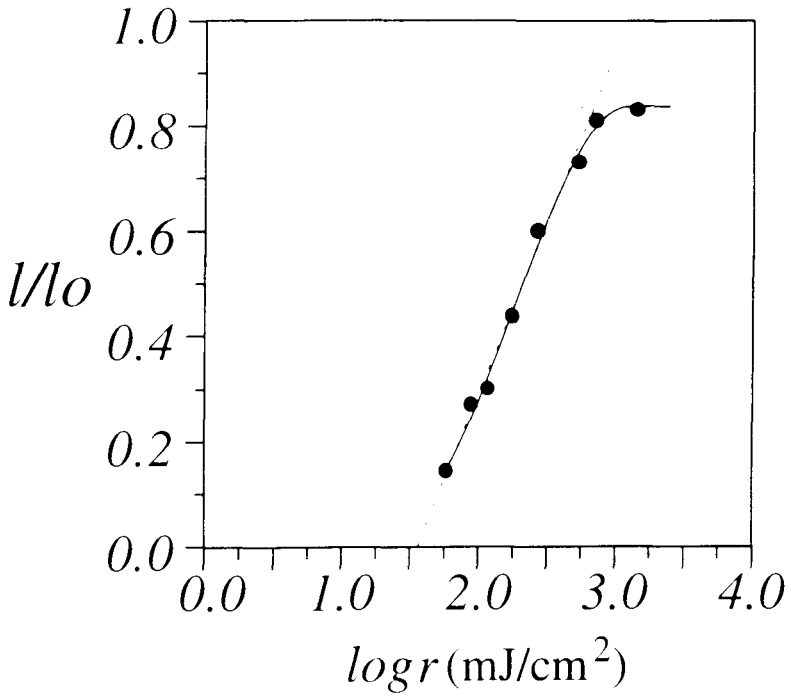

Figure III.14: Sensitivity plot of P3HT using 435 nm light

This curve was constructed by plotting the remaining thickness of polymer films after solvent development against exposure dose. The gel content (film thickness) increases with increasing exposure dose until the thickness remaining is equal to the original film thickness. In practice this maximum thickness is slightly less than the original film thickness due to volume contraction during the

crosslinking process.[136] Chain scission may also lead to a slight loss in the polymer' volume during the development process. The values of gel dose, r_{gel} or D_g^i, sensitivity, $D_g^{0.5}$, and contrast, γ, were calculated to be 38, 190 mJ.cm^{-2} and 0.8 respectively. The gel dose values determined from the solubility and sensitivity curves are in agreement to within ~25%.

III.6.2 Conventional Microlithography

P3HT, solvent cast from toluene, gave uniform films as shown by scanning electron microscopy. Flat films are required for contact printing since irregular surfaces can cause uneven exposure and distortion of the patterns.[132] Polymer architectures of controlled dimensions in the micron domain were readily obtained (Figure III.15). The thickness of the polymer patterns was tuned by controlling the exposure dose.

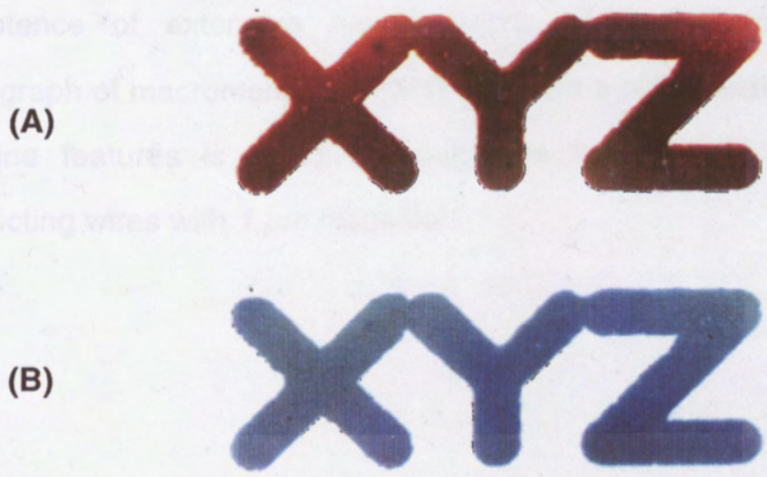

Figure III.15: Micrographs of P3HT images: (A) neutral polymer, (B) doped polymer ($FeCl_3$ dopant). Irradiation time = 1 min, Film thickness = ~1 μm, Resolution 0.5 mm.

III.6.3 Laser, Direct-write Microlithography

Processing of P3HT was demonstrated using conventional photolithography. Photomasks are, however, expensive and impractical for designing composite circuits. Direct-write microlithography is important since the photomask is replaced by computer-controlled mask information i.e. the mask information is controlled by software which can be programmed to provide any circuit pattern. Laser, direct-write microlithography was employed to examine the feasibility of processing P3ATs using these direct-write techniques.

Relief images were formed in thin polymer films on various surfaces by tracing a pattern onto the surface of the film with the focused laser beam. A faint contrast in color between the irradiated and non-irradiated regions could be observed due to a slight photobleaching of the polymer. Immersion of the relief pattern in a chloroform/acetone mixture (85/15% v/v) for 2 minutes at 20 ^{o}C caused the unexposed polymer to dissolve leaving only that polymer which was irradiated. The residual pattern was intensely red-colored signifying the persistence of extensive π-conjugation. Figure III.16 shows an optical micrograph of macromolecular P3HT wires on a silicon wafer. The resolution of the fine features is 4 μm, although we had no difficulty with depositing conducting wires with *1 μm* resolution.

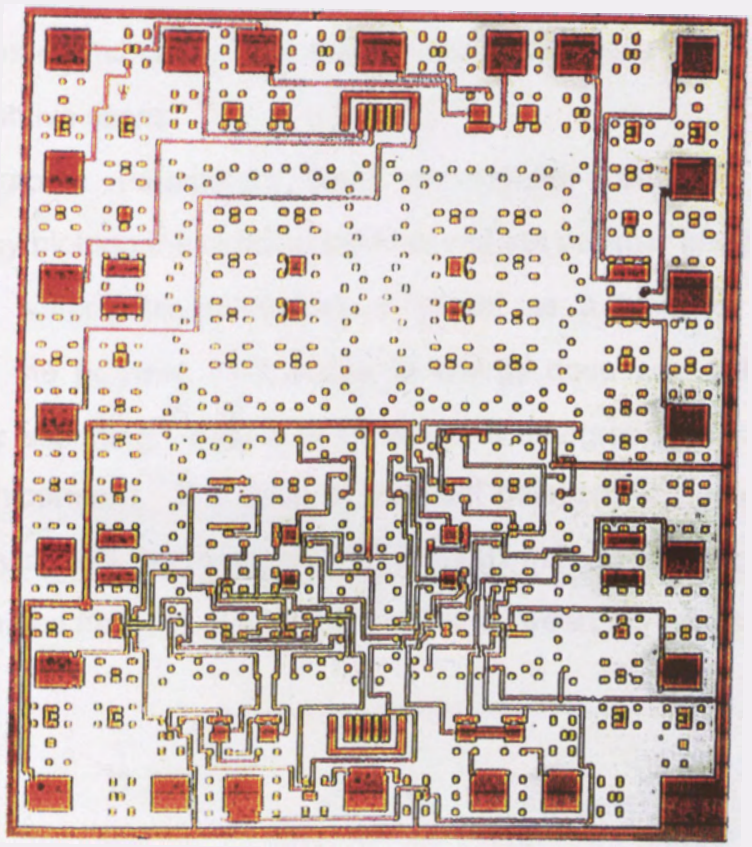

Figure III.16: Micrograph of P3HT-macromolecular wires

The optical density of the 160 nm thick polymer film at the wavelength of irradiation was 0.573, as determined from a calibration plot of film thickness versus optical density (OD). Assuming a density of 1.1 g cm^{-3} the extinction coefficient at 442 nm was 5480 mol^{-1} L cm^{-1}. Approximately 73% of the incident laser light was absorbed by the film and thus the energy absorbed per scan of laser light was 40 mJ cm^{-2}. The pattern shown in Figure III.16 was generated with four repetitive scans.

Lithographic parameters were determined from gel dose curves constructed by plotting the residual thickness of the polymer image deposited on Al-coated Si wafer after solvent development as a function of the energy absorbed by the polymer. Variations in energy dose was achieved through multiple laser scanning. Figure III.17 shows a lithographic sensitivity plot for poly(3-hexylthiophene). The dose of incipient gelation, D_g^i, was 7.7 mJ cm^{-2}. The sensitivity at 50% gel formation, $D_g^{0.5}$, was 61 mJ cm^{-2}. The contrast, γ_n, was 0.7 as determined from the gradient of the line between D_g^i and D_g^0.

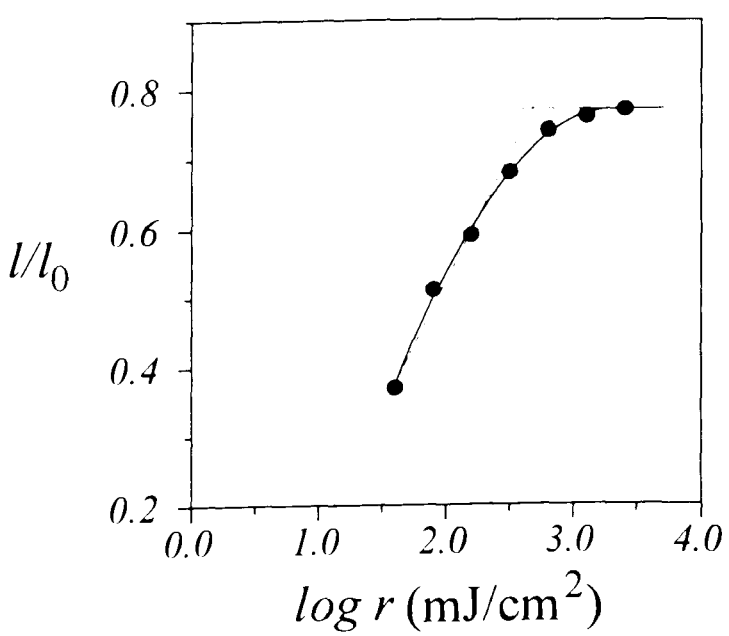

Figure III.17: Sensitivity plot of P3HT using blue laser (442 nm)

The discrepancy in values of the various lithographic parameters determined by laser lithography compared to conventional photolithography can be rationalized in terms three factors. The most important of these factors is the much higher intensity of lasers compared to Hg lamps. This leads to the generation of higher radical concentrations and thus greater probabilities for radical coupling. Top-side exposure on a reflective surface such as Al-coated Si may enhance photo-crosslinking due to the reflected radiation. The higher MW polymer used in laser lithography can also reduce the gel dose according to equation III.11.

Laser, direct-write microlithography gives high resolution polymer architectures if the processing parameters are carefully chosen. Resolution up to 1 μm, which is the limit of the laser system, was achieved. The conductivity of the resulting image and extent of π-conjugation following irradiation are points of concern. Sufficient π-conjugation exists, as evidenced by the red color of the residual patterns, after photolysis so that it should be possible to impart electronic conductivity to the material.

III.6.4 Irradiation, Conjugation length, and Conductivity Relationships

The effect of irradiation on the conjugation length and conductivity of P3HT was investigated. π-Conjugation can be monitored qualitatively by observing the change of optical density of the film with irradiation. Irradiation of thin films of P3HT at 435 nm in ambient air causes the optical density of the film to decrease. Figure III.18 shows a plot of optical density of the polymer film (at λ =500 nm) against the irradiation dose.

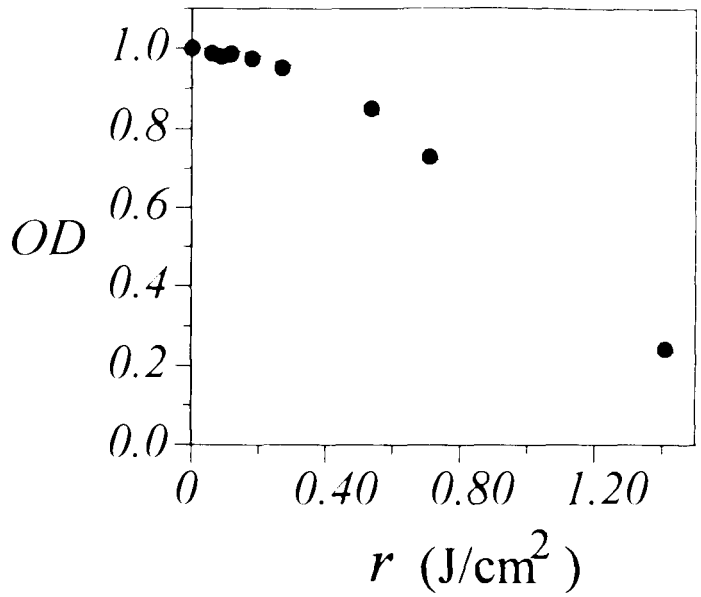

Figure III.18: Relative optical density (λ = 500 nm) of P3HT films versus irradiation dose. (Irradiation wavelength = 435 nm).

Neutral, undoped polymer film has a strong absorption band at 500 nm indicating a significant degree of π-conjugation along the polymer backbone (*cf.* Figure II.7). Noteworthy is the fact that the electronic transition of solid polymer films (80:20% HT-HH) is due to an effective conjugation length of ~6 thiophene units and not the persistent (actual) length of the polymer chains.[195,196] It can be concluded that the effective conjugation length of the polymer did not change appreciably with irradiation doses < 300 $mJ.cm^{-2}$, above this value the π-conjugation system was disrupted. This important observation illustrates that the polymer films can be photochemically insolubilized, yet still possess a high degree of conjugation which is essential for electronic conduction.

Neutral irradiated, and pre-irradiated, polymer films have low conductivity (~ 10^{-7} $\Omega^{-1}cm^{-1}$). Upon oxidative doping, using an anhydrous acetonitrile solutions of nitrosonium tetrafluoroborate ($NOBF_4$) or ferric chloride, the films turned blue in color and were found to be electronically conductive by the four-

point probe technique. The initial conductivity of heavily doped P3HT was ~5 $\Omega^{-1}cm^{-1}$.

In order to determine the effect of light on the conductivity of the films, several neutral films were irradiated, each to a different exposure dose. Following this, each film was oxidized and the conductivity measured by the four-point probe technique. The conductivity of the film decreased in a non-linear fashion with irradiation dose (Figure III.19) and fell by several orders of magnitude after prolonged photolysis. However, when the irradiation dose was kept low, (< 300 $mJ.cm^{-2}$), the change in electronic conductivity was negligible. This is consistent with the decrease in the effective conjugation length of the material with irradiation.

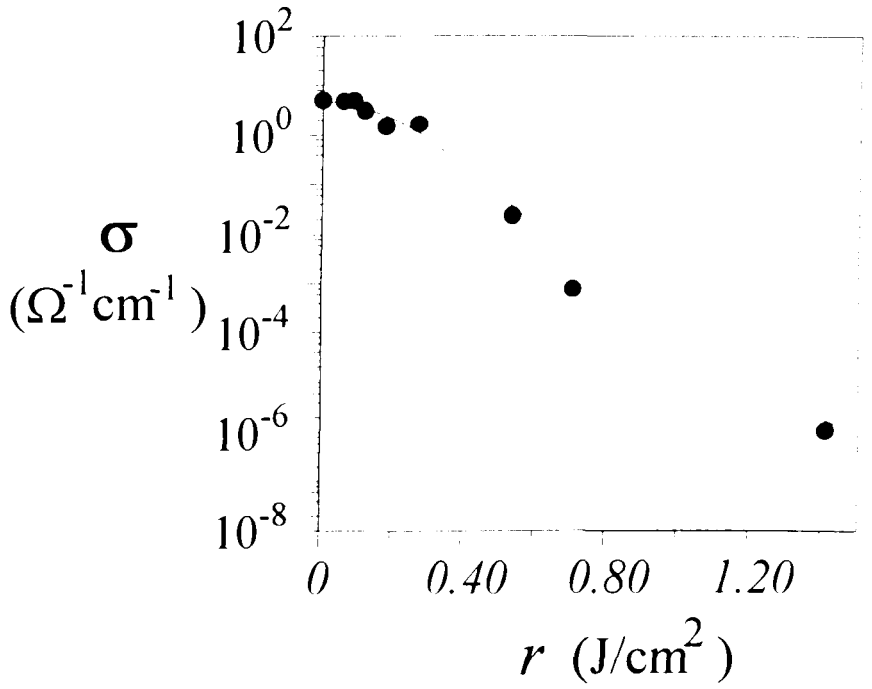

Figure III.19: Conductivity of oxidized P3HT versus irradiation dose.
(Irradiation wavelength = 435 nm)

The conductivity of the macromolecular P3HT wires shown in Figure III.16 was also investigated. Doping of the wires was carried out by application of an anhydrous acetonitrile solutions of nitrosonium tetrafluoroborate or ferric chloride. The oxidized polymer was blue in color indicating the presence of charge-carrying bipolarons.

Conductivities of oxidized polymer wires were determined by depositing five parallel polymer channels, each 40 μm wide, 200 μm long, 90 nm thick, and separated by 40 μm, onto glass slides as shown schematically in Figure III.20. Two aluminum contact pads were evaporated onto the ends of the polymer channels. The polymer was oxidized with nitrosonium tetrafluoroborate and the resistance between the two contact pads measured as 30 kΩ from which a resistance of 150 kΩ per channel was obtained. The bulk conductivity of the patterned material was ~5 $\Omega^{-1}cm^{-1}$ which is similar to the bulk conductivity of the non-irradiated material ~5 $\Omega^{-1}cm^{-1}$.

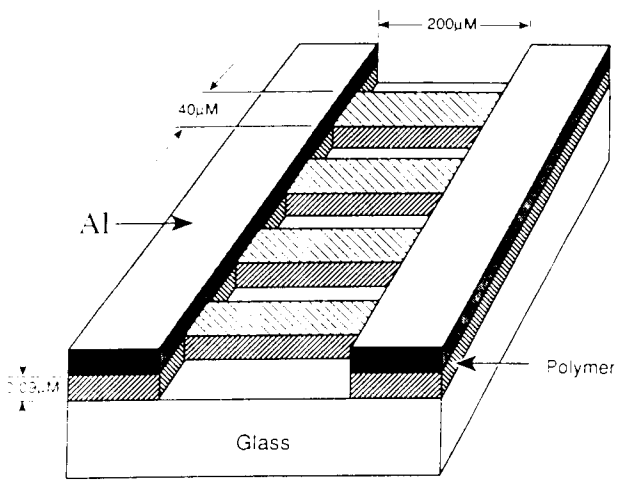

Figure III.20: Schematic diagram of a microstructure used for measuring conductivity of polymer wires.

The environmental stability of the oxidized form of the polymer is a point of concern. The oxidized, conductive patterns of P3HT are relatively stable under a nitrogen blanket but revert back to their neutral, semiconducting state shortly after exposure to the atmosphere. The process is considerably more rapid with micron-sized images compared to relatively thick free-standing films due to the small mass of the former. Investigation of the mechanism of these dedoping (loss of conductivity) processes and factors controlling them is the subject of *Chapter IV.* New strategies for improving the stability of polymer/counter ion pairs are also presented in *Chapter IV.*

III.6.5 Mechanisms of Photochemical Reactions of P3ATs

III.6.5.1 Solution Photochemistry

Spectroscopic Analysis. UV-vis absorption spectra of P3HT were recorded in various solvents. Typically, a broad absorption with a maximum of ~435 nm was observed in good solvents such as $CHCl_3$ indicative of extensive π -electron delocalization. Irradiation of the polymer in air-saturated $CHCl_3$ results in a decrease in the optical density (OD) (Figure III.21) and a blue shift in λ_{max} (Figure III.22).

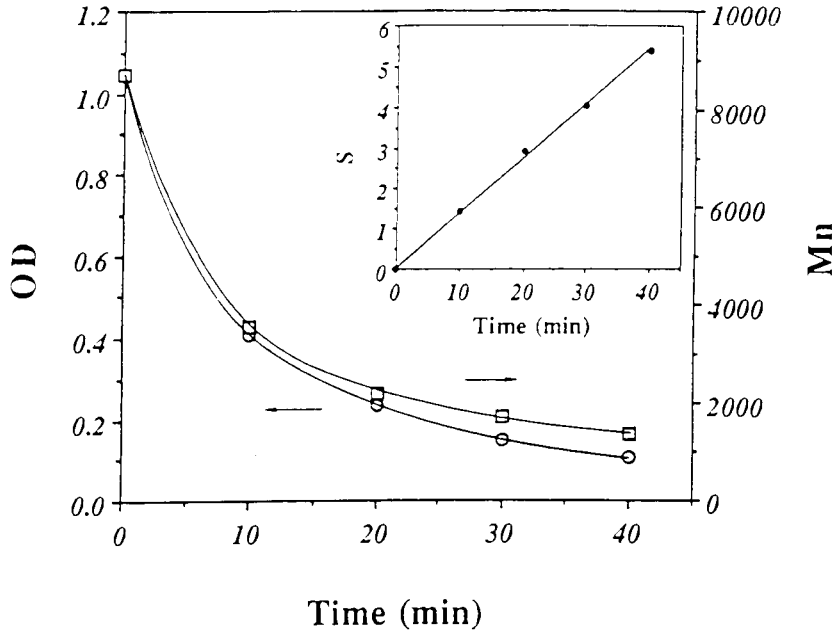

Figure III.21: Decrease in the optical density of P3HT solution (λ, 435 nm) and decrease in M_n with irradiation. Inset: number of chain scissions, s, versus irradiation time.

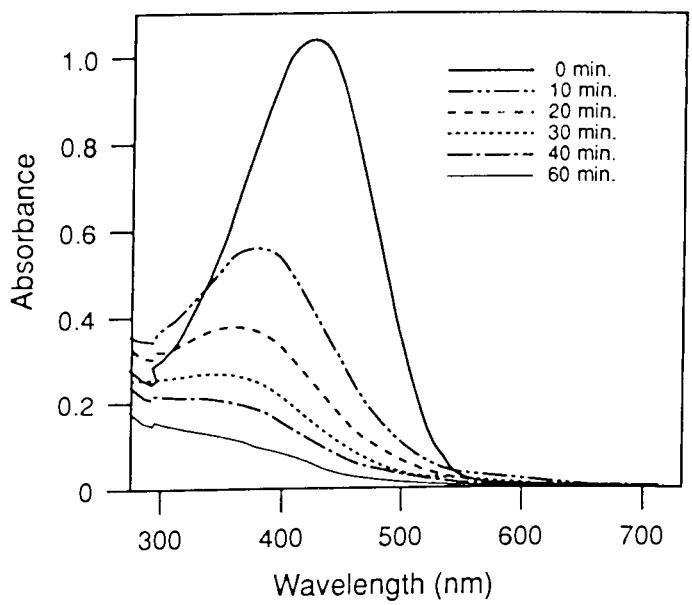

Figure III.22: Change in UV-vis absorption spectrum of poly(3-hexylthiophene) in $CHCl_3$ with time of irradiation. 150 W Hg lamp, 300 nm cut-off filter.

Photobleaching is attributed to disruption and shortening of the π-conjugated segments. Concurrent with photobleaching is a decrease in molecular weight of the polymer (photochain scission) (Figure III.21). Number-average molecular weights of pristine polymers were 8,500 representing a degree of polymerization ($\overline{P}_n$) >50. Following photolysis M_n decreased to values as low as 1,400 ($\overline{P}_n$~8). Later in the Chapter, it is shown that photobleaching and photochain scission follow from two independent reaction pathways.

FTIR vibrational spectroscopy of polythiophenes and derivatives of polythiophene is well documented. Data for the pristine polymer is summarized in Table II.2. FTIR of P3HT solution in $CHCl_3$ (1mg/ml) was monitored over a period of 30 minutes of irradiation (Figure III.23). Assignments were made taking into account supporting experimental data which is presented throughout this section. Several features concerning FTIR spectra of photolyzed samples require noting: (I) Formation of relatively strong absorption bands in the range 3700-3200 cm^{-1} which are characteristic of hydroxyl and hydroperoxy functionality. Several absorption bands indicate the presence of various hydroxyl species as confirmed by ^{13}C NMR. The broad absorption at 3450 cm^{-1} can be assigned to hydrogen-bonded -OH groups. The broad absorption is overlapped by a narrow band at 3580 cm^{-1} which is assigned to a hydroperoxy group.[197] This assignment is supported by the symmetric and asymmetric bending of the OH group at ~1395 and 1370 cm^{-1}, and in some cases by the O-O stretching vibration at ~ 877 cm^{-1}. The presence of -OOH groups was confirmed by their partial removal, and subsequent decrease of the 3580 cm^{-1} absorption band upon heating the sample *in vacuo* at 180 °C (thermal decomposition). (II) Evolution of a strong and complex band at 1800-1660 cm^{-1} characteristic various keto and/or aldehydic groups. Formation of carboxylic acids was ruled out since treatment of the photolyzed film with methanolic KOH

did not alter the spectrum and no carboxylate was observed at 1560 cm^{-1}. A weaker band at 1660 cm^{-1} is assigned to an unsymmetric olefin. These groups also have in- and out-of-plane bends at 1430 cm^{-1} and 790 cm^{-1}. (III) Formation of strong bands in the region 1260-1000 cm^{-1} which indicate sulfine residues of the structure $C=S^{+}-O^{-}$ or C=S=O.[198-200] The 1090 and 1020 cm^{-1} bands are attributed to a C=S stretching vibration and S→O vibrations respectively of $C=S^{+}-O^{-}$. Absorptions at 1253 and 1226 cm^{-1} are characteristic vibrational modes of the alternate resonance structure, C=S=O. It will be shown that these species originate from photochemical cleavage of thienyl rings. (IV) Decrease of the aliphatic CH stretching peak in the region 2900 cm^{-1} due to loss of the alkyl side chain. This is considered direct evidence for the participation of the alkyl chain in the photochemistry of poly(3-alkylthiophenes). (V) A decrease of the absorption bands characteristic of inter-annular stretching modes (1560, 15012, and 1460 cm^{-1}) and disappearance of the aromatic C-H stretch and C-H out-of-plane deformation at 3055 and 823 cm^{-1} respectively. This is attributed to disruption of the π-conjugated system. Absorption wavenumbers and the structural assignments for new IR bands are listed in Table III.3. IR data for pristine polymers is listed for comparison.

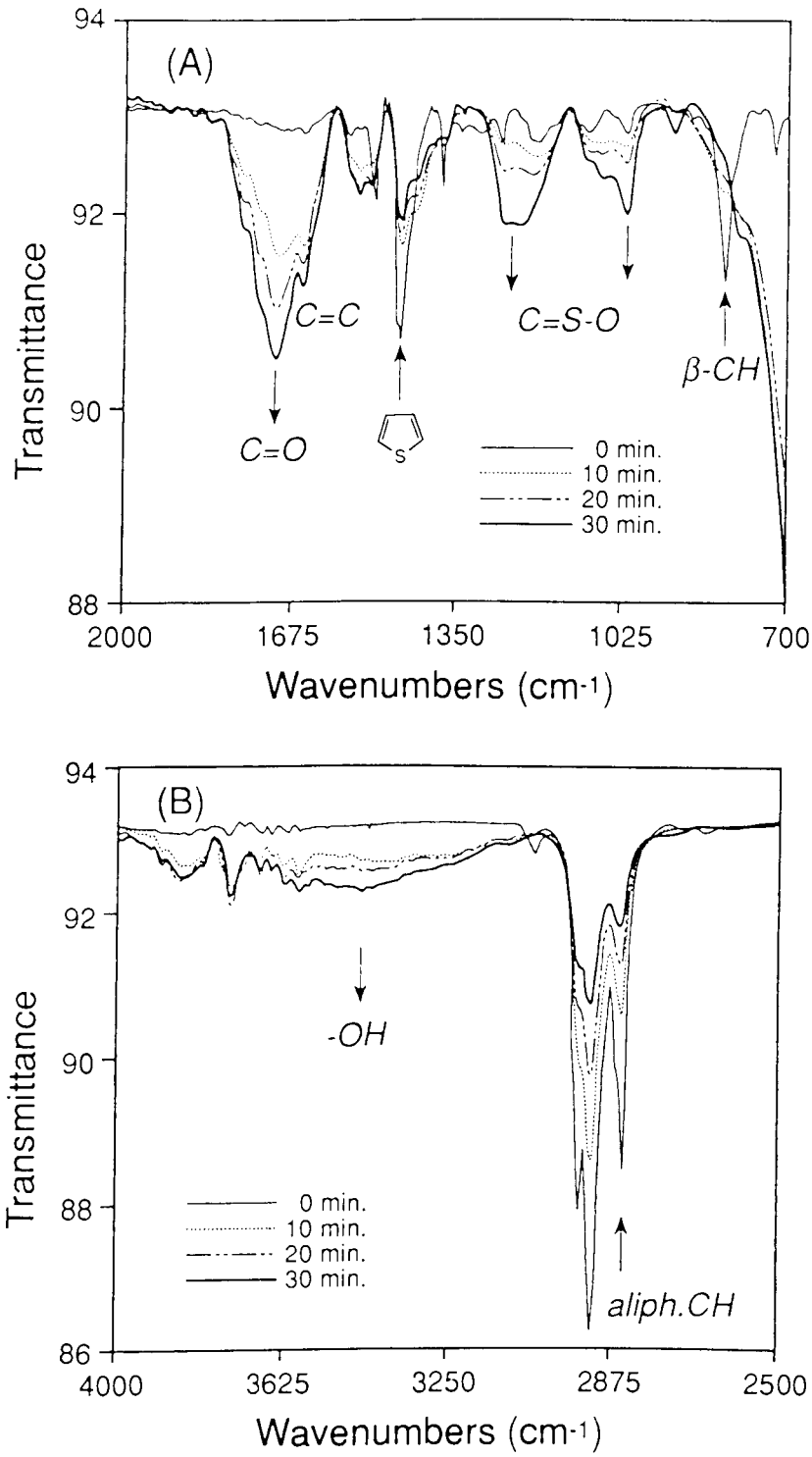

Figure III.23: (A&B) FTIR of P3HT films on KBr disks as a function of time of irradiation. Photolyzed in $CHCl_3$ (1mg/ml).

Table III.3. FTIR data of P3HT following irradiation*

(a) pristine polymer		(b) photolyzed polymer	
cm^{-1}	**assignment**	**cm^{-1}**	**assignment**
3055	C-H str.(aromatic)	3580	OOH str.
2955	CH_3 asym. str.	3450	OH str.
2926	CH_2 in-phase vib.	2955-2926	C-H str. (aliph.)
2870	CH_3 sym. str.	2857	
2856	CH_2 out-of-phase vib.	1765-1740	CHO str.
1655	overtone of thiophene ring.	1710-1685	C=O str. (ketone).
1560, 1512, 1460	C_2=C_3 & C_4=C_5 antisym. and sym. str. modes of thiophene ring.	1650-1625	C=C str.
1377	methyl def.	1431	C-H in-plane def. (olefin)
1260	C-C inter-ring bond str.	1395-1370	sym. and asym. bending of OH groups
1190-1155	wagging and twisting of methylene groups.	1253	C=S=O
1090	C-H in-plane bending of thiophene ring.	1226-1090	$C=S^+-O^-$
823	C-H out-of-plane def. of thiophene ring.	1920	
725	rocking mode of methylene groups.	924	C-O str.
		790	C-H def. (olefin).

* Films cast on KBr disks.

^{1}H and ^{13}C NMR data for P3HT in solution are well documented (*cf.* II.3.4). This enabled discernment of changes in NMR signals upon irradiation. ^{1}H NMR spectra of pristine and photolyzed spectra are shown in Figure III.24.

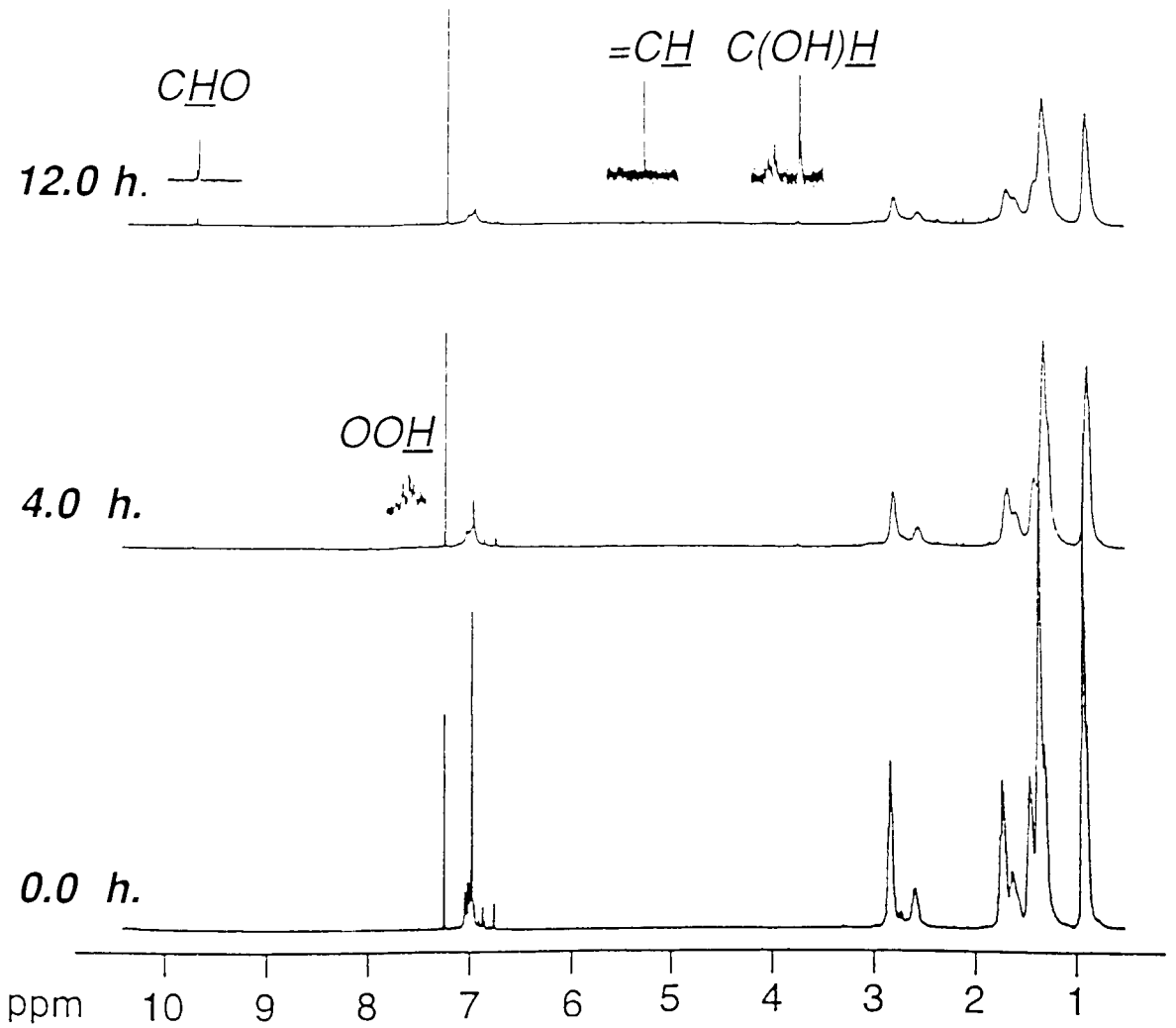

Figure III.24: ^{1}H NMR of P3HT in $CDCl_3$ before (a) and after photolysis: (b) 4 h; (c) 12 h. Photolyzed in $CDCl_3$ (7 mg/ml)

Evolution of the resonances are summarized as follows: (I) Formation of a weak signal in the region 5.3 ppm, characteristic of olefinic protons. (II) Formation of a signal at 3.75 ppm and a weak broad signal at ~7.7 ppm assigned to C<u>H</u>(OH) and hydroperoxy protons respectively.[201-203] (III) Evolution of a well resolved signal at 9.8 ppm assigned to α, β-unsaturated aldehydic protons. (IV) A decrease in the aliphatic proton resonance signals, in good agreement with changes in IR spectra. (V) A decrease in the aromatic proton signal indicating ring opening.

^{13}C NMR spectra of photolyzed polymers are in good agreement with IR and ^{1}H NMR results. Primarily, these indicate a decrease in aromatic and aliphatic signals in the regions 125-143 ppm and 14-32 ppm respectively; the appearance of new signals at 57 and 65 ppm assigned to primary and secondary alcohols; the formation of weak and complex signals at 120-140 ppm most likely due to olefinic structures. Carbonyl carbons in the region 200-230 could not be observed due to their long relaxation time.

Photosensitizing of singlet oxygen by P3HT. Thiophene oligomers are known to be efficient sensitizers of the lowest excited state of molecular oxygen ($^{1}\Delta_g O_2$), commonly termed singlet oxygen.[192,204-207] Polythiophene and its derivatives are also candidates for being efficient singlet oxygen sensitizers. This was confirmed by trapping photosensitized $^{1}O_2$ with anthracene as follows: An O_2-saturated $CHCl_3$ solution of P3HT containing various concentrations of anthracene ($0 \rightarrow 5x10^{-4}$ M) was irradiated at wavelength > 435 nm, ensuring that only the polymer absorbed light and the amount absorbed by anthracene was negligible. No ground state charge transfer complex of the two species was evident from UV-vis spectroscopy. Furthermore no mechanism of photosensitization or photo-induced electron transfer can take place between anthracene and poly(3-hexylthiophene) upon direct irradiation of the polymer.[208]

Upon irradiation of the polymer the optical absorption corresponding to the characteristic electronic and vibronic excitations of anthracene diminished. GCMS, IR, and UV-vis spectroscopic analysis confirmed the loss of anthracene and the build up of anthraquinone (GCMS, molecular ion: 208).[193,194] In the absence of anthracene the optical absorbance due to the π-π^* transition of the polymer decreased rapidly while in the presence of anthracene the rate of decrease at 435 nm was suppressed (Figure III.25, Table III.4).

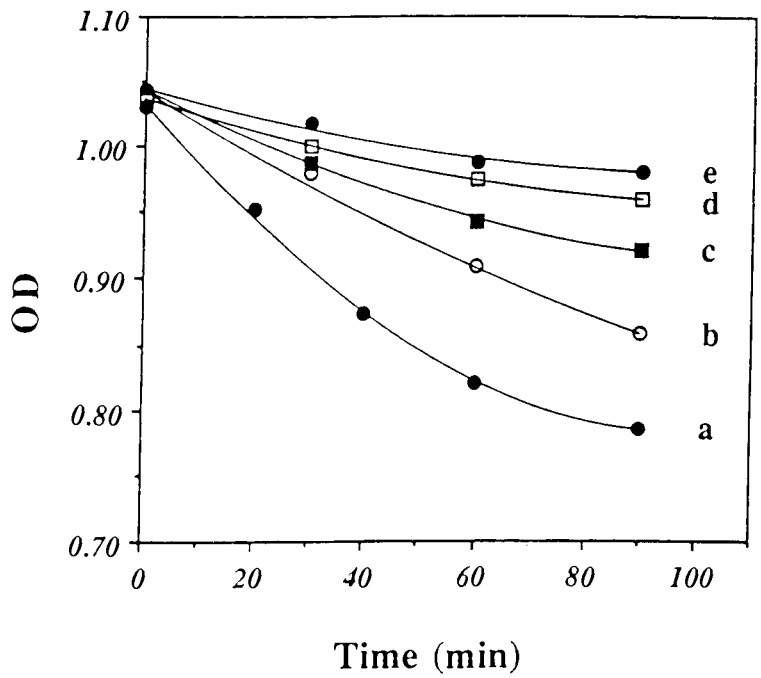

Figure III.25: Decrease in the optical density of poly(3-hexylthiophene) in $CHCl_3$ (1mg/ml) ((λ 435 nm) with time of irradiation and in the presence of anthracene. [Anthracene]: (a) 0 M, (b) 1.25×10^{-4}, (c) 2.5×10^{-4}, (d) 3.75×10^{-4}, (e) 5×10^{-4} M. Samples were irradiated at wavelength > 435 nm.

At concentrations of anthracene >$5.0x10^{-4}$ M, the rate of decrease in OD corresponding to the polymer was five times slower than when anthracene was absent. These results provide strong arguments that photosensitized $^1O_2$ is largely responsible for loss of π-conjugation and photobleaching of the polymer.

Table III.4: Relative rates of photochain scission and photobleaching of P3HT in presence of anthracene[a]

[anthracene] (M)	Relative Rates of Photochain Scission[b]	Relative Rates of Photobleaching[c]
0.00	1.00	1.00
$1.25x10^{-4}$	1.10	0.52
$2.50x10^{-4}$	1.00	0.38
$3.75x10^{-4}$	1.00	0.26
$5.00x10^{-4}$	1.10	0.19
$10.00x10^{-4}$	1.10	0.20

a P3HT in $CHCl_3$ (1mg/ml) at 25°C; Incident wavelength was > 435 nm.
b determined by GPC.
c determined from decrease in OD of P3HT at 435 nm.

In addition to monitoring the decrease in OD, the corresponding change in M_n was evaluated. Table III.4 gives the relative rates of photochain scission when the polymer is irradiated in the presence of anthracene singlet oxygen quencher. A negligible difference in rates of chain scission is observed indicating that chain scission is unaffected by quenching of photosensitized $^1O_2$.

Reaction of P3HT with chemically generated singlet oxygen. To test the hypothesis that photobleaching and photochain scission follow from two independent reaction pathways, singlet oxygen was generated by an independent route, i.e. ex-situ, and its effect on rates of chain scission and photobleaching was examined. The literature is rich in methodology for generation of singlet oxygen. Common systems use triphenyl phosphine/ozone,[209] hypochlorite/hydrogen peroxide,[190-192] microwave discharge,[210] or photosensitization.[211,212] The hypochlorite/ hydrogen peroxide system was chosen for our studies since it does not contaminate the test solution with impurities. Reaction of P3HT with singlet oxygen was monitored over a period of 16 hours. The OD of the solution at 435 nm decreased by ~ 30% whereas the molecular weight of the polymer remained unaltered (Figure III.26). Clearly chain scission does not originate from reaction with $^1O_2$.

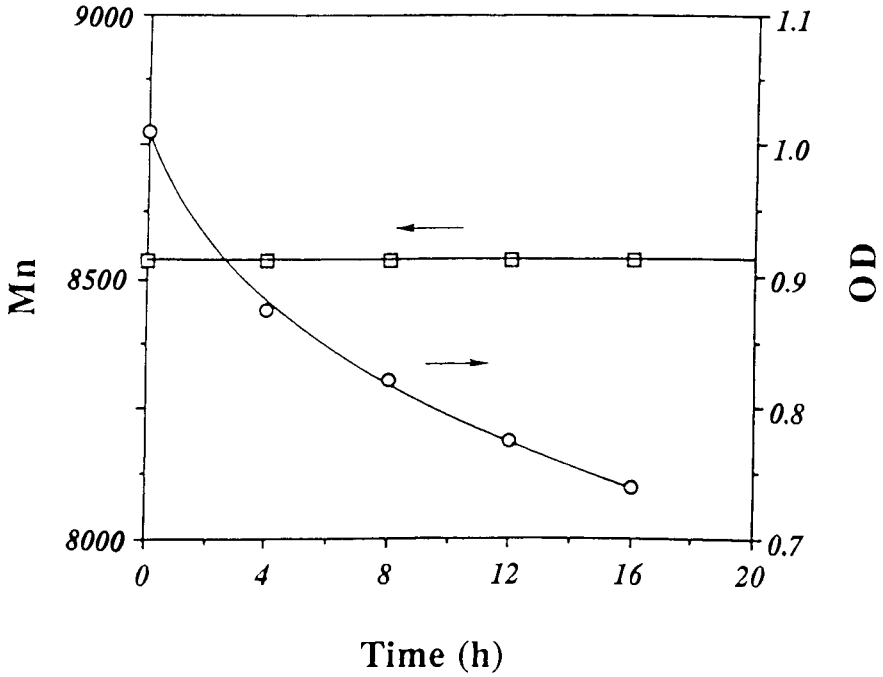

Figure III.26: Decrease in the optical density (λ-435 nm) and change in M_n of poly(3-hexylthiophene) in $CHCl_3$ (1mg/ml) during reaction with chemically generated singlet oxygen.

FTIR analysis of the polymer following exposure to $^1O_2$ showed strong signals due to sulfine (1090-1020 cm^{-1}), keto- (1730 cm^{-1}), and olefinic (1650 cm^{-1}) residues. Notably, no hydroxyl functionalities were observed (Figure III.27). The slight change in the aliphatic C-H stretching band is attributed to the new chemical environment following ring opening.

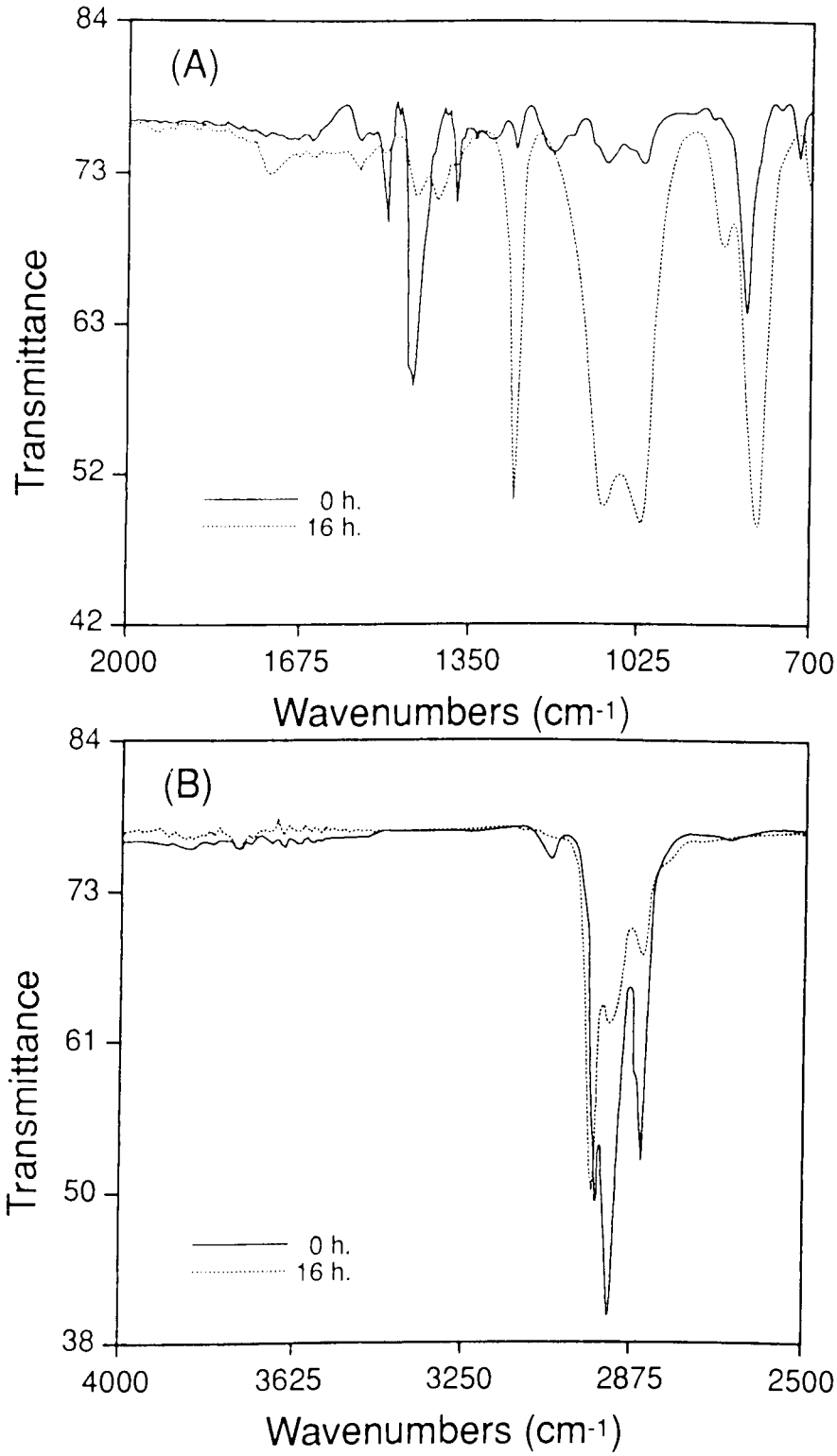

Figure III.27: (A&B) FTIR of P3HT before (0 h.) and after reaction with chemically generated singlet oxygen (reaction time, 16 h.).

Spectroscopic analyses of reaction products are consistent with reported mechanisms observed for the reaction of $^1O_2$ with small molecule thienyls.[213,214] A similar mechanism has been postulated for longer chain thienyls.[215] In this mechanism, shown in Scheme III.11 $^1O_2$ undergoes a 1,4 Diels-Alder addition with thienyl units.

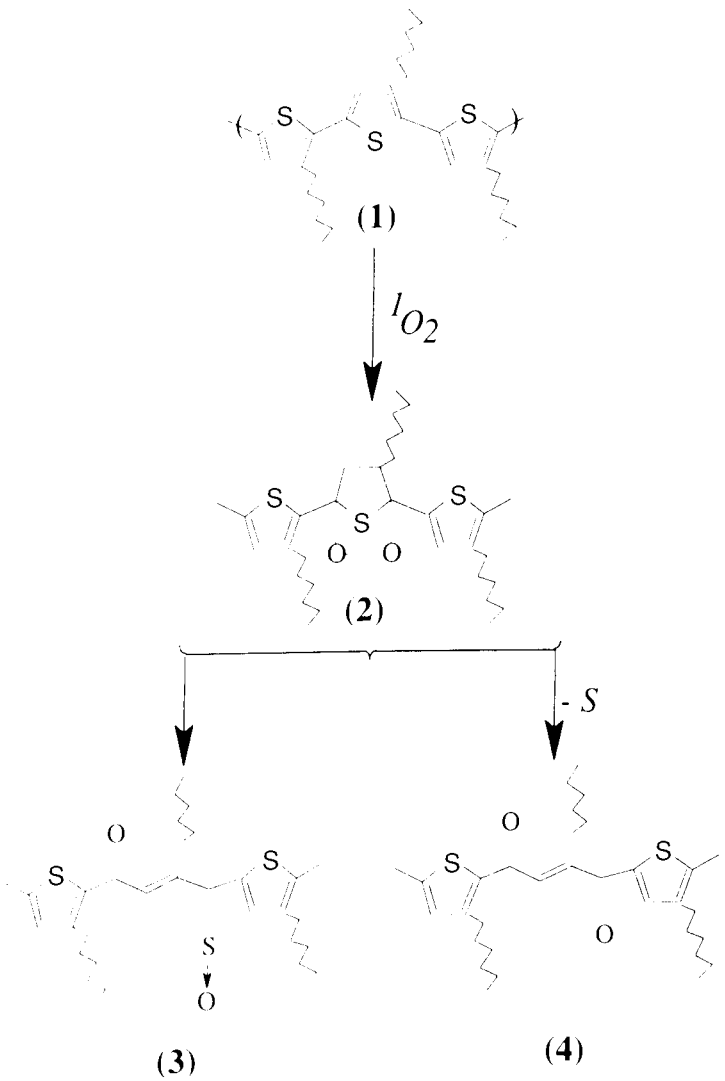

Scheme III.11

Endoperoxide residues **2** may be envisaged as intermediates in the formation of the sulfine. However, their formation as primary oxygenation products can only be inferred from the photochemical products because endoperoxides derived from heterocyclic 1,4-dienes are generally unstable at room temperature.[216] Isolation of highly unstable monomeric thiophene endoperoxides (thiaozonides) by reductive trapping with diazene at -78°C has been reported;[217] they, however, decompose at room temperature to the sulfine **3**, or the *trans*-diketone **4**. Spectroscopic analyses of reaction products between P3HT and singlet oxygen, and for photolyzed samples, are consistent with this mechanism.

The possibility of reaction between singlet oxygen and the alkyl side chain is highly improbable (*cf.* III.3.2). Saturated polymers such as polyethylene and polypropylene are completely inert to singlet oxygen,[218] and the participation of singlet oxygen in the mechanism of photo oxidation of more reactive polymers such as polystyrene is negligible.[219,220] In fact polystyrene has been used as a matrix for studying diffusion of $^1O_2$ in polymers,[221] and for photooxygenation of polynuclear aromatic hydrocarbons.[222]

Mechanism of singlet oxygen generation. The dominant reaction leading to polymer photobleaching involves photosensitization, and reaction, of singlet oxygen. Photosensitization of singlet oxygen is often the result of triplet-triplet annihilation according to Scheme III.12.

$$^1P_0 \xrightarrow{h\nu} {}^1P^*$$
$$^1P^* \xrightarrow{isc} {}^3P^*$$
$$^3P^* + {}^3O_2 \longrightarrow {}^1P_0 + {}^1O_2$$

Scheme III.12

Singlet oxygen generation ($^1O_2$) by triplet states of polythiophene ($^3P^*$) appears unlikely, given the recent phosphorescence and transient spectroscopic data which indicates a very low quantum yield of triplet formation.[66,223] The alternative explanation for photosensitization of singlet oxygen is based on dissociation of an excited state charge-transfer complex. Confirmation of this mechanism requires the detection of a charge transfer complex (CTC) between oxygen and P3ATs. CTC formation between molecular oxygen and P3ATs is discussed in *Chapter VI*.

Photochain scission. Singlet oxygen is not responsible for chain scission, and the products of reaction between singlet oxygen and thiophenes are photolytically inert,[224] a classical photo-oxidative route is proposed. Photooxidation of polyolefins is initiated by the photosensitization of free radicals by impurities such as residual transition metal catalysts.[225-229] In experiments designed to elucidate the role of free radicals in the chemistry of P3HT an independent source of radicals, namely the thermolysis of *t*-butyl peroxide, was used to successfully initiate chain scission in the absence of light. Molecular weights of the polymer in refluxing benzene/*t*-butyl peroxide, at 160 °C decreased from 8,500 to 5,000 over a period of 45 hours representing an average of ~0.8 chain scissions. In the absence of the free radical source no decrease in molecular weight was found, clearly indicating the role of free radicals in chain scission. Over the same period of time the optical density of the polymer decreased by only a negligible amount (~ 3%) in the presence of *t*-butyl peroxide.

The pristine polymer does not contain any obvious organic free radical initiators but as a consequence of the synthetic procedure residual inorganic salts remain as impurities even after extensive purification (*cf.* III.3.3).[230-232]

Mössbauer spectroscopic analysis indicated that the main impurity is Fe^{3+} (*cf.* II.3.2) . Quantitative analysis using atomic absorption spectroscopy yielded an iron (III) concentration in the polymer of 0.05 wt %. To test the hypothesis that photolysis of residual Fe salts are a source of free radicals, a polymer sample was prepared by oxidative coupling with $FeCl_3$ and subjected to various degrees of purification in order to provide different concentrations of iron impurities (*cf.* II.2.2). In all cases Mössbauer indicated the presence of iron (III). Atomic absoption analyses yielded various amounts of iron, while the polymers exhibited similar UV-vis absorption spectra. The corresponding relative efficiencies of photochain scission were 1.0 : 1.21 :1.44 for samples containing iron concentrations of 0.05 wt %, 1.3 wt %, and 3.2 wt %, respectively. The rate of chain scission increases with increasing the iron content confirming the role of residual metal salts on photochain scission of P3HT.

Mechanism of photochain scission. The dependence of the rate of chain scission on the concentration of residual iron impurities strongly points to a photo-oxidative free radical pathway in which the initial step is photolysis of $Fe^{3+}X^-$ ion pairs (*cf.* equation III.18). In P3HT, X is likely to be an OH or Cl, given the facts the polymer was prepared using $FeCl_3$ and that aqueous ammonia was used to reduce it.

IR and NMR spectroscopies show that alkyl side chains on polythiophenes play an essential role in the photochemistry of P3HT. We propose that the primary point of attack by free radicals is the α-carbon atom of the hexyl group, which possesses a labile H-atom. This is based on the lower dissociation energy of the α-C-H bond as a result of resonance stabilization of the radical. The mechanism is shown in Scheme III.13.

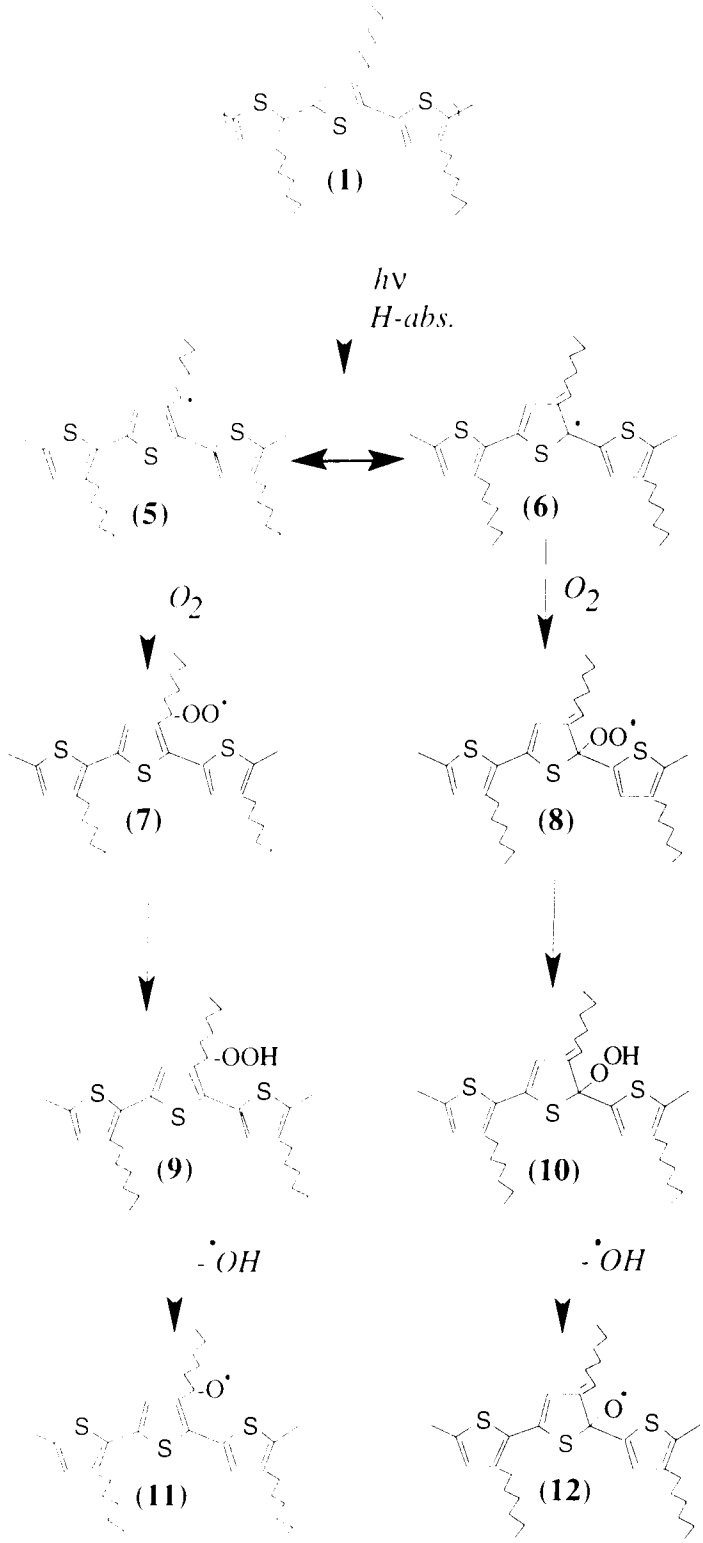

Scheme III.13

In this scheme the resulting P3HT radical is resonance stabilized by the π-system to yield radicals **5** and **6**.[233] Radicals **5** and **6** rapidly react with oxygen to produce peroxides **7** and **8** which can abstract a hydrogen from the polymer chain, or solvent, to yield hydroperoxides **9** and **10**. Cleavage of the hydroperoxide group by light results in alkoxy radicals **11** and **12**. Fe^{2+} produced from reaction III.18 might also take part in the cleavage of the OOH groups.[234,235] In this mechanism only rearrangement of the alkoxy radical **12** can cause chain scission with the formation of ketones **13** and thienyl radicals **14** (Scheme III.14).

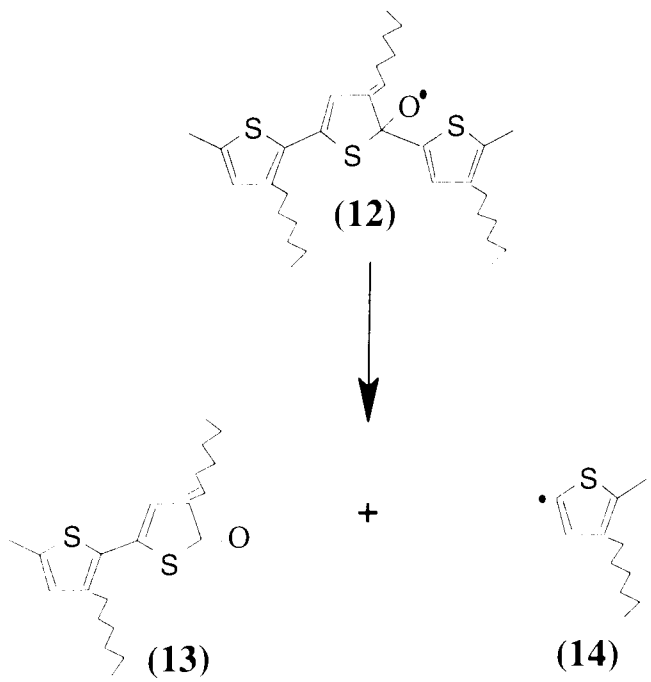

Scheme III.14

The Alkoxy radical **11**, on the other hand, can undergo several of the following possibilities as shown in Scheme III.15: (i) β-scission to yield an aldehyde **15**, and volatile hydrocarbons; (ii) hydrogen abstraction to give a secondary alcohol **16**, (iii) radical coupling to form a cross linked polymer. The latter possibility is suppressed in solution due to the low concentration of the polymer but this pathway is viable in solid films.

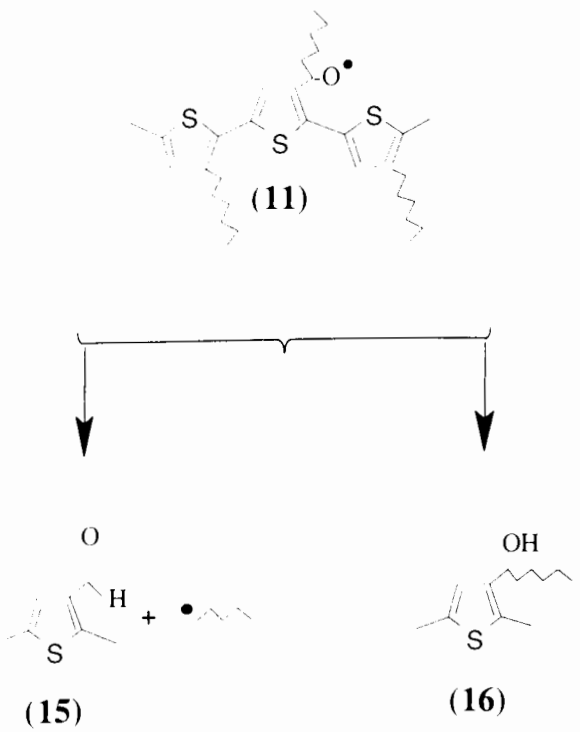

Scheme III.15

These results also provide a basis from which photochemical mechanisms in solid films of P3AT's can be deduced. The solid state photochemistry of these materials is presented below.

III.6.5.2 Solid-State Photochemistry

FTIR measurements on thin solid polymer films were used extensively to determine which chemical processes lead to an insoluble product upon irradiation. Figure III.28 shows FTIR spectra of thin films of polymer before and following irradiation in air with a polychromatic light (> 300 nm). The following new IR bands appear in the spectra following irradiation: 3400, 1743, 1610, 1230, and 1045 cm^{-1}. The band at 2962 cm^{-1} due to C-H stretching in the alkyl chain decreases with exposure time. Prolonged exposure causes this band to disappear completely. The bands at 1743, 1610, and 1045 cm^{-1} were assigned previously to C=O, C=C, and $C=S^{+}\text{-}O^{-}$ residues which result from a 1,4 Diels-Alder addition of photosensitized singlet oxygen to thienyl residues in the main chain (Scheme III.11). Kinetic studies (Figure III.29) establish that these absorption bands evolve immediately upon irradiation and that all three bands increase in intensity at relatively the same rate indicating they are the products of a common reaction pathway.

Assignment of the IR bands at 3400 (-OH), and 1230 (C-O-C), ether linkage) cm^{-1} is made by invoking a mechanism of oxidative degradation and crosslinking of the alkyl side chain in analogy to that observed in the photooxidation of polyolefins (*cf.* III.3). The mechanism of photooxidation of polyolefins, and presumably of alkyl side chains, begins with a initiation step in which an impurity, usually a transition metal ion, photosensitizes the generation of reactive free radicals. Potential photoinitiators of this process in films of P3HT are residual ferric salts originating from ferric chloride used in the polymerization of hexylthiophene. Extensive purification does not remove trace ferric salts. Even polymers purified by repeated recrystallization can contain trace Fe in the concentration range of 0.05 wt%.

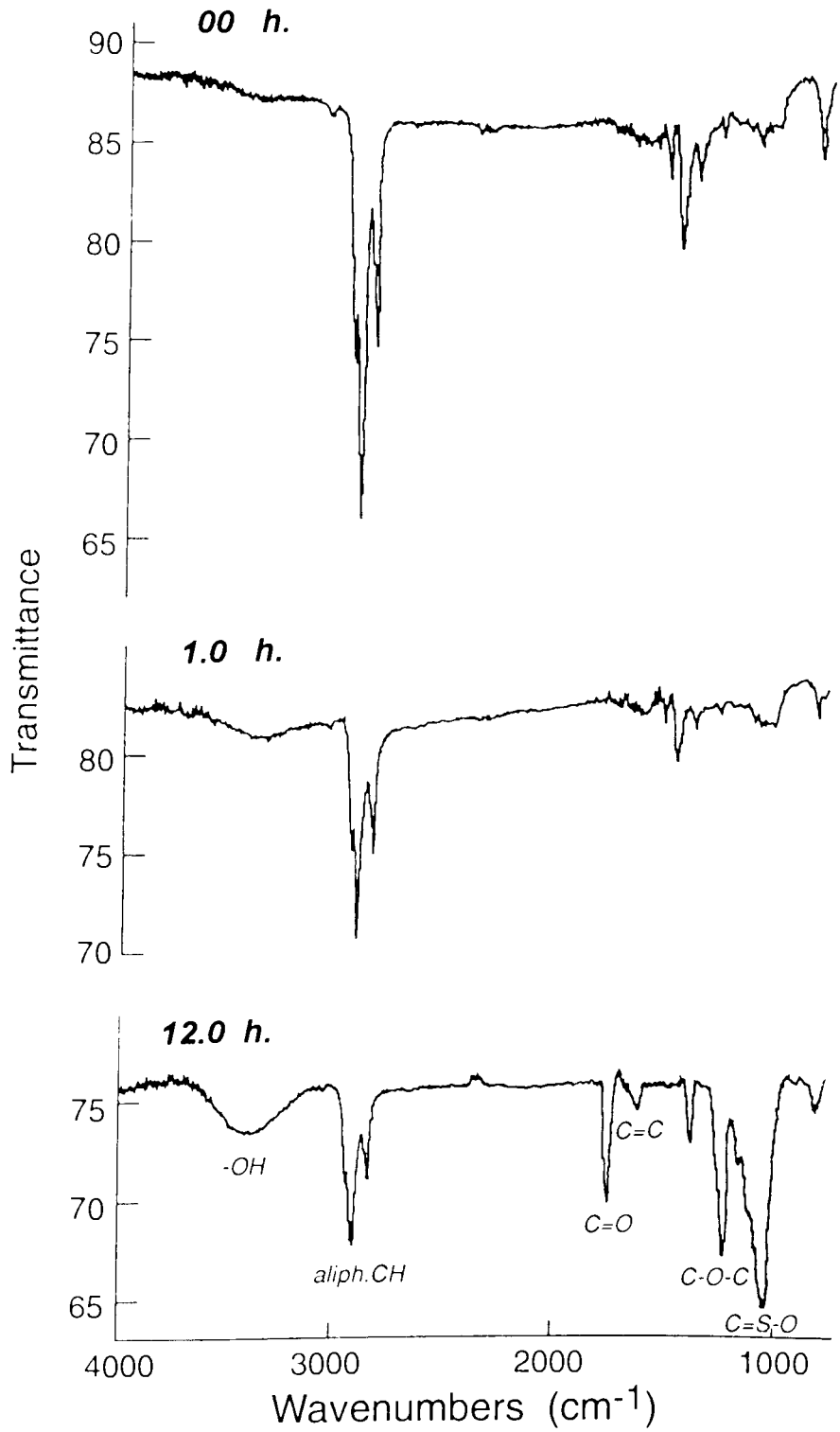

Figure III.28: FTIR spectra of P3HT films: (A) pristine polymer, (B) after 1 h irradiation, and (C) after 12 h irradiation. Irradiation in air with a polychromatic light (> 300 nm).

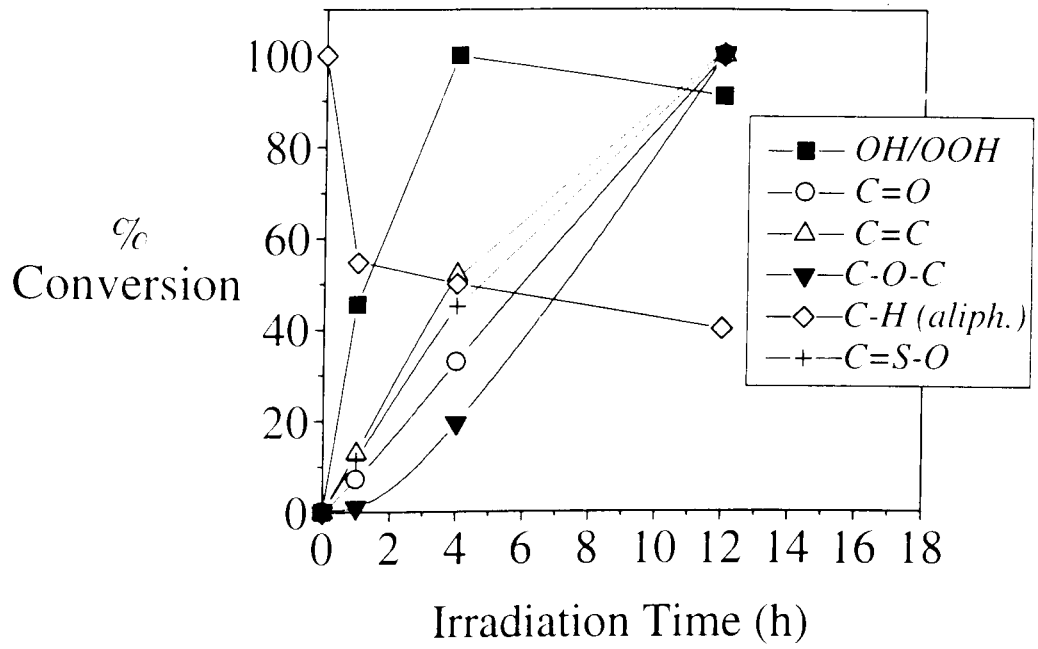

Figure III.29: Variation in intensity of IR-absorption of various functional groups of P3HT with irradiation time. Irradiation in air with a polychramatic light (>300 nm).

The primary point of attack by free radicals is the α-carbon atom of the hexyl group, which results in H-abstraction. This is based on the lower dissociation energy of the α-C-H bond (82 kcal/mol) compared to other methylenes (~95 kcal/mol) due to stabilization of the resulting radical.[147] Abstraction of a H-atom is followed by the addition of oxygen to the polymer-bound radical and the formation of hydroperoxide. The probability that alkyl radicals couple to give crosslinked polymer is low due to their low diffusion in the solid state. In contrast, the rate of oxygen addition is very high, close to the diffusion controlled limit (~ 10^9 L mol^{-1} s^{-1}).[161] Cleavage of the peroxide by the absorption of light produces alkoxy radicals which may couple with polymer-bound radicals to form ether linkages (Scheme III.16). OH radicals are also produced which may propagate the photoxidation process by abstracting a H-atom from the polymer. Dimerization of the hydroperoxides groups forms an

alternative pathway for polymer crosslinking yielding ether linkages (SchemeIII.17) (*cf.* III.3.3). Indeed, FTIR analyses of P3HT revealed the formation of ether groups following irradiation (Figure III.28).

A kinetic study of the evolution of 3400 (-OH) and 1230 (C-O-C) cm^{-1} bands (Figure III.29) supports this mechanism. The IR band at 3400 cm^{-1} reaches a steady state after only a relatively short period of irradiation. A steady state implies rate of formation of these residues is equal to their rate of depletion and is consistent with initial formation of hydroperoxide and its subsequent dimerization producing ether linkages and/or photolysis forming alkoxy radicals and OH. The band at 1230 cm^{-1} evolves only after a considerable period of time and does not reach a steady state value but continues to increase even after 12 h of photolysis indicating the functionality is the result of a secondary photochemical reaction. This is consistent with the formation of an ether linkage via the free-radical chain reaction.

The role of oxygen in photocrosslinking of P3HT was examined by photolyzing the polymer in an inert atmosphere. When thin P3HT films were irradiated in an argon atmosphere, the films remained soluble in toluene and changes in the IR spectra were minimal, even after 24 hours of photolysis. There was evidence for the formation of ketones (1760 cm^{-1}) but the relative intensity of the signal was extremely low, indicating that their concentrations were low, compared to films irradiated in air. No IR bands corresponding to C=S $\rightarrow$O or C-O-C were observed in the absence of oxygen.

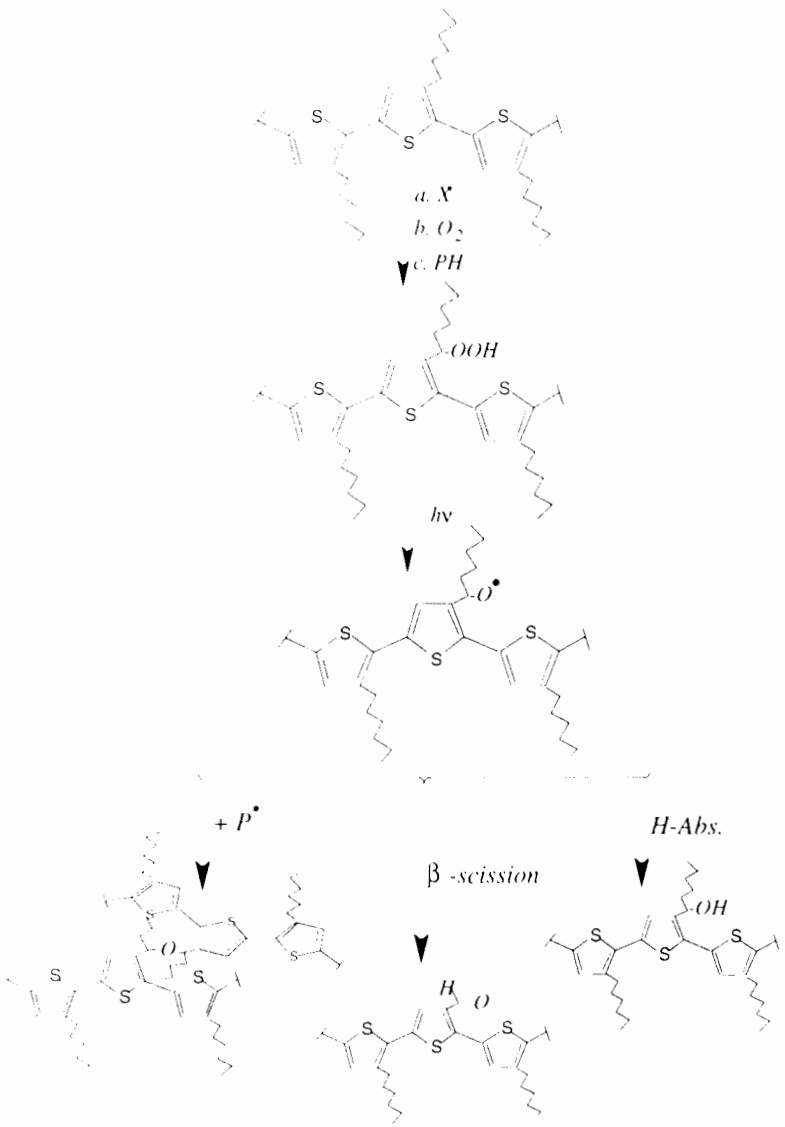

Scheme III.16

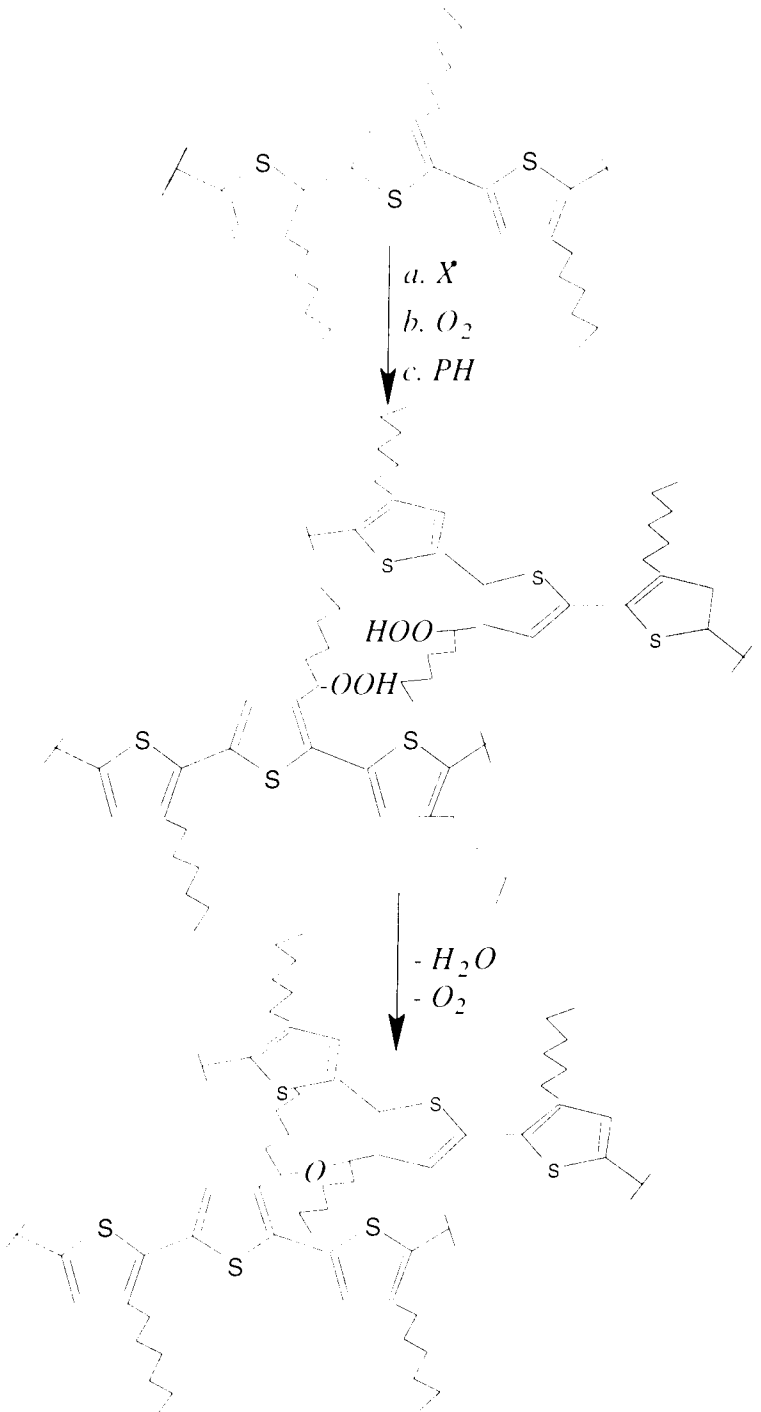

Scheme III.17

The role the alkyl substituents in the photochemistry of P3ATs was also examined. In the absence of the alkyl side chain one can anticipate that the photochemical properties will be different. Parallel studies with side chain-free, α -hexathiophene and electrochemically polymerized poly(thiophene) revealed the absence of photooxidation under the same experimental conditions used for P3HT, thus corroborating the hypothesis that the alkyl side-chain are involved in the photooxidation.

Thermal studies of poly(3-hexylthiophene) support an auto-oxidation process. Films of the polymer heated *in vacuo* at 200 °C for 15 h remained completely soluble in organic solvents. The IR spectra taken before and after thermal treatment were identical. When polymer films were heated for the same length of time and at the same temperature in an oxygen atmosphere the films were rendered insoluble. IR spectra of the films heated in oxygen exhibited almost identical absorption bands as those produced by irradiation of poly(3-hexylthiophene) in oxygen, i.e., a decrease in the intensity of the bands at ~2900 cm^{-1} (C-H), and an increase in the bands at 3400 (-OH) and 1230 cm^{-1} (C-O-C). The difference between the two IR spectra was the absence of a band at 1045 cm^{-1} ($C=S^{+}\text{-}O^{-}$) in the thermally treated sample. This IR absorption band is due to the sulfine residue which is a photochemically generated product. Indeed, photolysis of the thermally treated sample in oxygen generated this sulfine residue. It is evident that the reaction pathway involving singlet oxygen generation and Diels-Alder addition is not required for insolubilization of the polymer. The similarity of the thermal and photochemical products of poly(3-hexylthiophene) in the presence of oxygen infer similar chemical routes. It is well known from studies of polyolefins that thermal treatment in the presence of oxygen results in a auto-catalytic events beginning with H-abstraction; followed by formation of hydroperoxide; peroxide bond cleavage; and crosslinking by

ether bond formation.[162] These are essentially the same chemical events that occur in the photochemical process. The difference between the two processes is the initial H-abstraction which in one case is thermally driven, and in the other case, photochemically driven.

III.7 Conclusion

Poly(3-hexylthiophene) (P3HT) degrades in non-aqueous solvents containing dissolved molecular oxygen when irradiated with UV or visible light. Degradation takes the form of both reduced π-conjugation (photobleaching) and chain scission. The former is largely the product of photosensitization, and reaction of, singlet oxygen with thiophene moieties. Singlet oxygen reaction is believed to proceed via 1,4 Diels-Alder addition producing sulfine and unsaturated diketones. The mechanism of $^1O_2$ generation is primarily due to dissociation of an excited state charge-transfer complex between oxygen and P3HT. Chain scission occurs via free-radical chain reactions which are initiated by photolysis of residual impurities of the initiator/reagent used in polymerization of the material. Free radical attack on the alkyl-side chains results in H-abstraction. The resulting radical is resonance stabilized by the π-system to yield alkyl and thienyl radicals. In the presence of oxygen, these radicals are rapidly scavenged by molecular oxygen producing hydroperoxides. Thienyl peroxides is believed resposible for main-chain scission. Alkyl peroxides undergo β-scission and H-abstraction yielding carbonyl and hydroxyl functionalities.

In solid state, P3HT undergoes simultaneous crosslinking and chain scission when irradiated in air with a UV or vis light. The crosslinking density is ~ 4.5 times greater than the fracture (chain scission) density indicating that P3HT is a negative-type photoresist. The quantum yields of these two processes were determined using the Chalesby-Pinner theory. Although the quantum yield of crosslinking is relatively low, polymer patterns with relatively high degree of π-conjugation were achieved. The electronic conductivities of doped polymer patterns were similar to pristine polymers.

The mechanism of crosslinking and insolubilization proceeds via free-radical chain reactions which are initiated by photolysis of residual iron impurities originated from the initiator/reagent used in polymerization of the material. In the presence of oxygen, these chain reactions begin with H-abstraction; followed by formation of hydroperoxide, peroxide bond cleavage; and crosslinking by the formation of ether linkages between alkyl-side chains and thus insolubilization of the material.

Conventional photolithography and Laser, direct-write microlithography proved useful in designing three-dimensional molecular architectures of P3HT. Laser lithography gives higher resolution macromolecular P3HT wires if the processing parameters are carefully chosen. Resolution as high as 1 μm, which is the limit of laser system, was accomplished. It is believed that higher resolution could be achieved using more sophisticated lithographic systems.

The mechanisms of photodegradation of poly(3-hexylthiophenes) described in this work are believed applicable to poly(3-alkylthiophenes) in general. It appears that chain scission requires an α-CH_2 in the 3-position and would preclude poly(3-alkoxythiophenes) from exhibiting chain scission. However, photobleaching via the singlet oxygen route might still occur for these polymers.

Chapter IV: DOPING-DEDOPING BEHAVIOR OF π-CONJUGATED POLY(3-ALKYLTHIOPHENES)

IV.1 Introduction

P3AT-based macromolecular wires are semiconducting in the neutral form ($\sigma = 10^{-7}\ \Omega^{-1}\ cm^{-1}$) and doping of the polymer is necessary to achieve metallic conductivities. Unfortunately, the doped, conducting form of the material suffers from poor long-term stability and reverts back to its neutral form in a matter of hours. The reversion of the conductive form to the neutral, semiconducting counterpart is, in essence, a reductive electron transfer process. This process is commonly termed *de-doping;* and this description, while technically incorrect, is used throughout this chapter because of its common usage. Significant effort has been made towards understanding the instability of conducting P3ATs.[74,236-243] The majority of studies to date have been concerned with thermal de-doping processes. Although valuable, a complete mechanism is yet to be established.

Preliminary studies on dedoping of P3HT containing $FeCl_4^-$ dopant ion, which is reportedly the most thermally stable system, under ambient conditions have shown that ambient laboratory lighting has a dramatic effect on the stability of these polymer-dopant pairs. Thus, the rate of decrease in conductivity of $P3HT^{2+}\cdot 2FeCl_4^-$ in the absence of light was ~50 times slower than in its presence. A detailed photochemical study was undertaken to establish the mechanism of this de-doping process. Based on this study, new strategies for improving the stability of conducting P3ATs were devised. The important elements of the doping-dedoping behavior of P3ATs, and conjugated polymers in general, are discussed below.

IV.2. Energy Bands and Charge Carriers in Conducting P3ATs

IV.2.1 Doping of P3ATs

The concept of doping of conjugated polymers is different from the case of conventional inorganic semiconductors. In silicon, for instance, charge carrier generation is achieved by doping with part per million quantities of elements, such as boron (electron deficient), which fit into the silicon lattice either substitutionally or interstitially.[70] In the covalent bonding model, acceptor atoms can be visualized as shown in Figure IV.1A. A boron atom in the Si lattice has only three valence electrons to contribute to the covalent bonding, thereby leaving one bond incomplete. This gives rise to unpaired electrons which can be detected by electron spin resonance, ESR. This doping process leads to the appearance of acceptor levels associated with the boron atoms slightly above the silicon valence band. These levels are empty of electrons at 0 K (Figure IV.1B). At low temperatures, sufficient thermal energy is available to excite electrons from the valence band into the impurity level, leaving behind holes in the valence band. Acceptor impurities thus creates a semiconductor with a hole density greater than the conduction band electron density (p-type material).

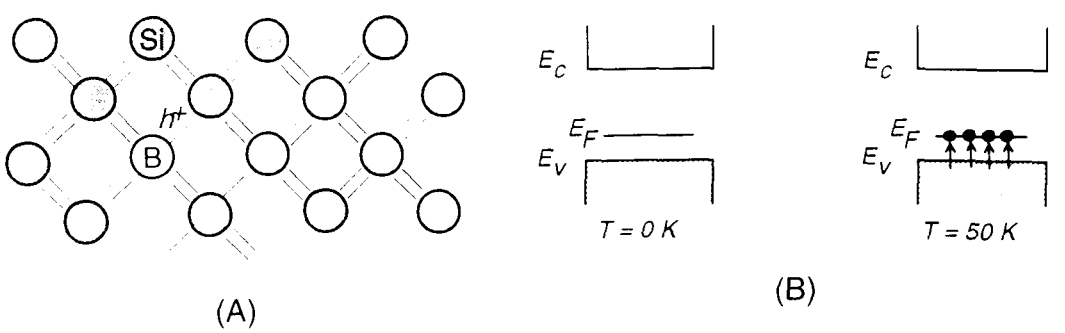

Figure IV.1: Energy band diagrams and covalent bonding model of p-doped Si

In conjugated polymers, doping is more appropriately described as a redox reaction because of the extensive charge transfer which takes place between the polymer and the dopant.[69] This process leads to incorporation into the polymer of several percent of dopant (counter ion). The term doping in conjugated polymers should thus be distinguished from that in inorganic semiconductors. Conjugated polymers can be doped by three main methods, namely; chemical (oxidizing agent, XY), electrochemical (current, i, and counter ion, X^-), and photochemical ($h\nu$, counter ion, X^-) as shown in Scheme IV.1.[69,175]

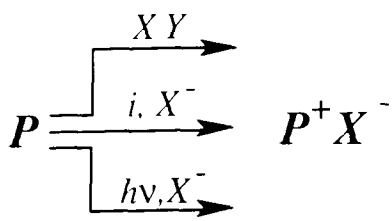

Scheme IV.1

Chemical p-type dopants include halogens, transition metal halides, and oxidizing salts of mineral acids , e.g. nitrosonium salt. Sodium naphthalide is a typical n-type dopant. Electrochemical methods allow doping with anions such as ClO_4^- , PF_6^-, or more complex species such as heparin. Photochemical doping employs photoacid generators such as triphenyl sulfonium salts.[175]

In addition to these doping methods, some polymers can self-dope.[244] The basic principle of self-doping originates from derivatization of the alkyl side chain of P3ATs with a strong protonating acid such as solfonic acids. Loss of a proton from the acid to the polymer backbone yields a p-type, self-doped polymer (Figure IV.2).

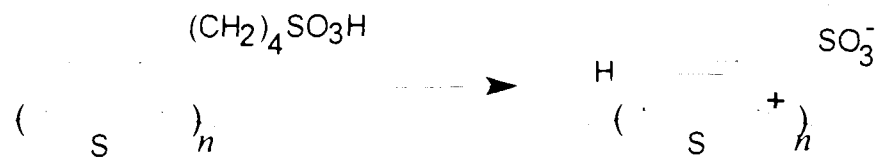

Figure IV.2: Self-doping of Poly(3-(alkylsulfonate)thiopnenes)

The nature of the dopant has a pivotal role in doped materials. It can affect morphology, mechanical properties, and more importantly, stability of the oxidized polymers.[236,245] Identification of the dopant is not always straightforward, for example, I_3^-, I_5^-, and I^- have all been observed in iodine doping of PA.[246] The nature of charge carriers associated with doped P3ATs has been explained in terms of the polaron-bipolaron theory.

IV.2.2 Polaron-Bipolaron Model[69,247,248]

The discovery that conductivity of π-conjugated polymers is associated with spinless charge carriers rather than unpaired electrons (carriers with spin 1/2) indicated that the nature of these carriers is different from conventional inorganic semiconductors. New models were required to explain the conductivity of these polymers. The soliton model was introduced by Su, Schrieffer, and Heeger in 1979.[249] The model assumes that defects (charged or uncharged carriers) in simple polyenes take the form of solitons. This model is useful for explaining the doping properties of PA, which is the only polymer known to date, that possesses a degenerate ground state. Figure IV.3 shows the two-fold degenerate ground-states of PA and the energy band diagrams of solitons.

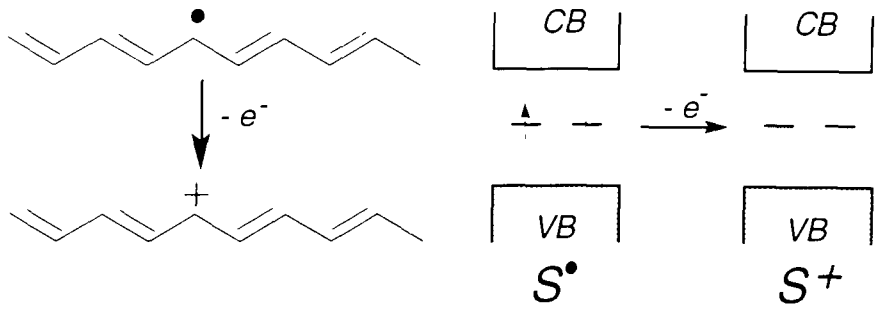

Figure IV.3: Molecular structure and energy band diagrams of soliton in PA.

Polyaromatics and heteroaromatics possess benzenoid and quinoid ground-state structures which are energetically non-equivalent. The quinoid ground-state structure is slightly higher in energy. The polaron-bipolaron model was developed to explain the doping behavior of these polymers.[69,247,248] The model assumes that oxidation of P3ATs, for example, gives rise to radical cations (spin 1/2), referred to as polaron ($P^{+\bullet}$) due to the relatively strong interaction with its molecular lattice vibration (phonon). Due to the quasi-1-D nature of the material, polaron-phonon interactions lead to generation of localized electronic states in the band gap of the polymer. These states are half-filled in case of p-type doping (Figure IV.4A). As the level of doping increases, polarons coalesce yielding spinless dications or bipolarons (BP^{2+}). BP^{2+} is associated with a stronger lattice distortion which suggests that the energy gained in this process is greater than the Coulombic repulsion energy between the two similar charges. Bipolarons are believed responsible for electronic conduction characteristics of doped P3ATs. The electronic states associated with bipolarons are empty in case of p-type doping (Figure IV.4B).

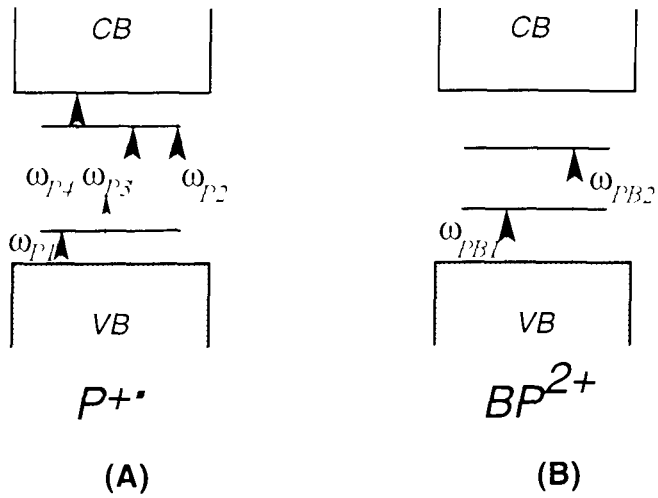

Figure IV.4: Energy band diagrams and electronic excitations of polaron and bipolaron in P3ATs

The generation of $P^{+\bullet}$ and BP^{2+} on the polymer chains upon doping can be monitored using optical and electron spin resonance spectroscopies.[250-255] ESR measurements on electrochemically-doped polythiphene have shown an initial increase in the spin density upon doping.[250,251] The spin density, as calculated from intensity of ESR signal, increases by more than two orders of magnitude up to a maximum of 2×10^{20} spins/g at a doping level of about 2-3 mol%. These data yield a spin density comparable to the number of injected charges, and are consistent with the creation of polarons. When the doping level exceeds 3 mol%, the ESR signal decreases, suggesting the formation of spinless charge carriers, bipolaron. The mechanism of bipolaron formation is believed to proceed via disproportionation of the radical cations as opposed to direct oxidation of radical cation (Figure IV.5).[256]

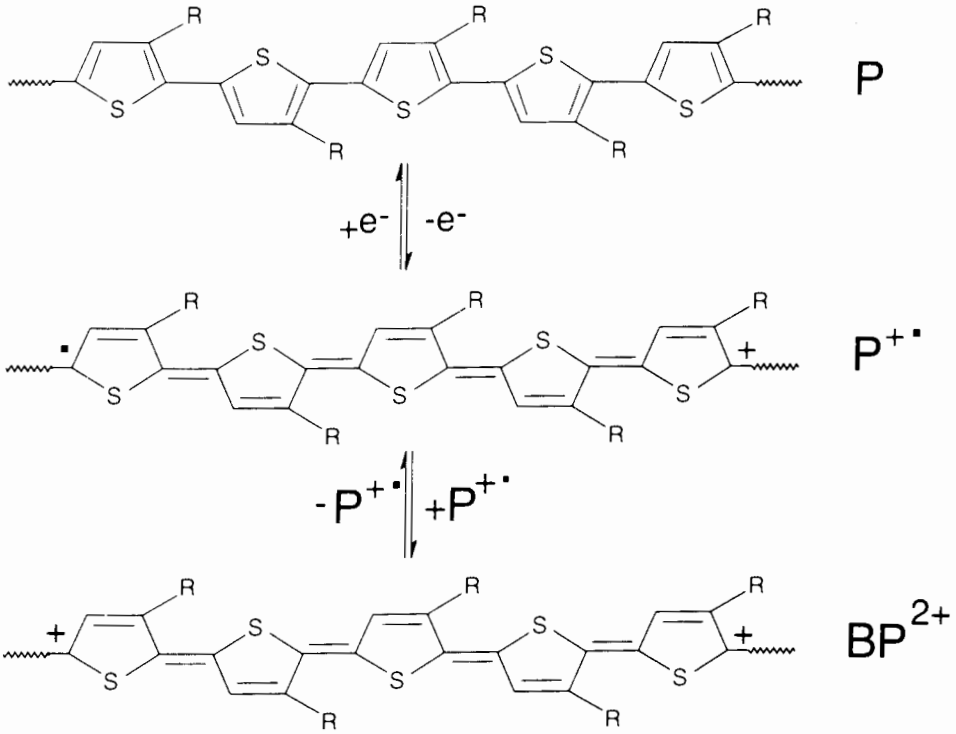

Figure IV.5: Molecular structures of polaron and bipolaron in P3ATs.

Polarons of P3ATs show three electronic transitions at 0.6, 1.3, and 1.5-1.8 eV (broad transition) which can be assigned to ω_{P1}, ω_{P2}, and ω_{P3}-ω_{P4} (Figure IV.4A).[252-255] In PTs, polarons have been detected at very low doping levels (≤ 3 mol%). At moderate and high doping levels bipolaron formation predominates. BP^{2+} has two electronic transitions; 0.65-0.70 (ω_{BP1}) and 1.5 (ω_{BP2}) eV (Figure IV.4B).

The band diagram of a bipolaron (Figure IV.4B) implies that [254]

$$\omega_{BP1} + \omega_{BP2} = E_g \qquad \text{(IV.1)}$$

Since a bipolaron is a doubly charged species, equation IV.1 was extended to account for the coulombic repulsion energy, U_B, between the associated charges. Thus

$$\omega_{BP1} + \omega_{BP2} = E_g - 2U_B \qquad \text{(IV.2)}$$

For polythiophene, bipolarons generated by photoexcitation are associated with two localized electronic states at 0.45 and 1.25 eV.[257] Accordingly, U_B was estimated to be ~0.25 eV, assuming a band gap, E_g, of 2.2 eV. However, the sum of the electronic transition energies for doping-induced bipolarons, in some cases, is ~2.32 eV, which is greater than E_g. Changes in the optical transition energies were attributed to interactions between charge carriers on the polymer chains (bipolarons) and counter ions introduced upon chemical doping. Equation IV.2 was further modified to account for these interactions in terms of the relation

$$\omega_{BP1} + \omega_{BP2} = E_g - 2(U_B - E_b) \qquad \text{(IV.3)}$$

where E_b is the binding energy of charged bipolarons to the counter ions. Optical absorption measurements in combination with equation IV.3 can thus be used for the determination of binding energies of counter ions.

IV.2.3 Electronic versus Ionic Conduction

Electronic conduction in doped polymers has been examined by Hall effect measurements.[258,259] The Hall coefficient is an important parameter because it yields values for the sign and concentration of charge carriers. Hall effect measurements conducted on PA and PPP have shown a positive coefficient for acceptor-doped polymers indicating that positively charged carriers are responsible for the observed conductivity. This proved that the electrical properties of conducting polymers are electronic in nature and charge transport occurs via the organic conductor.

IV.3 De-doping Behavior of P3ATs

IV.3.1 Polymer-Dopant Interactions

The electrostatic interaction between polymer charge carriers "bipolaron" and dopant ions has been studied by quantum chemical calculations.[260] The calculation employed dimers of thiophene, pyrrole and benzene with X^- being the dopant. For polythiophenes, it was predicted on the basis of electrostatic interaction between the dopant ion and polymer backbone that the most stable structure was one in which the two ions are centrosymetrically above and below the molecular plane. The calculations attempted to explain the lower thermal stability of doped poly(3-alkylthiophenes) compared to the parent polythiophene in terms of steric interactions of the bulky-side chains with the counter ions. The following mechanism was invoked. At relatively high temperatures, the alkyl side chains push the counter ion from its perpendicular position of stronger interaction towards a constrained situation of lower stability.

The location of the dopant and structural transformation accompanying doping of P3ATs has been studied by X-ray diffraction.[261,262] In a study conducted on chemical doping of P3ATs with iodine, it was found that, in contrast with the theoretical calculation, the dopant lies to the side of the main-chain stacks.[261] It was also demonstrated that iodide (I_3^-) which is a linear species (3.37 Å-diameter, 10.12 Å-length), has only a slight influence on the average interlayer chain-to-chain spacing. It should be noted, however, that the study was performed on poly(3-octylthiophene) and poly(3-dodecylthiophene) with long alkyl side chains of 8 and 12 carbon atoms, respectively.

In a similar study, it has been shown that structural transformation of the polymer upon doping depends on both the length of the alkyl-side chains and geometry of the dopant ions.[262] The model assumes the existence of a hexahedral vacant space (voids) in the crystal lattice of the polymer in which the

dopant is located. In contrast to P3OT, it was demonstrated that incorporation of BF_4^- into the crystal structure of P3BuT changed its crystallographic parameters. Accordingly, it was concluded that in P3ATs with long alkyl side chain (*hexyl and longer*), the size of the voids are sufficiently large to accommodate dopant ions such as BF_4^- whereas in P3ATs with chains shorter than butyl, space has to be made to accommodate the dopant ion. It has also been anticipated using this model, that thermal instability of P3ATs is derived by elimination of the dopant ions in order to relax the crystal structure.

IV.3.2 Diffusion and Distribution Profile of Dopants

The mechanism of diffusion of dopant and its distribution profile in doped polymers are important for understanding their doping-dedoping behavior. These two concepts have been demonstrated using the parent polymer PA and $FeCl_3$ and I_2 dopants.

Gravimetric methods using electromagnetic balance have been used to study diffusion.[263] The method is capable of continuous measurement of weight uptake of the dopant by the polymer as a function of time. From such correlations, the diffusion coefficient of the dopant were determined. The diffusion coefficient for $FeCl_4^-$ in PA at 25 ^oC is in the order of $\sim 10^{-18}$ cm^2 s^{-1}. The diffusion coefficient for iodine is greater by a factor of 100 ($\sim 10^{-16}$ cm^2 s^{-1}). The activation energies of diffusion were determined to be 1.0 and 0.2 eV for $FeCl_4^-$ and iodine, respectively. It has been proposed that diffusion of dopant ions into PA occurs via a three-step mechanism: 1) diffusion of the dopant molecules to the polymer surface, 2) adsorption of the dopant at the surface, and 3) solid state diffusion into the bulk. The last step was assumed rate-limiting. This model suffers from several drawbacks, including the fact that chemical reactions associated with diffusion were not considered.

The distribution profile of dopant ions in conducting polymers have been investigated by several techniques. ESR spectroscopy has been used to investigate the distribution profile of $FeCl_4^-$ in PA by monitoring changes in both line width and shape of the ESR signal following doping.[264] It has been shown that the distribution profile depends on the doping level. At low doping levels, the dopant is concentrated near the exposed film surface. As the doping level increases, the distribution profile becomes more uniform.

IV.3.3 Mechanism of Thermal De-doping

The majority of studies to date have been concerned with thermal instability of conducting polymers. A summary of the proposed mechanisms of thermal de-doping of conducting P3ATs are presented below.

Thermal stability of conducting P3ATs has been found to be highly dependent on the nature of the counter ion (X^-), as determined *qualitatively* using conductivity measurements.[239,241] In general, the rate of conductivity degradation of $BP^{2+}.2X^-$ ion pairs in the temperature range 25-100 ^oC is found to decrease in the order $FeCl_4^- < BF_4^- < I_3^-$.[238-241] Atmospheric conditions have a major influence on the stability. The presence of water vapor increases the rate of degradation of $BP^{2+}.2FeCl_4^-$ ion pairs at 80 ^oC by a factor of 5.[239b] The stability is also dependent on the length of the alkyl side chains and increases in the order P3BuT > P3HT > P3OT. The activation energies of thermal degradation lie in the range 10-30 kcal/mol.

Quantitative analyses of the thermal de-doping processes using kinetic models derived for homogeneous systems have been hampered by the non-linear response of doped materials.[239-241] Multiple conductivity degradation mechanisms and multi-order reaction kinetics have been invoked for these non-linear responses. William-Landell-Ferry, WLF, expressions which were originally

derived to describe free volume changes in macromolecules, have been adopted to model the reaction dynamics.[240b] Although they explained the kinetics of the de-doping of the $P3OT^{2+}.2FeCl_4^-$ system, WLF expressions failed to account for the de-doping of the $P3BuT^{2+}.2FeCl_4^-$ system which was investigated by the same group.

Changes in the nature of the dopant accompanying thermal de-doping has been studied by spectroscopic techniques. Mössbauer measurements have shown that exposure of $BP^{2+}.2FeCl_4^-$ ion pairs to ambient conditions results in a transformation of $FeCl_4^-$ into $FeCl_2$, in addition to normal de-doping process.[265] This was attributed to interaction of water with both the polymer and the counter ion. The origin and mechanism of the process were not, however, discussed. XPS studies have shown that the chemical nature of $FeCl_4^-$ did not change when doped polymer samples ($BP^{2+}.2FeCl_4^-$) were stored under ultra high vacuum conditions at 110 ^oC even after 26 h.[240a] Increasing the temperature of the sample to 195 ^oC resulted in slight changes. The authors have explained such changes as being due to the formation of $FeCl_2$ which results from de-doping of the material.

Thermal de-doping of P3ATs has been rationalized in terms of an equilibrium between rigid, coplanar chains in the oxidized form and flexible, non-planar chains in the neutral state.[239-241] At high temperatures, the equilibrium shifts in favor of the less planar conformation and the oxidized polymer reverts back to its undoped state.

Based on these mechanisms, several strategies for improving the stability of conducting polymers have been suggested. These strategies were based on two proposals: 1) creation of a "space" in the polymer to accommodate the dopant ions,[243b] and 2) suppression of the polymer chain flexibility.[243a,c,d] Polythiophene-copolymers containing a long and short alkyl chains, such as 3-

octylthiophene-3-methylthiophene copolymer have been used to examine the first proposal.[243b] This approach was unsuccessful in improving the stability and rates of conductivity degradation were comparable to doped P3HT and P3OT. Suppression of polymer chain flexibility by blending of P3ATs with crosslinkable polymers have been attempted.[243c,d] Although chain mobility was lowered, as shown by DSC measurements, rates of conductivity degradation at 120 ^{o}C in air, for example, were decreased only by a factor of 1.8 compared to pure polymers.[243d]

IV.4 Experimental

Polymer. Polymers used in this study were prepared by oxidative-coupling according to the procedure described in Chapter II. The polymer had number average molecular weight, M_n, and a molecular weight distribution of 8,500 and ~3, respectively. The head-to-tail:head-to-head dyad ratio was 80:20, as determined by ^{1}H NMR. In solid films, λ_{max} was 500 nm. The concentration of iron in polymers was 0.05 wt% as determined by atomic absorption. The oxidation state of this iron species was +3 as determined by Mössbauer spectroscopy. Iron free polymer was prepared by electrochemical polymerization and was used for Mössbauer measurements and as a control for the analytical determination of Fe and Cl.

Chemicals. Anhydrous ferric chloride (BDH Chemicals), gold trichloride (Aldrich Chem.) and ammonia solution (BDH) were used as received. Solvents including chloroform (Caledon, spec. grade), acetonitrile (BDH, Spec. grade), and nitromethane (BDH, Spec. grade) were dryed under N_2. $(Et_4N)_2FeCl_2$ was prepared by mixing methanol solutions of Et_4NCl and $FeCl_2$ in a 2:1 ratio under a nitrogen blanket.[266]

Instrumentation:

Mössbauer. Mössbauer spectroscopy was used to determine the nature of the iron chloride dopant before and after photolysis. Details of measuring procedures are described in Chapter II. Acquisition time of each run was 10 days. Absorbers, containing ca. 80 mg of polymer sample, were mounted in Teflon holders in oxygen-free nitrogen, and the cross-sectional area of the sample was 2 cm^2. Samples photolysed *in vacuo* were transferred in a dry box into the Teflon holder and sealed with silicon grease. The isomer shifts are quoted with respect to iron metal as a reference.

Humidity. Humidity was measured using a hygro-thermograph (Friez Instruments, USA) which is capable of simultaneous recording of both the relative humidity and air temperature.

Electrochemistry. The redox potentials of P3ATs were determined electrochemically using a PAR 170 electrochemistry system.[267] The measurements were performed in a three-electrode cell equipped with saturated calomel reference electrode (SCE), and a Pt foil auxiliary electrode. The working electrode was made by casting a thin polymer film (0.2 μm) onto platinum disk (0.07 cm^2). A solution of tetrabutylammonium perchlorate (0.1M) in acetonitrile was used as electrolyte. Cyclic voltammogram of the polymer was recorded by scanning the potential from -0.2 to +1.6 V at a scan rate of 20 mV/s. The standard electrochemical potential of $FeCl_4^-/FeCl_4^{2-}$ system was determined from its voltammetry using Pt-working electrode.

Four-point probe method. Conductivity of doped polymer films were measured by co-linear four-point probe method.[268] The technique utilizes four-linear, equi-spaced point-probes (Figure IV.6). When the area of contact is small (point-contacts) and the spacing between the probes, s_P, is much larger than the thickness of the sample, l, and the conductivity is given by

$$\sigma = \frac{ln\,2}{\pi\, l}\,\frac{i}{V} \qquad \text{(IV.4)}$$

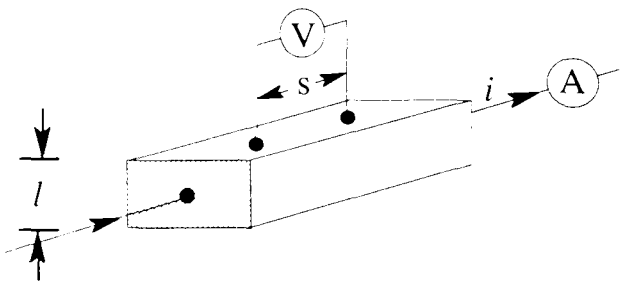

Figure IV.6: Co-linear four point-probe.

i represent the current passing though the two outer probes and V is the potential drop across the two inner probes.

Surface Analysis.[269,270] Surface analysis by electron spectroscopy for chemical analysis (ESCA) involves irradiation of a solid *in vacuo* with monoenergetic soft X-ray followed by analysis of the emitted electron energy. The X-ray photons have a limited penetration power and interact with atoms at the solid's surface. These interactions result in emission of a core electron (photo-electron), creating a vacancy in the inner orbitals of the atom. Upon relaxation, an outer electron falls into the inner orbital vacancy, and a second electron (Auger electron) is emitted carrying off the excess energy. Photoionization, thus, leads to emission of two electrons, a photoelectron and an Auger electron. Figure IV.7 shows a comparison between these two processes.

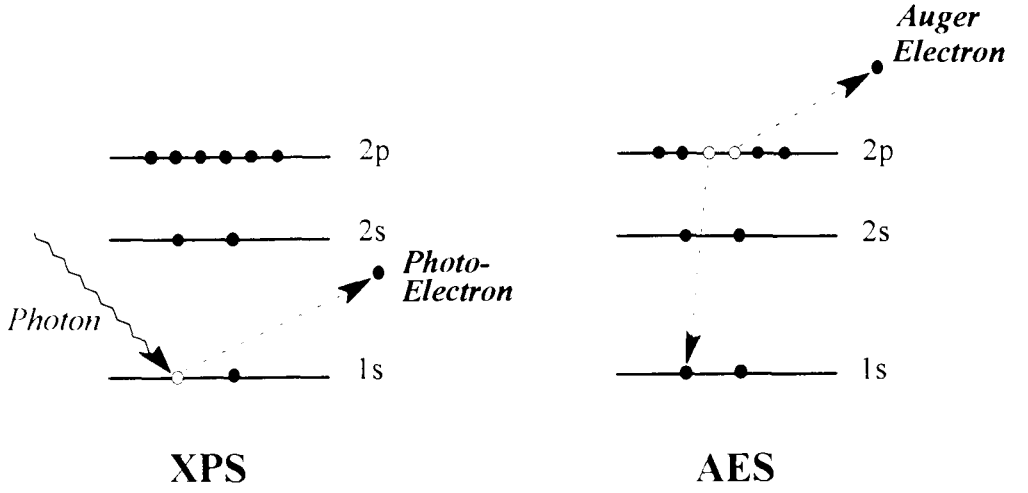

Figure IV.7: Photoelectron and Auger electron emissions.

The information obtained from X-ray photoelectron spectroscopy (XPS) and Auger-electron spectroscopy (AES) are different. XPS depends on the binding energy of one shell, while Auger data are dependent on the behavior of three shells. In AES, the binding energy is related essentially to the valence

shell orbitals which are characteristic of the molecule or solid as a whole. With core electron, binding energy changes in unison with alternation of the oxidation state and chemical environment of the material. XPS is thus useful for identification of elements and their oxidation states while AES is limited only for elemental description. Since the mean free path of electrons in solids is very small, the detected electron originates from only few atomic layers (~5-10 Å) at the surface.

XPS was used to determine the oxidation state of the gold species of the oxidized polymer films at various levels of doping. Both the polymer/solution and polymer/substrate interfaces were examined. Elements and their oxidation states were identified from their XPS core energies: Cl-$2p_{3/2}$ (198.5, Δ=1.60 eV), C-1s (284.5 eV), and S-$2p_{3/2}$ (164.0, Δ 1.18 eV).[271] The binding energy of Au-$4f_{7/2}$ depends on its oxidation state: Au(0) is 83.6 eV, Au(I) ~85 eV, and Au(III) is ~86 eV with a separation energy, Δ, between $4f_{7/2}$ and $4f_{5/2}$ of ~3.6 eV.[302] The binding energies were referenced to the Au-$4f_{7/2}$ binding energy of a vacuum deposited gold, taken as 83.6 eV.

XPS spectra were obtained using an AEI ES200B spectrometer with a Mg Kα X-ray excitation source (1253.6 eV line). The oxidized polymer samples were held under vacuum (10^{-10} Torr) for 2 h before measurements in order to remove surface contaminations adsorbed during sample preparation and transfer. The operating pressure was also 10^{-10} Torr. Data were collected using IBM software. The curve fitting and deconvolution were carried out using a nonlinear least-square curve fitting program with a Gaussian function. The actual data is represented by symbols while fitting is represented by lines.

AES was performed using a Perkin-Elemer 595 Scanning Auger microprobe. This technique was employed to investigate the concentration profile of the gold species in the direction perpendicular to the plane of the

sample (i.e. depth profile). AES spectra were obtained using a primary Auger current density of 35 mA/cm^2 and a 3 keV electron energy. For depth profile analysis, sputtering with Ar^+ was used at a beam energy of 1keV. During the measurements, the operating pressure was 10^{-9} Torr. Elements were identified from their Auger energies: Au (69 eV), S (152 eV), Cl (181 eV), and C (272 eV).[272] XPS and Auger measurements were carried out with assistance of K. Myrtle of the Department of Physics, Simon Fraser University.

Chemical Doping. Thin films of *P3HT* (0.25 μm), spin-cast onto quartz slides from chloroform solutions (2000 rpm, 30 s), were oxidatively doped using solutions of $FeCl_3$ (0.1M) in dry nitromethane. The doped samples were washed with nitromethane and dried under vacuum in the dark. The level of doping was determined by elemental analysis and mass uptake measurements to be ~24 mol% based on repeating thienyl units. Tetrahedral $FeCl_4^-$ is the dominant iron species incorporated in the polymer following oxidation. This assertion is made on the basis of elemental analysis (*Fe:Cl* = 1:4); UV-vis-NIR spectroscopy (λ_{max}: 240, 316 & 368 nm);[273] and Mössbauer spectroscopy (quadrupole doublet: isomer shift, δ, of 0.253 mm s^{-1} and quadrupole splitting, Δ, of 0.284 mm s^{-1})[107,274].

The mechanism of oxidation of *P3HT* is shown in the following scheme:[275]

$$P3HT + 4FeCl_3 \longrightarrow BP^{2+} \cdot 2FeCl_4^- + 2FeCl_2 \qquad \text{(IV.5)}$$

where BP^{2+} represents the bipolaronic charge carriers. $FeCl_2$ formed during the course of the oxidation process precipitates from solution.[263] Mössbauer spectroscopy of doped polymers indicated the absence of iron (II).[276] Electronic conductivities were measured on thin films by the four-point-probe technique.

IV.5 Results and Discussion

IV.5.1 Photochemical Stability of Conducting P3ATs

Photolytically-induced decrease in conductivity. Oxidized, conducting films of *P3HT* (σ~6 S/cm) were exposed to ambient laboratory lighting. Figure IV.8 shows pseudo first-order kinetic plots for the decrease in conductivity of oxidized polymer films with time. By comparison the rate of decrease in conductivity in the absence of light is ~50 times slower. The half-life time values, $t_{1/2}$, are given in Table IV.1. This preliminary result illustrates the dramatic effect of light on the stability of *P3HT-$FeCl_4^-$*.

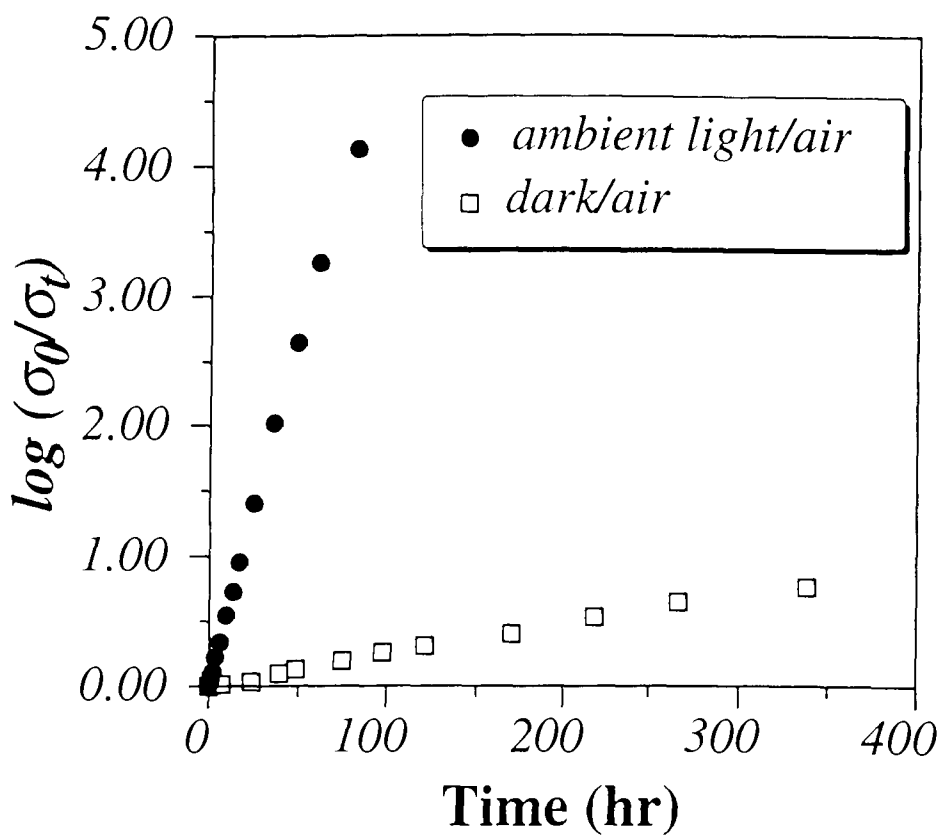

Figure IV.8: Decrease in σ of *P3HT-$FeCl_4^-$* films during exposure to ambient light.

Table IV.1: Effect of irradiation on the decrease in conductivity of oxidized poly(3-hexylthiophene)-$FeCl_4^-$ films[a]

Conditions[b]	$t_{1/2}$ (min)[c]
ambient light/air[d]	114
366 nm/air	0.9
435 nm/air	40
580 nm/air	5790
dark/air	5830

a film thickness: 0.25 μm, 298 K;

b Relative humidity of ambient air: 25;

c half life of conductivity. Data for 366, 435, and 580 nm were determined using comparable light intensities.

d Fluorescent lighting

The photochemical stability of the polymer-counter ion pair was studied using 366, 435, and 580 nm monochromatic light. Figure IV.9 shows the change in conductivity with irradiation time in air using 366 and 435 nm monochromatic light. $t_{1/2}$ values for the decrease in conductivity are 0.9 min and 40 min respectively for incident intensities normalized to the irradiation dose. Degradation using 366 nm light is 44 times greater than with 435 nm light.[277] The optical density of $FeCl_4^-$ at 366 nm is 47 times larger than at 435 nm which might account for the difference if direct excitation of $FeCl_4^-$ is responsible for photodegradation. Irradiation with 580 nm light did not lead to photodegradation. At this wavelength, light is absorbed only by polymer charge carriers; the

extinction coefficient of $FeCl_4^-$ is zero. This is direct evidence that photodegradation is primarily due to excitation of the counter ion.

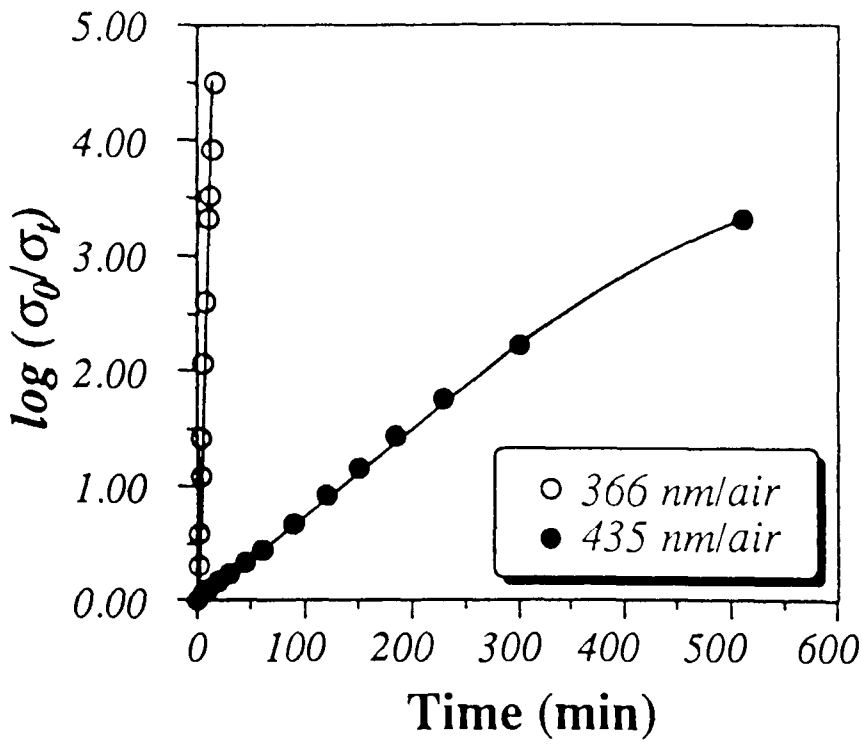

Figure IV.9: Effect of irradiation wavelength on the photochemical degradation of σ of *P3HT-$FeCl_4^-$* films.

Irradiation of doped films with 366 nm light was also conducted under various atmospheres; namely, ambient air (relative humidity, RH, 25%), dry O_2, and *in vacuo*. $t_{1/2}$ values, calculated from pseudo-first order kinetic plots, are given in Table IV.2. Moisture clearly accelerates photochemical degradation.

Table IV.2: Effect of Ambient Conditions on Photochemical de-doping of poly(3-hexylthiophene)-$FeCl_4^-$ films[a]

Conditions	$t_{1/2}$ (min)[b]
laboratory air[c]	0.9
humidified O_2[d]	1.4
dry O_2	3.3
vacuum	5.1

[a] Incident wavelength: 366 nm (I_0=1.4 mW/cm^2). film thickness: 0.25 μm, 298 K;

[b] half life of conductivity;

[c] Relative humidity =25;

[d] Relative humidity: 15

Spectroscopic analysis: (i) UV-vis-NIR The photochemistry of $BP^{2+}.2FeCl_4^-$ was studied in detail in order to understand the photolytic de-doping processes. Doped polymers show the characteristic bipolaronic electronic transitions at 780 and ~1750 nm[252-255] (Figure IV.10), in addition to absorption bands at 240, 316 and 368 nm due to $FeCl_4^-$.[273] The change in UV-vis-NIR absorption spectra of oxidized polymer films exposed to 366 nm light in ambient air is also shown in Figure IV.10. The absorption bands due to $FeCl_4^-$ decrease, indicating loss of $FeCl_4^-$. A broad band emerges at ~485 nm due to the π-π^* transition of the neutral polymer. Bipolaron absorption bands at 780 and ~1750

nm concurrently decrease. The spectra evolve in a similar manner when either 435 nm monochromatic irradiation or ambient light is employed.

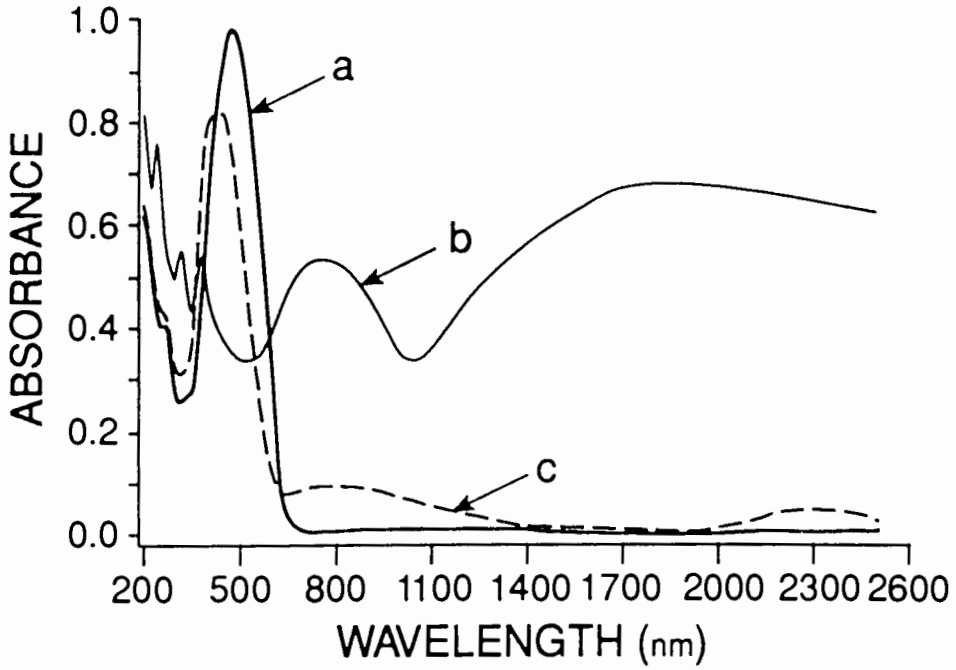

Figure IV.10: UV-vis-NIR spectra of oxidized P3HT films under ambient atmosphere: (a) pristine, neutral polymer; (b) oxidized polymer; (c) following irradiation with a 366 nm light.

Kinetic analysis shows that the bipolaron concentration decreases in a pseudo-first order manner during photolysis. A plot of optical density at 780 and 485 nm *versus* irradiation time in shown in Figure IV.11. In contrast, the rate of

loss of $FeCl_4^-$ is not first order. Loss of $FeCl_4^-$ is much slower during the initial stages of photolysis. Prolonged photolysis leads to the complete disappearance of $FeCl_4^-$. Mössbauer spectroscopic measurements on photolyzed samples in air yields a doublet resonance with δ = 0.42 mm s^{-1} & Δ = 0.60 mm s^{-1} indicative of an octahedral iron(III) complex.[107,278] Elemental analysis of photolyzed samples yields a molar Fe:Cl ratio of 1:1.6, which indicates loss of Cl during photolysis.

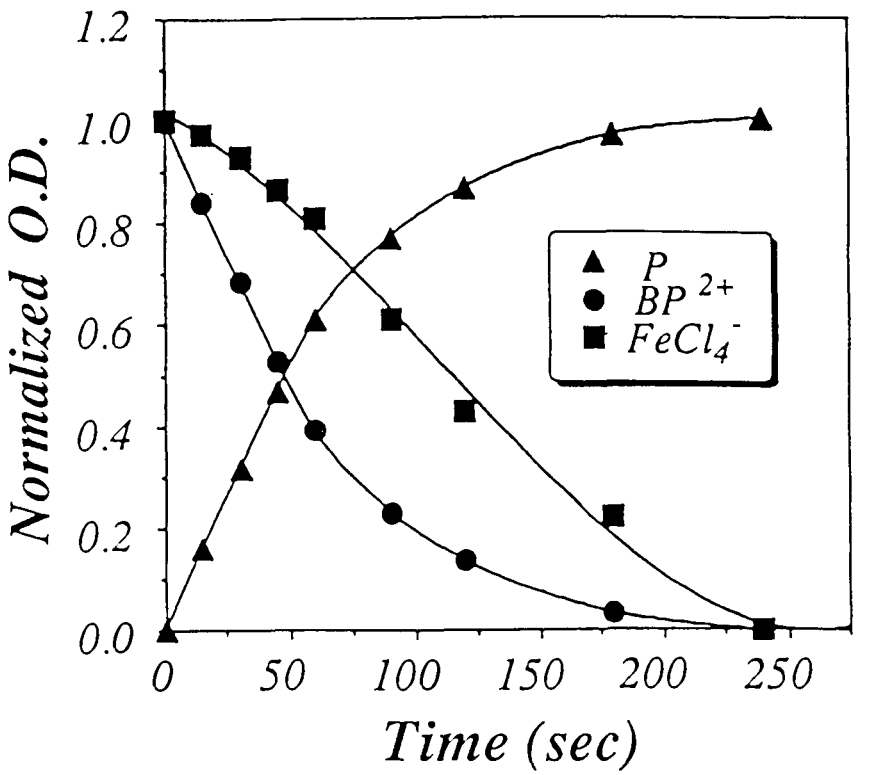

Figure IV.11: Kinetic plots of the decrease of optical density of *P3HT-$FeCl_4^-$* films with irradiation time. Irradiation at 366 nm under ambient conditions.

(**ii) FTIR**. FTIR was used to probe chemical changes of the polymer chain as a result of irradiation. Chemical doping results in a broad absorption in the IR region 4000-600 cm^{-1}. Figure IV.12 shows FTIR spectra of doped films prior to photolysis and following photolysis. Steady state FTIR spectra were obtained after 15 min photolysis, beyond which prolonged photolysis resulted in no additional spectral change. It should also be noted that no additional decrease in conductivity (σ ~10^{-5} *S/cm*) was observed following this extended period of photolysis. The persistent broad FTIR spectrum is attributed to residual charge carriers. Photolyzed films were therefore subjected to a reducing atmosphere of ammonia gas following irradiation in order to compensate residual polaronic and bipolaronic species and enable examination the chemical nature of the polymer chain following photolysis.[279] The reduced, photolyzed polymer acquired a new IR band at 1667 cm^{-1} (*-C=O)* and a broad band at 3400 cm^{-1} (*-OH*) relative to the pristine polymer, in addition to those associated with NH_4^+ (1414, 3050, 3145 cm^{-1}).[108] Noteworthy is the reduction in intensity of the C-H stretching at ~2900 cm^{-1}. This will be discussed later in this Chapter as being evidence for reactions involving the alkyl side chain.

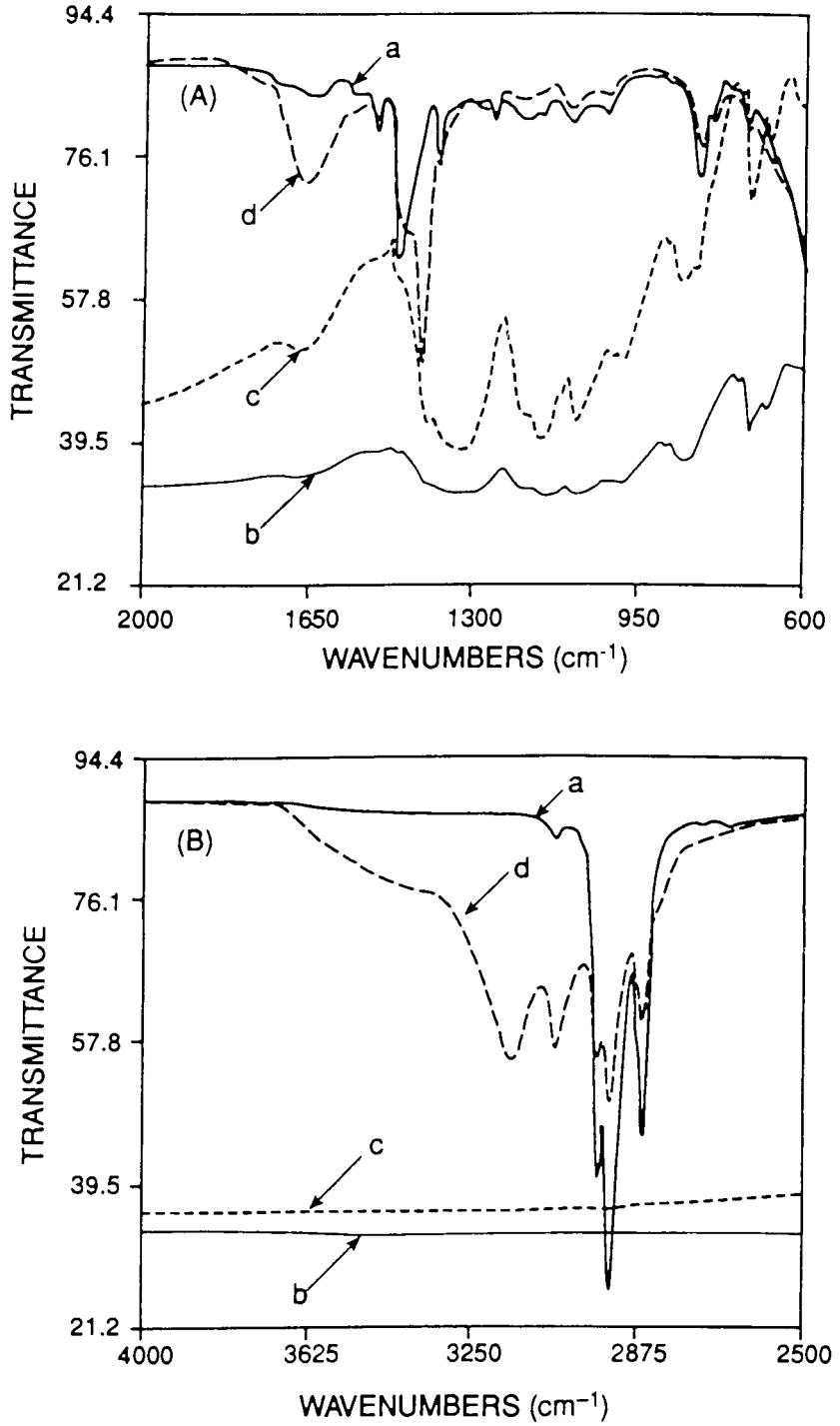

Figure IV.12: FTIR (A,B) of P3HT films on KBr disks. (a) pristine, neutral polymer,; (b) oxidized polymer; (c) following irradiation; (d) same as in c but after complete chemical reduction with ammonia vapor. Irradiation wavelength 366 nm, ambient atmosphere.

Photochemistry *in Vacuo*: Evidence of an $FeCl_4^{2-}$ intermediate. Results obtained from the decrease in conductivity as a function of the wavelength of incident light indicates photodegradation results from direct photolysis of $FeCl_4^-$. Indeed, in the presence of moisture this anion is known to undergo photoreduction:[280,281]

$$FeCl_4^-(H_2O) \xrightarrow{h\nu} [FeCl_4^{2-} + (HOH)^{+\bullet}] \rightarrow H^+FeCl_4^{2-} + {}^{\bullet}OH \qquad \text{(IV.6)}$$

It is known that Fe(II) salts oxidize to Fe(III) in the presence of oxygen.[282] Thus in order to determine whether Fe(II) is indeed an intermediate, photolyses were carried out *in vacuo*. Figure IV.13 shows UV-vis-NIR spectra of photochemically de-doped polymer films using 366 nm light under vacuum.

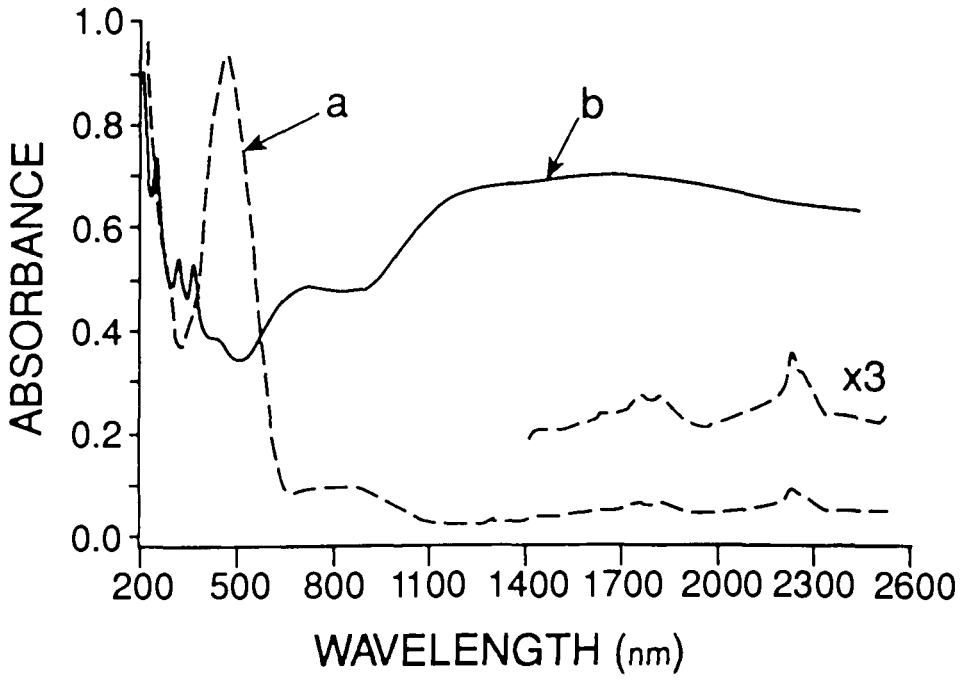

Figure IV.13: UV-vis-NIR spectra (a)of oxidized P3HT films following irradiation with a 366 nm light *in vacuo* and (b) following exposure of photochemically reduced $P3HT\text{-}FeCl_4^-$ films to dry oxygen.

A new absorption band is observed at ~2240 nm which is consistent with tetrahedral $FeCl_4^{2-}$.[283] Mössbauer analysis of the photolyzed sample confirmed the presence of Fe(II) (quadrupole doublet: δ=0.985 mm s^{-1} & Δ=1.623 mm s^{-1}) (Figure IV.14).[107,284]

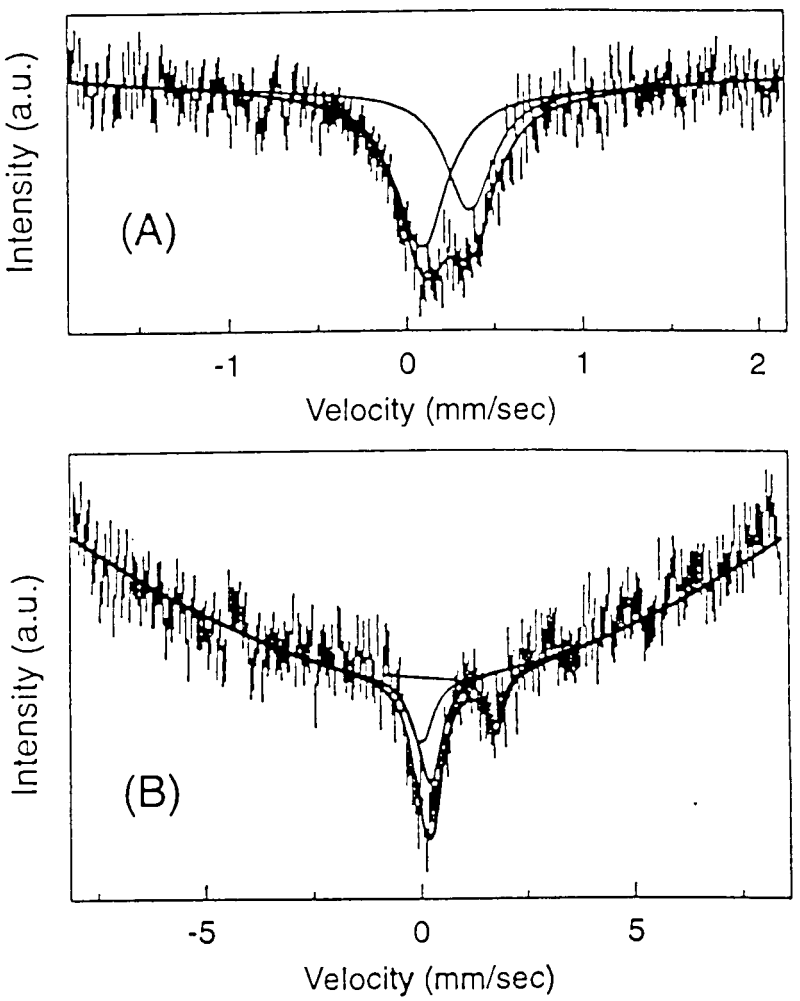

Figure IV.14: Mössbauer spectra of *P3HT-$FeCl_4^-$* films (77 K). (A) oxidized polymer; (B) following irradiation at 366 nm *in vacuo*.

Similarly to photolysis under ambient atmosphere the bipolaron concentration decreases in a pseudo-first order manner during photolysis, whereas the rate of loss of $FeCl_4^-$ is not first order (Figure IV.15). Initially the concentration of $FeCl_4^-$ remains constant even though polymer is being reduced from its oxidized to neutral form. After prolonged photolysis $FeCl_4^-$ also disappears. The nature of these kinetics and the information they provide on the mechanism of photolysis is discussed later.

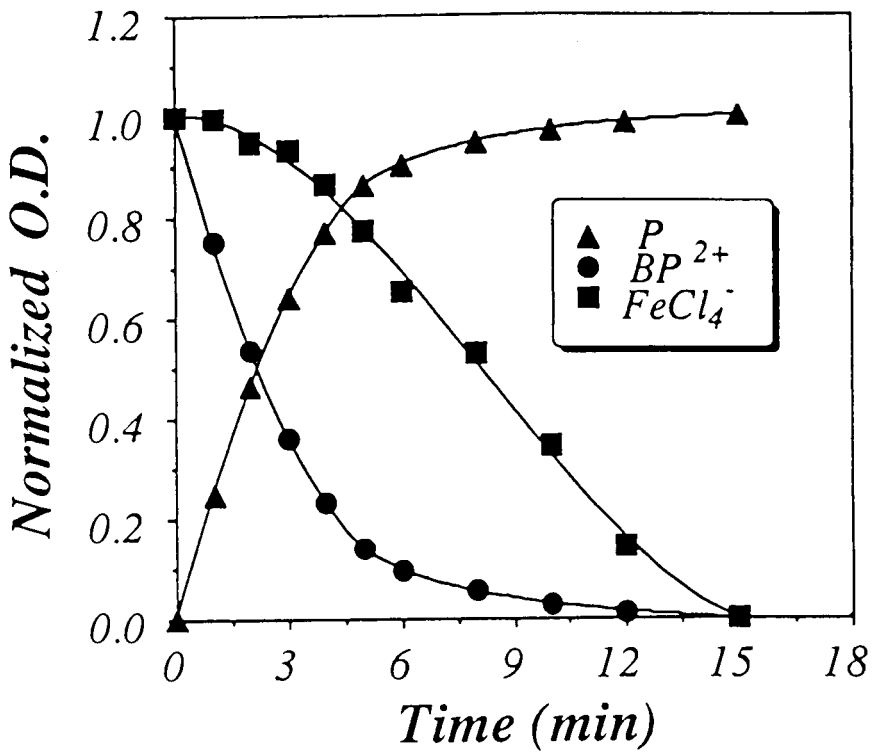

Figure IV.15: Kinetic plots of the decrease of optical density of $P3HT\text{-}FeCl_4^-$ films with irradiation time. Irradiation at 366 nm *in vacuo*.

When photolytically de-doped films were exposed to dry oxygen they reverted back to their doped conductive form and the characteristic absorption bands of $FeCl_4^-$ and BP^{2+} were regenerated (Figure 13b). The efficiency of recovery of the doped form was >90 % efficiency as calculated from the bipolaron absorption band. The electronic conductivity of the regenerated conducting polymer was 1 S/cm which compares well to 6 S/cm for the pristine conducting polymer.

Relationship between bipolarons, polarons, and neutral polymer. The precise molecular nature of bipolarons and polarons cannot be accurately represented due to uncertainty in the degree of localization. However, it is useful to realize approximate molecular forms of these species in order to understand their photochemical redox reactions.

Contrary to most depictions of bipolarons, the double charge associated with this species must be distributed, on average, over eight thienyl rings. This assertion is based on the fact that: (i) elemental analysis shows the doped polymer as possessing one counter ion for every four rings; (ii) the bipolaron is a doubly charged species; and (iii) UV-vis spectroscopy indicates the absence of neutral conjugated segments at this level of doping. The bipolaron can be thought as comprising two partially-delocalized regions of positive charge density which are maximized four thienyl units apart which possess minimum charge density in between. The quinoidal character is maximized at the position of highest positive charge density. This position was assumed to be juxtaposed to the counter ion. In this region, interannular bonds possess more double bond character. In the region of minimum charge density, interannular bonds possess more single bond character. However, for simplicity, the bipolaronic residue depicted in Scheme IV.2 is shown as being comprised of quinoidal units rather than the partial-delocalized system.

Bipolarons, polarons, and neutral polymer are related by successive one electron redox reactions, e.g., electron transfer to the bipolaron results in the corresponding polaron. The charge associated with a polaron may be represented, for simplicity, as being distributed over several rings, with the highest quinoidal character and density of charge being situated close to the location of the counter ion. Except for very low concentrations of polarons, polarons are unstable with respect to bipolarons and the following disproportionation process occurs $P^{+\bullet} + P^{+\bullet} \rightarrow BP^{2+} + P$.[256] Where P represents neutral polymer. Neutral segments of the polymer will self-interact in order to maximize π-stabilization. The mechanism of reduction of bipolarons to polarons is shown below (Scheme IV.2).

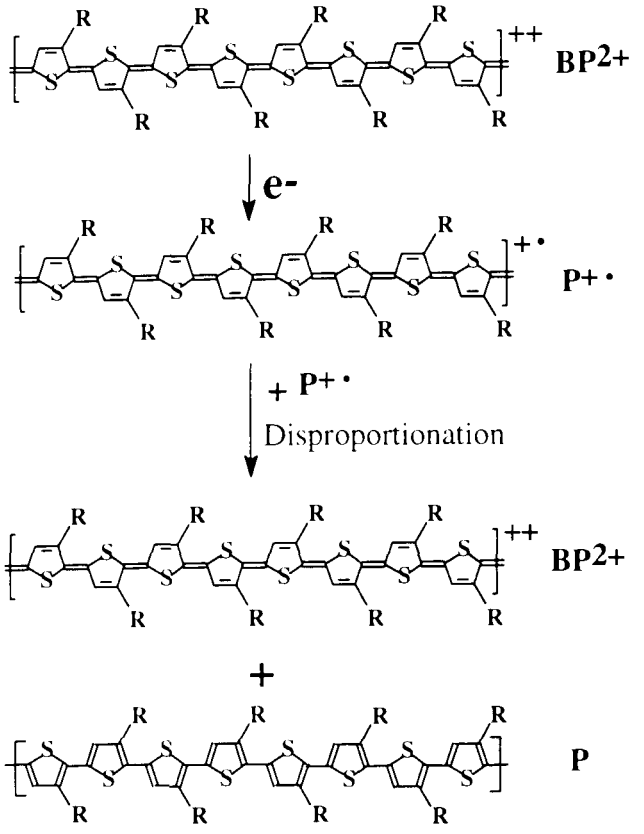

Scheme IV.2

Mechanism of photo-dedoping. UV-vis-NIR spectrosopy has been used to determine the mechanism of photodegradation of electronically conducting polymers. Photolysis in air and *in vacuo* show similar manifestations associated with reduction of the oxidized polymer, disappearence of $FeCl_4^-$, and loss of conductivity. However, subtle deviations in these observations provide important information on the photochemical mechanism. Since photolysis *in vacuo* is not complicated by concurrent reactions involving moisture or oxygen, this aspect is treated first.

Photolyses *in vacuo*: $FeCl_4^-$ is known to undergo photoreduction.[280,281] In presence of hydrocarbons (*RH*) photoexcitation is followed by electron transfer and proton transfer:

$$FeCl_4^- \xrightarrow{h\nu} [\, FeCl_4^- \,]^* \xrightarrow{RH} [\, FeCl_4^{2-} + RH^{+\bullet} \,] \rightarrow H^+ FeCl_4^{2-} + R^\bullet \quad \text{(IV.7)}$$

$FeCl_4^{2-}$ is believed to be both an intermediate and a reducing agent in the dedoping reaction. In the present system, there is some doubt as to whether photoreduction of the excited counter ion proceeds by electron transfer from the polymer backbone or from the alkyl side chain. However, the data clearly show the polymer being photolytically reduced not oxidized beyond its original level. Thus, the net reaction must involve oxidation of the side chain followed by rapid proton transfer as illustrated in Scheme IV.3.

The intermediate, $FeCl_4^{2-}$, is a strong reducing agent. The formal redox potential of the $FeCl_4^-/FeCl_4^{2-}$ couple was determined to be 0.275 V *vs* SCE whereas the oxidation potential (anodic peak potential) of *P3HT* was determined to be 0.97 V. Thus $FeCl_4^{2-}$ can thermodynamically reduce BP^{2+} and $P^{+\bullet}$. Indeed, prepared solutions of $(Et_4N)_2FeCl_4^-$ in acetonitrile completely reduce doped polymer films.

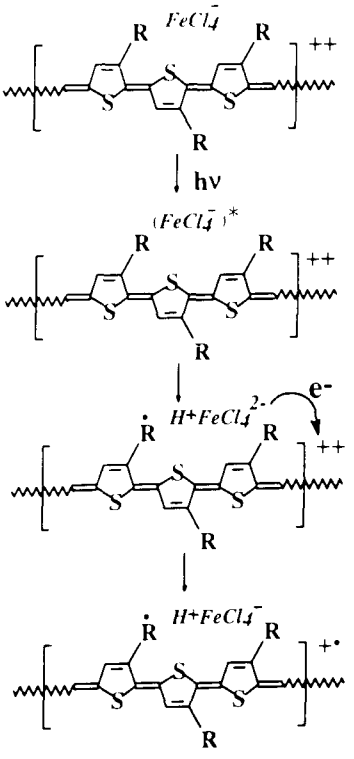

Scheme IV.3

Given that two $FeCl_4^-$ molecules are associated with each bipolaron, the following reaction scheme is proposed:

$$(RH)BP^{2+}.2FeCl_4^- \xrightarrow{h\nu} [(R^\bullet)BP^{2+}.FeCl_4^-.H^+FeCl_4^{2-}] \qquad \text{(IV.8)}$$

$$[(R^\bullet)BP^{2+}.FeCl_4^-.H^+FeCl_4^{2-}] \xrightarrow{e\ transfer} (R^\bullet)P^{+\bullet}.FeCl_4^- + H^+FeCl_4^- \qquad \text{(IV.9)}$$

where (RH) and $(R^\bullet)$ represent an alkyl side chain and alkyl radical linked to the polymer backbone. During the initial stages of photolysis, polarons undergo disproportionation to form neutral polymer and bipolarons (see Scheme IV.2). During the latter stages of photolysis, the polaron can undergo further reduction via

$$(RH)P^{+\bullet}.FeCl_4^- \xrightarrow{h\nu, e-transfer} (R^\bullet)P + H^+FeCl_4^- \qquad \text{(IV.10)}$$

The net overall reaction for the reduction of the oxidized polymer is thus

$$(RH)BP^{2+}.2FeCl_4^- \xrightarrow{h\nu} (2R^\bullet)P + 2H^+FeCl_4^- \qquad \text{(IV.11)}$$

Kinetic analysis of the photochemical de-doping process (Figure IV.15) is consistent with photogeneration of $FeCl_4^{2-}$ and subsequent electron transfer from this species to oxidized polymer. Concentration-time profiles for depletion of $FeCl_4^-$ and bipolarons are significantly different. The concentration of $FeCl_4^-$ changes little during initial photolysis while the concentration of bipolarons decreases in a first order fashion. This observation indicates that $FeCl_4^-$ is regenerated while oxidized polymer is initially reduced i.e. oxidized polymer is photocatalytically reduced by $FeCl_4^-$.

Photolysis of $FeCl_4^-$ does not stop upon photoreduction of the oxidized polymer; prolonged photolysis converts $H^+FeCl_4^-$ to $2H^+.FeCl_4^{2-}$, i.e., Fe(III) to Fe(II), by the following reaction

$$H^+FeCl_4^- \xrightarrow{h\nu,(RH)P} 2H^+.FeCl_4^{2-} + (R^\bullet)P \qquad \text{(IV.12)}$$

Where $(RH)P$ represents a neutral polymer segment possessing pendent alkyl functionality. According to this mechanism, residual iron should be in a +2 oxidation state following photolysis. This was confirmed using NIR and Mössbauer spectroscopies (see Figures IV.13 and IV.14).

Strong evidence supporting this mechanism is provided by regeneration of the oxidized, conducting form of the polymer upon exposure of photolyzed films to dry oxygen. Oxygen is known to oxidize iron(II) in acid medium.[283] The oxidation of $2H^+.FeCl_4^{2-}$ by oxygen proceeds by the reaction:

$$2(2H^+.FeCl_4^{2-}) + \tfrac{1}{2}O_2 \rightarrow 2(H^+.FeCl_4^-) + H_2O \qquad \text{(IV.13)}$$

While $H^+FeCl_4^-$ is unable to oxidize P3HT, it readily dissociates into HCl and $FeCl_3$ (K_{diss} ~95).[285]

$$H^+FeCl_4^- \rightleftharpoons HCl + FeCl_3 \qquad \text{(IV.14)}$$

$FeCl_3$ is a known oxidant for poly(3-hexylthiophene) (see equation IV.5). Furthermore, $FeCl_2$ generated from this reaction (equation IV.5) is oxidized to $FeCl_3$ in the presence of oxygen and acid:

$$2FeCl_2 + \frac{1}{2}O_2 + 2HCl \longrightarrow 2FeCl_3 + H_2O \qquad \text{(IV.15)}$$

Conducting polymer containing the $FeCl_4^-$ counter ion is thus regenerated almost quantitatively via equations IV.13-15, and IV.5.

Photolyses in ambient air. In the absence of moisture we assert the inital photoreduction of $FeCl_4^-$ to $FeCl_4^{2-}$ involves electron transfer from the alkyl functionality attached to the main chain. However, sacrificial electron donors can readily compete with this process. It has been shown, for example, that excitation of $FeCl_4^-$ in the presence of moisture leads to oxidation of water:[281]

$$FeCl_4^- \xrightarrow{h\nu, H_2O} H^+FeCl_4^{2-} + OH^\bullet \qquad \text{(IV.16)}$$

Equation IV.16 is the anologous reaction to equation IV.7 for which the hydrocarbon, RH, is replaced by H_2O. A series of chemical events follows equation IV.16 which are analogous to equations IV.8-13, except the sacrificial donor is trace water, not the alkyl side chain. A generalized reaction scheme is shown below (Scheme IV.4).

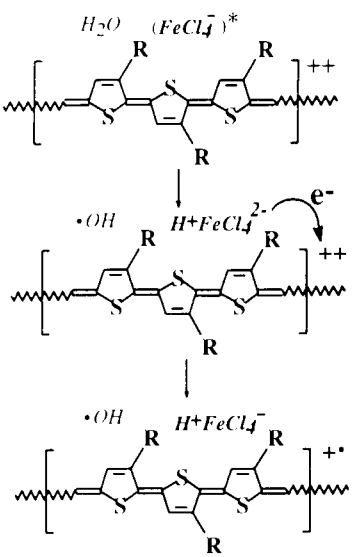

Scheme IV.4

When moisture is the predominant sacrificial electron donor $OH^{\bullet}$ radicals are formed. It has previously shown that $OH^{\bullet}$ radicals abstract H-atoms from the alkyl side and lead to the formation of polymer-bound aliphatic alcohols (*cf.* III.6.5). FTIR confirmed the formation of *-OH* groups (Figure IV.12). In addition, the concentration of aliphatic *C-H* groups is reduced which is consistent with *H*-abstraction.

During photolysis, $FeCl_4^-$ is converted to an octahedral Fe(III) complex. The reactions by which this occurs cannot be readily described because of the complexity of coordination reactions involving iron species, radicals, and water. We can, however, speculate the mechanism initially involves reaction of hydroxyl radicals with Fe(II) species according to equation IV.17.[286]

$$Fe^{2+} + OH^{\cdot} \rightarrow Fe^{3+} + OH^{-} \qquad \text{(IV.17)}$$

OH^- produced in this process has a strong affinity for coordination with Fe (III). The affinity of Fe^{3+} for OH^- is 10^{13} times greater than for Cl^- thus OH^- can replace Cl^- in the coordination sphere.[163] Elemental analysis of photolyzed films yielded a ratio of Fe:Cl of 1:1.6, while Mössbauer spectroscopy revealed the presence of octahedral iron (III). Given this, residual iron is most likely takes the form as an Fe(III) hydroxychloro-complex in which the cationic charge is compensated by a combination of hydroxy and chloro ions, and in which an octahedral configuration is stabilized by coordination with water.[287] A general reaction is given below.

$$FeCl_4^- \xrightarrow{h\nu,\, H_2O} Fe(III)\,hydroxy\,chloro-complex$$
$$e.g.,\ [Fe(H_2O)_4(OH)_2]^+Cl^- \qquad \text{(IV.18)}$$

IV.5.2 Enhanced Stability of Conducting P3ATs

The selection of a thermostable, photostable counter ion is critical for designing stable conducting polymers. Gold and platinum compounds were chosen as dopants. $Au(III)$ and $Pt(II)$ ions belong to the third transition series and are known by their eight electrons in the d shell. They generally form four coordinate square planar complexes. Pt(II) complexes are known by their thermal and photochemical stabilities.[280] Thus, $PtCl_4^{2-}$ complex is insensitive to light of wavelengths ≥313 nm, and is thus photostable under visible light.[288] Gold(III) complexes are the isoelectronic counterparts and anticipated to be photochemically stable. Gold(III) halides possess higher oxidizing power than the corresponding Pt(II) halides. The standard electrochemical potential, E^o, of (Au^{3+}/Au^{+}) is 1.16 V SCE in aqueous solution at 25 °C compared to 0.51 for E^o (Pt^{2+}/Pt^{0}).[289] Based on these attributes, Au(III) halides are anticipated to be suitable dopants for P3ATs. Dopind-dedoping behavior of P3ATs/$AuCl_3$ systems was undertaken to test this hypothesis.

IV.5.2.1 Oxidative Doping and Electroless Metal Deposition Using $AuCl_3$

(i) Oxidative doping of P3HT using acetonitrile solutions of $AuCl_3$.

Electrochemical potential of Au^{3+}/Au^{+} is 1.16 V (SCE)[289] whereas the oxidation potential of P3HT, as determined from its voltammetry, is 0.97 V. Thus, $AuCl_3$ can thermodynamicaly oxidize P3HT. Red films of P3HT (0.25 μm) cast onto quartz slides turned blue upon contact with acetonitrile solutions of $AuCl_3$ (0.01-0.1 M). UV-vis absorption spectra of neutral and oxidized films are shown in Figure IV.16. After doping, two broad absorption bands developed at λ_{max} 765 and 1690 nm consistent with the formation of charge-carrying bipolaronic states.[252-255] In addition, oxidized films show two transitions at 232

and 324 nm which were assigned to ligand-to-metal charge transfer bands of $AuCl_4^-$.[290,291]

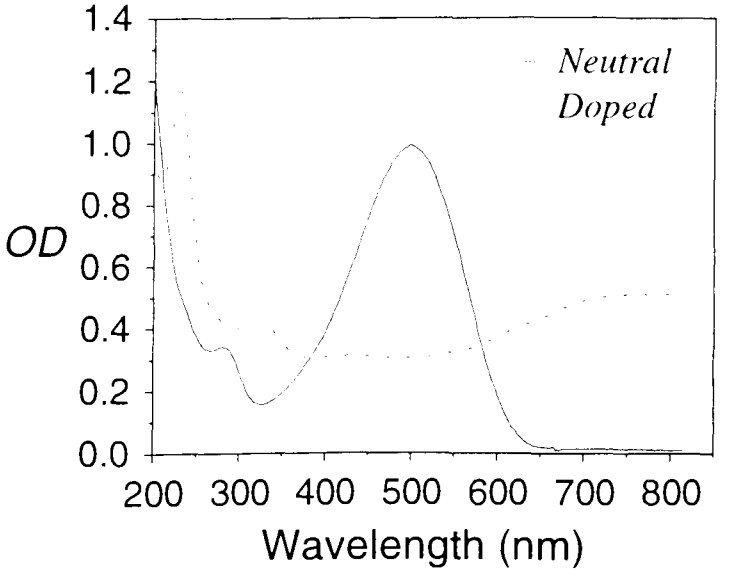

Figure IV.16: UV-vis spectra of P3HT films in the neutral and oxidized forms. Oxidant, $AuCl_3$ (0.01 M) in acetonitrile.

The electronic conductivity of $AuCl_3$-oxidized films was 13-15 S cm^{-1}, as determined by the four-point probe technique.

Kinetic analysis of the doping process was studied using optical spectroscopy. A plot of the optical density (OD) at 500 and 230 nm versus time is shown in Figure IV.17. Using a 0.01M Au(III) chloride and 0.25 μm thick films, the doping process was complete within 120 s and no additional change in the OD was observed upon prolonged exposure.

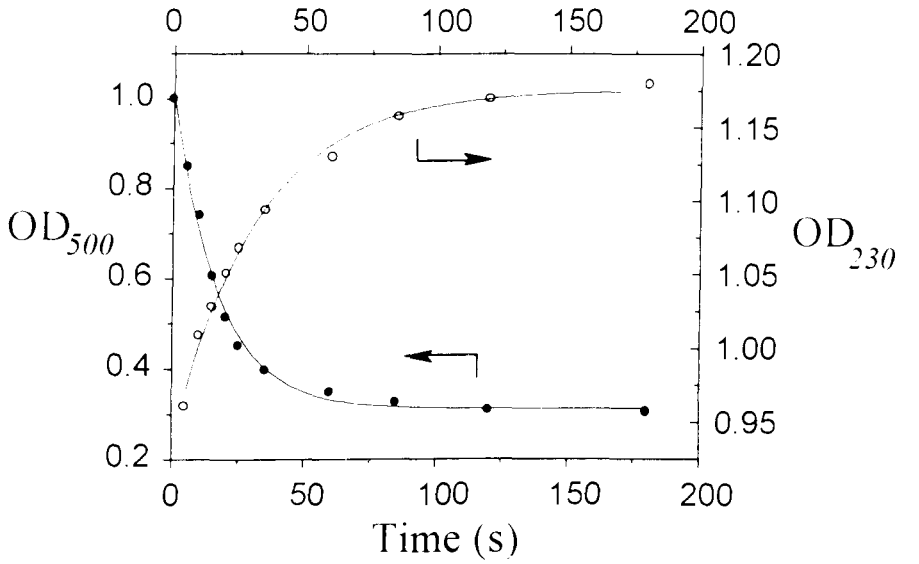

Figure IV.17: Kinetic plots of the change in OD of *P3HT-AuCl*$_4^-$ with doping time.

The nature of the counter ion was also studied using surface analysis techniques. XPS spectra of oxidized polymer show the presence of only one gold species at both the polymer/solution and polymer/substrate interfaces. The binding energies of the of this species were 86.3 and 89.9 eV (Figure IV.18). These were assigned to the $4f_{7/2}$ and $4f_{5/2}$ levels of *Au(III)*[270,271] which is consistent with UV-vis measurements. The characteristic XPS spectra of Cl-2p at 197.7 and 199.6 eV were also detected at both interfaces in addition to S-2p and C-1s (Figures IV.19 and IV.20).[270,271] Cl is associated with the dopant ion, while C and S are due to the polymer. Noteworthy is the absence of Au(0) on polymer samples doped using $AuCl_3$/acetonitrile system.

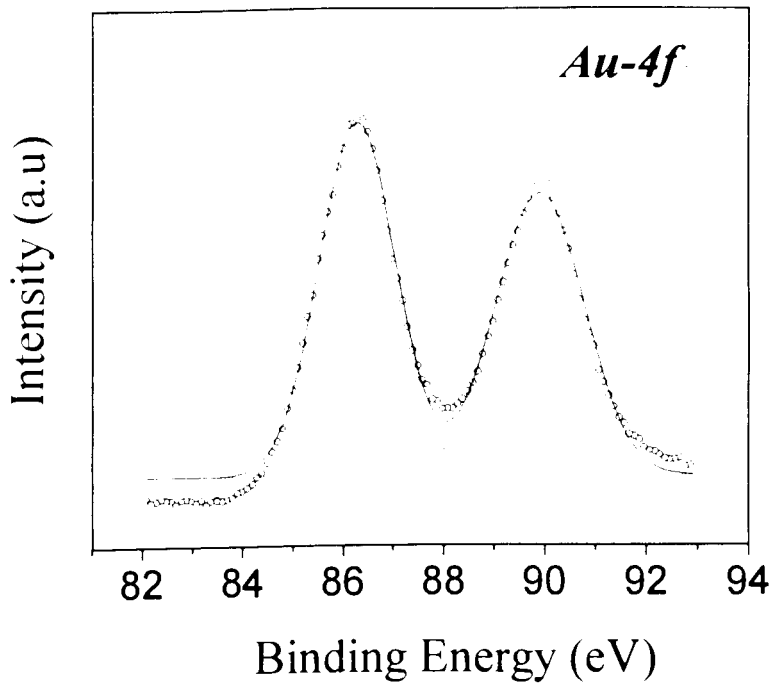

Figure IV.18: *Au-4f* XPS spectrum of P3HT films doped with $AuCl_3$ solution in acetonitrile.

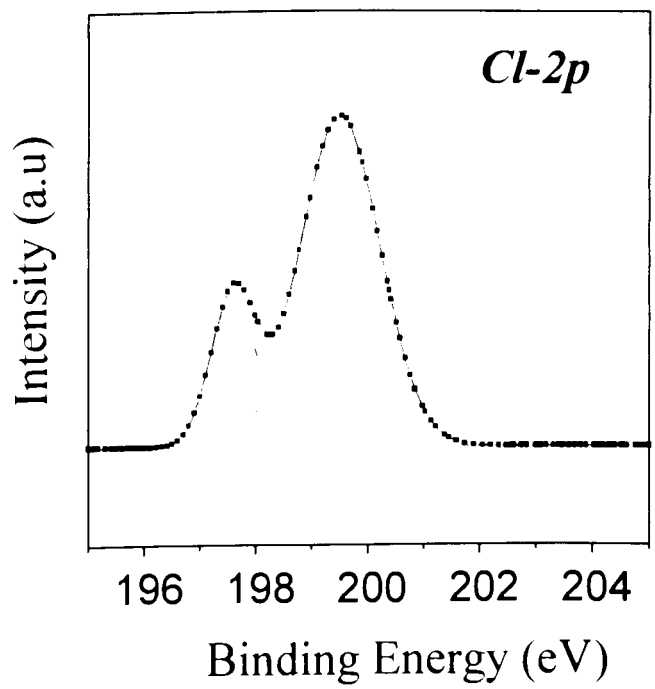

Figure IV.19: Cl-2p XPS spectrum of P3HT doped with $AuCl_3$ solution in acetonitrile.

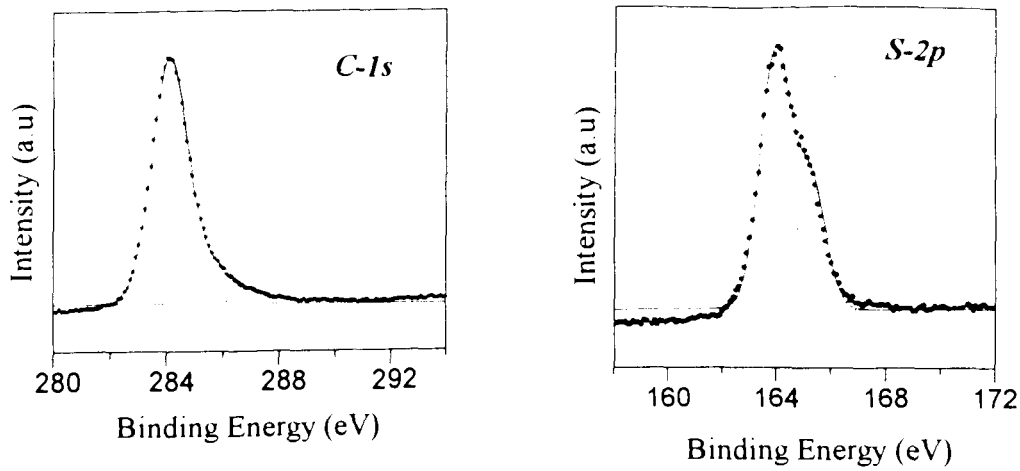

Figure IV.20: C-1s and S-2p XPS spectra of P3HT doped with $AuCl_3$ solution in acetonitrile.

Mechanism of Oxidation. Organic nitriles dissolve and coordinate $AuCl_3$.[306,307] A square planar complex ($AuCl_3(CH_3CN)$) is formed in acetonitrile which exhibits ligand-to-metal charge transfer absorption bands at 227 and 319 nm.[290-293] Au^{3+} compounds are readily reduced to the Au^{2+} species.[294-296] Gold(II) compounds are highly unstable and disproportionate to Au^{3+} and Au^{+}. The rate constant, k, of disproportionation at $[Au^{2+}]$ = 10^{-6} M is ~10^{10} $M^{-1}s^{-1}$.[296] However, Au^{+} ions are soluble in acetonitrile forming *stable* $Au(CH_3CN)_nCl$ complexes.[297,298] In the presence of Cl^-, the formation constant of $AuCl_4^-$ (β_4 = 10^{26}) is much larger than that of $Au(CH_3CN)_nCl_2^-$ (β_2 = 10^{17}) indicating that association of Cl^- with $AuCl_3(CH_3CN)$, which, in our case, is in excess, will form $AuCl_4^-$.[299] $AuCl_4^-$ serves as the counter-ion for oxidized polymer. This assertion was supported by optical and XPS measurements since $AuCl_4^-$ is the only gold species identified in the polymer following oxidation.

Accordingly, the following mechanism for oxidation of the polymer in acetonitrile was proposed.

$$P + AuCl_3(CH_3CN) \rightarrow P^{+\bullet} + Au(CH_3CN)_nCl_2 + Cl^- \quad \text{(IV.19)}$$

$$2Au(CH_3CN)_nCl_2 \xrightarrow{k} Au(CH_3CN)Cl_3 + Au(CH_3CN)_nCl \quad \text{(IV.20)}$$

$$Cl^- + AuCl_3(CH_3CN) \rightarrow AuCl_4^- \quad \text{(IV.21)}$$

$$2P^{+\bullet} \rightarrow BP^{2+} + P \quad \text{(IV.22)}$$

$$P + 3AuCl_3(CH_3CN) \rightarrow BP^{2+} 2AuCl_4^- + Au(CH_3CN)_nCl \quad \text{(IV.23)}$$

where P represents neutral polymer, and $P^{+\bullet}$ and BP^{2+} represent oxidized polymer polaron and bipolaron, respectively.

(ii) Oxidative doping of P3HT using nitromethane solutions of $AuCl_3$.

When thin films of P3HT (0.25 μm) were exposed to nitromethane solutions of $AuCl_3$ the polymer immediately turned blue in color. However, in contrast to oxidation in acetonitrile, the films rapidly acquired a metallic gold luster. The quality of the gold layer improved with increasing doping time. For polymer films doped for 600 s, the quality/homogeneity of the gold layer was visually indistinguishable from films obtained by metal evaporation. The electronic conductivity of the material increased with increasing doping time as shown in Figure IV.21. Conductivities as high as 1.1×10^4 S cm^{-1} were obtained for these polymer/metal bilayers and can be attributed solely to the metal layer. This was confirmed by de-doping the polymer, whereupon the high conductivities remained.

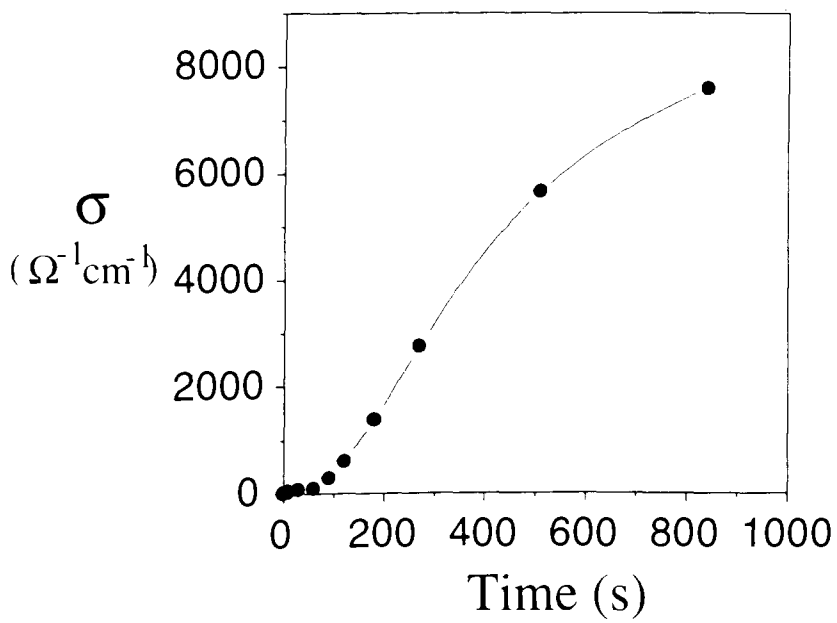

Figure IV.21: Increase in the conductivity of oxidized P3HT films with doping time. Thickness of the polymer/metal bilayer increases at a rate of ~1.4 nm/s, as calculated from AES depth profile.

Oxidation of thin films of P3HT (0.25 μm) was also monitored by optical spectroscopy. UV-vis absorption spectra of films oxidized for 100 s, which is insufficient time for formation of a homogeneous gold layer, showed two absoptions at 232 and 324 nm confirming the presence of $AuCl_4^-$. In addition, a weak and broad characteristic absorption band due to gold(0) was observed at ~520 nm.[300] The conductivities of polymer/metal composites after 100 s doping were 10-15 S cm^{-1} indicating that the polymer film was fully doped during this time. Figure IV.21 therefore implies that gold deposition is autocatalytic in nature since the deposition process continued even after the polymer was fully oxidized.

X-ray electron spectroscopy (XPS) was performed to provide further information on the nature of the gold species. Figures IV.22 and IV.23 show

XPS spectra of polymer/solution interface corresponding to the *Au-4f* region after exposure to $AuCl_3$ solutions in nitromethane for 100 s and 600 s, respectively.

The XPS spectra at a doping time of *100 s* were fitted to three sets of doublets (Figure IV.22). The binding energy of 83.6 and 87.3 eV are typical of *Au(0)*[270,271] whereas the chemical shifts at 86.3 (shoulder) and 89.9 eV are due to *Au(III)*. The chemical shifts corresponding to the fitted curves (Figure IV.22) at 84.8 and 88.2 eV were assigned to the $4f_{7/2}$ and $4f_{5/2}$ levels of *Au(I)* species. At this stage of doping (100 s), elements including S, C and Cl were also detected on the polymer surface.

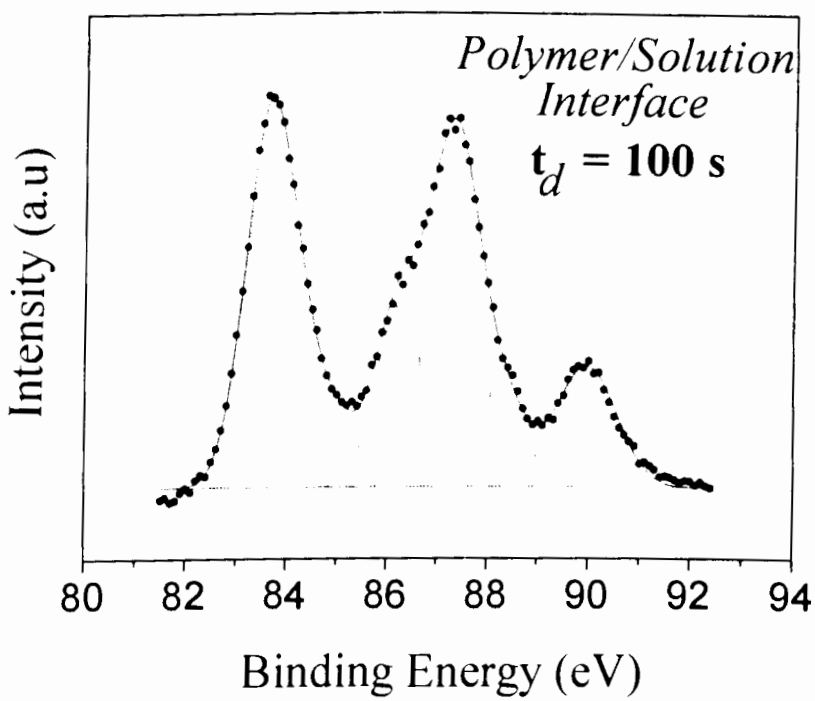

Figure IV.22: *Au-4f* XPS spectrum of P3HT films doped with $AuCl_3$ in nitromethane for **100 s**. Polymer/solution interface.

In contrast to XPS spectra obtained at 100 s, the XPS spectra of the polymer/solution interface of polymer films doped for *600 s* were fitted to two set of doublets (**Figure IV.23**). The 83.6 and 87.3 eV species are due of *Au(0)*. The higher binding energy species at 86.4 and 88.9 (fitted curves) are shifted with respect to *Au(III)* species identified in Figure IV.22. It is also important to note that the intensity of the *Au(0)* species at 83.7 eV is at least 10 times greater than that at 86.4 eV. The latter can be assigned to *Au(III)* species and is believed due to adsorbed $AuCl_3$, originally used for doping. Noteworthy is the absence of elements such as S at this interface which indicates that the polymer film is completely covered with gold metal.

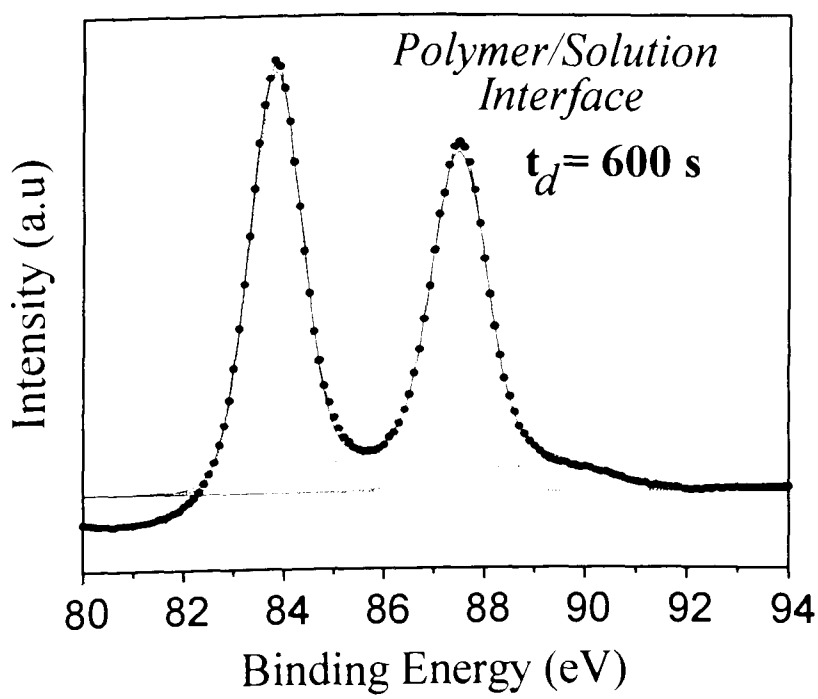

Figure IV.23: *Au-4f* XPS spectrum of P3HT films doped with $AuCl_3$ in nitromethane for **600 s**. Polymer/solution interface.

XPS was also performed at the *polymer/substrate* interfaces in order to identify the nature of the gold species which diffused through the polymer film during the doping process. Figure IV.24 shows the *Au-4f* XPS spectrum after 100 s doping. The chemical shifts are 86.3 and 89.9 eV; indicative of *Au(III)* species. Polymers doped for 600 s provide similar XPS spectrum confirming the common nature of the gold species at the polymer/substrate interfaces for short and long doping times.

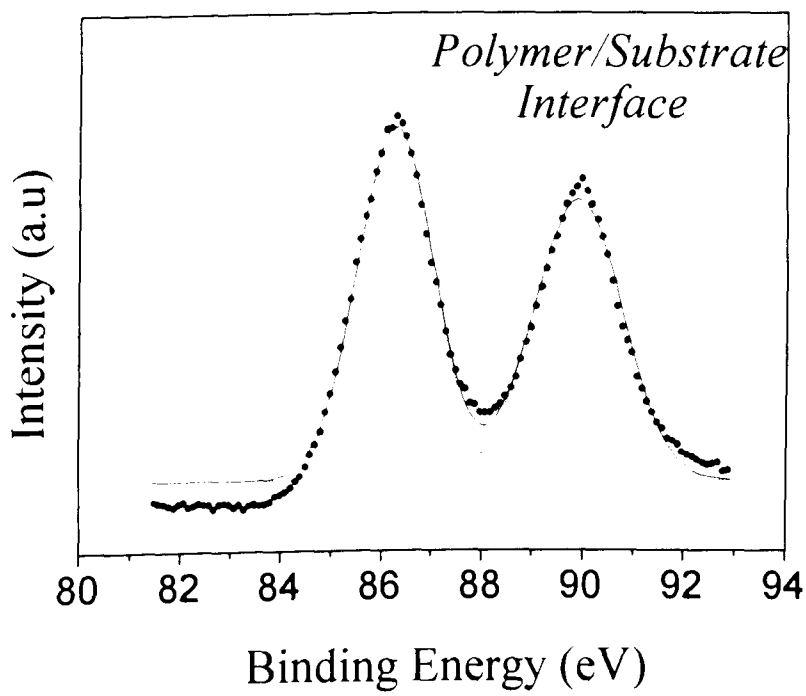

Figure IV.24: *Au-4f* XPS spectrum of P3HT films doped with $AuCl_3$ in nitromethane. Polymer/substrate interface

The common features of the XPS results are: (1) For short doping times, three gold species were identified at the *polymer/solution* interface: namely *Au(0)*, *Au(I)*, and *Au(III)*, while *Au(0)* was the dominant species at longer doping times, (2) No *Au(0)* was detected at the *polymer/substrate* interface even at longer doping times. These features imply that the formation of *Au(0)* is limited to the

polymer/solution interface and that the extent of interdiffusion of Au(0) in the bulk of the polymer is minimal. This was investigated further by depth profiling using Auger electron spectroscopy (AES). AES is a useful surface technique which allows in-depth distribution analysis of chemical composition.[270] Figure IV.25 shows the AES depth profile of an oxidized polymer sample doped for 600 s using a nitromethane solution of $AuCl_3$. The depth profile illustrates that the Au^0 is confined to the surface since other elements than gold could not be detected.

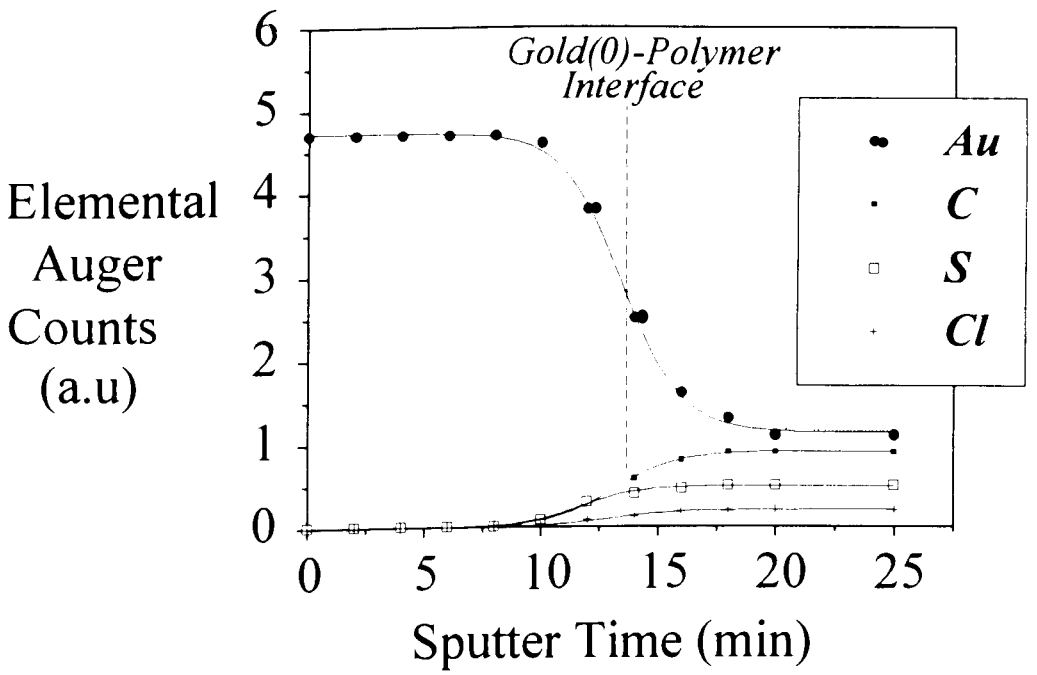

Figure IV.25: AES depth profile of P3HT/Au bilayer, The dotted curve represents the derivative of the Au signal.

By knowing the rate of sputtering the sputtering time can be converted to a distance scale. The sputtering rate z (nm/s) of an element is determined by[270]

$$z = \frac{M}{\rho N_A e} S_y i_p \qquad \text{(IV.24)}$$

where M is the atomic mass of the element, ρ its density, N_A Avogardro number, e electron charge, S_y is the sputtering yield, and i_p is the primary ion current density. With this equation the rate of sputtering can be calculated if S_y is known. Determination of the sputtering yield is not, however, a trivial matter. The literature value of S_y for normal incidence of Ar^+ gas ion at a bombarding energy of 1 keV for polycrystalline gold, as determined using in-situ measurements of sputter-induced weight loss, is 3.08 atom/ion.[301] Using this value, an approximate sputtering rate for gold was calculated to be 1.1 nm/s. The depth resolution function, shown as the dotted curve on Figure IV.25, indicates that 13 min of sputtering was required to sputter away the gold(0) layer, thus the thickness of the gold layer deposited on the polymer was estimated to be ~*890 nm*. Electroless deposition of Au^0 occurs, therefore, solely at the *polymer/solution* interface and not at the *polymer/substrate* interface. In confirmation of this is the observation that the electronic conductivity of polymer films at the polymer/substrate interface was measured to be 15 $\Omega^{-1}cm^{-1}$ while the conductivity at the polymer/solution interface, where the gold layer was formed, was ~10 000 $\Omega^{-1}cm^{-1}$.

Mechanism of Oxidation and Au(0) Deposition. In contrast to the $AuCl_3$/acetonitrile doping system, oxidation of P3HT using solutions of $AuCl_3$ in nitromethane results in deposition of metallic gold, in addition to formation of $AuCl_4^-$ doped polymers. It is thus clear that the nature of the solvent plays a

significant role in the mechanism of oxidation. Although nitromethane is a good solvent for gold trichloride it is a relatively poor coordinating solvent, and thus does not form a square planar complex with $AuCl_3$.[292] This assertion is supported by a single absorption band of the $AuCl_3/CH_3NO_2$ solution at 340 nm. Furthermore, the stability of $Au(I)$ complexes is highly dependent on the nature of the solvent. Au^+ is stable if coordinated with solvents such as acetonitrile[300] but uncoordinated Au^+ is reported to disproportionate forming Au^{3+}, Au^0, and Cl^-.[302,303] Accordingly, the following mechanism was proposed for oxidation of P3HT with nitromethane solutions of $AuCl_3$.

$$P + AuCl_3 \rightarrow P^{+\bullet} + AuCl_2 + Cl^- \quad \text{(IV.25)}$$

$$2AuCl_2 \xrightarrow{k} AuCl_3 + AuCl \quad \text{(IV.26)}$$

$$Cl^- + AuCl_3 \rightarrow AuCl_4^- \quad \text{(IV.27)}$$

$$3AuCl \rightarrow AuCl_3 + 2Au^0\downarrow \quad \text{(IV.28)}$$

$$2P^{+\bullet} \rightarrow BP^{2+} + P \quad \text{(IV.29)}$$

$$3P + 8AuCl_3 \rightarrow 3(BP^{2+} 2AuCl_4^-) + 2Au^0 \quad \text{(IV.30)}$$

The formation of $AuCl$ and $AuCl_4^-$ during the course of the oxidation reaction was confirmed using optical and XPS spectroscopies (see Figure IV.22). Au^0 was confirmed by XPS analyses and the exceptionally high electronic conductivity of doped materials. The mechanism of oxidation and metal deposition are explained as follow. The equilibrium constant for reaction IV.28 is $10^{7.74}$ in aqueous solution.[303] In nitromethane the equilibrium constant is anticipated to be even greater due to its poor coordinative properties. Support of equation IV.30 was achieved by carrying out the oxidation/metal deposition of

polymer films in nitromethane/$AuCl_3$ in the presence of acetonitrile (5 vol/vol%). Small amounts of CH_3CN were sufficient to completely suppress metal deposition since acetonitrile complexes with Au^+ to form a stable species.

The proposition that electroless deposition of $Au(0)$ is an autocatalytic process was examined by comparing the thickness of the gold layer determined experimentally using AES with that the estimated theoretically based on the stoichiometry of the overall reaction (equation IV.30). According to equation IV.30, the following expression was derived to determine the thickness of the gold layer

$$l_{Au^0} \quad \frac{3}{2} \; l_{P3HT} \; \frac{\rho_{P3HT}}{\rho_{Au^0}} \; \frac{AW_{Au^0}}{MW_{P3HT}} \qquad \text{(IV.31)}$$

l and ρ are the film thickness and density. MW_{P3HT} is the molecular weight of P3HT and AW_{Au} is the atomic weight of gold. The factor 3/2 represents the stoichiomety of the reaction whereby 3 moles polymer produces 2 mole of $Au(0)$. It is also important to notice that molecular weight of the polymer was calculated based on 4 thiophene units which is the number of rings per $AuCl_4^-$ dopant ion for oxidized polymers. For a 250 nm thick polymer film, the estimated thickness of $Au(0)$ layer was *6.3* nm. The experimentally determined value for polymer film of similar thickness, as calculated from AES depth profiling measurements, was *~890* nm. This value is ~140 times greater than the stoichiometric value and thus deposition of gold on P3HT is autocatalytic in nature. The autocatalytic step, however, requires a sacrificial reducing agent. It was anticipated that moisture plays this role. Subsequently, this proposition was supported by the observation that electroless deposition of gold was suppressed by carrying out the oxidation under dry nitrogen conditions and using dry solvents.

The mechanism of reduction/precipitation of gold on solid polymer films may be regarded as occurring in six steps:[304,305]

1. Diffusion of the reactant molecules to the surface.
2. Adsorption of the molecules on the surface
3. Reaction at the surface.
4. Desorption/precipitation of the product.
5. Diffusion of the dopant into the bulk of material.
6. Autocatalytic electroless metal deposition.

It can be envisaged that the oxidation process begins with a nucleation step whereby Au^0 particulates are formed on the polymer surface followed by an autocatalytic electroless deposition step on these Au^0 nuclei. XPS and conductivity measurements support this mechanism. At 100 s doping, which is insufficient time for the formation of a homogeneous $Au(0)$ layer, XPS confirms the presence of both $Au(III)$ and $Au(0)$ on the polymer/solution interface. Furthermore, the electronic conductivity at 100 s doping was similar to polymer samples doped using $AuCl_3$/acetonitrile (15 Ω^{-1} cm^{-1}). In contrast, at 600 s doping the conductivity was $6x10^3$ Ω^{-1} cm^{-1} and $Au(0)$ was the only species detected on the polymer/solution interface.

IV.5.2.2 Enhanced Ambient Stability of $AuCl_4^-$-doped P3ATs

Armed with the knowledge that photodegradation of $P3HT\text{-}FeCl_4^-$ is correlated to photolability of the anion, the photochemistry of oxidized P3HT containing various counter ions was investigated. The majority of polymer/counter ion systems were insufficiently thermally stable that photochemical degradation could not be distinguished from thermal degradation. The exception to this was $AuCl_4^-$ -containing conducting polymers which were produced by oxidizing thin films of P3HT with 0.01M $AuCl_3$ in acetonitrile. A

comparison of the stability of polymers doped with gold chloride versus ferric chloride is discussed below.

Oxidized films of P3HT (0.25 μm), using $AuCl_3$/acetonitrile dopant, remained oxidized even after several months exposure to ambient conditions on a laboratory bench at 25 °C. This is in contrast to polymers oxidized using $FeCl_3$ which reverted back to their neutral forms in less than one day. A comparison of the change in the level of conductivity of $BP^{2+}.FeCl_4^-$ and $BP^{2+}.AuCl_4^-$ as a function of time is shown in Figure IV.26. $t_{1/2}$ value for the rate of decrease in σ for $P3HT\text{-}AuCl_4^-$ films was 3.6×10^3 hours compared to 1.9 hours for $FeCl_4^-$-containing polymers.

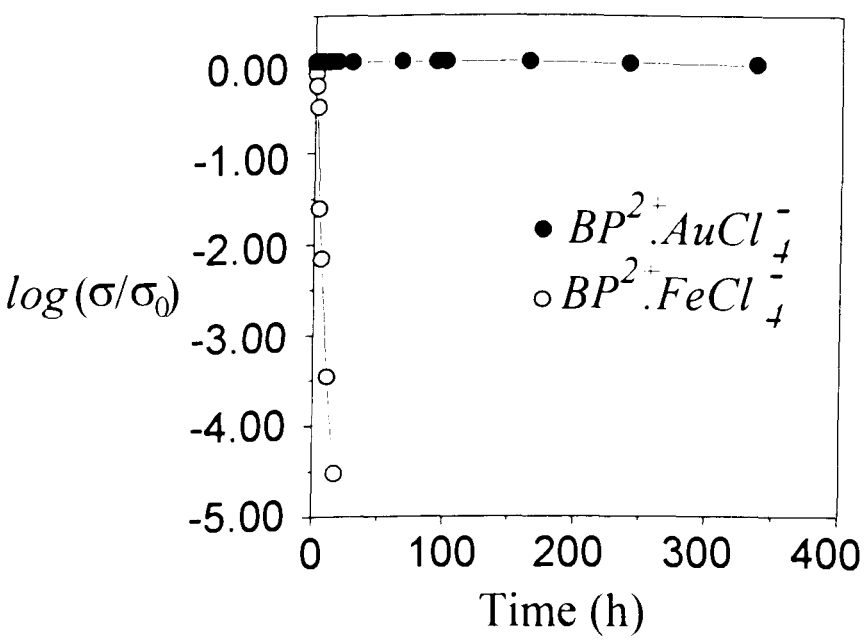

Figure IV.26: Normalized plots of electronic conductivity versus time for oxidized films of P3HT. dopant, 0.01M in acetonitrile; (•) $AuCl_3$ and (o) $FeCl_3$.

The photochemical stability of polymers containing the $AuCl_4^-$ counter ion was investigated. $AuCl_4^-$ is photochemically stable relative to $FeCl_4^-$,[306] and consequently, thin films doped with $AuCl_4^-$ are anticipated to be more stable. $t_{1/2}$

values for the rate of decrease of σ for $P3HT\text{-}AuCl_4^-$ films is 250 min for irradiation with 366 nm (I_0=1.4 mW/cm^2) compared to 0.9 min for $FeCl_4^-$-containing polymer for the same absorbed light intensity. Photochemical stability of $P3HT\text{-}AuCl_4^-$ is ~300 times greater than $P3HT\text{-}FeCl_4^-$. It was, therefore, concluded that photochemical stability of the dopant is a necessary requirement for designing stable conducting polymers.

IV.6 Conclusion

Irradiation of electronically conducting poly(3-alkylthiophenes) doped with the $FeCl_4^-$ counter ion results in a loss of electronic conductivity (6 S/cm $\rightarrow 10^{-5}$ S/cm). The mechanism proceeds by: (i) direct photolysis of $FeCl_4^-$; (ii) photoreduction of $FeCl_4^-$ to $FeCl_4^{2-}$; followed by (iii) electron transfer to bipolaronic residues. Upon prolonged photolysis the products are neutral, non-conductive polymer and octahedral iron(III) complexes. Photochemical de-doping occurs *in vacuo* but is greatly accelerated by moisture. The reaction is sufficiently facile to occur significantly under ambient light. Armed with the knowledge that instability of *P3HT*-$FeCl_4^-$ is correlated to photolability of the anion, the photochemistry of oxidized *P3HT* containing various counter ions was investigated.

Oxidative doping of thin π-conjugated polymer films using *acetonitrile* solutions of gold trichloride yields electronically conductive polymers (15 $\Omega^{-1}cm^{-1}$) containing the $AuCl_4^-$ counter ion. Thin oxidized films containing $AuCl_4^-$ counter ion are orders of magnitude more stable in ambient atmosphere at 25 °C than polymers oxidized using conventional oxidants such as iron trichloride. Oxidation of polymer films using solutions of $AuCl_3$ in *nitromethane* results in electroless deposition of zero-valent gold in addition to formation of $AuCl_4^-$ doped polymer. Long doping times (>2 min) afford growth of a homogeneous and continuous metallic layer on top of the polymer film. As a result, conductivities of the metal/polymer bilayers are as high as 10,000 $\Omega^{-1}cm^{-1}$. Mechanism of oxidative doping proceeds via Au^{II} and Au^{I} intermediates. Au^{II} ions disproportionate very rapidly (k= 10^{10} $M^{-1}.s^{-1}$) yielding Au^{I} and Au^{III}. Stability of the Au^{I} species is highly dependent on the nature of the solvent. Au^{I} forms a stable, soluble complex in acetonitrile. In contrast, Au^{I} undergoes a disproportionation reaction in nitromethane yielding Au^{0} and Au^{III}. Au^{III}

associates with Cl^-, formed in the course of oxidation reaction, forming $AuCl_4^-$ doped polymer. The stoichiometric thickness of the gold layer is only ~6 nm and can not account for the exceptionally high conductivites of polymer/metal bilayers. Autocatalytic electroless deposition mechanisms were invoked to explain this phenomenon.

Poly(3-alkylthiophenes) containing $AuCl_4^-$ dopant are orders of magnitude more stable in ambient atmosphere at 25 ^oC than polymers oxidized using the more common oxidant, such as iron trichloride. The improved stability is largely due to the photochemical stability of the counter ion. Oxidative doping and electroless deposition of $Au(0)$ is not restricted to poly(3-alkylthiophenes). Stable, oxidized and conductive forms of poly(thienyl vinylene), polypyrrole, poly(3-alkoxythiophenes), and even unsubstituted polythiophene, which have a relatively high oxidation potential, have been obtained, illustrating that the stability of $AuCl_4^-$-doped polymers is a general effect.

Chapter V: ELECTRONIC PROPERTIES OF π-CONJUGATED POLY(3-ALKYLTHIOPHENES)

V.1 Introduction

Inorganic materials have dominated the field of semiconductor physics for the last forty years and have been the material of use in microelectronic and optoelectronic technologies up to the present time. However, in recent years enormous interest in conjugated organic materials has developed, largely as a result of much fundamental research in finding new materials that meet future requirements of miniaturization and complex system designs.

Conjugated organic polymers (or macromolecular semiconductors) offer a viable alternative to the traditional inorganics because of their small size, diversity, and ease of preparation and processing. For example, the typical dimensions of macromolecular structure of polymers are ~100 Å which are two to three orders of magnitude smaller than the existing and proposed devices developed by current state-of-the-art lithographic techniques. Macromolecular semiconductors offer an additional feature in that their electronic and optical properties can be controlled by tailoring the molecular structure by creative chemistry.

The work presented in this chapter was prompted by a lack of understanding of the origin of charge carriers in π-conjugated polymer-based devices.[307,308] In this study, electrical characteristics of poly(3-hexylthiophene) (P3HT) synthesized by chemical oxidative coupling using $FeCl_3$, were investigated by chemical and spectroscopic analyses, electrical characterization of Thin-Film Metal-Insulator-Semiconductor Field Effect Transistor (TF-MISFETs) based on P3HT macromolecular semiconductor, and Capacitance-Voltage measurements on P3HT-based Metal-Insulator-Semiconductor diodes. Three samples of poly(3-hexylthiophene) were investigated. The samples were

chemically identical but differed in their relative concentration of residual iron impurity. Electrical parameters were determined in order to examine the relationship between residual impurities, charge carriers and transport properties of poly(3-alkylthiophenes).

Spatial control of the electrical properties of macromolecular semiconductor-based devices is another intriguing property of molecular systems. As a result of the photochemical study described in Chapter III of this thesis, it was found that semiconducting π-conjugated polymer regions can be spatially converted to insulating regions by virtue of their photo-oxidative chemistry (*cf.* III.5.6). This concept was used to tailor the electrical properties P3ATs, and convert the resistor-like characteristics of thick film polymer-MISFETs into devices possessing encapsulating insulating layers.

The physics of macromolecular semiconductors and techniques of probing their properties are the subject of the following discussion.

V.2 Physics of Macromolecular Semiconductors

The semiconductor physics of conjugated polymers is expected to differ markedly from inorganic semiconductors such as GaAs or Si. The latter is a three dimensional bonded material with rigid lattice structure and possessing strong electron-electron interactions.[70] Macromolecular semiconductors are, however, quasi-one-dimensional possessing strong electron-phonon interactions which result in lattice distortion in presence of added charges (polarons and bipolarons).[71] These charges are mobile and are thus expected to dominate charge transport in the materials. In addition, their generation gives rise to new electronic levels in the band gap.

V.2.1 Electrical Properties

π-Conjugated polymers, in the pure (undoped) states, are best described as electrical insulators. This is because of their relatively large band gap energy, (E_g > 1 eV). Conductivity (σ) of P3ATs, for example, in the "neutral" form is, however, ~10^{-7} $\Omega^{-1}cm^{-1}$ which is much higher than most insulators (σ=10^{-18} $\Omega^{-1}cm^{-1}$).[309] This conductivity is not an intrinsic property of the polymer and is believed, but not proven, due to structural defects and impurities. The electrical conductivity (σ, $\Omega^{-1}cm^{-1}$) is proportional to the product of the free-carrier concentration (n, number of free charge carrier per unit volume, cm^{-3}) and the carrier mobility (μ, cm^2. V^{-1} s^{-1}).[310] Thus

$$\sigma = e\, n\, \mu \qquad \text{(V.1)}$$

where e is the unit electronic charge (1.6x10^{-19} C). For intrinsic semiconductors, the carrier concentration decreases exponentially with increasing band gap according to

$$n = N_C\, e^{(E_c - E_F)/kT} \qquad \text{(V.2)}$$

where E_C is the conduction band energy, N_C is the density of states in the conduction band, and E_F is the Fermi level energy. At room temperature (T=298 K), the thermal energy kT is 0.026 eV. The band gap energies of conjugated polymers, in general, are relatively large (> 1 eV). The concentration of thermally-generated charge carriers is, therefore, very low at room temperature.

Equation V.1 can also be written as[311]

$$I = e\, n\, \mu\, E \qquad \text{(V.3)}$$

This equation describes the current characteristics, I, of the material under low applied electric fields, E, according to low field approximation. Under low applied electric fields, the current follows the field in a linear fashion due to charge balance between the available carriers in the material and injected carriers from electrodes, assuming ohmic contact. In contrast, as the field

increases charge inbalance is produced due to the relatively low concentration of free charge carriers in the polymer compared to the injected carriers and current flow becomes limited by space charges.

V.2.2 Nature and Origin of Charge Carriers

The nature of charge carriers in conjugated P3ATs has been discussed in terms of the polaron-bipolaron model (*cf.* IV.2). The origin of these carriers in the "neutral" form of the polymer is more complex. In general, there are two mechanisms responsible for carrier generation in materials; namely intrinsic and extrinsic.[310] In the intrinsic mechanism, electrons and holes may be generated by thermal- or photo-excitation from the valence band to the conduction band. The excitation energies must be greater than the band gap energy of the material. Thermal energy at room temperature is 0.026 eV which is much smaller than E_g of conjugated polymers. This mechanism, thus, cannot account for the relatively high dark conductivities of the material. Photoexcitation is important only in photoconduction and photoluminescence of materials (*cf.* I.3.1). The extrinsic mechanism infers that generation of charge carriers is due to the presence of extrinsic or foreign material, i.e. impurities. Based on electron affinities/ionization potentials of the impurities relative to that of the host material, impurities may act as electron donors or electron acceptors. These lead to an increase of charge carriers density and to the creation of electronic states in the band gap of the host material. This mechanism of carrier generation is quite conceivable in conjugated polymers due to the high level of impurities in the material as a result of the catalyst used in the polymerization processes.

Other possible mechanisms of carrier generation include:[310] (a) carrier injection from electrodes which are governed by the nature of both semiconductor/electrode (metal) contact and the space charge region formed in

the semiconductor, and (b) field-assisted carrier generation which separates carriers before recombination or modifies the potential barrier profile of traps i.e. de-trapping and liberation of carriers. These two mechanisms are discussed in section V.3.

V.2.3 Mechanism of Charge Carrier Transport

Transport of charge carriers in conjugated polymers is controlled by their mobility. Although conjugated polymers have backbone structures well suited for carrier transport, effective charge carrier mobility, μ_{eff}, is usually low. Three main components contribute to carrier transport (Figure V.1).[312-314] These are *intra*-chain (quasi-one dimensional transport, process 1), *inter*-chain (process 2), and *inter*-particle transports (process 3).

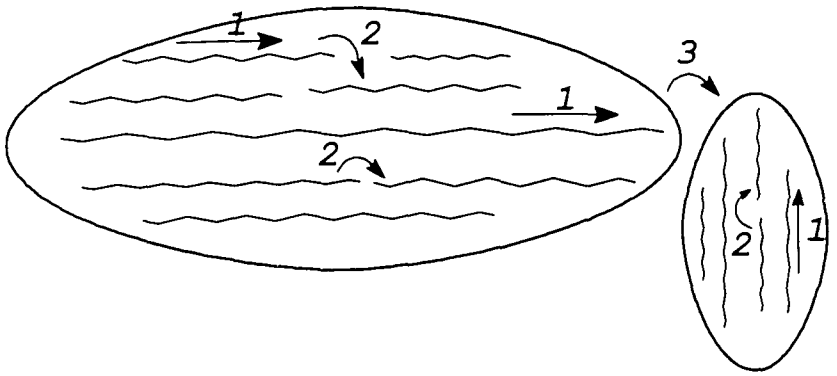

Figure V.1: Charge transport in conjugated polymers

This transport model has been demonstrated using Polyacetylene (PA). PA films have fibrillar structure with ~30% void volume.[310] Charge carriers have to traverse these *inter*-particle voids which affect the effective mobility, μ_{eff} (Figure V.1 process 3). On the microscopic level, the persistence length of a polymer chain is usually much longer than the effective conjugation length, since

the π-system along the polymer backbone is interrupted by structural defects. These defects necessitate transport of charge carriers from one chain to another (*inter*-chain transport, process 2). This process is believed to be the rate limiting step for 3D-transport since the transport distance and transport barrier between chains is much larger than along the chain. The large anisotropy of electrical conductivities of the material supports this model.[315] Thus, the conductivities measured in the direction of chain orientation ($\sigma_{||}$) is 10-100 times greater than that measured in the perpendicular direction ($\sigma_{\perp}$). This, of course, is a direct consequence of the higher carrier mobilities along the polymer chains.

The mechanism of charge carrier transport can be best described in terms of the hopping models in which the carrier transport occurs by random jumping (hopping) over barriers of a certain energy and width.[316,317] The barrier energy is approximately equal to the ionization energy of the material. If hopping occurs over the potential barrier separating two adjacent molecular, or ionic sites, the charge transport process is a "phonon-assisted hopping". The hopping between non-adjacent molecular, or ionic sites, is described as "long-, or variable-range hopping". This process is known as "percolation". The three dimension variable-range hopping (3D-VRH) appears to be the dominant mechanism in P3AT semiconductors since conductivity-temperature relationships are best described by the exponential dependence $\sigma \propto exp\ (-T^{-1/4})$.[318,319]

V.3 Macromolecular Semiconductor Device Physics

The electronic and transport properties of macromolecular semiconductors have been investigated using semiconductor devices such as metal-insulator-semiconductor (MIS) structures.[307-309] These include MIS-diodes (MISDs), and MIS-field effect transistors (MISFETs). The basic aspects of the device physics and operation are discussed in the following sections. The

discussion will be limited to unipolar devices, in which only one type of carriers usually participates in the conduction processes. These devices are the common type of conjugated polymer-based device. The metal-semiconductor contacts play a central role in the device operation and this is discussed first.

V.3.1 Metal-Semiconductor Contacts

At the surface of any solid there is an energy barrier which holds the electrons in the material. Two main parameters are necessary to define this energy barrier.[320,321] The electron affinity, χ, is defined as being the energy required to remove an electron from the bottom of the conduction band to a point in vacuum just outside the solid. The other parameter is the work function, ϕ_F, which is defined as the work required to remove an electron at the Fermi level to the vacuum level. For semiconductors, the relationship between the two parameters is given by equation V.4. This is shown schematically in Figure V.2

$$\phi_s = \chi_s + (E_c - E_F) = \chi_s + \phi_o \qquad \text{(V.4)}$$

E_C and E_F represent the energy of the conduction band and Fermi level, respectively, and ϕ_S is the work function of the semiconductor. Figure V.2 also shows the work function of metals for comparison.

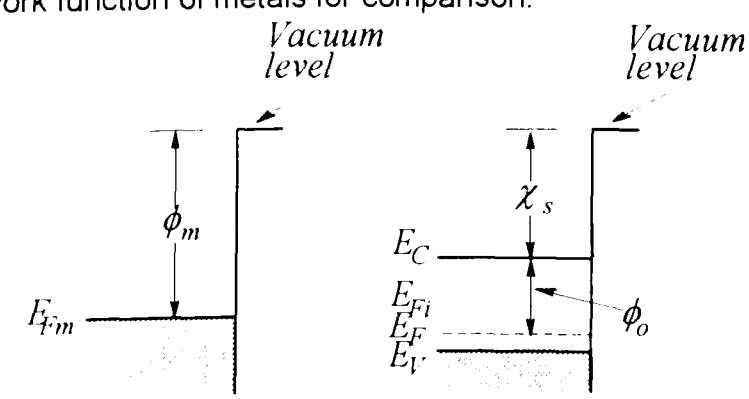

Figure V.2: Energy band diagrams for the surface regions of (a) Metals, and (b) p-type Semiconductors. E_{Fi} represents the intrinsic Fermi level.

When an electrical contact is made between the metal and semiconductor, a potential difference, known as the contact potential, is created between the two materials and is equal to the difference between the work functions of the two solids. Considering a contact between p-type semiconductor and a metal with a work function, ϕ_m, that is lower than that of the semiconductor, ϕ_s, the contact potential, ϕ_b is given by

$$\phi_b = \phi_s - \phi_m \qquad \text{(V.5)}$$

ϕ_b drops across the space-charge region created in the semiconductor. Figure V.3 shows the energy-band diagrams for such a contact.

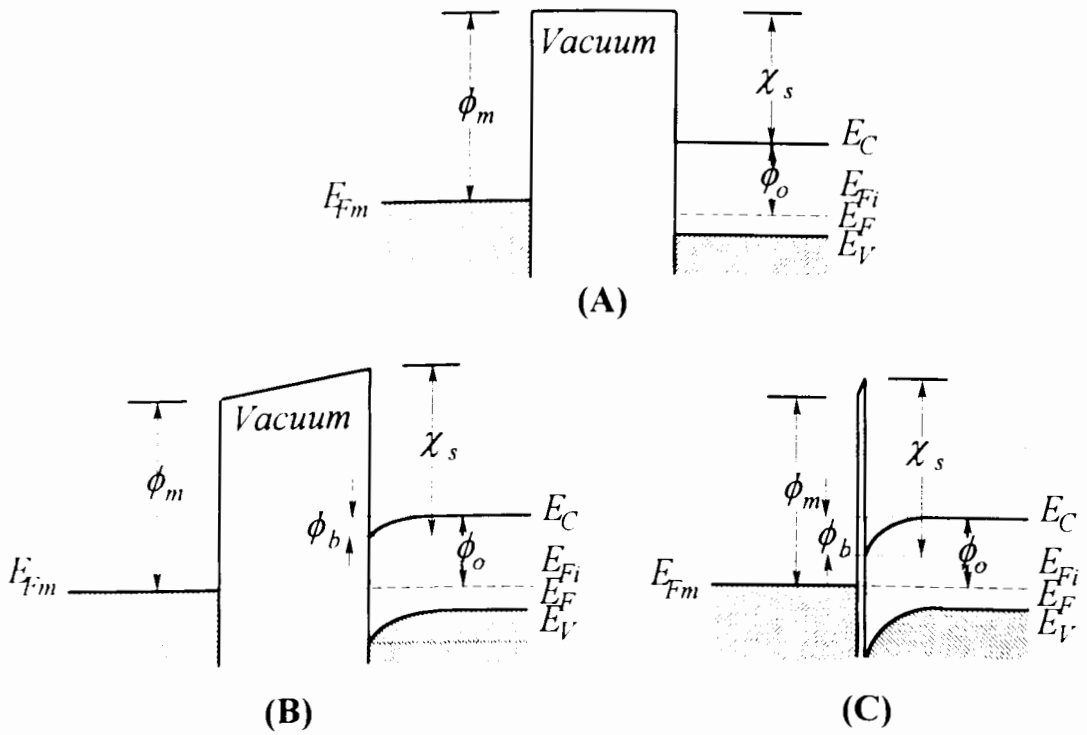

Figure V.3: Energy-band diagram for a metal-p-type semiconductor contact: (A) Isolated, (B) Thermal equilibrium, and (C) Intimate contact.

In Figure V.3, the work function of the metal is lower than the semiconductor, electrons in the metal thus flows into the semiconductor. This flow continues until the Fermi levels are adjusted to the same height, corresponding to thermal equilibrium conditions, as shown in Figure V.3B. The electrostatic field established by the accumulated space charge is sufficient to stop any further charge transfer. Because the separation of the metal and the semiconductor is large, the contact potential is dropped mostly across the vacuum, as shown in Figure V.3B. Accordingly, the energy bands of the semiconductor bend slightly downward at the surface corresponding to a small space charge region. As the separation between the metal and semiconductor decreases until the surfaces are at atomic distances, the bending of the bands increases until the contact potential is dropped completely across the space-charge region (Figure V.3C). At such separations, despite the height of the energy barrier between the metal and the semiconductor, the barrier width is sufficiently small that electrons are able to penetrate the barrier by tunneling. It is also to be noted that because the free carrier density in the semiconductor is much less than in the metal, the space charge region extends much further into the bulk of the semiconductor. In contrast, the space charge region at the metal surface is very thin.

According to equation V.5, ϕ_b depends on the work function of the metal and on the affinity and doping level of the semiconductor. In addition, the values of ϕ_m and ϕ_s determine the nature and type of contact. The contact shown in Figure V.3 is referred to as a Schottky contact where ϕ_m is lower than ϕ_s. In general, there are two types of contacts: Schottky contacts (discussed above) and ohmic contacts. The contact between a metal and a p-type semiconductor is ohmic if the work function of the metal, ϕ_m, is larger than ϕ_s of the semiconductor. In this case, electrons transfer from the semiconductor to the

metal in order to equalize the Fermi levels. As a result, an accumulation layer forms in the semiconductor.

V.3.2 Metal-Insulator-Semiconductor Diodes (MISDs)

These devices are useful in studying semiconductor surfaces and the mechanism of device operation.[321] The basic structure of a MIS diode is shown in Figure V.4. The device consists of a metal or polysilicon gate (G) overlaying an insulator layer, usually SiO_2. The structure is completed by deposition of the semiconductor film and a suitable metal to form an ohmic contact (B).

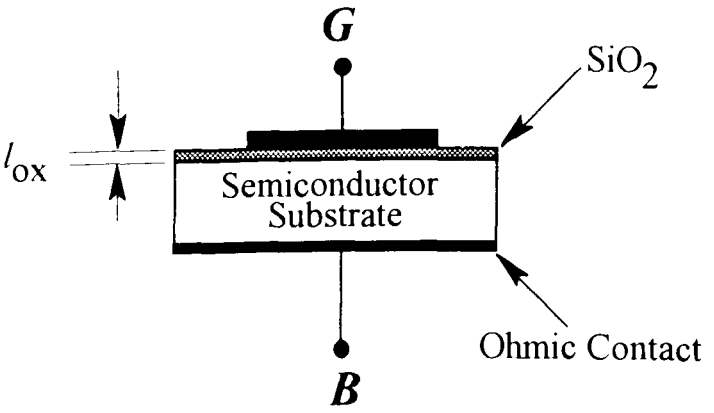

Figure V.4: A typical MIS structure, G and B are the gate and base electrodes, respectively, and l_{ox} is the thickness of the oxide layer

A complete energy band diagram for a MIS diode formed on a p-type semiconductor is shown in Figure V.5. In this diagram, the work functions of the metal and semiconductor are assumed equal so that the Fermi energies in the gate and substrate coincide at a zero bias, V_{GB} = 0. When the MIS diode is biased with positive or negative voltages, three cases may exist at the semiconductor surface.

When a positive bias is applied to the gate (V_{GB}), holes are repelled from the semiconductor and the semiconductor energy bands bend as shown in Figure V.7. As the holes leave the surface, immobile, ionized acceptor ions remain, forming a surface *depletion region*.

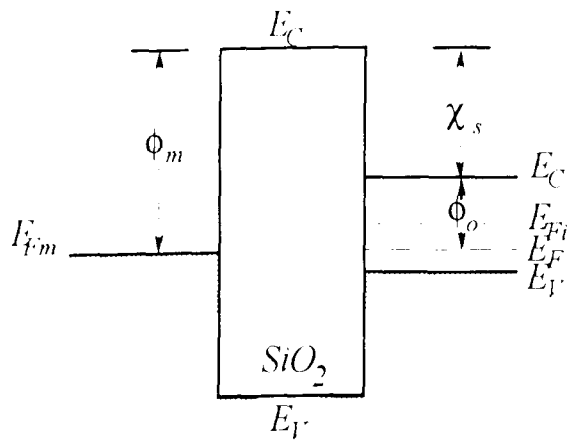

Metal - Insulator - Semiconductor

Figure V.5: Band diagram of MIS diodes

If V_{GB} is made more positive, the bands in the semiconductor will continue to bend downward and E_F at the surface will, eventually, lie midway between the conduction and valence band edges. At this point the surface electron concentration, n_S, is equal to the surface hole concentration, p_S. A further increase in V_{GB} causes n_S to be greater than p_S, so that the semiconductor surface is inverted forming an *inversion layer* (Figure V.7B).

In contrast, if V_{GB} is made negative, holes are attracted to the semiconductor surface, and the band diagram appears as shown in Figure V.7C. In this case the surface accumulates excess holes forming an *accumulation layer*.

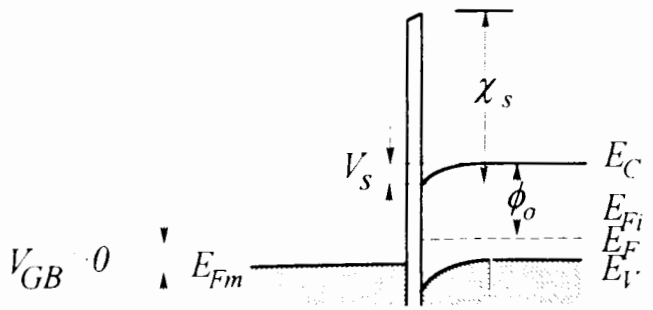

(A) Depletion layer

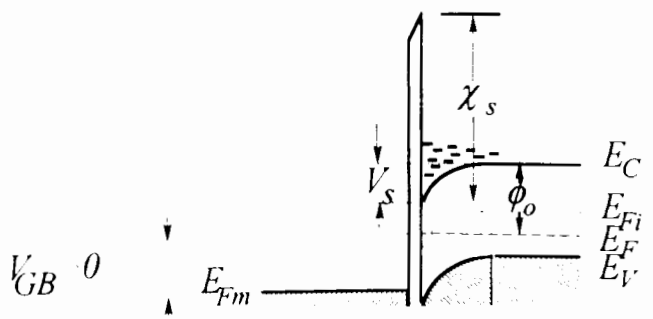

(B) Inversion layer

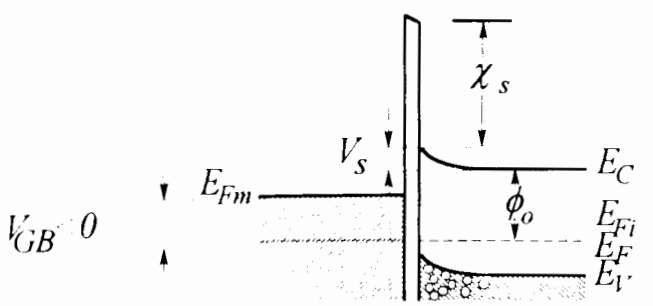

(C) Accumulation layer

Figure V.6: Energy band diagrams and charge distribution of a MIS diode. (A) Depletion, (B) Inversion, and (C) Accumulation layers. V_S is the potential drop across the semiconductor.

The possibility of band bending at the semiconductor-insulator interface and the formation surface-charge layer may be demonstrated through the relationships between the device capacitance and the bias voltage. The measured capacitance, C, is that of the series combination of the insulator capacitance, C_{ox}, and the capacitance of the active region of the semiconductor, C_s, and is given by[322]

$$C = \frac{C_{ox}\, C_s}{C_{ox} + C_s} \qquad \text{(V.6)}$$

Because C_s is large for the accumulation and inversion layers, C is equal to the geometric capacitance of the insulator layer, but falls to a lower value if the depletion layer is formed. In some cases where an inversion layer can not be formed at high positive biases, a deep depletion layer is formed instead. The equivalent circuit and typical C-V response for a MIS capacitor is shown in Figure V.7. In this Figure C_S is shown as a variable capacitor because it is bias dependent.

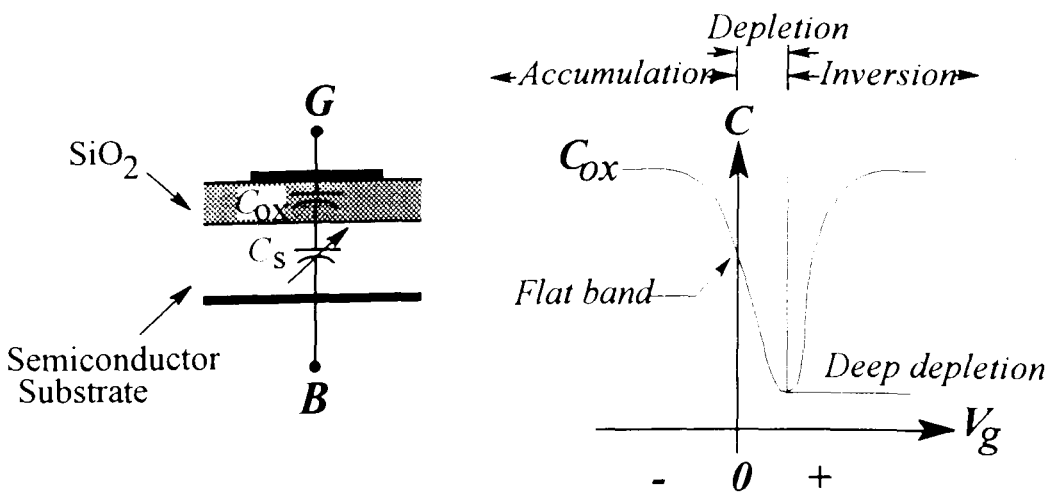

Figure V.7: Equivalent circuit and typical C-V response of MIS capacitor

The variation of capacitance in the deep depletion regime can be modeled as[322]

$$\left(\frac{C_i}{C_c}\right)^2 - 1 = \left(\frac{C_i}{A}\right)^2 \frac{2(V - V_f)}{qN_A \varepsilon\varepsilon_0} \qquad \text{(V.7)}$$

where A is polymer-MIS diode area, N_a is the number of ionized impurities that give rise to charge carriers (majority carrier concentration), C_i is insulator capacitance, V is the applied voltage, V_f is the flat band potential and ε and ε_0 are the dielectric constants of the semiconductor and insulator respectively. Equation V.7 is important in determining the concentration of charge carriers in the material.

V.3.3 Metal-Insulator-Semiconductor Field Effect Transistors (MISFETs)

The device employs an insulated metal (gate) to control the resistance of a semiconducting substrate and the current flow between two ohmic contacts; source and drain. MISFETs are useful for evaluation of the electrical parameters and transport properties of semiconductors. The characteristics and operational features of the Thin-Film MISFETs are discussed below.

Silicon-based MISFETs are based on modulation of the conductance of an *inversion layer* which is created using a rectifying p-n junction contact and appropriate gate biases.[321] Conventional MISFETs are, thus, minority carrier devices. In the case of p-type semiconductors the current carriers are electrons. Thin-Film MISFETs (TF-MISFETs),[323-325] in contrast, are majority carrier devices. These devices are based on modulation of the conductance of an *accumulation layer* at ohmic contacts formed between the semiconductor and metals of suitable work function. These contacts permit majority carrier flow but are usually unable to provide minority carrier currents due to the low supply and slow mobility of these carriers.

V.3.3.1 Structure of TF-MISFETs

The structures of TF-MISFETs comprise of two laterally spaced electrodes, a source and drain, connected by a thin semiconductor film whose conductivity can be modulated by a third electrode called the gate (Figure V.8).[323] The source and drain make ohmic contacts to the semiconductor, but the gate is separated from the semiconductor by a thin layer of insulator. Materials such as glass are usually used as a substrate.

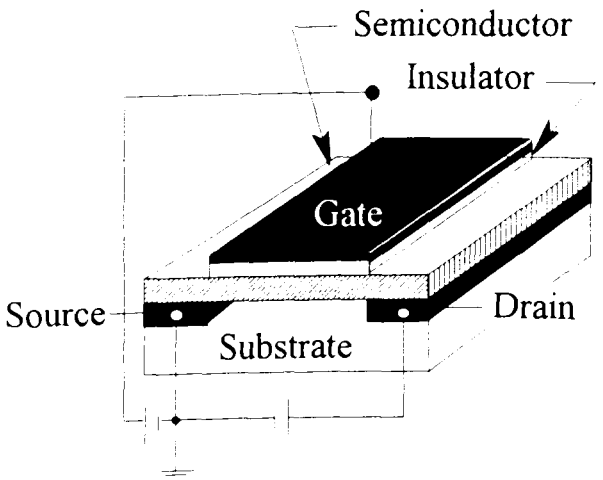

Figure V.8: Structure of Thin-Film Metal-Insulator-Semiconductor Field Effect Transistors (TF-MISFETs)

The device may be constructed to operate in the depletion-, or enhancement-modes.[323] In depletion-mode devices, the semiconductor conductivity is normally *high* but can be reduced by the action of the gate. In contrast, in an enhancement-mode device, the initial conductivity is small but can be enhanced by the gate action. Since the goal of this study is to characterize the electrical properties of macromolecular P3AT semiconductors in the neutral form (σ = 10^{-7} $\Omega^{-1}cm^{-1}$), the enhancement-type devices were

employed in the study. The following discussion will thus be focused on enhancement-type TF-MISFETs.

V.3.3.2 Electrical Characteristics of TF-MISFETs

Modulation of the semiconductor conductivity in the TF-MISFETs by the variation of gate potentials results from control of the concentration of charge carrier in the source-drain regions. In enhancement-type devices utilizing p-type semiconductors, the drain current is essentially zero at the zero gate bias and increases by many orders of magnitude as the gate voltages are raised from zero to several volts negative with respect to the source. The typical drain current-voltage characteristics (I-V) for TF-MISFETs are shown in Figure V.10.[323]

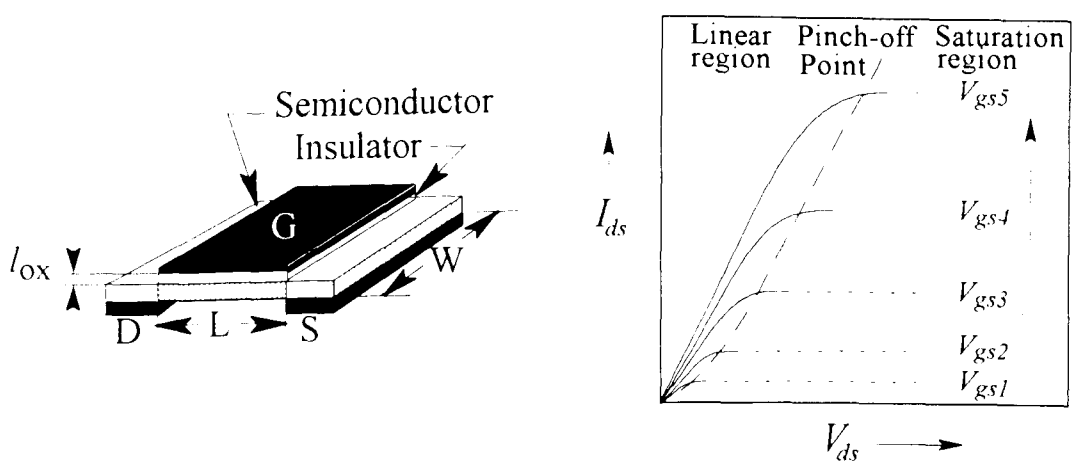

Figure V.10: (A) TF-MISFET structure used in the I-V analyses
(B) Typical I-V characteristics of enhancement-type TF-MISFETs

Increasing voltage steps applied to the gate yields a family of drain current-voltage curves which are linear at low bias and saturate at higher drain voltage.

In the linear region of operation, the drain (or channel) current (I_{ds}) is given by the expression[324,325]

$$I_{ds} = \mu_{FET} C_{ox} \frac{W}{L}\left\{(V_{gs} - V_{th})V_{ds} - \frac{1}{2}V_{ds}^2\right\} \qquad \text{(V.8)}$$

and for the saturation region

$$I_{ds} = \frac{1}{2} \mu_{FET} C_{ox} \frac{W}{L} (V_{gs} - V_{th})^2 \qquad \text{(V.9)}$$

where L and W are channel length and width respectively, C_{ox} is capacitance of oxide layer, and V_{gs}, V_{ds} and V_{th} are the gate, drain and threshold voltages respectively. The threshold voltage is defined as the gate voltage required for pinch-off of the drain current. The other current component is the bulk current (I_{bk}) which can be represented as

$$I_{bk} = \sigma \frac{W}{L} l V_{ds} \qquad \text{(V.10)}$$

where l and σ are thickness and bulk conductivity of the polymer film.

The initial linear increase in the drain current can be explained in terms of the following model.[324] At zero gate bias, the semiconductor energy bands are bent down at the semiconductor-insulator interface as shown in Figure V.10. When the gate is biased negatively, holes are drawn toward the interface, causing the bottom of the conduction band at the interface to be higher relative to the Fermi level. This gives rise to highly conducting channels close to the insulator surface and results in higher conductivities of the semiconductor film.

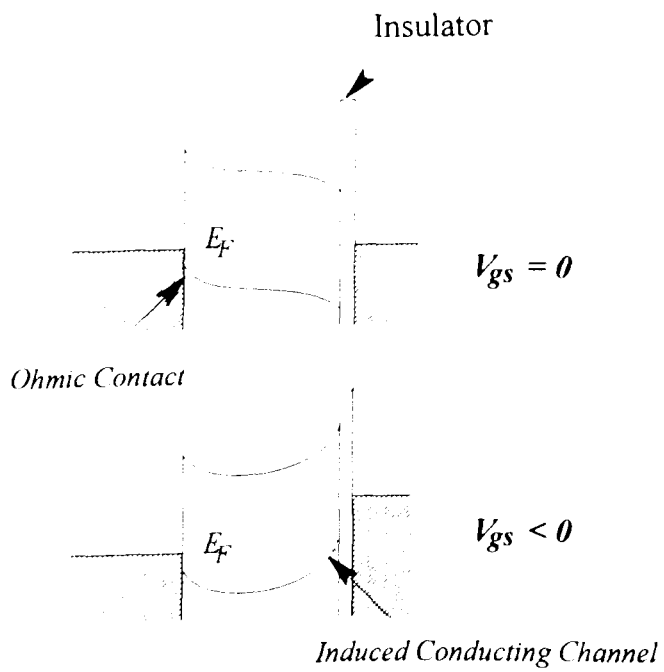

Figure V.10: Energy band diagrams of enhancement-mode TF-MISFETs

Saturation of the drain current can be explained in terms "pinch-off" model.[323-325] As the drain voltage becomes more negative than the gate, the conducting channels near the drain gradually increases in length by an amount sufficient to hold the drain current substantially constant, and the channels are said to be "pinched off". The failure of the drain current to saturate results from the existence of non-modulated current paths existing in series or in parallel with the conduction channel. These paths exist if the semiconductor is too thick or too conductive.

During the course of this study a number of reports concerning polymer-based MISFETs have appeared. A brief summary is presented below.

V.4 A Survey on π-Conjugated Polymer-Based MIS Devices

Several studies have been reported concerning polymer- and oligomer-based metal-insulator-semiconductor devices.[81,326-331] Of these, polythiophene-based structures have attracted the most attention.[328-336] The electronic properties of these polymers, as determined by electrical characterization of MIS structures, are found to be highly dependent on the method of polymer preparation, the nature and level of impurities, and the thickness of the polymer film. Typical electrical parameters of TF-MISFETs based on polythiophene (PT) and poly(3-alkylthiophenes) (P3ATs) semiconductors prepared by electrochemical and Grignard polymerization techniques are summarized in Table V.1.

Table V.1 : Electrical Properties of Poly(3-Alkylthiophenes)

Electrical Parameter	***Synthetic Method***	
	Electrochem.	***Grignard***
σ ***(S/cm)***	5×10^{-8}	10^{-6}
μ_{FET} ***(cm²/V.s)***[a]	10^{-5}	10^{-4}-10^{-5}
n (cm⁻³)[b]	3×10^{16}	3×10^{17}
V_{th} ***(V)***[c]	-13	--
[Impurity] (cm⁻³)	ClO_4^-, --	I^-, 10^{18} [d]
Reference	328,329,336	330,332-335

[a] field effect mobility, [b] carrier concentration, estimated from I-V characteristics of polymer-MISFETs using $\sigma = e\mu n$, [c] threshold voltage, [d] determined by ESR and Rutherford Back Scattering.

In addition to those described above, a number of studies have utilized FETs possessing novel device configurations. For example, Schottky gated FETs using free standing poly(3-alkylthiophene) films with Schottky gated electrode configurations have been reported.[332, 337-339] Mobilities were estimated to be ~10^{-3}-10^{-5} $cm^2/V.sec$. Nano-transistors and transistors fabricated on nanometer metal islands have also been investigated.[340,341] The field effect mobility of carriers in these transistors was similar to micro-scale devices (~10^{-5} $cm^2/V.sec$). The effect of enhanced molecular order via stretch orientation and Langmuir-Blodgett (LB) techniques on device performance have also been investigated. Field effect mobilities, however, were similar to conventional polymer devices.[331,335]

Thiophene oligomers (α-nT, n=3-8) have also been studied, as models of the parent polythiophene.[326,327,342-356] Oligomers have conductivities of ~10^{-6} S/cm. This relatively high conductivity is attributed to the presence of bulk impurities which give rise to free charge carriers.[348] The field effect mobility and charge density of α-6T oligomer based-MISFETs are reported to be ~10^{-4}-10^{-5} $cm^2/V.sec$ and 10^{14} cm^{-3}, respectively.[353,355] The field effect mobility is found to be dependent on the nature of the insulating material used in the MIS device. Cyanoethylpullulane insulator-based devices (ε = 18.5) yields μ_{FET} of 2x10^{-1} $cm^2/V.sec$ while SiO_2 -based devices (ε = 3.9) yield values of 5.0x10^{-5} $cm^2/V.sec$.[347-349] This difference is attributed to the influence of the insulator on the crystallinity of the oligomers at the semiconductor-insulator interface. Derivatization of thiophene oligomers is found to have a dramatic effect on μ_{FET}. Oligomers end-capped with alkyl groups have much higher field effect mobilities (1.5x10^{-2} $cm^2/V.sec$) by virtue of self-organization of the constituent molecules on the insulator.[351-354] Substitution at the β-position of thienyl

moieties with alkyl groups, however, results in a substantial decrease in μ_{FET} ($5x10^{-6}$ $cm^2/V.sec$).[350]

Capacitance-voltage (C-V) measurements of MIS structures complement field effect transistor studies. For p-type semiconductors, ramping the bias from positive to negative voltage usually increases the overall capacitance of the structure, after which a constant capacitance is reached having a value equal to the geometric capacitance of the oxide layer. This behavior is typical of most polymer-MIS structures indicating that the conduction channel is due to accumulation of majority positive carriers at the insulator/polymer interfaces. A depletion layer is formed under positive gate bias, but no inversion of majority carriers has been observed for polythiophene-based devices.[329,345] The C-V characteristics are qualitatively similar to metal-insulator-p-type silicon structures, which operate under the formation of an accumulation layer under negative bias. C-V investigations also provide information on the nature of polymer/metal interfaces and the dopant distribution profile.[357,358] Measurements on Al/polymer/Au and ITO/polymer/Au Schottky diodes show that the dopant is not homogeneously distributed in the polymer film, but is concentrated at the polymer/metal interface. Furthermore, application of an electric field for prolonged periods (2 *V* back bias for 3.5 hours) caused migration of dopant. It is important to note that the polymer used in the study was prepared by the Grignard route which produces highly mobile iodide impurities. Whether or not dopant diffusion is important in polymers which contain less mobile impurities, such as those obtained during the oxidative coupling, remains to be seen.

The parent π-conjugated polymer, polyacetylene (PA), has also been actively studied as the semiconducting component in MISFETs.[81,359-361] The polymer is also a p-type semiconductor and the mobility of charge carriers is

similar to that of other π-conjugated polymers (~10^{-5} $cm^2/V.sec$). The density of charge carriers, as calculated from measurements of depletion widths in Schottky barrier diodes, is calculated to be ~10^{16} cm^{-3}. Electron spin resonance (ESR) results show a rather high spin concentration (10^{19} cm^{-3}). The origin of these carriers is attributed to defects, and impurities associated with isomerization from *cis* to *trans*. It is concluded that dopants associated with the carriers do not readily migrate under an applied electric field as evidenced by C-V measurements.[360]

The work described above highlights the interesting electrical properties of π-conjugated polymers and the significant efforts that have been made to understand these properties. However, the origin of charge generation and factors controlling the transport properties are poorly understood. *Pure* conjugated polymers should be insulators (conductivity ~10^{-18} S/cm) because of their wide band gap. It is believed, but not proven, that unintentional doping of the material by residual catalyst used in the polymerization process leads to the formation of acceptor states in the band gap and the semiconducting properties. Field effect transistors, thus, operate by controlling the space charge density, which modulates the conductance of the polymer film. It is not clear, however, whether the electric field applied across the gate and source generates new carriers or simply modulates the distribution of charge carriers already existing in the polymer.

V.5. Experimental

Polymer. Polymerization of 3-hexylthiophene was achieved by chemical oxidative-coupling according to the procedure described in Chapter II (*cf.* II.2). The solid product was purified following procedures described in Chapter II (*cf.* II.2.2). Polymer samples of identical chemical structure but different concentration of residual iron impurity contents were obtained. **P3HT-A** contained 3.2 wt% (9.6 mol%) based on the ratio of Fe to thienyl rings; **P3HT-B** contained 1.32 wt% (4.15 mol%); and **P3HT-C** contained 0.05 wt% (0.15 mol%) of iron.

EPR. Electron paramagnetic resonance (EPR) measurements were performed on an X band (9.5 GHz) Bruker ECS106 Spectrometer at room temperature. Freshly recrystallized DPPH (α,α'-diphenyl-β-picrylhydrazyl) was used as the reference for g-value and intensity calibration. The EPR linewidth for DPPH was ca. 1.5 G. The microwave power was set to well below the sample saturation level and the modulation amplitude was kept at ca. 25% of the peak-to-peak line width. Spectra were obtained at 25 ^{o}C and ambient pressure.

Fabrication and analysis of MIS devices. Silicon was chosen as the support substrate for the fabrication of polymer devices because it can be heavily doped to form a gate electrode, and thermally oxidized to yield a silicon oxide insulating layer. The Si substrate plays no *active* role in the device operation. Two inter-digital structures of gold were deposited photolithographically on top of the insulator and used as source and drain. The polymer semiconductor layer was spin cast onto the structure to form working devices. A detailed description of the fabrication process is given below and depicted in Figure V.11: (A) The substrate was an oriented *n*/p-type silicon wafer. After performing standard degrease and clean procedures,[362] the dopant source (B-155 Allied-Signal Inc.) was spin cast onto the wafer. Thermal diffusion

of dopants was carried out at 1100 °C under a N_2 atmosphere. The heavily doped layer served as a gate for the polymer-FET structure; (B) A layer of silicon oxide (200 nm) was grown by a combination of dry and wet oxidation procedures at 1100 °C;[362] (C) AZ 1312SFD (Allied-Signal Inc.) photoresist was used to perform laser direct writing photolithography on the oxide layer in order to open connection windows. The procedure for photolithography was: spin casting of the photoresist and baking at 95 °C for 0.5 h; exposure to 442 nm light; development using by AZ developer (Shipley) and post-baking at 120 °C for 0.5 h; (D) Vacuum evaporation of gold (20 nm); (E) Photolithography using AZ 1312SFD photoresist, etching of exposed gold, and patterning of one hundred gold inter-digitated fingers of width 10 μm and length 300 μm, and spaced 14 μm apart; (F) Exposure of the active region by photolithography. Followed by spin-casting of dilute polymer solution (7000 rpm, film thickness = 0.25 μm) and lift-off of the remaining photoresist. A schematic representation of the polymer-MISFET used in this study is shown in Figure V.12.

MIS structures for capacitance-voltage measurements were also fabricated on a silicon wafer substrate, with silicon oxide as the insulator, and a heavily doped silicon layer acting as one of the electrodes. Aluminum was evaporated and patterned as contact pads, and polymer was spin cast from solution (0.25 μm). Silver epoxy glue was applied to the top of polymer, and the structure was annealed in N_2 at 120 °C for 1h. This structure is shown in Figure V.13. The electrical contacts with the polymer were ohmic. The use of silver expoxy was preferred over metal evaporation in order to prevent exposure of the polymer to high temperature. This structure was bonded to a dual in-line package (DIP), and plugged into a HP 16058 test fixture with electrical and magnetic radiation shielding. C-V measurements were performed in a dark environment.

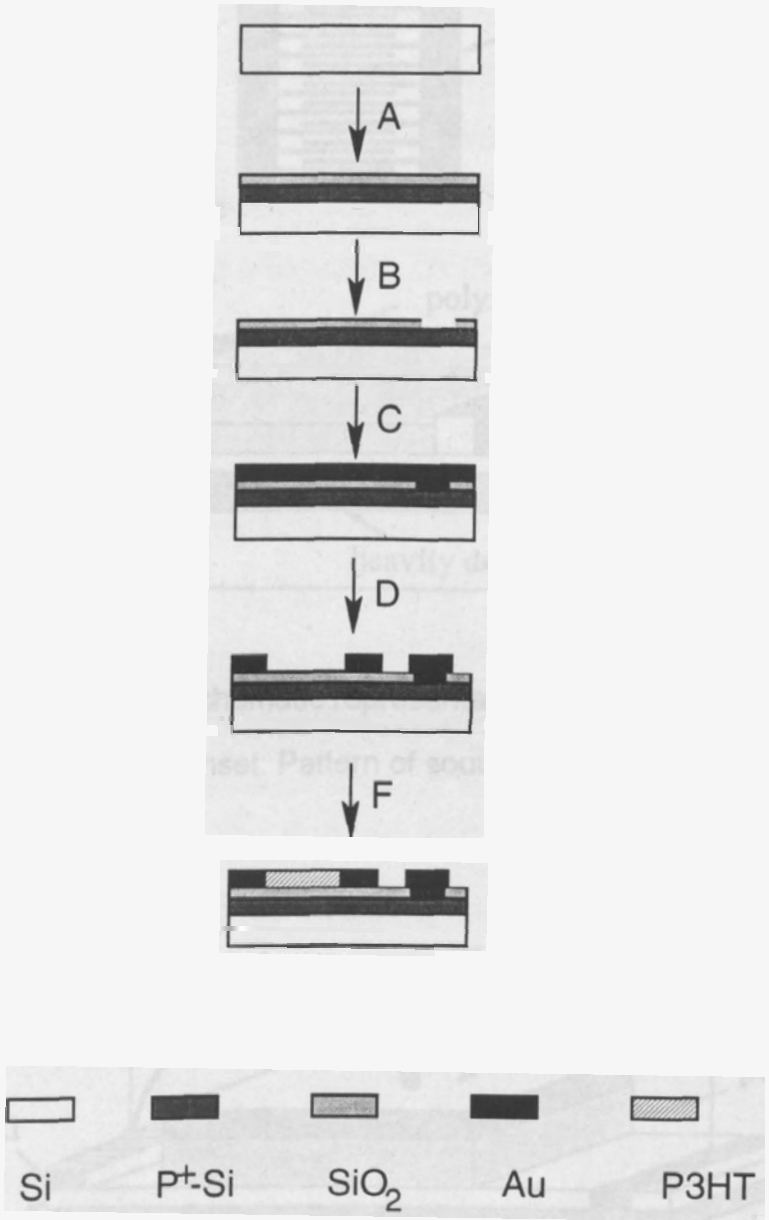

Figure V.11: Fabrication scheme for polymer-MISFET.

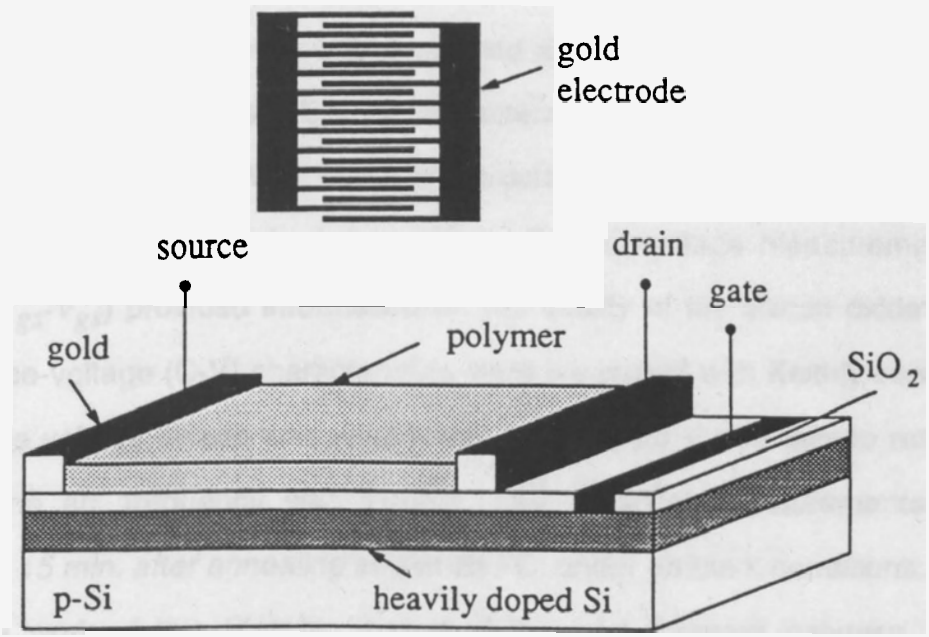

Figure V.12: Schematic representation of polymer-MISFET (inset: Pattern of source and drain contacts)

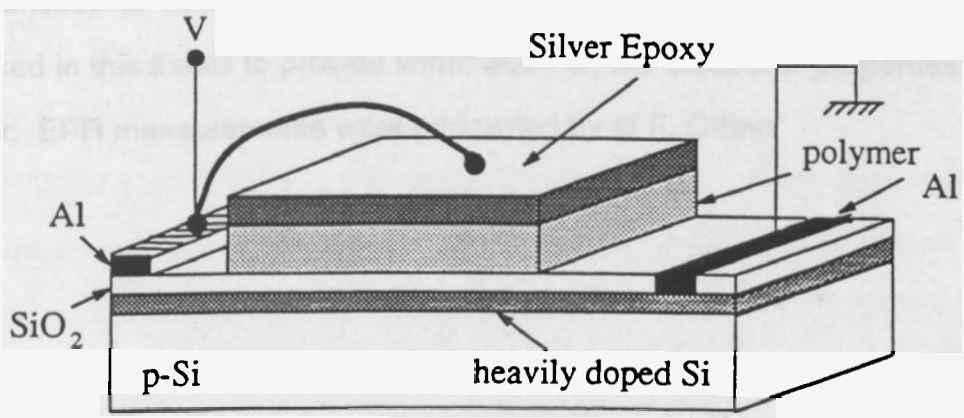

Figure V.13: Polymer-MIS structure prepared for capacitance-voltage measurements

Current-voltage characteristics of polymer MISFETs were measured with a semiconductor parameter analyzer HP4145 and a Bausch and Lomb wafer probing station. Drain current was measured at different drain-source voltages (I_{ds}-V_{ds}) to observe polymer FET-like characteristics, while plots of drain current versus gate voltage (I_{ds}-V_{gs}) were constructed to determine the gate bias modulation of the FET conductive channel. Current-voltage measurements at the gate (I_{gs}-V_{gs}) provided information on the quality of the silicon oxide layer. Capacitance-voltage (C-V) characteristics were measured with Keithly series CV meter. The voltage sweep was varied from -20 V to 20 V at a sweep rate of 2 V/min. The ac. frequency was 1 MHz. All electrical measurements were conducted *15 min. after annealing* and at 25 ^{o}C, under ambient conditions.

The work of this Chapter is part of the joint program between Dr. S. Holdcroft and Dr. M. J. Deen at the School of Engineering Science, Simon Fraser University. The Polymer-MISFETs were constructed by Dr. Z. Xie and I-V and C-V measurements were carried out by X. Lu. In this collaboration, the School of engineering was concerned with modeling and simulating the electrical characteristics of MISFETs (SPICE simulations), whereas I-V measurements were used in this thesis to provide information on the electronic properties of the polymer. EPR measurements were performed by of F. Orfino.

V.6 Results and Discussion

V.6.1 Effect of Impurities on the Electrical Properties of π-Conjugated Poly(3-alkylthiophenes)

V.6.1.1 Chemical Characterization of Impurities

P3HT prepared by oxidative coupling using $FeCl_3$ was found to contain a relatively high amount of residual iron impurities. As described in the experimental section of Chapter II (*cf.* II.2.3), purification of the polymer was performed to varying degrees so as to produce three samples of polymer containing different levels of impurity. This ensures that the polymer's structure and molecular weight were identical and that the variation in electrical properties originated only from the difference in impurity concentration. Atomic absorption spectroscopic analysis indicated the concentrations of residual iron were 0.05 wt% (P3HT-C), 1.3 wt% (P3HT-B), and 3.2 wt% iron (P3HT-A). Elemental analysis determined that the molar ratio of Fe:Cl was 1:1 for each polymer. Mössbauer spectroscopy indicated that the iron impurities exist in the form of an iron(III) octahedral complex. FTIR studies of neutralized P3HT revealed the presence of -OH groups whose concentration is dependent on the concentration of iron impurities.

(P3HT-A), (P3HT-B), and (P3HT-C) exhibit similar absorption spectra in the UV-vis region but small perturbations are observed in vis-NIR region which depend on the concentration of iron impurities. These perturbations are shown in Figure V.14. For each of these films the thicknesses and optical densities at maximum absorbance were similar. The polymers show weak, broad transitions in 650-900 nm region which are interpreted as being due to the presence of low concentrations of (bi)polarons. These transitions become more pronounced with increasing iron concentration. There is some evidence that polaron formation is

preferred with lower impurity concentrations while bipolaron formation is more favored at higher concentrations.[125] This would be consistent with the fact that the bipolaron is thermodynamically more stable than two polarons so that coalescence of polarons occurs at higher concentrations. However, the lack of clearly defined absorption bands in this region and the presence of a strong π-π^* transition indicates that the polaron and bipolaron concentrations are very low.

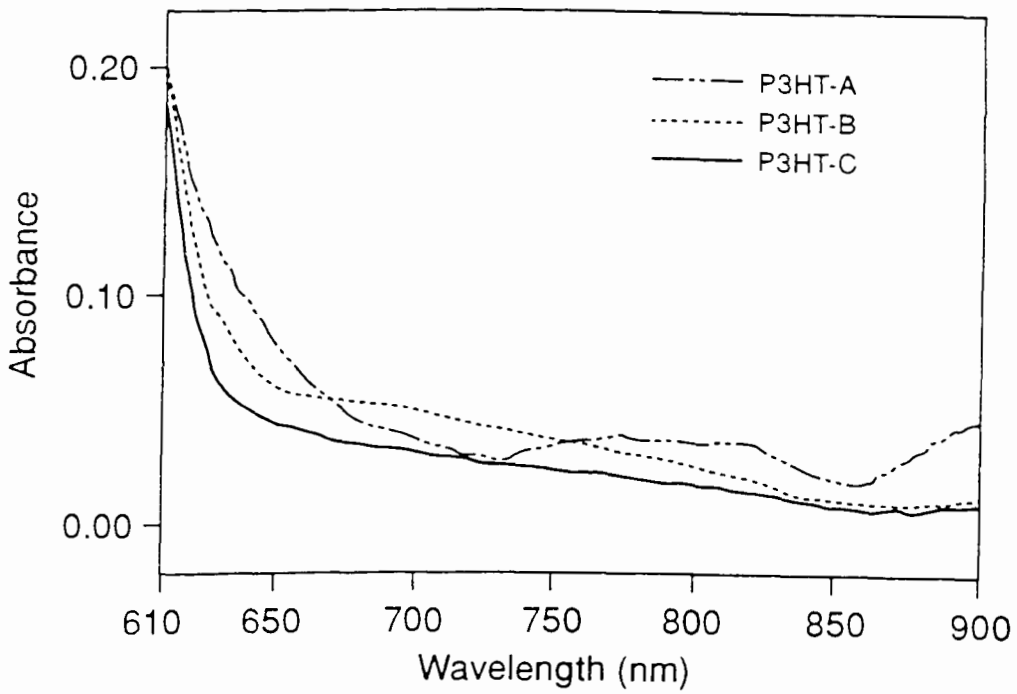

Figure V.14: Effect of residual iron concentration on the vis-NIR spectra of P3HT.

EPR Analysis. EPR analysis of the polymers gave rise to several characteristic signals. The dominant signals were characteristic for Fe^{3+} (g=2.02).[363] The peak-to-peak line widths for these signals varied from 560 G for P3HT-C (0.05 wt% Fe) to 410 G for P3HT-A (3.2 wt% Fe). The lineshapes exhibited a Lorentzian character which indicates relatively fast spin-lattice relaxation times. As expected, the doubly integrated intensity of the Fe^{3+} dispersion curves increased with increasing impurity content.

Centered at 3350 G, and superimposed on the broad Fe^{3+} signal, was a much narrower dispersion curve which was intrinsic to the polymer. These polymer signals are shown in Figure V.15, and the extracted data is presented in Table V.2 for (P3HT-A), (P3HT-B), and (P3HT-C).

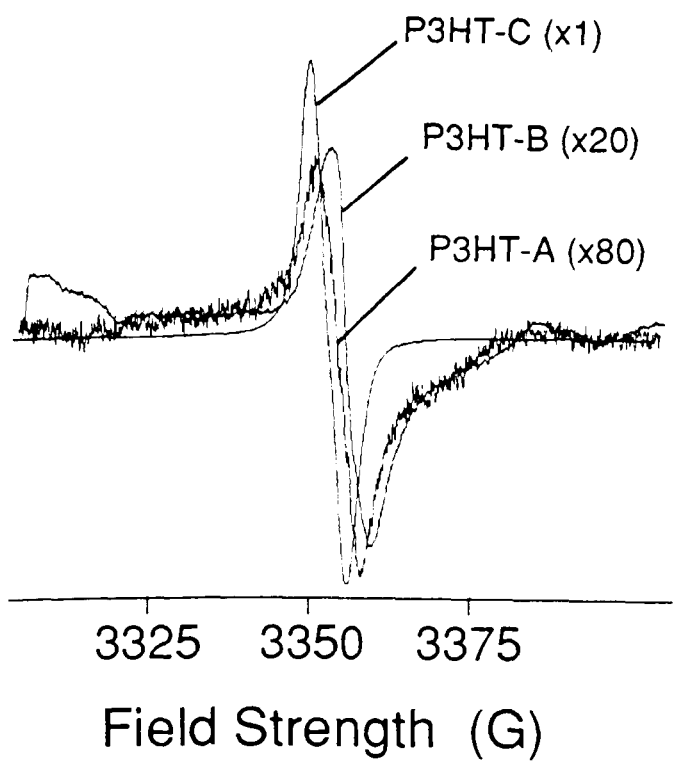

Figure V.15: EPR spectra of P3HT containing different level of iron impurities: (A) P3HT-A, (B) P3HT-B, (C) P3HT-C.

Table V.2. EPR Data of Poly(3-hexylthiophenes).

Polymer	*Fe Content (wt%)*	*Polymer[a] (10 16 #spins/g*	*g-value[b]*	*ΔHp-p (G)*	*Line shape*
P3HT-A	3.20	7.6	2.0029	6.43	Lorentzian
P3HT-B	1.32	4.6	2.0028	7.58	Gaussian
P3HT-C	0.05	127.4	2.0032	6.00	Gaussian

a These values are accurate to 15%.

b The g-values were obtained with DPPH as a marker.

The signal for P3HT-C has a g-value of 2.0032, a line width of 6.00 G, a gaussian line shape, and a spin density of $1.3X10^{18}$ spins/g which indicates 1 spin per 2820 thienyl rings. These parameters are consistent with values found in the literature.[364] The g-value is similar to the free electron value of 2.00232 [365] indicating localization of the electron on the polymer backbone rather than on the sulphur heteroatoms.[366] For the high iron impurity level sample (P3HT-A, 3.2 wt% Fe) the spin density decreases to $7.6X10^{16}$ spins/g revealing a correlation between the impurity concentration and the number of unpaired electrons in the polymer. A similar decrease in spin density has been noted for polythiophene[366] and poly(3-hexylthiophene)[364] doped electrochemically with BF_4^- at high doping levels.

Annealing of Polymer-MISFETs. It was found that annealing of polymer-MISFETs under N_2 atmosphere at 180 ^oC is necessary to achieve a FET-like response for electrical characterization. In order to explain the annealing effect, we note that spin coating alone often renders polymer films with a large free volume (~15%) and retention of 10-20% solvent.[367] Annealing above the glass transition or melting point of the polymer can help in reducing the free volume and the amount of trapped solvent thus leading to a more compact and ordered film. The melting point of the polymer was determined by DSC to be 175 ^oC (*cf.* II.3.3). Following annealing at 180 ^oC in N_2, the chemical structure of the polymers did not change as determined by FTIR. The polymer does however undergo a thermal degradation process under O_2 at this temperature so that rigorous exclusion of oxygen is necessary during annealing (*cf.* III.6.5.2). The physical properties of the polymer are affected by annealing. X-ray diffraction analysis of thin films shows that the reflection signals are narrower and more pronounced for annealed films indicating an increase in crystallinity of the polymer (Figure V.16). This has been recently reported for an analogous polymer, poly(3',4'-dibutyl-2,2':5'2''-terthiophene).[368] UV-vis absorption spectroscopy shows a red shift in the absorption edge upon annealing (Figure V.16-inset) attributed to a decrease in the band gap energy due to increased π-interaction. Annealing therefore results in an enhancement of molecular order and π- interaction.

The effect of annealing on the concentration of charge carriers and nature of the iron impurities was also investigated. The results revealed that the chemical nature and concentration of the iron complexes did not change after annealing as evidenced by EPR and Mössbauer measurements. The concentration of charge carriers, on the other hand, decreases after annealing and then increases upon exposure to air as evidenced by the EPR

measurements. The rate of increase of the carrier concentration was however slow and the changes were insignificant within the time period of the electrical or EPR measurements. A separate study was undertaken to investigate these effects (Chapter VI).

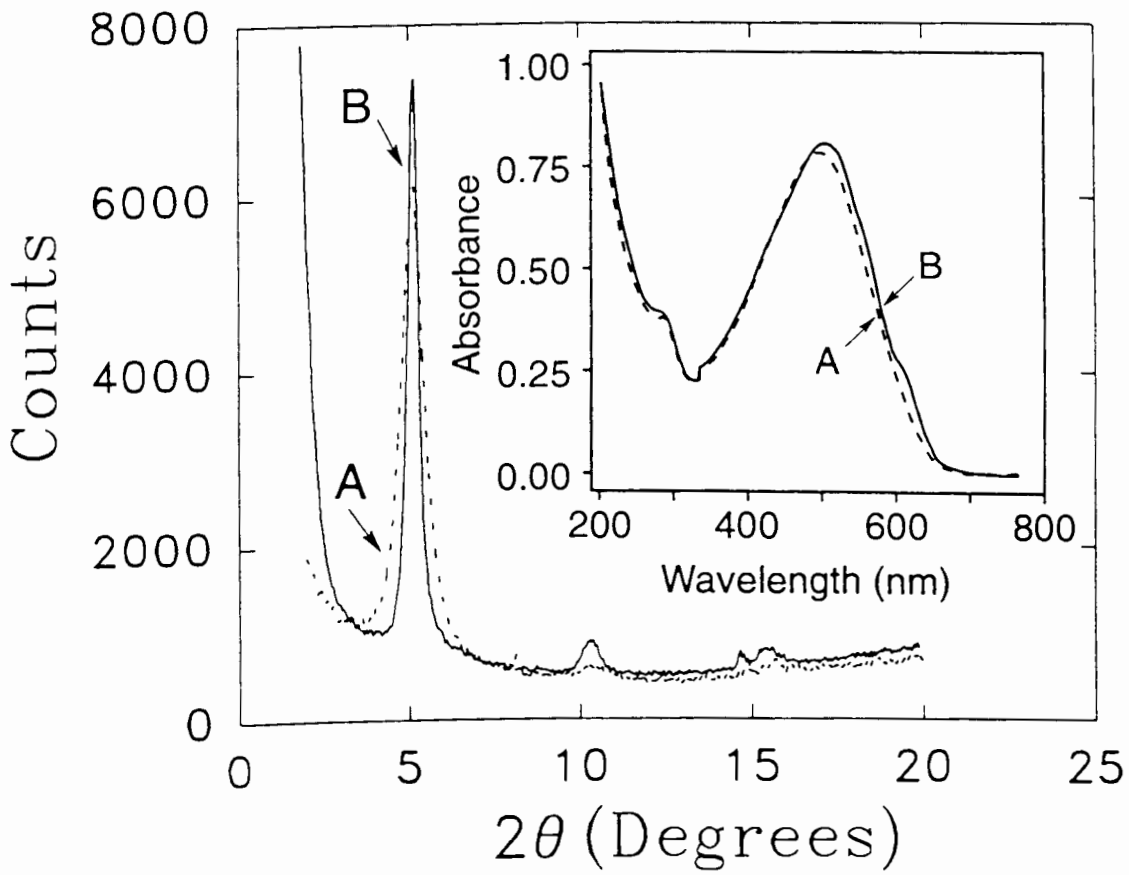

Figure V.16: X-ray diffraction profiles of P3HT-C before and after annealing. Inset: Comparison of UV-vis absorption spectra of P3HT-C. (A) Before annealing, (B) After annealing

V.6.1.2 Polymer-MISFET I-V Characteristics. Prior to thermal annealing at 180 °C under a N_2 atmosphere, I_{ds}-V_{ds} curves of polymer-MISFETs showed a large resistive current, a small gate bias modulation, and the absence of a saturation region (Figure V.17A).

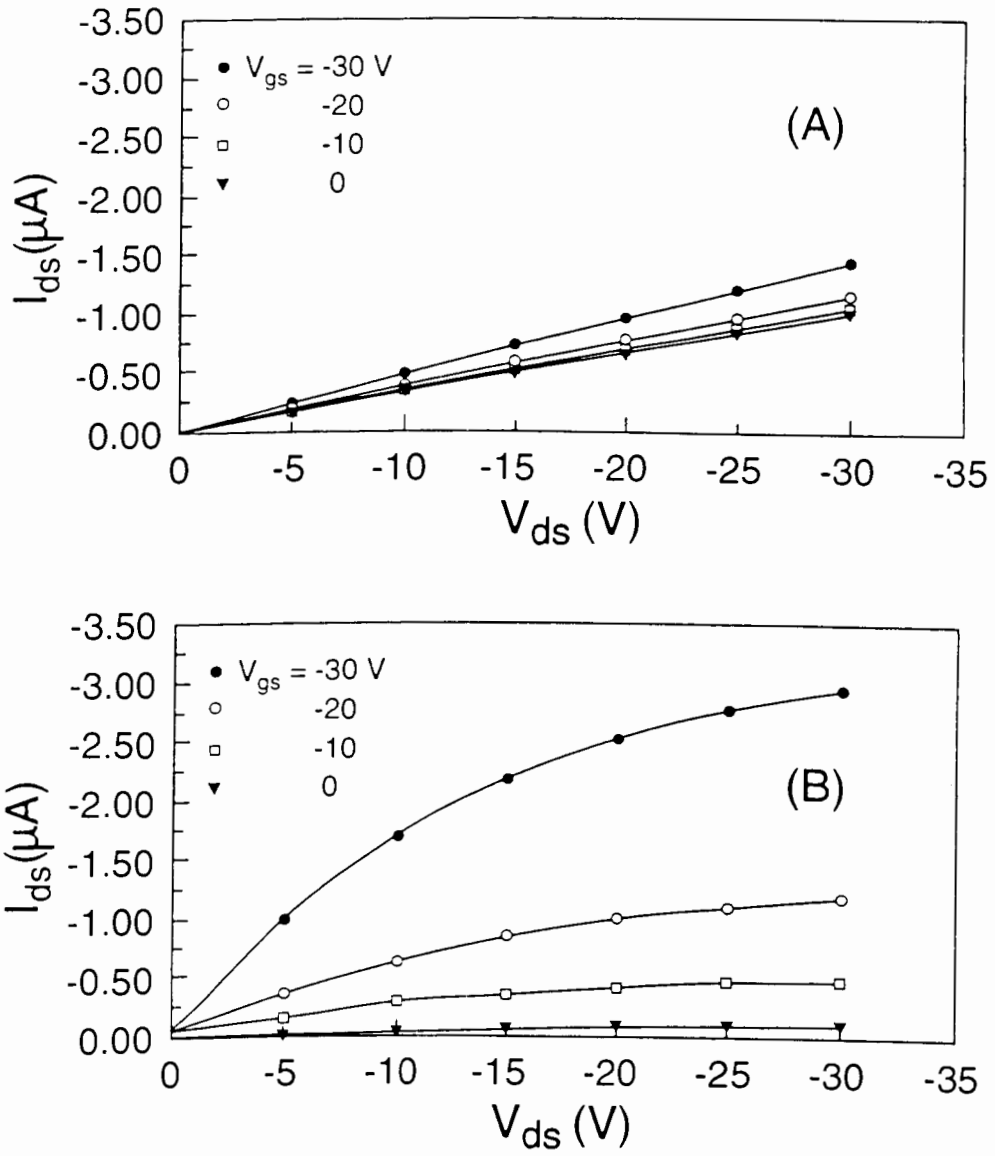

Figure V.17: I_{ds}-V_{ds} characteristics of (P3HT-C)-MISFET (Fe content = 0.05 wt%): (A) Before annealing, (B) After annealing.

Figure V.17B shows typical I_{ds}-V_{ds} curves for an annealed (P3HT-C)-MISFET (0.05 wt% Fe). FET-like behavior is observed with typical linear and saturation regions. For positive V_{gs} bias greater than 0 V, there is almost no change in the drain current, even for V_{ds} biases as high as 30 V. At negative gate bias, I_{ds} increases with V_{gs} indicating that the polymer is a p-type semiconductor and that polymer TF-MISFETs operate through the modulation of an accumulation layer at the semiconductor-insulator interfaces. Similar mechanisms have been observed in devices based on P3ATs that were prepared by Grignard or electrochemical polymerization i.e. P3ATs containing ClO_4^- or I^- impurities.[329,330]

The bulk conductivity can be determined from plots of I_{ds}-V_{ds} at zero bias using equation V.10. To determine the FET-like channel currents, the bulk current is subtracted from drain currents (I_{ds}) at negative biases. Mobilities are determined using equation V.8. The field effect mobility of P3HT was determined to be 2.3 x10^{-5} $cm^2/V{\cdot}sec$ from data presented in Figure V.17B. This is consistent with other reports.[332-336] In comparison with other polythiophenes, the mobility is higher than 3-octyl and 3-dodecylderivatives 10^{-6}-10^{-7} $cm^2/V{\cdot}sec$,[15] but lower than 3 -methyl and 3-butyl substituted analogs 10^{-3}-10^{-4} $cm^2/V.sec$.[334]

Modulation of the semiconductor conductivity by the gate voltage results in changes in the drain current. At low gate biases, the drain current follows a linear relationship with gate voltage according to equation V.8. In contrast, there is a square law dependence of the drain current on gate voltage at high gate biases (equation V.9). I_{ds}-V_{gs} responses of annealed devices at different V_{ds} are shown in Figure V.18. At zero gate bias, I_{ds} has a small current value which is the bulk current. For a small gate bias, I_{ds} increases linearly with V_{gs}. As V_{gs} is made more negative (-20→-40 *V*), I_{ds} shows a sharp increase, which

corresponds to large gate bias modulation in the saturation region. At even higher gate biases (>-50 *V*), the current increment decreases. This is presumably due to the increased carrier concentration at the polymer-insulator interface and subsequent surface scattering of the carriers.

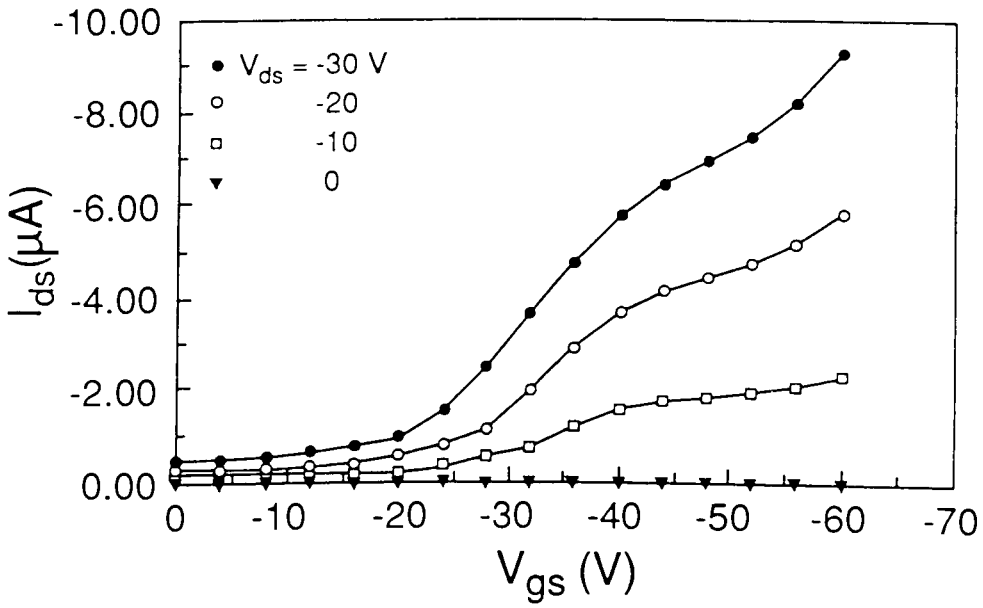

Figure V.18: I_{ds}-V_{gs} responses at different V_{ds} for annealed polymer-MISFET. Data extracted from Figure V.18B.

Figure V.18 can be replotted as $\sqrt{I_{ds}}$ versus V_{gs} at V_{ds}=V_{gs} according to equation V.9 (Figure V.19). At this bias the MISFET operates in the saturation region. From the intercept of this plot with voltage axis, a threshold voltage of -7.1 *V* was obtained, and from its gradient a mobility of 6.9x10^{-5} $cm^2/V \cdot sec$ was calculated. The mobility values estimated at the linear and saturation regions of operation (equations V.8 and V.9) are in good agreement.

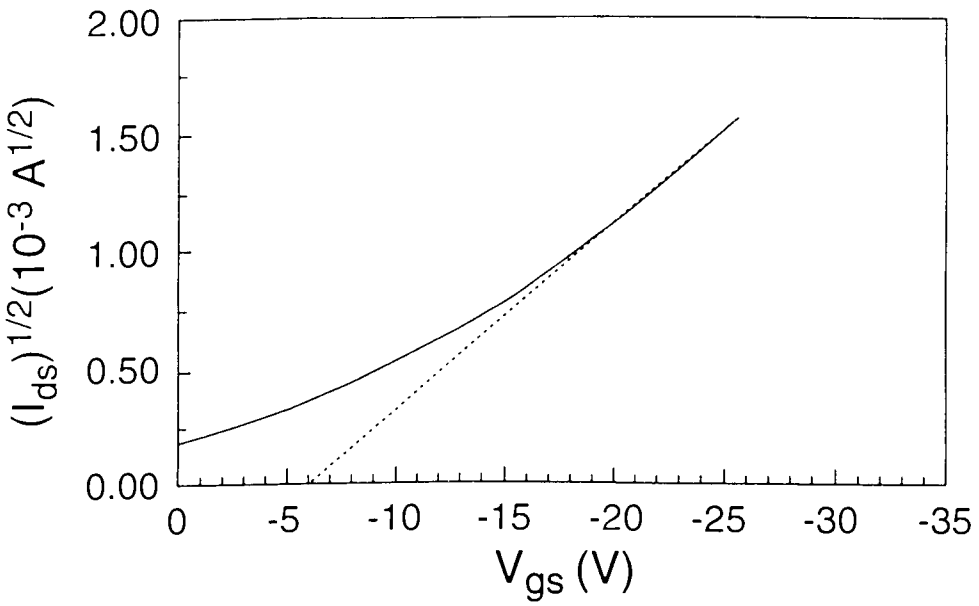

Figure V.19: $\sqrt{I_{ds}}$ versus V_{gs} at $V_{ds}=V_{gs}$ for annealed polymer-MISFET. Data taken from Figure V.17B.

Effect of Impurity Concentration on Electrical Properties of Polymer MISFETs. Poly(3-alkylthiophenes) are p-type semiconductors. A possible source for extrinsic doping are residues remaining from use of polymerization initiator. In order to investigate the role of residual initiator/reagent on FET characteristics, P3HT samples were prepared with varying levels of residual impurities. Figure V.20 shows I_{ds}-V_{ds} curves of MISFETs based on polymers (P3HT-A) and (P3HT-B). When these figures are compared with Figure V.17B (P3HT-C), the former can be observed to possess more resistive character and a lesser field effect response. Values of mobility and conductivity for the polymer-MISFET were extracted from I_{ds}-V_{ds} characteristics and are given in

Table V.3 together with values of σ . As the external impurity concentration increases, the bulk current, and the field effect mobility decrease. These results verify that impurities play an important role in carrier transport.

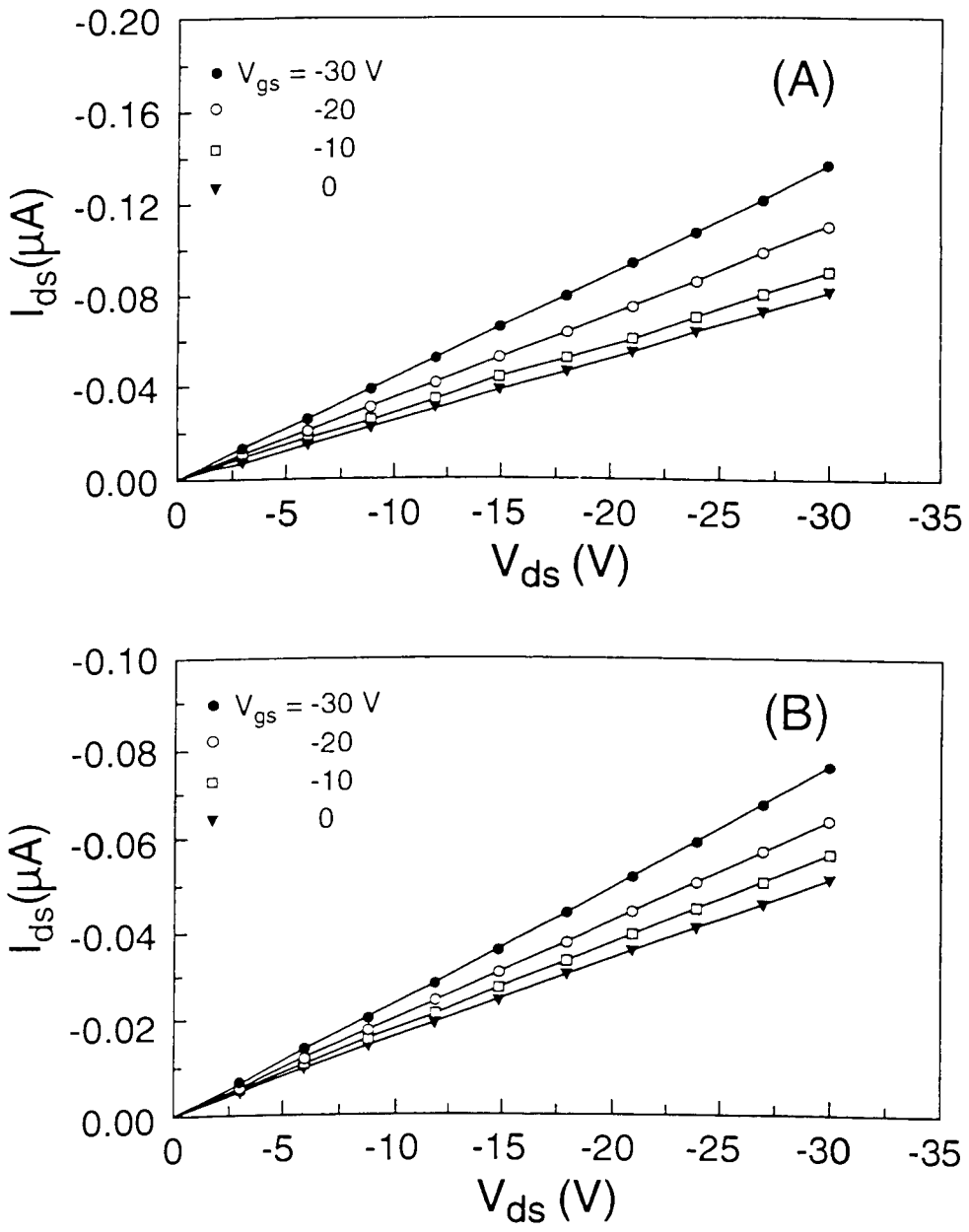

Figure V.20: I_{ds}-V_{ds} curves of MISFETs based on polymers with iron contents of: (A) 3.2 wt% (P3HT-A), (B) 1.32 wt%(P3HT-B).

Table V.3: Field effect mobilities, conductivities and acceptor concentrations of P3HT

Polymer	*Fe Content wt% (cm^{-3})[a]*	*μFET ($cm^2/V \cdot sec$)[b]*	*σ(S/cm)[b]*	*N_a (cm^{-3})[c]*
P3HT-A	3.2 (3.9×10^{20})	6.4×10^{-8}	3.7×10^{-9}	5.8×10^{17}
P3HT-B	1.32 (1.7×10^{20})	8.4×10^{-7}	1.4×10^{-8}	1.7×10^{17}
P3HT-C	0.05 (5.9×10^{18})	2.3×10^{-5}	1.2×10^{-7}	5.1×10^{16}

a determined by Atomic Absorption.

b determined by analysis of polymer FETs.

c determined by C-V measurements.

V.6.1.3 C-V Characteristics for Polymer-Based MIS Capacitors

C-V measurements were analyzed by X. Lu. It was useful to include these results in order to compare the impurity content determined chemically with that determined from electrical measurements. The capacitance of polymer-MIS structures has been analyzed under high frequency (1 *MHz*). The dc. voltage was ramped from -20*V* to 20*V* at a rate of 2*V/min*. A high frequency and slow sweep rate was chosen to exclude effects of long relaxation times of charge carriers. Figure V.21 shows the C-V responses for polymer devices at 1 MHz for relatively thick films (~1 μm) of (P3HT-C). As expected from the I-V measurements, for negative gate voltages the capacitance tends to the geometric capacitance of the insulator indicating thus the formation of an

accumulation layer. The decrease in the measured capacitance when the applied voltage is made positive reveals the formation of a depletion layer. Such layer extends through the polymer since the capacitance remains constant for large positive biases i.e. deep depletion. No obvious minimum capacitance is observed for a high positive voltage. This indicates the absence of an inversion layer. No inversion layer has ever been observed in polythiophene MIS structures. Its absence is presumably due to a combination of difficulty in generating stable negatively charged carriers in the depletion region, and their very low rate of migration.

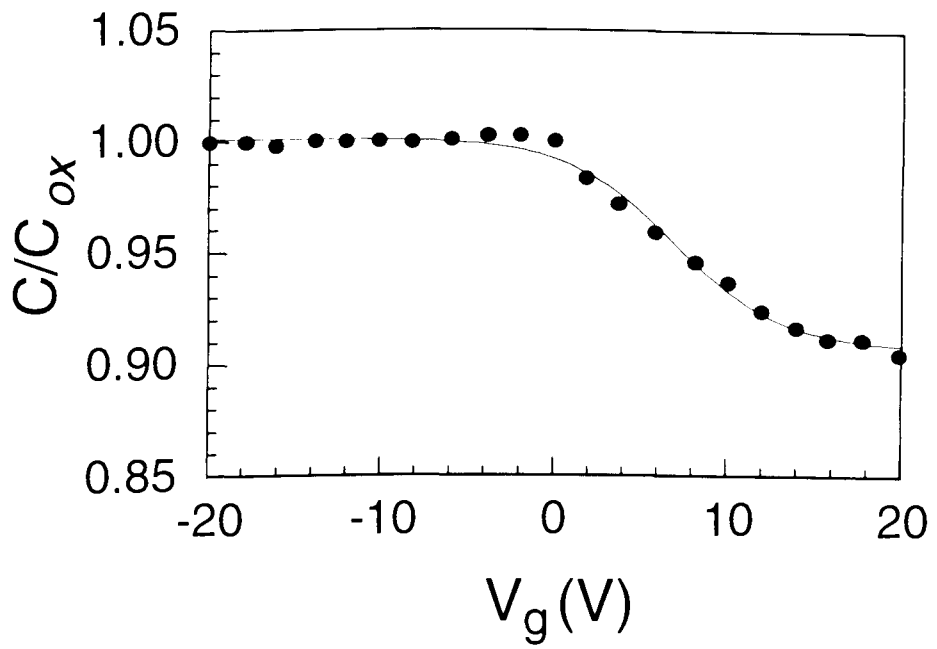

Figure V.21: Capacitance-Voltage characteristics of P3HT-C-MIS structures. C is the overall capacitance of the MIS structure, C_{ox} is the capacitance of the oxide layer.

In the deep depletion regime, the number of ionized impurities that give rise to charge carriers (majority carrier concentration), N_a, was calculated according to equation V.7. Values for N_a of 5.44x10^{17}, 1.54x10^{17}, and 4.7x10^{16} cm^{-3} were estimated from the slope of plots of $(C_i/C)^2$ against voltage for polymers P3HT-A, P3HT-B, and P3HT-C (Figure V.22). Thus N_a increases with impurity (Fe-complex) concentration. Upon closer inspection of the relationship between impurity concentration and carrier concentration, we note that the latter is orders of magnitude smaller. For example, the Fe impurity content was determined to be 5.9x10^{18} cm^{-3} for P3HT-C, whereas N_a was measured to be 5.1x10^{16} cm^{-3}. Clearly not all iron species take the form of ionized impurities.

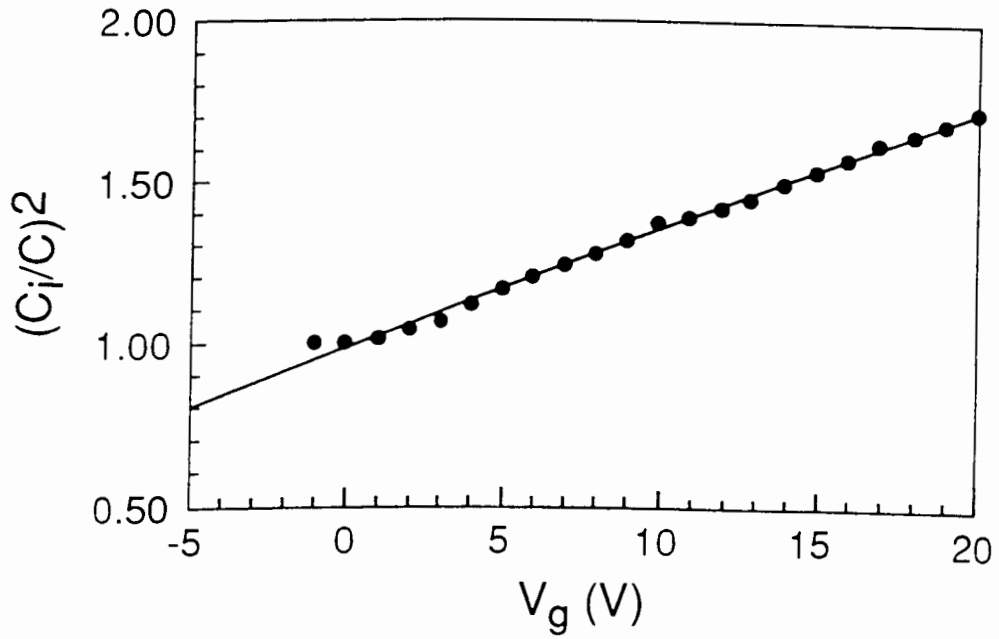

Figure V.22: $(C_i/C)^2$ versus gate bias of (P3HT-C)-MIS diode.

Chemical characterization of these polymers reveals that the iron impurities exist in the form of an iron(III) octahedral complex. The chloride to iron ratio is 1:1. For complete compensation of charge the Fe-complex requires two other anions. Given that purification was performed using ammonia solutions it is reasonable to assume these as hydroxyl groups. Furthermore, Mössbauer spectroscopy indicates an octahedral complex so that additional molecules must be coordinated to Fe^{3+}. These are most likely H_2O molecules. FTIR analyses indeed supports the presence of OH functionality although they cannot be specifically assigned to the Fe(III) complex. The possibility exists that the complex is coordinated to the polymer backbone.[109,110] Two main sites are available for coordination: π (η^5) coordination and S-bonded (η^1). Thus charge transfer between the conjugated polymer and the Fe^{3+} complex, as shown in Figure V.23, might possibly be the origin of charge carriers. The equilibrium shown in Figure V.23 must lie heavily to the left because: 1) the concentration of carriers is orders of magnitude lower than the concentration of impurities; and 2) the iron species are known to be overwhelmingly in the form of Fe (III).

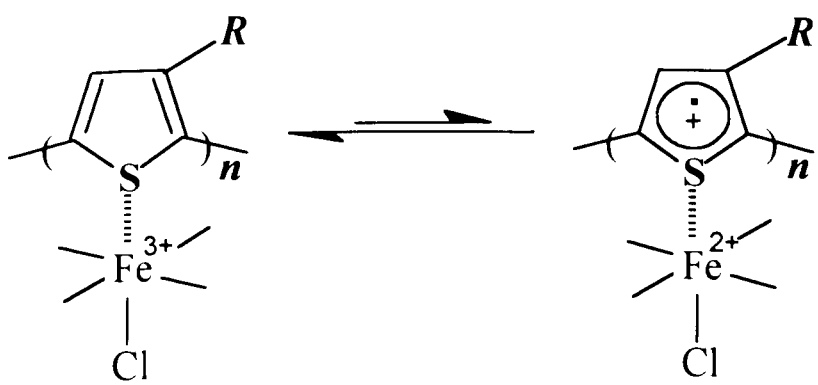

Figure 23: Scheme illustrating possible charge transfer between P3HT and residual Fe^{3+} impurities.

Insight into the origin of charge carriers in semiconducting π-conjugated polymers has been provided by electro-optical measurements on polymer-MIS structures in which modulation of the optical transmission through the active polymer layer is observed as a function of bias voltage i.e. voltage-modulated transmission (VMT).[369,370] The study revealed the presence of polaron and bipolaron states only upon application of a negative bias across polymer-MIS structures. Furthermore, the formation of these charged species was confirmed by voltage modulated photoluminescence for which application of a negative bias resulted in a 5% decrease in luminescence. Field-induced quenching of luminescence was attributed to non-radiative recombination of singlet polaron-excitons at charged polaronic sites. Both these studies indicate that localized charged states were largely absent in the absence of an applied field and were subsequently generated by the electric field.

This information is useful in interpreting the results in the present study regarding the origin of charge carriers and the field-effect response of MIS structures. In the absence of an applied field transverse to the polymer film, the positive charge carriers originating from charge transfer between the polymer and Fe(III) impurities are distributed homogeneously throughout the polymer film. Thus for polymers P3HT-A, P3HT-B, P3HT-C there exists a single positive charge (polaron) for every 80000, 3000, and 1250 thienyl rings respectively. The relative concentration of bipolaronic species is unknown, but for the latter, the dominant charged species are polarons. A low concentration of carriers as indicated here barely perturbs the electronic structure of the π-system and thus the π-π^* transition energy appears to be independent of impurity concentration; although weak transitions are observed in the region of 700-900 nm where polaron and bipolaron excitations are usually observed (Figure V.14). Upon application of the electric field across a MIS structure, the positive charges

(holes) are redistributed, and accumulated at the polymer/insulator interface so that an individual positive charge is distributed over only a relatively few thiophene rings. It is important to note, however, that these carriers are not associated with acceptor ions (counter ions). The accumulated charge takes the form of (bi)polarons which can be observed by optical spectroscopy.[369,370] The charge concentration in the accumulation layer is thus much higher than in the bulk. Since mobility of charge carriers, according to polaron-bipolaron hopping model, is governed by a percolation phenomenon and is determined by the percolation paths across the polymer chains, the effective carrier mobilities will increase rapidly with carrier concentration.[371] This increase can be explained in terms of a decrease in the hopping barrier energy and the barrier width with increasing the concentration of charge density. It is considered thus that this mechanism accounts for the behavior of the I_{ds} versus V_{ds} plots in the linear regime shown in Figure V.17. Field assisted carrier generation may also assist increasing carrier concentration by modifying the potential barrier profile of traps i.e. de-trapping and liberation of carriers. A possible source of carrier trapping in conjugated polymers is also the catalyst impurities. The latter mechanism is consistent with the "trapping" model which has recently been adapted to analyse the effect of trap density and trap energy on the current-voltage characteristics of organic based-TF-MISFETs.[372]

In contrast to a previous study of polythiophene, no evidence was found for migration of impurities under an applied field as evidenced by C-V measurements, since no hystresis was observed on ramping the gate voltage either directions, starting with negative or positive and scanning to the opposite direction. . This might be due to the bulkiness, and therefore slow migration, of the octahedral Fe-complex. In the study, where impurity migration was

observed, the polymer were prepared by the Grignard route for which impurities are mobile iodide species.

EPR spectroscopy has been used to provide information on the presence and concentration of charge carriers which possess spin, i.e., polarons. Previous studies correlating spin concentration with levels of doping (achieved electrochemically) have shown that the former decreases as the doping level is increased due to coalescence of polarons into spinless bipolarons. Ambiguity arises as to what level of doping is required to observe this decrease. A study on poly(3-methylthiophene) provides evidence that the spin concentration is maximum at 0.2 mol% doping (one spin per 500 thienyl rings).[364d] Whereas studies from another group place this transition at 3 mol% and 16 mol% for polythiophene and poly(3-hexylthiophene) respectively.[364a,366a] In our studies, in which the dopant is an impurity, the polaron concentration is observed to drop by a factor of 25 as the iron impurity concentration is increased. Simultaneously, the effective carrier concentration is apparently increasing as inferred from electrical characterization. Both these phenomena can be explained on the basis of coalescence of polarons into bipolarons. However, UV-vis data indicate only a small increase in bipolaron content as the impurity concentration is increased which implies the levels of doping are relatively low, consistent with one of the previous studies mentioned. If a much higher doping/impurity level was necessary to observe a decrease in spin concentration then this would be reflected in strong polaron and bipolaron absorptions in the vis-NIR region, but this was not the case. In the case where the spin concentration falls above 0.2 mol% doping, the concentration of polarons and bipolarons, and thus their absorption intensities are low, which is consistent with our studies.

These results provide unambiguous evidence that impurities are integrally related to carrier generation. While it is anticipated that the carrier concentration in the polymer increases with iron impurity concentration no chemical technique is yet available for direct measurement of carrier concentrations. However, the decrease in conductivity of the samples with increasing impurity content is more likely to be due to a decrease in carrier mobility and not a decrease in carrier concentration. In fact, the field effect mobility is observed to decrease with impurity content. Furthermore, the ionized acceptor concentration, as determined by capacitance-voltage measurements, is observed to increase with impurity content. The ionized acceptor concentration increases only 10 fold for a one hundred fold increase in iron content and varies non-linearly with the impurity concentration. The origin of this is yet unknown.

V.6.2 Photolytic Tuning of Thick Film Polymer MISFETs

Semiconducting π-conjugated polymer regions can be spatially converted to insulating regions by virtue of their photo-oxidative chemistry (*cf.* III.5.6). This concept was used to tailor the electrical properties P3ATs, and convert the resistor-like characteristics of thick film polymer-MISFETs into devices possessing encapsulating insulating layers.

When the semiconductor film thicknesses are too thick (~ 1μm) to be completely pinched off by the gate field, the drain currents fail to saturate due to the existence of non-modulated current paths in series or in parallel with the conduction channel. *I-V* curves for "thick film" MISFETs are shown in Figure V.24A. These electrical responses show a large ohmic contribution and the I-V curves are largely resistive. In order to fine-tune the MISFET electrical characteristics and eliminate the large ohmic current observed, photochemically induced degradation of P3ATs were utilized.

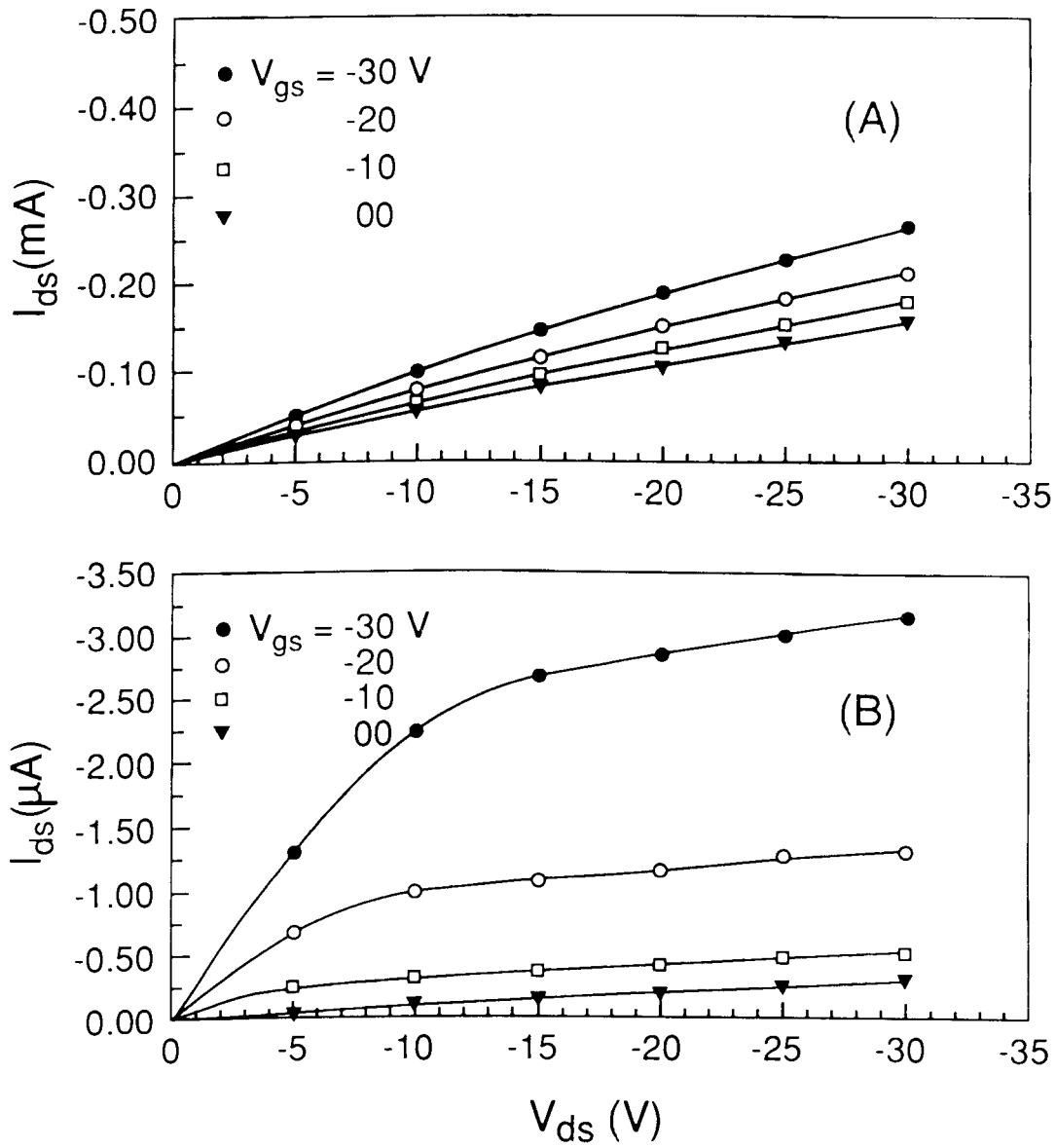

Figure V.24: I_{ds}-V_{ds} characteristics of annealed thick film P3HT MISFET (A) Before irradiation, and (B) After irradiation.

The principle is shown schematically in Figure V.25. P3ATs undergo photobleaching and photooxidation when exposed to UV-vis light in presence of oxygen (*cf.* III.5.6). As a result, irradiation results in loss of conjugation, and a decrease in the electrical conductivity.

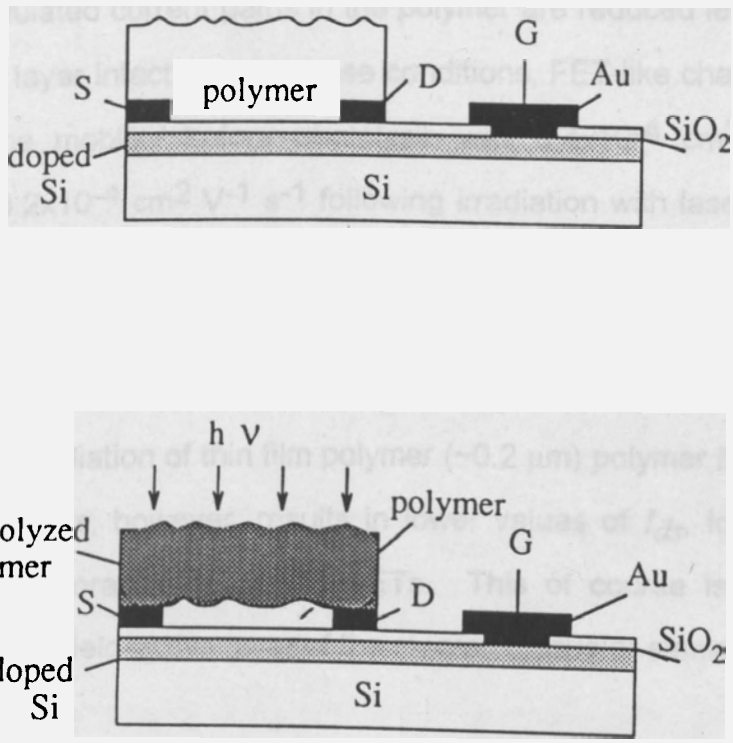

Figure V.25: Schematic representation of the photolysis experiment. The effect of the incident light is to reduce the non-modulated current paths.

In this experiment, thick film P3AT MISFET was irradiated using laser light (blue laser, 442 nm). Upon irradiation to an exposure dose of 400 mJ cm^{-2}, the I_{ds} drops considerably and the field response is observed. Upon irradiation bulk conductivity of the polymer is reduced by photochemical degradation from the surface down. As photolysis proceeds and the surface layer of the polymer is photobleached, the depth of penetration increases. Eventually, the π-conjugated region providing ohmic, bulk conductivity is rendered highly resistive, and the unmodulated current paths in the polymer are reduced leaving the field-active polymer layer intact. Under these conditions, FET-like characteristics are observed. The mobility before photolysis was 6.4×10^{-4} cm^2 V^{-1} s^{-1} but decreased to 3.2×10^{-4} cm^2 V^{-1} s^{-1} following irradiation with laser light. These field-effect mobilities are, however, larger than thin film MISFETs, presumably because the former retains a thicker π-conjugated layer than 0.25 μm. This is evident from the small yet observable unsaturation in the I-V curves shown in Figure V.24B. Irradiation of thin film polymer (~0.2 μm) polymer MISFETs under the same conditions, however, results in lower values of I_{ds}, lower mobilities, and general deterioration of the MISFETs. This of course is due to direct degradation of the field-active layer of the macromolecualar semiconductor.

V.7 Conclusion

Macromolecular semiconductor-based TF-MISFETs were constructed using conventional MOS technology. The mechanism of operation of polymer TF-MISFETs was proposed based on the I-V characteristics of MISFETs and substantiated by C-V measurements. The device operates through the modulation of an accumulation layer at the polymer-insulator interface under negative gate biases.

Octahedral Fe (III) complexes contribute to the origin of charge carriers in poly(thiophenes) prepared via oxidative coupling using ferric chloride. For the polymer of highest purity, the ratio of unpaired electron spins to thienyl groups is 1:2900. This value falls by a factor of one hundred with increasing impurity concentration. Optical spectroscopy shows that even though the impurity concentration is high, the polymer can be considered to be in the low doping-level regime.

The field effect carrier mobility of the polymers decreases with increasing levels of impurities, presumably due to scattering by ionized impurities. Given that mobilities decrease with increasing impurity levels, it is concluded that polymers with low impurity concentrations are more suitable for MISFET applications. The bulk conductivity is found to decrease with increasing impurity levels most likely because the decrease in carrier mobility is larger than the increase in charge carrier concentration. The correlation of impurity with electrical properties is likely to be a general effect for π-conjugated polymers although the origin of charge carriers/nature of impurities will vary depending on the synthetic route.

Electrical properties of macromolecular poly(3-alkylthiophene) semiconductors can be tailored by virtue of their photo-oxidative chemistry. This process provides devices possessing encapsulating insulating layers.

Chapter VI: POLY(3-ALKYLTHIOPHENES)-OXYGEN CHARGE TRANSFER COMPLEXES

VI.1 Introduction

P3ATs show interesting photochemical and electrical properties. Thin films of P3HT undergo crosslinking and insolubilization when irradiated with a UV or visible light in air, thus allowing the deposition of π-cojugated polymer patterns (*cf.* chapter III). Prolonged irradiation of the polymer in the presence of oxygen, however, leads to disruption of the conjugated system and a decrease of its conductivity. The electronic properties of the material are also sensitive to the presence of oxygen (*cf.* chapter V). In general, the conductivities of thin films of P3ATs increase upon exposure to oxygen. These phenomena point to a specific interaction of oxygen with the polymer. In order to explain such phenomena, a study was undertaken to investigate the existence of a charge transfer complex (CTC) between poly(3-hexylthiophene) and molecular oxygen.

In this study, evidence for a charge transfer complex between poly(3-hexylthiophene) and molecular oxygen is presented using electronic absorption and EPR spectroscopies. The concentration and diffusion coefficient of oxygen in P3HT were determined using the time-lag method. The Benesi-Hildebrand equation was employed to determine the thermodynamic parameters of the complex including stability constant, free energy change, and binding energy. The role of the CTC on the photochemical and electronic properties of P3ATs was evaluated. The important elements of the theory of charge transfer complexes and the spectroscopic and thermodynamic properties of these complexes are discussed below.

VI.2 Charge Transfer Complexes

The association of a molecule of low ionization potential (an electron donor, D) with a molecule of relatively high electron affinity (an electron acceptor, A) that leads to a *weakly* bound, stoichiometric structure is known as donor-acceptor complex or charge transfer complex (CTC) (equation VI.1).[373-375]

$$D + A \rightleftharpoons [D^{\delta+} \cdot A^{\delta-}] \xrightarrow{h\nu} [D^{+}, A^{-}] \qquad \text{(VI.1)}$$

Upon association, the physical properties of the donor and acceptor are perturbed and new properties arise. For example, an electronic absorption extra to the absorption of both components is often observed. This is the result of an intermolecular charge-transfer transition involving electron transfer from the donor to the acceptor and appears as a structureless red-shifted transition in the absorption onset of the donor molecule.

The relationship between the energy of the charge-transfer transition, E_{CTC}, the ionization potential of the donor, IP_D, and the electron affinity of the acceptor, EA_A, is given by[373]

$$E_{CTC} = h\nu_{CTC} = IP_D - EA_A - W \qquad \text{(VI.2)}$$

where ν_{CTC} is the frequency characteristic of the intermolecular charge-transfer transition and W is the energy of stabilization of the excited state (Coulombic attraction energy) of the complex. E_{CTC} or $h\nu_{CTC}$ can be estimated with reasonable accuracy using the empirical relation[376,377]

$$E_{CTC}(eV) = E^{D}_{1/2} - E^{A}_{1/2} + 0.15(\pm 0.10) \qquad \text{(VI.3)}$$

$E^{D}_{1/2}$ and $E^{A}_{1/2}$ represent the half wave potentials of the donor and acceptor respectively. These potentials can be used as a measure of the ionization potential and electron affinity assuming the electrochemical system is reversible. The 0.15 component is an empirical factor determined from the linear correlation

of the CTC energy with the energy calculated via ($E^{D}_{1/2}$-$E^{A}_{1/2}$). The 0.10 eV error is a result of uncertainty in the solvation energy of the separate ions. The spectral characteristics of a CTC can be related to its thermodynamic properties through the Benesi-Hildebrand equation.[378] These properties form the criteria for defining the nature of the complex.

The classical procedures to determine the equilibrium constant, K, of a CTC from its spectroscopic data is via the Benesi-Hildebrand equation which describes the equilibrium constant for complex formation in the form[378a]

$$K_c = \frac{[CTC]}{([D]-[CTC])([A]-[CTC])} \qquad \text{(VI.4)}$$

where [A], [D], and [CTC] are the concentration of acceptor, donor, and charge transfer complex, respectively. For a donor molecule in large excess with respect to the acceptor, the optical density of the CTC is related to the concentration of the acceptor and donor through the Benesi-Hildebrand equation (B-H), assuming the Beer-Lambert law is valid. For a polymer film, the B-H equation can be written as

$$\frac{l[A]}{OD_{CTC}} = \frac{l}{\varepsilon_{eff}} + \frac{l}{K_x \varepsilon_{eff} x_D} \qquad \text{(VI.5)}$$

where l is the film thickness (i.e. the optical path length) and x_D represents the mole fraction of donor. OD_{CTC} and ε_{eff} are the optical density and the effective extinction coefficient of the complex. K_X is the equilibrium constant of the complex based on mole fractions of the constituent species. The B-H equation permits K_X and ε_{eff} to be determined from the slope and the intercept of the line obtained by plotting $l\,[A]\,/\,OD_{CTC}$ versus $1/x_D$. Depending on the value of K, the nature of the complex can be determined. For $K \rightarrow 0$ the CTC is very weak. This CTC has been coined by Mulliken as "contact" charge transfer complex and arises from statistical collisions between donor and acceptor molecules.[373] The large the value of K the stronger the donor-acceptor interaction. While K values

> 1 M^{-1} are indicative of pure complexes, values of K < 0.1 M^{-1} are typical of "contact"-type CTCs.[374,379,380] Mixed complexes have formation constants between these two limits. The thermodynamic parameters of the complexes may also assist in the assessment of their nature. This can be established through the determination of free energy changes and enthalpies of molecular association. The relationship between standard free energy change (ΔG^o) for a reaction and its equilibrium constant K is given by[381]

$$\Delta G^o = - RT \ln K \qquad \text{(VI.6)}$$

The standard heat of formation (ΔH^o) can be determined according to

$$\Delta G^o = \Delta H^o - T\Delta S^o \qquad \text{(VI.7)}$$

Knowing the standard entropy change (ΔS^o) of complexation, the binding enthalpy (or energy) of the charge transfer complex can be determined. Typical ΔS^o of complexation falls in the range -8 to -14 cal deg^{-1} $mole^{-1}$.[379,382] Accordingly, ΔH^o of contact CTCs are small, in the order ~1 kcal/mol at 298 K. The binding energies of pure complexes are typically ≥ 4 kcal/mol.

VI.3 Properties of Charge Transfer Complexes

The formation of donor-acceptor complexes is accompanied by intercomponent electron transfer, and corresponding changes in the electrical, optical (photochemical and photophysical), and sometimes magnetic properties of the components. Changes in electrical properties can provide qualitative information concerning charge transfer.[383] The formation of CTCs usually leads to anomalous quenching kinetics of flourescence and phosphorescence of the donor (non-linear Stern-Volmer plots).[384] CTCs also influence bimolecular photochemistry.[385] EPR spectra can often identify and determine the spin or carrier concentration of paramagnetic complexes.[386] The electrical, optical and

magnetic properties of π-conjugated polymer-based CTCs, if they exist, are anticipated to have similar properties to lightly doped conjugated polymers.

For complexes which are formed by the interactions of gases with solid materials, the diffusion phenomenon is also important since interpreting the interaction requires information on the dynamics and solubility of the gas in the material.

VI.4 Diffusion of Gases in Solid Polymers

There are a number of theories describing the mechanism of diffusion of gases in solid polymers. The Hole theory was the first descriptive model of diffusion and employed the conceptual model of discrete holes (microvoids) which may be either mobile or fixed within and throughout the polymer matrix.[387] These holes are created by Brownian motion of the molecular segments of the polymer chains. A molecule of penetrant can move only when there is a space available to receive it. The energy necessary to form a hole of proper dimensions forms the activation barrier in the diffusion process. Recently, a more advanced mathematical model has been developed.[388,389] The basic principle of this model is that mobilities of both the polymer segment and the diffusant molecule are primarily determined by the amount of free volume present in the polymer.

The diffusion process begins with sorption of the gas at the polymer surface.[389] This is followed by a dissolution process and finally an equilibrium is established at the gas-membrane interface. These processes cause build up of a concentration gradient between the surface layer and the polymer bulk in the direction of diffusion and drive diffusion of the gas through the polymer film. A complete balance is established when the gas is uniformly distributed in the entire polymer film and an equilibrium state of gas sorption is obtained. The

equilibrium level of gas sorption (or solubility) in polymers depends on the magnitude and nature of interaction forces.[390] Mechanisms for penetrant immobilization/binding include chemical or physical interactions with polymer groups (backbone or side chains) and sorption into pre-existing microvoids. For conventional, unsaturated polymers the interaction forces are usually weak physical forces such as dipole-dipole and dipole-induced-dipole interactions, and London dispersion forces. Consequently, the equilibrium level of gas sorption is low. For π-conjugated polymers, the ionization potentials are low and the interactions of gases of high electron affinity, e.g. oxygen, are anticipated to be relatively strong, thus higher solubilities or levels of gas sorption are not unexpected.

Solubility of gases in polymers can be determined by several techniques including luminescence,[391] ESR,[392] UV-vis,[393] time resolved IR,[394] and time-lag techniques.[395-400] The time-lag method was employed in this study for determining the interaction of molecular oxygen with poly(3-alkylthiophenes) (P3ATs). The advantage of this method lies in the fact that both diffusion (D) and permeability (P) coefficients can be evaluated simultaneously.

The time-lag method is a Barometric or constant volume technique. It is based on solving Fick's second law of diffusion (equation VI.8) under specific boundary conditions

$$\frac{\partial c}{\partial t} = D \frac{\partial^2 c}{\partial x^2} \qquad \text{(VI.8)}$$

Barrer (1939)[395] was able to solve this diffusion equation for transmission of gases though thin polymer membranes using a constant value of D and under boundary conditions of: (a) an initially gas-free polymer film, (b) attainment of equilibrium at the inlet gas-polymer interface, and (c) a zero concentration of gas

at the outflow face. The solution of equation VI.8 under the above conditions for steady state diffusion yields

$$Q_t = \frac{D c_l}{l}\left[t - \frac{l^2}{6D}\right] \qquad \text{(VI.9)}$$

where Q_t is the amount of permeant passing though a polymer film of thickness l at time t, and c_l is the permeant concentration at the upstream face. Equation VI.9 permits the determination of the diffusion coefficient, D, and permeability, P, of gases in solid polymer films by plotting of the amount of gas Q_t against time t. The slope of the linear portion is directly related to P, while the intercept on the t axis gives the time lag θ which is defined by the equation[395-397]

$$\theta = \frac{l^2}{6D} \qquad \text{(VI.10)}$$

From the time lag θ the diffusion coefficient D can be determined.

The solubility of gases in polymer films is usually assumed to follow Henry's law (equation VI.11)[395-397]

$$c = S_g p \qquad \text{(VI.11)}$$

where c is the concentration of gas in the polymer film, p is the partial pressure of the gas at the gas-polymer interface, and S_g is the solubility coefficient. This assumption is valid for the condition of equilibrium, since S_g is essentially an equilibrium partition coefficient of the gas between the two phases. The relationship between S_g and the permeation coefficient, P, is given by

$$P = D\ S_g \qquad \text{(VI.12)}$$

The solubility coefficient and concentration of a gas in polymer films can be determined using equations VI.11 and VI.12.

VI.5 Experimental

Polymers containing 0.05 wt% (0.15 mol%) iron were used in this study. Details of the synthesis anf purifications are described in Chapter II (*cf.* II.2).

UV-vis spectra were recorded on a Cary E1 spectrophotometer at 25°C. Polymers films (~20 μm) were cast onto quartz substrates from $CHCl_3$ solutions. Oxygen-free films were obtained from degassed polymer solutions (freeze-pump-thaw method) by casting under an oxygen-free N_2 atmosphere. For UV-vis absorption measurements the films were enclosed in an air-tight stainless steel cell and vacuum pumped for several days to remove residual oxygen. The effect of oxygen was studied by introducing oxygen with controlled pressure and allowing it to equilibrate with the polymer films. Electron paramagnetic resonsnce (EPR) measurements were performed by F. Orfino (*cf.* V.5).

Thin-Film Metal-Insulator-Semiconductor Field Effect Transistors (TF-MISFETs) were used to probe the effect of oxygen on the electrical properties of the polymer. P3HT containing 0.05 wt% iron impurities were employed in this study. The polymer semiconductor layer (0.1 μm) was cast on the MISFET structure from degassed polymer solutions under oxygen-free N_2, and placed in an integrated circuit carrier sealed inside an air-tight compartment. Vacuum and oxygen were applied as required. Before measurements, the devices were allowed to come to equilibrium with the applied oxygen. Current-voltage characteristics of polymer-FETs were measured with a semiconductor parameter analyzer HP4145 and a Bausch and Lomb wafer probing station. Details of the procedure are given in Chapter V (*cf.* V.5.1). The bulk conductivity was determined from I_{ds}-V_{ds} at zero bias (equation V.10). Field effect mobilities were determined using equation V.8.

The apparatus employed for the determination of permeability and diffusion is illustrated in Figure VI.1.[399] The diffusion cell is composed of in-going and out-going compartments. A free standing polymer film is supported by a fine copper gauze. The two halves of the assembly are pressure sealed by Teflon rings as shown (Figure VI.1). The pressure of low and high pressure sides were measured by various pressure gauges. A Pirani gauge connected to the out-going cell was capable of measuring pressure from 10^{-3} to 10^{2} Torr with an accuracy of 1% per decade. Free standing polymer films of P3HT were prepared by solvent evaporation on glass slides under controlled vacuum conditions and subsequent peeling of the film. The thickness of the film was controlled by both the concentration of the polymer solutions and the quantity of polymer deposited. Polymer films 30 μm thick were used in these measurements. Oxygen was introduced into one-half of the degassed cell at a pressure of 760 Torr. Permeation of the gas through the membrane was monitored by measuring the change in pressure in the outgoing compartment with time. Steady state diffusion was indicated when the pressure-time plot was linear. Under these conditions, the permeability coefficient (P $cm^2.sec^{-1}$) was calculated according to[396-399]

$$P = \frac{273}{T}\,\frac{V}{p_I}\,\frac{l}{A}\,\frac{l}{76}\,\frac{dp}{dt} \qquad \text{(VI.13)}$$

where V is the volume of the in-going chamber (cm^3), l is the thickness of the polymer film (cm) of area A (cm^2), $\frac{dp}{dt}$ is the slope of the plot at steady state flow (cmHg/s), T is the temperature (K), and p_I is the pressure of oxygen in the in-going compartment (cmHg). Extrapolation of the linear region of the pressure-time plot to zero pressure yielded the time lag θ. The diffusion coefficient (D $cm^2.sec^{-1}$) was determined from equation VI.10. The solubility coefficient (S_g)

expressed as volume of gas , measured at STP, per unit volume of polymer is given by

$$S_g = \frac{76\,P}{D} \qquad \text{(VI.14)}$$

The units and dimensions of P, D, and S_g were adopted according to references 399, 400, and 401.

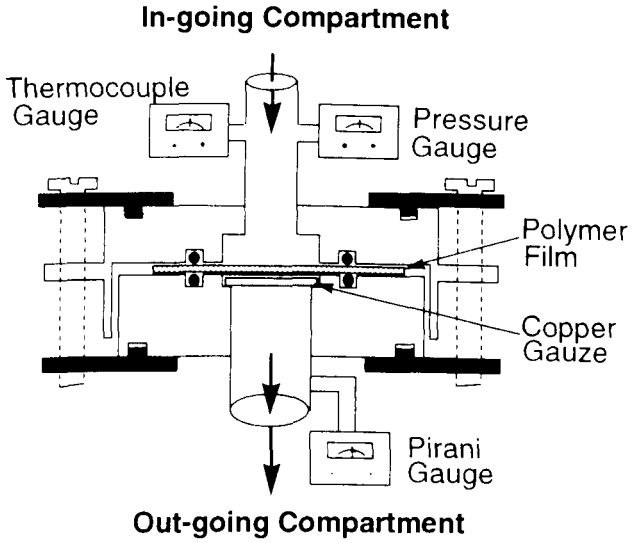

Figure VI.1: Time-lag diffusion cell

VI.6 Results and Discussion

UV-vis Spectroscopy. The energy of a possible charge-transfer transition for P3HT-O_2 complex was determined according to equation VI.3. Using measured $E_{1/2}$ values of -0.82 and ~0.94 *vs.* SCE in CH_3CN/TEAP for oxygen and P3HT, respectively, E_{CTC} was estimated to be ~1.9±0.1 eV which corresponds to a wavelength of 648 ±33 nm.

In order to detect this absorption, films of P3HT were subjected to variable pressures of oxygen and the visible spectrum recorded *in situ*. Films of P3HT possess a broad absorption spectrum with a maximum absorption at ~505 nm and an absorption tail which extends to 620 nm. The presence of oxygen was found to perturb the optical density of the absorption tail of P3HT. The difference spectra of the polymer in the presence and absence of oxygen shows a structureless band at ~630 nm (Figure VI.2).

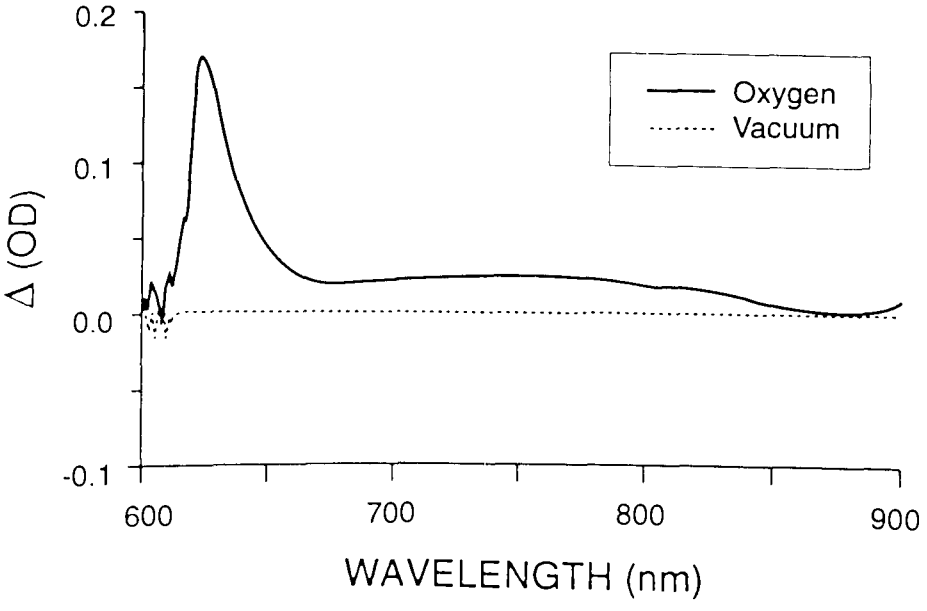

Figure VI.2: UV-vis absorption difference spectra of a P3HT thin film (20 μm) in contact with oxygen (10 atm) and *in vacuo*.

The proximity of this band to the predicted value for E_{CTC} and the fact that the absorbance of the charge transfer complex was proportional to the pressure of oxygen within the range 1-10 atm were considered as strong evidences for a charge transfer complex between molecular oxygen and poly(3-hexylthiophene). The structure proposed for the P3HT-O_2 CTC is depicted in Scheme VI.1.

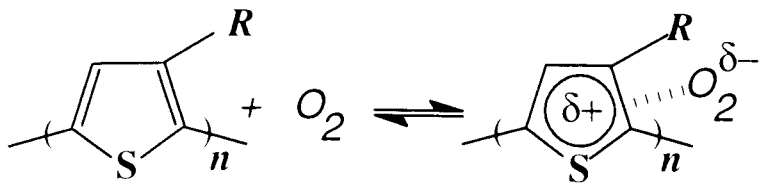

Scheme VI.1

The equilibrium constant of CTC formation can be determined using the Benesi-Hildebrand relation (equation VI.5) if the concentration of the acceptor [A] in the polymer is known. This was not the case and therefore the time-lag technique was employed to determine the concentration of oxygen, [A], in the polymer film.

Solubility and Diffusion Coefficient of Oxygen. Figure VI.3 shows the pressure-time relationship of films of P3HT under oxygen atmosphere (760 mmHg). From the time lag, θ, the diffusion coefficient, D, was determined according to equation VI.0. The value for the diffusion of O_2 in P3HT films was estimated to be 1.2×10^{-8} $cm^2.sec^{-1}$. The slope of the linear portion provides a measure of the permeation coefficient. The permeation coefficient, P, of O_2 in P3HT films was estimated to be 3.4×10^{-11} $cm^2.sec^{-1}$. Accordingly, solubility of oxygen in P3ATs was determined to be 0.22 vol/vol at STP. This solubility coefficient was used to determine the concentration of oxygen in the polymer, [A], at various oxygen pressures according to equation VI.11. The equilibrium constant of complexation of oxygen with P3ATs can thus be determined using these values of concentrations.

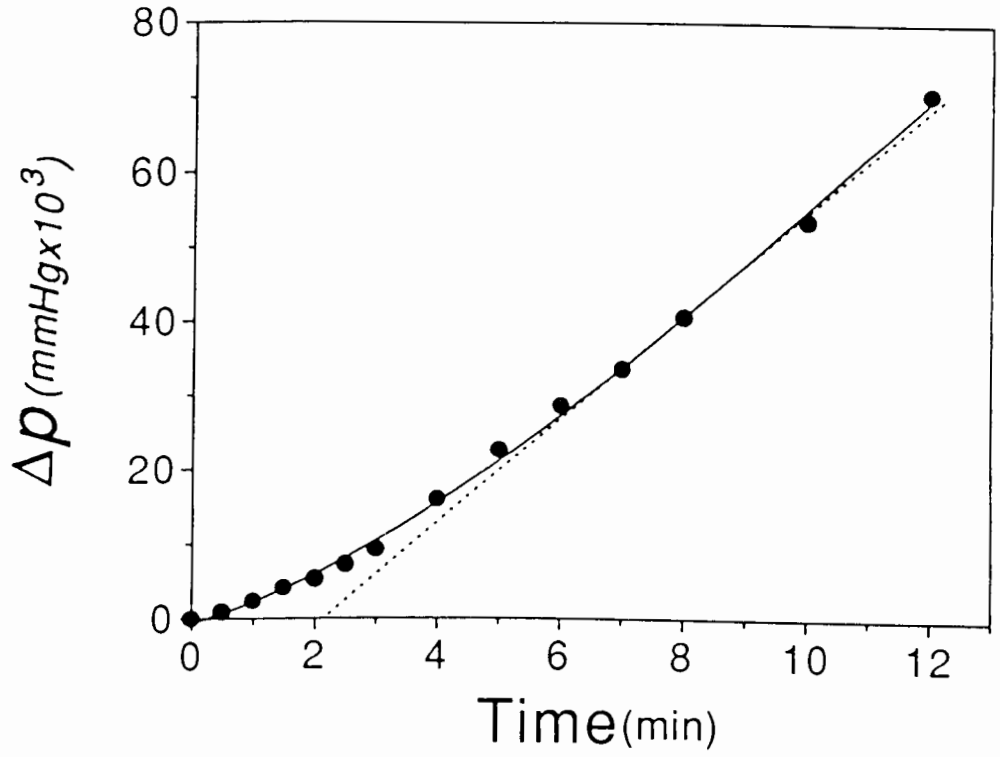

Figure VI.3: Rate of permeation of oxygen across a film of P3HT

Equilibrium Constant and Energetics. A Benesi-Hildebrand plot of $[A]/OD_{CTC}$ versus $1/x_D$ (Figure VI.4) obtained by varying the pressure of oxygen provides estimates of ε_{eff}, and K_X. The concentration of the donor in the film, $[D]_{film}$ can be estimated by considering the minimum number of conjugated thienyl rings required to form a detectable CTC. It is postulated that the interaction of oxygen with long π-conjugation lengths will dominate over interactions with short conjugation lengths due to the lower ionization potential of the former. knowing that the oligomer, α-sexithienyl, has a degree of

conjugation similar to that of the polymer, the donor unit was taken as being represented by a sexithienyl segment.[195] Accordingly, $[D]_{film}$ was calculated to be 1.09 M (assuming a density of 1.1 g/cm^3).[187] The concentration of acceptor in the film, $[A]_{film}$ was 0.98×10^{-2} M at 298 K and 1 atm of oxygen as estimated from solubility of oxygen in P3HT. ε_{eff} and K_Y are thus calculated to be ~800 $M^{-1}cm^{-1}$ and 0.52, respectively.

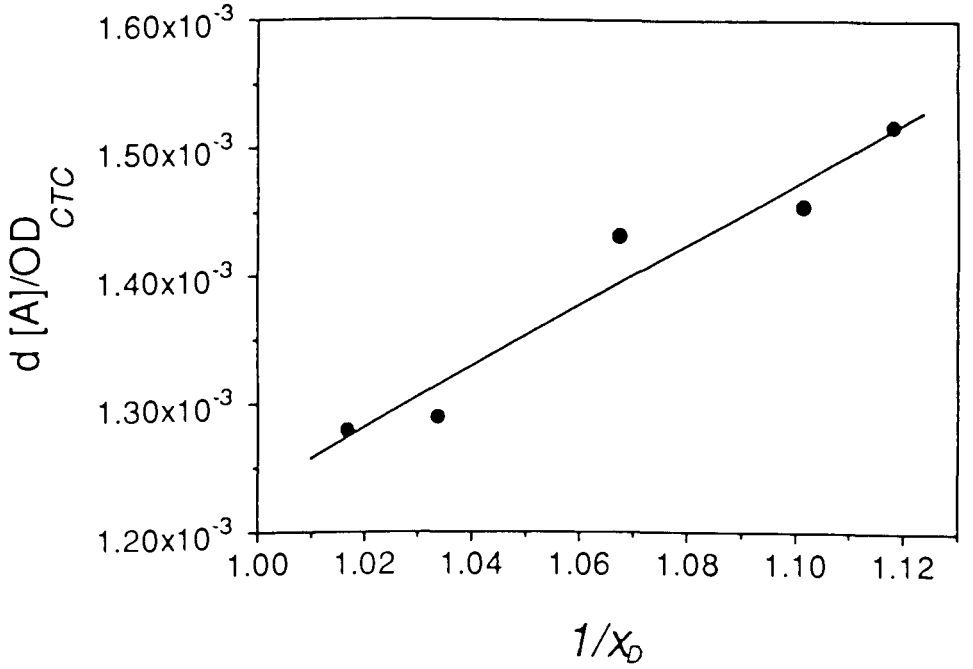

Figure VI.4: B-H plot of P3HT-O_2 charge transfer complex

It is noteworthy that the evaluation of K_X, unlike ε_{eff}, is independent of the concentration of dissolved oxygen used in the calculations.[387b] K_X can be readily converted to a concentration-based constant, K_C, since in the absence of solvent, and where the donor is in large excess, $K_C = K_X \overline{V_D}$, where $\overline{V_D}$, 0.91 M^{-1}, is the molar volume of the donor based on the sexithienyl segment. K_C was calculated to be 0.47 M^{-1}. From equation VI.4, the concentration of CTC was calculated to be 1.32×10^{-3} M when films are exposed to air (152 mmHg O_2). The value of the equilibrium constant lies between the values of contact and pure complexes and is thus indicative of a mixed donor-acceptor complex. This was supported in part by the relatively high extinction coefficient of the complex.

Energetics of CTC formation can be established through determination of free energy change and binding energy of molecular association. From equation VI.6, the standard free energy change (ΔG^o) for formation of P3HT.O_2 CTC was determined to be 4.5×10^{-1} kcal/mol at 298 K. The binding energy can be determined if the standard entropy change (ΔS^o) of complexation is known. Since CTC's exhibit ΔS^o values in the range of -8 to -14 J deg^{-1} mol^{-1},[379,382] a -10 J deg^{-1} mol^{-1} was taken as a reasonable estimate of ΔS^o. Accordingly, the binding energy (ΔH^o) of P3HT.O_2 CTC was calculated to be -2.48 kcal/mol (0.11 eV).

EPR. EPR spectra of P3HT were obtained under reduced pressure (4 mm Hg), in air and at 1 atm of O_2. Analysis of the data indicates that introduction of oxygen gives rise to a small increase in the EPR signal. The data also shows a reversible interaction between O_2 and P3HT. At 1 atm of oxygen, the polymer's EPR signal exhibits a gaussian lineshape with a peak-to-peak width of 6.00 Gauss and a g-value of 2.0032. Similar EPR results were obtained in air. At reduced pressure (4 mm Hg), the peak-to-peak width was found to decrease to 5.57 Gauss while the g-value increased to 2.0039. The

concentration of spins were determined from integrals of the EPR signals. Under vacuum, the polymer was found to contain 5.4×10^{17} spins/g ($\sim 4.9 \times 10^{17}$ spins/cm^3). Introduction of oxygen at a pressure of ~1 atm resulted in an increase in the spin density to 7.1×10^{18} spins/g ($\sim 6.4 \times 10^{18}$ spins/cm^3) which is consistent with the value of CTC concentration estimated using the equilibrium constant K_C.

The observed increase in intensity of the polymer's EPR absorption in the presence of oxygen is indicative of the ionic character of the P3HT.O_2 CTC i.e. P3HT and O_2 contain unpaired electrons.[386] The g-value (g = 2.0023) is typical of free electrons indicating that the electrons are delocalized on the polymer backbones.[365,366] The oxygen radical anions, $O_2^{-\bullet}$, give broad absorption lines which are not resolved at atmospheric pressures.[402] The P3HT.O_2 CTC can thus be represented as

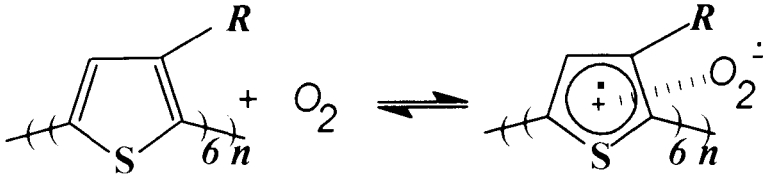

Scheme VI.2

Electronic Properties. A charge transfer complex between the polymer and O_2 should affect the conductivity and charge transport properties of the material. In order to evaluate the validity of these assertions, thin film field effect transistors (TF-FETs) incorporating π-conjugated P3ATs were used to characterize their electrical properties in the presence and absence of oxygen. These microelectronic structures are particularly useful since charge generation and charge migration processes can be separated, and information on charge carrier concentration, charge mobility, and conductivity extracted. Several reports have indicated that polythiophene-based FETs are sensitive to the presence of oxygen.[68,336] Here, a correlation of electrical parameters of devices with the P3HT-O_2 charge transfer complexes was derived by studying the behavior of P3HT-FETs at different pressures of oxygen (1-10 atm).

Figure VI.5 shows FET I-V characteristics in *vacuo* and under 10 atm oxygen. In the absence of oxygen, a typical FET-like response is observed, i.e., clear saturation currents which are proportional to the gate bias.[325] In the presence of oxygen, the current increases by an order of magnitude and the curves take on considerable "ohmic" behavior. This effect can be attributed to the increase in the concentration of charge carries upon exposure to oxygen as evidenced by EPR measurements. These I-V curves (Figure VI.5) are fully reversible upon the removal or addition of oxygen.

The carrier mobility decreases with increasing oxygen pressure. The inverse relationship between carrier concentration and mobility is typical of both organic and inorganic materials alike.[321] Under high oxygen pressures, the carrier concentration at the polymer/insulator surface is anticipated to be sufficiently large that surface scattering may occur. As a result, the conductivity of the films ($\sigma = n e \mu$) increases linearly with low oxygen pressure (4×10^{-8}

S/cm *in vacuo*, $4x10^{-7}$ S/cm at pO_2=0.2 atm, and $2x10^{-6}$ S/cm at pO_2=1 atm), and non-linearly with higher pressures (Figure VI.6).

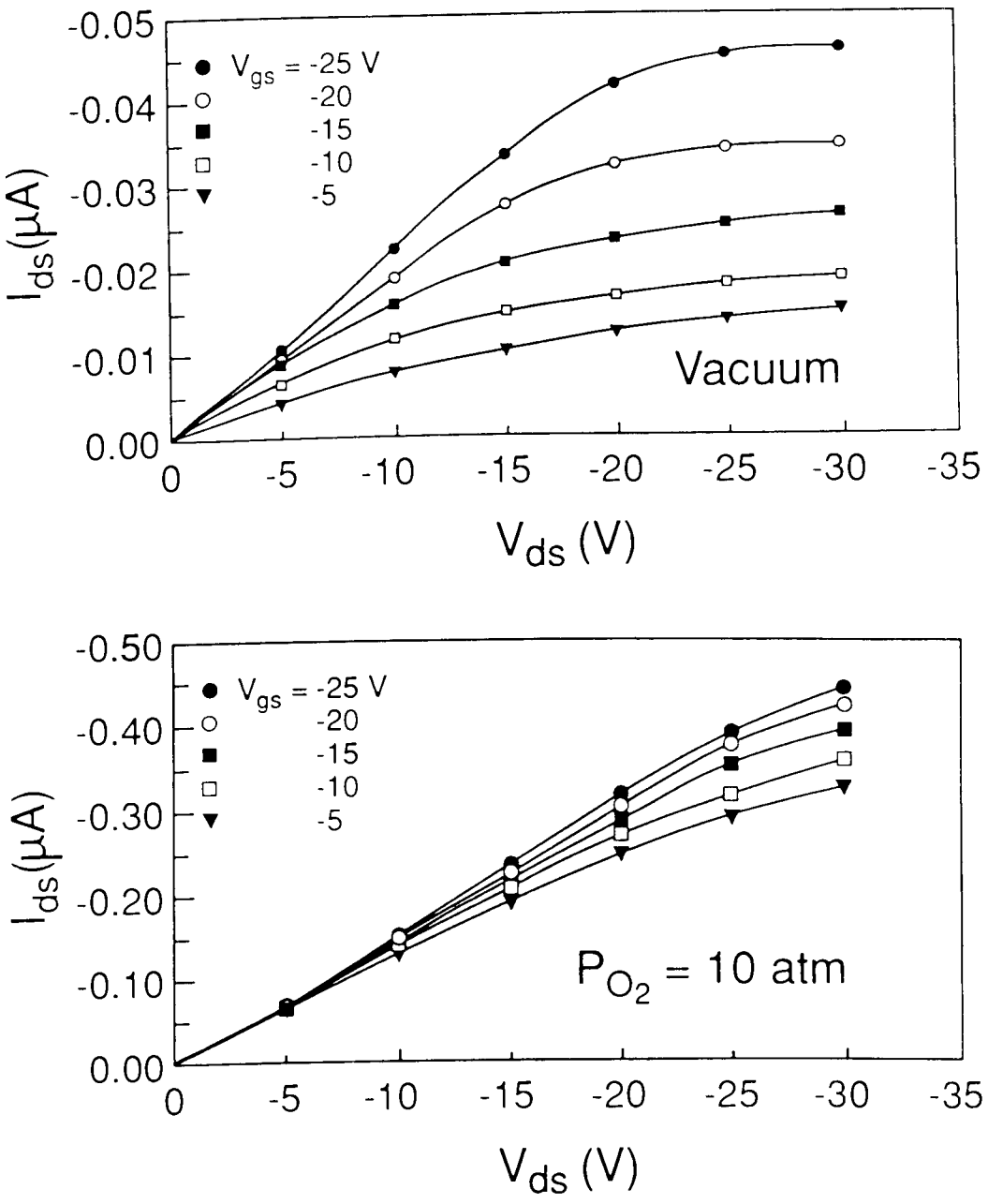

Figure VI.5: I_{ds}-V_{ds} characteristics of polymer-FETs *in vacuo* and under 10 atm. O_2.

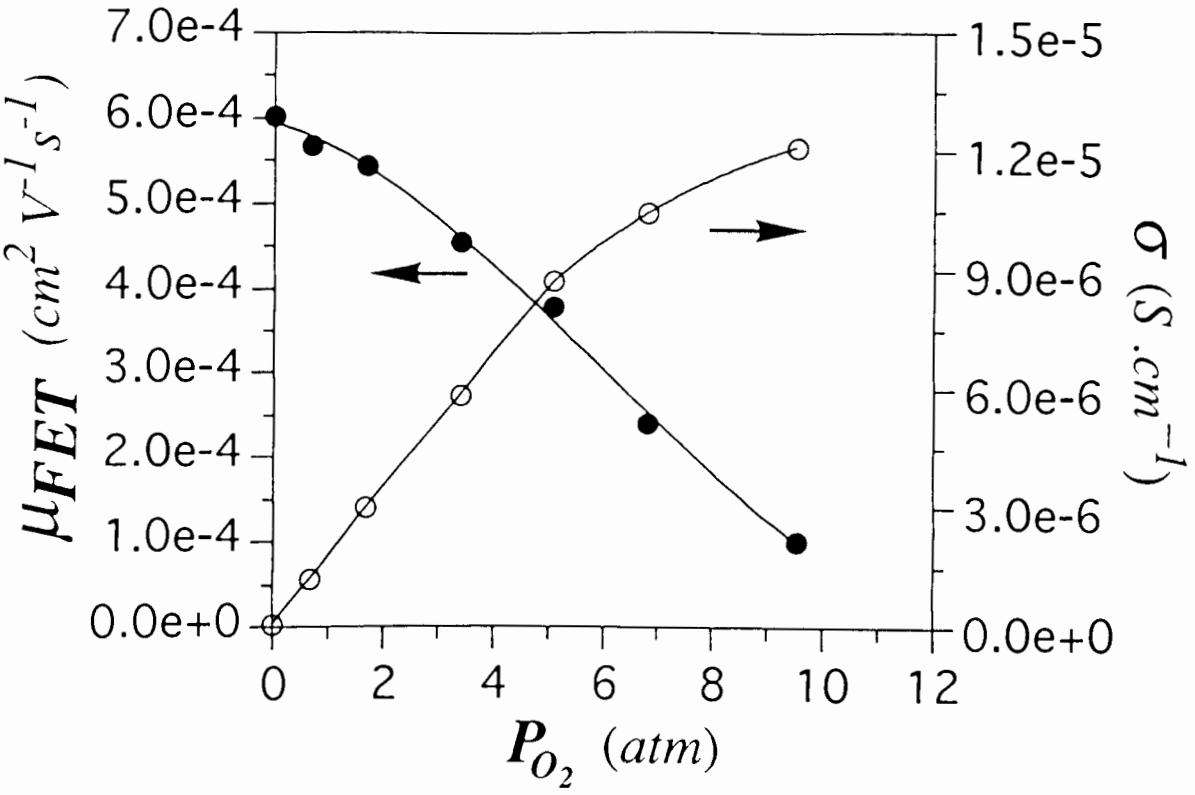

Figure VI.6: Effect of oxygen pressure on the conductivity and charge carrier mobility in P3HT films.

The change in conductivity upon contact with oxygen is indicated in Figure VI.7. This plot indicates the time response of the film upon application of oxygen or vacuum. The long equilibration time can be attributed to the relatively slow diffusion of oxygen into the bulk of the polymer. It should be remembered that thin films of P3HT are semicrystalline, and this will serve to retard diffusion.

In addition to providing valuable insights on the interactions between conjugated polymers and oxygen, these FETs are attractive as oxygen sensors since the sensing macromolecular materials can be spatially deposited with micron resolution by microlithographic techniques, and easily integrated into

microelectronic circuitries. However, it will be necessary to substantially reduce the response time of the devices. In this context, amorphous polymers with low glass transition temperatures may enhance the diffusion process and would prove interesting to investigate.

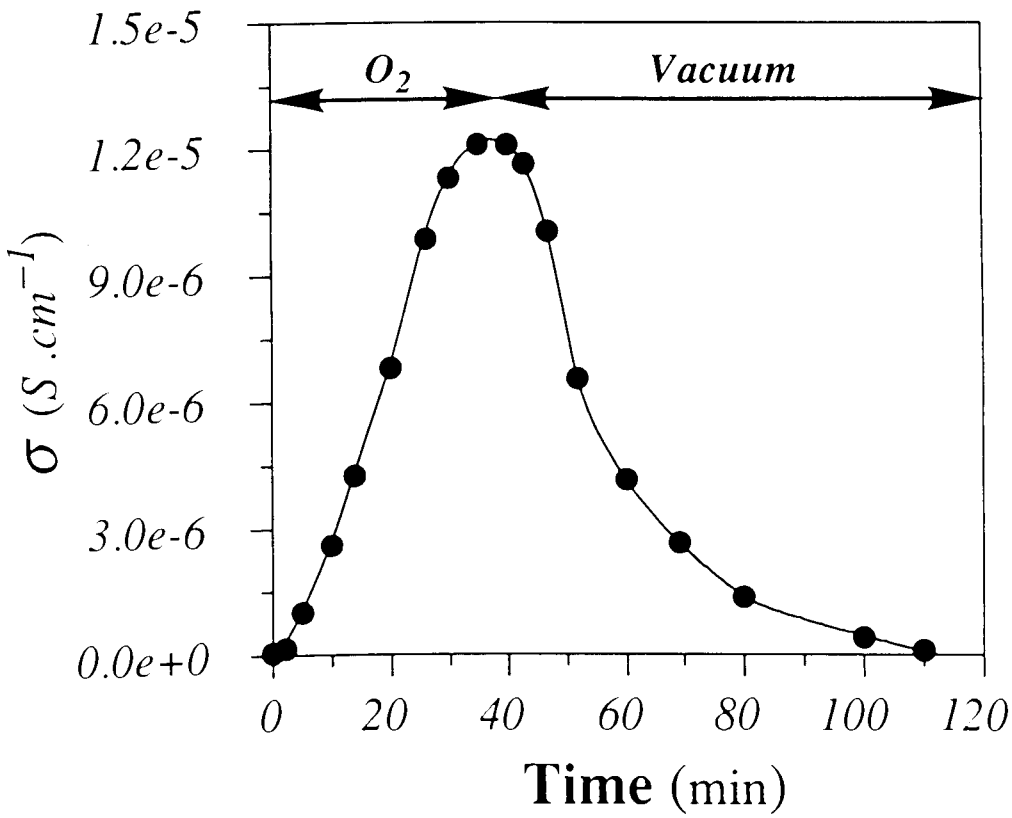

Figure VI.7: Time response for change in conductivity of P3HT thin films upon application and removal of O_2. pO_2= 10 atm.

Photochemical Properties. P3ATs are susceptible to photodegradation in the presence of oxygen (*cf.* III.6.5). Photobleaching is the main reaction leading to degradation and involves photosensitization, and reaction, of singlet oxygen. The mechanism of reaction of $^1O_2$ with P3HT was demonstrated in Chapter III (*cf.* Scheme III.11). The mechanism of $^1O_2$ photosensitization by P3HT is yet to be resolved. Photosensitization of singlet oxygen by triplet states of P3HT was ruled out based on the very low quantum yield of triplet formation as shown by recent phosphorescence and transient spectroscopic data.[66,223] The observation that P3ATs form a CTC with molecular oxygen provides an alternative explanation.

Recently, it has been demonstrated that photogeneration of singlet oxygen in solid films of polystyrene results from irradiation of oxygen-polystyrene charge transfer complexes.[221] One can anticipate a similar mechanism for P3ATs. Indeed, singlet oxygen emission at 1270 nm was detected following irradiation of P3HT in the presence of molecular triplet oxygen.[404] The following mechanism might explain this photosensitization process (Scheme VI.3).

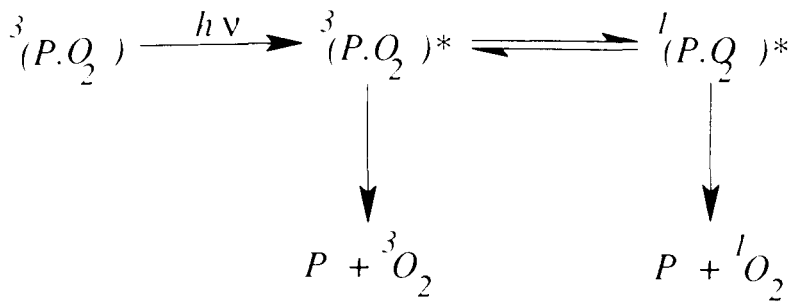

Scheme VI.3

In this scheme, the ground state of P3HT.O_2 CTC is a triplet due to multiplicity multiplication of singlet ground state of P3HT and the triplet ground state of molecular oxygen. Excitation of P3HT.O_2 CTC gives rise to a triplet excited state which is usually very close in energy to the excited singlet-state.[403] Dissociation of the latter yields singlet oxygen. The formation $^1O_2$ from ^{3}CTC* is improbable because it is a spin forbidden process. Further photophysical investigation is, however, necessary to clarify this mechanism.

VI.7 Conclusion

In summary, oxygen forms a weak charge transfer complex with conjugated poly(3-alkylthiophenes). The complex exhibits an absorption maximum in the visible region of the spectrum as predicted from empirical relationships. The CTC is largely responsible for the generation of charge carriers in semiconducting π-conjugated polymers exposed to air. The conductivity of the polymer increases with oxygen pressure. Because these polymers act as both the amplifying and sensing medium, thin film transistors using poly(3-alkylthiophenes) might prove to have interesting oxygen-sensor applications.

The O_2.P3ATs complexes are believed responsiple for photosensitization of singlet oxygen by poly(3-alkylthiophenes).

The formation of a charge transfer complex with π-conjugated polymers is anticipated to be a general effect. The degree of charge transfer and the magnitude of the equilibrium constant of complex formation will certainly be a function of the ionization potential and morphology. Those polymers possessing low ionization potentials and having an amorphous nature, to facilitate diffusion of oxygen into the bulk, will be particularly susceptible to charge transfer complex formation in the presence of oxygen.

CONCLUDING REMARKS

In this thesis, the potential for constructing macromolecular wires and macromolecular transistors was demonstrated. Microlithography has been used in fabrication of conjugated polymer-based macromolecualr wires with micron resolution. Macromolecular poly(3-alkylthiophene) semiconductor-based thin-film field-effect transistors were constructed using conventional MOS technology.

The lithographic performance of π-conjugated poly(3-alkylthiophenes) (P3ATs) was evaluated using conventional photolithography and Laser, direct-write microlithography. A detailed photochemical study of P3ATs in the solid state and in solution has been conducted to establish the mechanism of the photochemical reactions involved in these light-induced processing techniques. This photochemical study revealed that the alkyl substituents play a central role in the photochemistry and photoimaging of P3ATs. This mechanism facilitates new strategies for designing conjugated polymers which possess even greater quantum efficiencies of crosslinking and higher resolution architectures. In this context, derivatization of the alkyl-side chains with vinyl-functionality may prove interesting to investigate.

Macromolecular wires are semiconducting in the neutral form ($\sigma = 10^{-7}\ \Omega^{-1}cm^{-1}$), and doping is necessary to impart metallic conductivity. P3ATs doped using conventional oxidants such as ferric chloride suffer from poor long-term stability. The photo-instability (de-doping) of $FeCl_4^-$-doped polymers has been shown to be a direct consequence of the photolability of the counter ion $FeCl_4^-$. Photochemical de-doping is an efficient route by which these materials lose conductivity. New strategies using photostable counter ions such as $AuCl_4^-$, which were produced by doping P3ATs with $AuCl_3$ in *acetonitrile*, provided solutions for improving the stability of doped, conducting polymers. In contrast to

polymers doped with $FeCl_4^-$, which revert back to their neutral form in a matter of hours even in the dark, $AuCl_4^-$-doped polymers are stable for several months. Oxidation of P3ATs films using solutions of $AuCl_3$ in *nitromethane* results in electroless deposition of gold metal in addition to formation of $AuCl_4^-$-doped polymers. The electronic conductivities of the metal/polymer bilayers are as high as 10, 000 Ω^{-1} cm^{-1}. These bilayers may prove useful in the fabrication of π-conjugated-based current carriers, interconnects and contact pads in microelectronics applications such as integrated circuitry.

Macromolecular devices complement macromolecular wires in the design of organic macromolecular electronics. Investigations of the electronic properties of poly(3-alkylthiophene)-based thin-film field effect transistors permit understanding the origin of charge carriers and transport properties of the materials in the neutral form. Residual-iron impurities (internal impurities) of the initiator used in polymerization of the material contribute, in part, to the origin of charge carriers and significantly affect the transport properties of P3ATs. The electrical properties of P3ATs are sensitive to the presence of oxygen (external impurities). O_2 forms a weak charge transfer complex with P3ATs. These complexes are largely responsible for the generation of charge carries in macromolecualr semiconductors exposed to air. Controlling the level of both internal and external impurities is essential for designing high performance devices.

REFERENCES AND NOTES

1. Robinson, A. , *Science*, **1984**, *223*, 267.
2. Aviram, A.; Ratner, M. A., *Chem. Phys. Lett.*, **1974**, *29*, 281.
3. Smith, R. A., *Semiconductors*, Cambridge University Press, London, **1967**.
4. Faraday, M., *Experimental Researches in Electricity*, **1833**, *IV*, 433.
5 Braun, F., *Ann. Phys. Chem.*, **1874**, *153*, 55.
6. Smith, W., *J. Soc. Telegraph Engrs.* **1873**, *2*, 31.
7. Gudden, B., *Ergebn. exakt. Naturw.* **1924**, *3*, 143.
8. Wagner, C., *Z. Chem. Phys. B,* **1930**, *11*, 163.
9. Grondahl, L. O.; Geiger, P. H., *Trans. Amer. Inst. Elect. Engrs.*, **1927**, *46*, 357.
10. Bardeen, J.; Brattain, W. H., *Phys. Rev.*, **1948**, *74*, 230.
11. Shockley, W.; Pearson, G. L.; Haynes, J. R., *Phys. Rev.*, **1948**, *74*, 232.
12. Meyer, K. H., *Natural and Synthetic High Polymers*, Interscience Pub., **1942**.
13. Pochettino, A., *Acad. Lincei., Rendic.*, **1906**, *15*, 355.
14. Koenigsberger, J.; Schilling, K., *Ann. Physik.*, **1910**, *32*, 179.
15. Szent-Gyorgyi, A., *Science*, **1941**, *93*, 609.
16. Szent-Gyorgyi, A., *Nature*, **1946**, *157*, 875.
17. Ely, D. D., *Nature*, **1948**, *162*, 819.
18. Topchiev, A. V.; Geyderkh, M. A., *Dokl. Akad. Nauk, SSSR*, **1959**, *128*, 312.
19. Dokukina, E. S., *Dokl. Akad. Nauk, SSSR*, **1961**, *137*, 893.
20. Dacey, J. R.; Barradas, R. G., *Can. J. Chem.*, **1963**, *41*, 180.

21. Dacey, J. R.; Cadenhead, A., *Proc. fourth Carbon Conference*, Buffalo, Pergamon Press, N.Y., **1960**, pp. 315.

22. Topchiev, A. V.; Geyderkh, M. A.; Davydov, H. E.; Kargin, V. A.; Krenstel, B. A.; Kustanovich, I. M.; Polak, L. S., *Chem. Ind.*, (London), **1960**, 184.

23. Maithia, S. B.; Kronick, P.L.; Labes, M. M., *J. Chem. Phys.*, **1962**, *37*, 2509.

24. Shvartsberg, M. S.; Kotlyarevsky, I. L., *Russ. Chem. Rev.*, (Engl. Trasl.), **1960**, *29*, 662.

25. Dulov, A. A.; Slinkin, A. A.; Liogonky, B. I.; Robinstein, *Dokl. Akad. Nauk. SSSR*, **1962**, *143*, 1355.

26. Hatano, M.; Kambara, S.; Okamato, S., *J. Polym. Sci.*, **1961**, *51*, 526.

27. Hatano, M.; *J. Chem. Soc. Japan, Ind. Chem. Sect.*, **1962**, *65*, 728.

28. Goldfinger, G., *J. Polym. Sci.*, **1949**, *4*, 93.

29. Glaesson, S.; Gehm, R.; Seibel, M., *Makromol. Chem.* **1951**, *7*, 46.

30. Kern, W., Gehm, R.; Seibel, M., *Makromol. Chem.* **1955**, *15*, 170.

31. Kovacic, P.; Kyriakis, A., *Tetrahedron Lett.*, **1962**, 467.

32. McNeill, R., Siudak, R., Wardlaw, J. H.; Wiess, D. E., *Australian J. Chem.*, **1963**, *16*, 1056.

33. Weiss, D. E.; Bolto, B. A., *Australian Pat.*#263 238, **1965**.

34. Shirakawa, H.; Ito, T.; Ikeda, S., *Polymer J. (Tokyo)*, **1973**, *4*, 460.

35. Ito, T.; Shirakawa, H.; Ikeda, S.; *J. Polym. Sci., Polym. chem. Ed.*, **1974**, *12*, 11.

36. Ito, T., Shirakawa, H.; Ikeda, S., *J. Polym. Sci., Polym. Chem. Ed.*, **1975**, *13*, 1943.

37. Shirakawa, H.; Louis, E. J.; MacDiarmid; A. G., Chiang, C. K.; Heeger, A. J., *J. Chem. Soc. Chem. Commun.*, **1977**, 578.

38. Shirakawa, H.; Ito, T.; Ikeda, S., *Makromol. Chem.* **1978**, *179*, 1565.

39. Chaing, C. K.; Fincher, C. R.; Park, Y. W.; Heeger, A. J.; Shirakawa, H., Louis, E. J.; Gau, S. C.; MacDiarmid, A. G., *Phys. Rev. Lett.*, **1977**, *39*, 1098.

40. Chaing, C. K.; Gau, S. C.; Fincher, C. R.; Park, Y. W.; MacDiarmid, A. G.; Heeger, A. J., *Appl. Phys. Lett.*, **1978**, *33*, 18.

41. Chaing, C. K.; Park, Y. W.; Heeger, A. J.; Shirakawa, H.; Louis, E. J.; MacDiarmid, A. G., *J. Chem. Phys.*, **1978**, *69*, 5098.

42. Park, Y. W.; Denenstein, A.; Chaing, C. K.; Heeger, A. J.; MacDiarmid, A. G., *Solid State commun.*, **1979**, *29*, 747.

43. Fincher, C. R.; Peebles, D. L.; Heeger, A. J; Druy, M. A.; Matsumura, Y.; MacDiarmid, A. G.; Shirakawa, H.; Ikeda, S., *Solid State commun.*, **1978**, *27*, 489.

44. Naarmann, H.; Theophilou, N., *Synth. Met.* **1987**, *22*, 1.

45. Ivory, D. M.; Miller, G. G.; Sowa, J. M.; Shacklette, L. W.; Chance, R. R.; Baughman, R. H., *J. Chem. Phys.*, **1979**, *71*, 1506.

46. Shacklette, L. W.; Chance, R. R.; Ivory, D. M.; Miller, G. G.; Baughman, R. H., *Synth. Met.* **1979**, *1*, 307.

47. Wnek, D. E.; Chien, J. C. W.; Karasz, F. E.; Lilya, C. P., *Polymer*, **1979**, *20*, 1441.

48. Rabolt, J. F.; Clarke, T. C.; Kanazawa; K. K.; Reynolds, J. R.; Street, G. B., *J. Chem. Soc. Chem. Commun.*, **1980**, 347.

49. Chance, R. R.; Shacklette, L. W.; Miller, G. G.; Ivory, D. M.; Sowa, J. M.; Elsenbaumer, R. L.; Baughman, R. H., *J. Chem. Soc. Chem. Commun.*, **1980**, 349.

50. Diaz, A. F.; Logan, J. A., *J. Electroanal. Chem.*, **1980**, *111*, 111.

51. Diaz, A. F.; Kanazawa, K. K., *J. Chem. Soc. Chem. Commun.*, **1979**, 635.

52. Yamamoto, T.; Sanechika, K.; Yamamoto, A., *J. Polym. Sci., Polym. Lett. Ed.*, **1980**, *18*, 9.

53. Tourillon, G.; Garnier, F., *J. Electroanal. Chem.*, **1982**, *135*, 173.

54. Wudl, F.; Kobayashi, M.; Colaneri, N.; Boysel, M.; Heeger, A. J., *Mol. Cryst. Liq. Cryst.* **1985**, *118*, 199.

55. Rughooputh, D. D. V.; Hotta, S. ; Heeger, A. J.; Wudl, F., *J. Polym. Sci., Polym. Phys.*, **1993**, *25*, 1071.

56. Inganas, O.; Salaneck, W. R.; Ösreholm, J.-E.; Laakso, J., *Synth. Met.* , **1988**, *22*, 395.

57. Garnier, F.; Tourillon, G.; Gazard, M.; Dubois, J. C., *J. Electroanal. Chem.*, **1983**, *148*, 299.

58. Salaneck, W. R.; Inganas, O.; Nilsson, J. O.; Ösreholm, J.-E.; Themans, B.; Bredas, J-L., *Synth. Met.*, **1989**, *28*, C451.

59. Themans, B.; Salaneck, W. R.; Bredas, J-L., *Synth. Met.*, **1989**, *28*, C359.

60. Yoshino, K.; Kaneto, K.; Inuishi, Y., *J. J. Appl. Phys.*, **1983**, *22*, L157.

62. Friend, R. H.; Bradley, D. D. C.; Townsend, P. D., *J. Phys. D.: Appl. Phys.* **1987**, *20*, 1367.

63. Ruhe, J.; Colaneri, N. F.; Bradley, D. D. C.; Friend, R. H.; Wegner, G., *J. Phys.: Condens. Matter.* **1990**, *2*, 5465.

64. Hayashi, S.; Kaneto, K.; Yoshino, K., *Solid State Commun.* **1987**, *61*, 251.

65. Dyreklev, P.; Inganas, O., Paloheimo, J.; Stubb, H., *Synth. Met.* , **1993**, *55-57*, 4139.

66. Xu, .B.; Holdcroft, S., *J. Amer. Chem. Soc.* **1993**, *115*, 8447.

67. Xu, .B.; Holdcroft, S., *Thin Solid Films*, **1994**, *242*, 174.

68. Binh, N. T.; Gailberger, M.; Bassler, H., *Synth. Met.*, **1992**, *47*, 77.

69. Skothiem, T. A. *Handbook of Conducting Polymers*, Marcel Dekker,USA, **1986**.

70. Kittel, C. , *Introduction to Solid-State Physics*, Wiley, 3rd. Ed., **1967**.

71. Heeger, A. J., *Faraday Discuss. Chem. Soc.*, **1989**, *88*, 203.

72. Mao, H.; Holdcroft, S., *Macromolecules*, ***25***, **1992**, 554.

73. McCullough, R.; Lowe, R. D., *J. Chem. Soc. Chem. Commun.*, **1992**, 70.

74. Wang, Y.; Rubner, M. F., *Polymer Preprints*, **1991**, *31*, 402.

75. A. Aviram, *J. Amer. Chem. Soc.*, **1988**, *110,* 5687.

76. (a) Tour, J. M.; Wu, R.; Schumm, J. S., *J. Amer. Chem. Soc.*, **1990**, *112*, 5662., (b) Tour, J. M.; Wu, R.; Schumm, J. S., *J. Amer. Chem. Soc.*, **1991**, *113*, 7064.

77. Spangler, C. W.; Liu, P. K.; Dembek, A. A.; Havelka, K. O., *J. Chem. Soc., Perkin 1*, **1991**, 799.

78. Franssila, S.; Paloheimo, J.; Kuivalainen, P., *Electronic Lett*, **1993**, *29*, 713.

79. (a) Burn, P. L.; Holmes, A. B.; Kraft, A.; Bradley, D. D. C.; Brown, A. R.; Friend, R. H.; Gymer, R. W., *Nature*, **1992**, *356*, 47., (b) Gustafsson, G.; Cao, Y.; Treacy, G. M.; Klavetter, F.; Colaneri, N.; Heeger, A. J., *Nature*, **1992**, *357*, 477.

80. Sailor, M. J.; Ginsburg, E. J.; Gorman, C. B.; Kumar, A.; Grubbs, R. H.; Lewis, N. S., *Science*, **1990**, *249*, 1146.

81. Burroughes, J. H.; Jones, C. A.; Friend, R. H., *Nature*, **1988**, *335*, 137.

82. White, H. S.; Kittlesen, G. P.; Wrighton, M. S., *J. Amer. Chem. Soc.*, **1985**, *106*, 5375.

83. Rosner, R. B.; Rubner, M. F., *Mater. Res. Soc. Symp. Proc.* **1990**, *173*, 363.

84. Belanger, D.; Nadreau, J.; Fortier, G., *J. Electroanal. Chem.* **1989**, *274*, 143.

85 (a) Naegele, D.; Bittihn, R., *Solid State Ionics*, **1988**, *28-30*, 983., (b) Maxfield, M.; Jow, T. R.; Sewchok, M. G.; Shacklette, L. W., *J. Power Sources*, **1989**, *26*, 93.

86. Miller, L.; Zhou, Q. X., *Macromolecules*, **1987**, *20*, 1594

87. Mastragostino, M.; Marinangeli, A. M.; Corradini, A.; Giacobbe, S. *Synth. Met.* **1989,** *28*, C501.

88. Yoshino, K.; Tabata, M.; Kaneto, K.; Ohsawa, T., *J. J. Appl. Phys., Pt. 2*, **1985**, *24*, 693.

89. Jen, K. Y.; Oboodi, R.; Elsenbaumer, R., *Polym. Materials: Sci. Eng.* 1985, 53, 79.

90. Sugimoto, R.; Takeda, S.; Gu, H.B.; Yoshino, K. *Chem. Express*, **1986**, *1*, 635.

91. Tamao, K.; Kodama, S.; Nakajima, J.; Kumada, M., *Tetrahedron*, **1982**, *38*, 3347.

92. Hotta, S., *Synth. Met.* ***22***, **1987**, 103.

93. Quarmby, C., Grimshaw, H. M. *Analyst*, **1967,** *92*, 305.

94. Stevens, M. P., *Polymer Chemistry*, Oxford University Press, N.Y., **1990**.

95. Holdcroft, S., *J. Polym. Sci., Polym. Phys.*, **1991**, *29*, 1585.

96. Hunt, B. J.; James, M. I., *Polymer Characterization*, Chapman & Hall, Great Britain, **1993**.

97. Niemi, V. M., Knuuttila, P., Österholm, J.-E.; Korvola, J., *Polymer*, **1992**, *33*, 1559.

98. Sato, M.; Morii, H., *Macromolecules,* **1991**, *24*, 1196.

99. Mao, H., Xu, B.; Holdcroft, S., *Macromolecules, **26**,* **1993**, 1163.

100. McCullough, R.; Lowe, R. D., Jayaraman, M.; Anderson, D. L., *J. Org. Chem.*, **1993**, *58*, 904.

101. Paloheimo, J.; Stubb, H.; Yli-Lahti, P.; Kuivalainen, P., *Synth. Met.*, **1991**, *41-43*, 563.

102. Zotti, G.; Schiavon, G., *J. Electroanal. Chem.* **1988**, *246*, 467.

103. Roncali, J. *Chem. Rev.* , **1992**, *92*, 711.

104. Wei, Y.; Tian, J.; Glahn, D.; Wang, B.; Chu, D., *J. Phys. Chem.*, **1993**, *97*, 12842.

105. Leclerc, L.; Diaz, F. M.; Wegner, G., *Makromol. Chem.*, **1989**, *190*, 3105.

106. Foot, P.; Ritchie, T.; Mohammad, F.,, *J. Chem. Soc. Chem. Commun.*, **1988**, 1536.

107. Greenwood, N. N., Gibb, T. C., *Mössbauer Spectroscopy*, Chapman and Hall Ltd., london, 1971.

108. Nyquist, R. A.; Kagel, R. O., *Infrared Spectra of Inorganic Comounds*, Academic Press, N.Y., 1971.

109. Angelici, R. J., *Coordination Chem. Rev.*, ***105***, **1990**, 61.

110. Pannel, K. H.; Kalsotra, B. L.; Parkanyi, C., *J. Hetrocycl. Chem.*, ***15***, **1978**, 1057.

111. Aimé, J. P., Bargain, F., Schott, M., Eckhardt, H., Elsenbaumer, R. L., Miller, G. G., McDonnell, M. E.; Zero, K., *Synth. Met.* **1989**, 28, C407.

112. Heffner, G. W.; Pearson, D. S., *Macromolecules*, **1991**, *24*, 6295.

113. Zerbi, G., Chierichetti, B., Inganas, O. J. *Chem Phys.*, **1991**, *94*, 4637.

114. Zerbi, G., Chierichetti, B., Inganas, O. J., *J. Chem Phys.*, **1991**, *94*, 4646.

115. Schulte, K. E., Kreutzberger, A., Bohn, G. *Chem. Ber.*, **1964**, *97*, 3263.

116. Hotta, S., Shimotsuma, W., Taketani, M. *Synth. Met.*, **1984**, *10*, 85.

117. Akimoto, M., Furukawa, Y., Takeuchi, H., Harada, I., Soma, Y., Soma, M. *Synth. Met.*, **1986**, *15*, 353.

118. Furukawa, Y., Akimoto, M., Harada, I. *Synth. Met.*, **1987**, *18*, 151.

119. Souto Maior, R. M., Hinkelmann, K., Eckert, H.; Wudl, F., *Macromolecules*, **1990**, *23*, 1268.

120. Sato, M.,Shimizu, T., Yamauchi, A. *Synth. Met.*, **1991**, *41-43*, 551.

121. Stein, P.C., Bolognesi, A., Catellani, M., Zetta, L. *Synth. Met.*, **1991**, *41-43*, 559.

122. Bovey, F. A., *Polymer Coformation and Configuration*, Academic Press, N.Y., **1969**.

123. Barbarella, G., Bongini, A.; Zambianchi, M., *Macromolecules*, **1994**, *27*, 3039.

124. Hotta, S. , Rughooputh, D. D. V., Heeger, A. J., Wudl, F. *Macromolecules* , **1987**, *20*, 212.

125. Patil, A. O.; Heeger, A. J.; Wudl, F. *Chem. Rev.*, **1988**, *88*, 183.

126. Brodsky, M. H., *Amorphous Semiconductors*, Springer-Verlag, Germany, **1985**.

127. Kakudo, M.; Kasai, N., *X-ray Diffraction by Polymers*, Kodansha Ltd., Japan, **1972**.

128. Winokur, M. J., Spiegel, D., Kim, Y. H., Hotta, S.; Heeger, A. J.,*Synth. Met.*, **1989**, *28*, C419.

129. (a) Mardalen, J., Samuelsen, E., Gautun, O.; Carlsen, H., *Solid State Commun.* **1991**, *80*, 687., (b) Mardalen, J., Samuelsen, E., Gautun, O.; Carlsen, H., *Synth. Met.*, **1992**, *48*, 363.

130. Chen, S-A.; Ni, J-M., *Macromolecules*, **1992**, *25*, 6081.

131. Hsu, W-P., Levon, K., Ho, K-S., Myerson, A. S.; Kwei, T. K., *Macromolecules*, **1993**, *26*, 1323.

132. Moreau, W.M. *Semiconductor Lithography*, Plenum Press: New York, **1988**.

133. Hitchman, M. L.; Jensen, K. F., Eds., *Chemival Vapor Deposition*, Academic Press, San Diego, **1993**.

134. Bredas, J. L.; Silbey, R., Eds., *Conjugated Polymers*, Kluwer Acadamic Pubs., Dordrecht, Netherland, 1991., p. 363

135. DeForest, W. S., *Photoresist*, McGraw-Hill Inc., USA, **1975**.

136. Thompson, L.F.; Wilson, C.G.; Bowden, M.J. Eds., *Introduction to Microlithography*, ACS Symposium Series 219; American Chemical Society: Washington, DC, 1983.

137. Albert, M., School of Engineering Science , Simon Fraser University.

138. Turner, S. R.; Ahn, K. D.; Willson, C. G., *Proc. ACS Division Polymer Material Science and Engineering*, ACS, 1986.

139. Charlesby, A., *Atomic Radiation and Polymers*, Pergamon Press Ltd., N.Y., **1960**.

140. Reiser, A., *Photoactive Polymers*, John Wiley, USA, **1989**.

141. *Aspects of Degradation and Stabilization of Polymers*, Jellinek, H. H. G., Ed., Elsevier Scientific Pub. Amsterdam, **1978**.

142. Stockmayer, W. H., *J. Chem. Phys.*, **1944**, *12*, 125.

143. Charlesby, A.; Pinner, S. H., *Proc. Roy. Soc.*, **1958**, *A249*, 367.

144. Calvert, J. G.; Pitts, J. N., Jr., *Photochemistry*, Wiley, N.Y., **1966**.

145. Jaffe, H. H.; Orchin, M., *Theory and Applications of Ultraviolet Spectroscopy*, Wiley, N.Y., **1962**.

146. Pleskov, Y. V.; Gureich, Y. Y., *Semiconductor Photoelectrochemistry*, (English Translation), Consultant Bureau, N.Y. 1986.

147. Ranby, B.; Rabek, J. F., *Photodegradation, Photooxidation and Photostabilization of Polymers*, John Wiley, Great Britain, **1975**.

148. McKeller, J.F., Allen, N.S., *Photochemistry of Man-Made Polymers*, Applied Science Publishers, London, **1979**.

149. Guillet J.E., *Polymer Photophysics and Photochemistry*, Cambridge University Press, New York, **1985**.

150. Birks, J.B., *Photophysics of Aromatic Molecules*, Wiley, London, **1970**.

151. Ogilby, P.R., Dillon, M.P., Kristiansen, M., Clough, R.L., *Macromolecules*, **1992** , *25*, 3399.

152. Gollnick, K.; Schenck, G. O., *in 1,4-Cycloaddition Reactions*, Hamer, J. Ed., Academic Press, N.Y., **1967**, Chap. 10.

153. Sawyer, D. T., *Oxygen Chemistry*, Oxford University Press, N.Y., **1991**.

154. Tsubomura, H.; Mulliken, R.S., *J. Amer. Chem. Soc.*, 1960, 82, 5966.

155. Wilkinson, F.; Helman, W. P.; Ross, A. B., *J. Phys. Chem. Ref. Data*, **1993**, *22*, 113.

156. Turro, N. J., *Modern Molecular Photochemistry*, Benjamin/Cummings Pub., California, **1978**.

157. Schiller, K.; Muller, F. W., *Polymer International*, **1991**, *25*, 19.

158. Kearns, D., *Chem. Rev.*, **1971**, *71*, 395.

159. Gollnick, K., in *Singlet Oxygen-Reaction with Organic Compounds and Polymers*, Ranby, B., Rabek, L. F., Ed., John Wiley, 1978.

160. Winslow, F. H., Trozzolo, A. M. *Macromolecules*, **1968**, *1*, 98.

161. Ingold, K. U., *Acc. Chem. Res.*, **1969**, *2*, 1.

162. Reich, L., Stivala, S. S. *Autoxidation of Hydrocarbons and Polyolefins*, Marcel Dekker Inc., N.Y., 1969.

163. Uri, N., *Chem. Rev.* **1952**, *52*, 357.

164. Ingold, K. U., *Pure Appl. Chem.*, **1967**, *15*, 49.

165. Mayo, F. R., *Acc. Chem. Res.*, **1968**, *1*, 193.

166. Allen, P.C.; Bott, D.C.; Brown, C.S.; Connors, L.M.; Gray, S.; Walker, N. S.; Clemonson, P.I.; Feast, W.J., *Electronic Properties of Conjugated Polymers III*, Kuzmany, H.; Mehring, M.; Roth, S., Eds., Springer-Verlag, Berlin, 1989.

167. Clemonson, P.I., Feast, W.J., Ahmad, M.M., Allen, P.C., Bott, D.C., Brown, C.S., Connors, L.M., *Polymer*, in press.

168. Novak, B.M.; Hagen, E.; Viswanathan, A.; Magde, L. *Polymer Preprints*, **1990**, *31*, 482.

169. Crivello, J. V.; Lam, J. H. W., *J. Poly. Sci., Poly. Chem. Ed.*, **1980**, *18*, 2677.

170. Das, P. K.; DesLauriers, P. J.; Fahey, D. R.; Wood, F. K.; Cornforth, F. J., *Macromolecules*, **1993**, *26*, 5024.

171. Filho, A. T.; Lenz, R., *J. Polym. Sci., Polym. Phys.*, **1993**, *31*, 959.

172. Onoda, M.; Nakayama, H.; Yoshino, K., *IEEE Trans. Elect. Ins.*, **1992**, *27*, 636.

173. Bullot, J.; Dulieu, B.; Lafrant, S., *Synth. Met.* **1993**, *61*, 211.

174. Angelopoulos, M.; Shaw, J.M.; Huang, W.-S.; Karplan, R.D. *Mol. Cryst. Liq. Cryst.*, **1990**, *189*, 221.

175. Angelopoulos, M.; Shaw, J.M.;Lee, K-L.; Huang,W-S.; Lecorre, M-A.; Tissier, M.,. *Poly. Engin. Sci.*, **1992**, *32*, 1535.

176. Kuwabata, S.; Takahashi, N.; Hirao, S.; Yoneyama, H., *Chem. Mater.*, **1993**, *5*, 437.

177. Yoneyama, H., *Adv. Mater.*, **1993**, *5*, 394.

178. Jin, J.Y.; Teramae, N.; Haraguchi, H., *Chem. Lett.*, **1993**, 101.

179. Wuu, Y-M.; Fan, F. F.; Bard, A., *J. Electrochem. Soc.*, **1989**, *136*, 885.

180. Neoh, K. G.; Kang, E. t.; Tan, K. L., *Polymer*, **1992**, *33*, 2292.

181. Okano, M.; Itoh, K.; Fujishima, A.; Honda, K. *J. Electrochem. Soc.*, **1987**, *134*, 837.

182. Segawa, H.; Shimidzu, T.; Honda, K. *J. Chem. Soc. Chem. Commun.*, **1989**, 132.

183. (a) Nannini, A.; Serra, G., *J. Molec. Electon.*, **1990**, *6*, 81., (b) Behnck, W.; Bargon, J., *Synth. Met.* **1993**, *54*, 223.

184. Van Dyke, L. S.; Brumlik, C. J.; Martin, C. R.; Yu, Z.; Collins, G. J., *Synth. Met.* **1993**, *52*, 299.

185. Cai, S. X.; Kanskar, M.; Wybourne, M. N.; Keana, F. W., *Chem. Mater.*, **1992**, *4*, 879.

186. Yan, M.; Cai, S. X.; Wybourne, M. N.; Keana, F. W., *J. Amer. Chem. Soc.*, **1993**, *115*, 814.

187. van der Leur, R.H.M., de Ruiter, B., *Synth. Met.*, **1991**, *44*, 327.

188. Bamford, C.H., Tipper, C.F.H., Eds., *Comprehensive Chemical Kinetics*, Elsevier, New York, Volume 14, 1975.

189. David, C.; Demarteau, W.; Geuskenes, G., *Polymer*, **1967**, *8*, 497.

190. Richardson, R. J., Wiswall, C. E., Carr, P. A. G., Hovis, F. E., Lilenfeld, H. V. *J. Appl. Phys.*, **1981**, *52*, 4962.

191. Seliger, H. H. *J. Chem. Phys.*, **1964,** *40*, 3133.

192. Foote, C. S., Wexler, S., Ando, W., Higgins, R. *J. Amer. Chem. Soc.*, **1968**, *90*, 975.

193. Sugiyama, N.; Iwata, M.; Yoshioka, M.; Yamada, K.; Acyama, H. *J. Chem. Soc.*, **1969**, *42*, 1377.

194. Livingston, R.; Rao, V. S., *J. Amer. Chem. Soc.*, **1959**, *63*, 794.

195. Bredas, J. L.; Silbey, R.; Boudreaux, D. S.; Chance, R. R., *J. Amer. Chem. Soc.*, **1983**, *105*, 6555.

196. Scott, J. C.; Pfluger, P.; Krounbi, M. T.; Street, G. B., *J. Chem. Phys.*, **1983**, *78*, 3212.

197. (a) Bellamy, L., *Advances in Infrared Group Frequencies*, Bellamy, L, Ed., Methuen & Co.Ltd., 1968., (b) Socrates, G., *Infrared Characteristic Group Frequencies*, Wiley, **1980**.

198. Zwanenburg, B., Strating, J. *Quart. Rep.Sulfer Chem.*, **1970**, *5*, 79.

199. Detoni, S., Hadzi, D. *J. Chem. Soc.*,**1955**, 3163.

200. Price, C. C., Gillis, R. J. *J.Amer. Chem. Soc.*, **1953,** *75*, 4750.

201. Swern, D., Clements, A. H. , Lung, T.M. *Anal.Chem.*, **1969**, *41*, 412.

202. Ward, G. A., Mair, R. D. *Anal.Chem.*, **1969**, *41*, 538.

203. *Sadtler Standard NMR Spectra*, Researchers, Eds. and Pub., USA, 1987.

204. D. McLachlan, T. Arnason, J. Lam, *Photochem. Photobiol.* **39** (1984) 177.

205. C. Evans, D. Weir, J. C. Scaiano, A. Mac Eachern, J. T. Arnason, P. Morand, B. Hollebone, L. C. Leitch, B. J. R. Philogene, *Photochem. Photobiol.* **44** (1986) 441.

206. Reyftmann, J.P., Kagan, J., Santos, R., Moliere, P., *Photochem. Photobiol.* **41** (1985) 1.

207. Evans, C. Scaiano, J.C., *J. Am. Chem. Soc.*, **112** (1990) 2694.

208. E_{0-0} transitions are ~ 3.2 and 2.1 eV for anthracene (Berlman, I.B., *Fluoresence Spectra of Aromatic Molecules*, Academic, New York, 1971). $E_{1/2}$ for oxidation and reduction of anthracene are ~-2.0 and +1.0 V (vs. SCE) respectively (Meites, L., Zuman, P., *CRC Handbook Series in Organic Electrochemistry,* CRC, Ohio). The onset for oxidation of P3HT is ~ +0.5 V (SCE) (Roncali, J., Garreau, R., Yassar, A., Marque, P., Garnier, F., Lemaire, M., *J. Phys. Chem.*, **91** (1987) 6706) which places the LUMO at ~-1.6 V and precludes any possibility of electron transfer between excited state P3HT and anthracene on thermodynamic grounds.

209. Thompson, Q. E. *J. Amer. Chem. Soc.*, **1961**, *83,* 845.

210. Scheffer, J. R., Ouchi, D. *Tetrahedron lett.*, **1970,** *3,* 223.

211. Neckers, D. C. *J. Photochem. Photobiol. A,* **1989**, *47,* 1.

212. Attempts to interpret reaction of singlet oxygen by photosesitization of singlet oxygen using Rose-Bengal dye were hampered by the formation of free radicals which arise from photodegradation of the dye (see ref. 206).

213. Skold, C. N.; Schlessinger, R. H.; *Tetrahedron. Lett.*, **1970**, 791.

214. Wasserman, H. H.; Strehlow, W., *Tetrahedron. Lett.*, **1970**, 795.

215. Holdcroft, S. *Macromolecules*, **1991**, *24,* 4834.

216. Gollnick, K., in *Singlet Oxygen-Reaction with Organic Compounds and Polymers*, Ranby, B., Rabek, L. F., Ed., John Wiley, 1978.

217. Adam, W., Eggelte, H. J. *Angew. Chem. Int. Ed. Engl.*, **1979**, *17,* 765.

218. Rabek, J. F., *Singlet O_2*, Frimer, A. A.,Ed.,CRC Press Inc., Florida1985.

219. Rabek, J. F.; Ranby, B., *J. Poly. Sci., A1*, **1974**, *12*, 273.

220. Rabek, J. F.; Ranby, B., *Polym. Degrad. Stabil.*, **1979**, *1*, 251.

221. Ogilby, P.R., Dillon, M.P., Kristiansen, M., Clough, R.L., *Macromolecules*, **1992**, *25,* 3399.

222. Bystritskaya, E. V., Karpukhin, O. N., *Vysokomol. Soedin. Ser. A*, **1976,** *18*, 1963.

223. Wintgens, V., Valat, P., Garnier, F., *J. Phys. Chem.*,**1994**, *98*, 228.

224. Zwanenberg, B., Wagenaar, A., Strating, J., *Tetrahedron. Lett.*, **1970,** 4683.

225. Richters, P., *Macromolecules*, **1970**, *3*, 262.

226. Cicchetti, O., *Adv. Polymer Sci.*, **1970**, *3*, 70.

227. Ya-Shiyapintokh, V., *Photochemical Conversion and Stabilization of Polymers*, Hanser Pub., N.Y., 1984.

228. Beachell, H.C., Nemphos, S.P., *J. Polym., Sci.*, **1956**, *21*, 113.

229. Kujiai, C., Hasiya, S., Furuno, H., Terada, N., *J. Polym., Sci., Part A-1*, **1968**, *6*, 589.

230. Tomozawa, H., Braun, D., Phillips, S., Heeger, A.J.; Kroemer, H. *Synth. Met*, **1987**, *22*, 63 .

231. Garnier, F. ; Horowitz, G. *Synth. Met.*, **1987**, *18*, 693.

232. Tomozawa, H., Braun, D., Phillips, S.D., Worland, R., Heeger, A.J.; Kroemer, H. *Synth. Met*, **1989**, *28*, C687.

233. Although structure **5** is believed the thermodynamically-favored structure, only a small percentage of **6** is required to account for the observed chain scission.

234. Chalk, A. J.; Smith, J. F., *Trans. Faraday Soc.*, **1957**, *53*, 1214.

235. Ingold, K. U., *Chem. Rev.*, **1961**, *61*, 563.

236. Billingham, N.C.; Calvert, P.D.; Foot, P.J.S.; Mohammad, F. *Poly. Degrad. Stab.* **1987**, *19*, 323.

237. Tourillon, G.; Garnier, F. *J.Electrochem. Soc.* **1987**, *130*, 2042.

238. (a) Jen, K.Y.; Miller, G.G.; Elsenbaumer, R.L. *J. Chem. Soc. Chem. Commun.* **1986**, 1346., (b) Elsenbaumer, R.L.; Jen, K.Y.; Miller, G.G.; Shacklette, L. W., *Synth. Met.* **1987**, *18*, 277.

239. (a) Druy, M.A.; Rubner, M.F.; Walsh, S.P. *Synth. Met.* **1986,** *13*, 207. (b) Wang, Y.; Rubner, M.F. *Synth. Met.* **1990,** *39*, 153.; **1991**, *41-43*, 1103.

240. (a) Gustafsson, G.; Inganas, O.; Nilsson, J.O.; Liedberg, B. *Synth. Met.*, **1988,** *26*, 297. (b) Granstrom, M.; Inganas, O., *Synth. Met.*, **1992,** *48*, 21.

241. (a) Osterholm, J.E.; Passiniemi, P.; Isotalo, H.; Stubb, H. *Synth. Met.*, **1987,** *18*, 213. (b) Loponen, M.T.; Tak, T.; Laasko, J.; Vakiparta, K.; Suuronen, K.; Valkeinen, P.; Osterholm, J.-E. *Synth. Met.*, **1991,** *41-43*, 479. (c) Isotalo, H.; Ahlskog, M.; Stubb, H.; Laasko, J.; karna, T.; Jussila, M.; Osterholm, J.-E. *Synth. Met.*, **1993,** *55-57*, 3581, (d) Taka, T. *Synth. Met.*, **1993,** *55-57*, 4985, (e) de Leeuw, D. M. *Synth. Met.*, **1993,** *55-57*, 3597.

242. Daoust, D., Leclerc, M. *Macromolecules*, **1991**, *24*, 455.

243. (a) Pei, Q.; Jarvinen, H.; Osterholm, J.E.; Inganas, O.; Laasko, J. *Macromolecules*, **1992**, *25*, 4297., (b) Pei, Q.; Inganas, O. *Synth. Met.*, **1992,** *46*, 353. (c) Punkka, E., Laakso, J., Stubb, H.; Kuivalaine, P, *Phys. Rev. B.*, **1990**, *41*, 5914., (d) Wang, Y.; Rubner, M.F. *Macromolecules*, **1992**, *25*, 3284.,

244. Patil, A. O., Ikenoue, Y., Wudl, F.; Heeger, A. J., *J. Amer. Chem. Soc.*, **1987**, *109*, 1858.

245. Ito, M., Tsuruno, A.; Ogawa, S., Tanaka, K., *Polymer*, **1988**, *29*, 1161.

246. Baughman, R. H., Hsu, S. L., Pez, G. P.; Slgnorelli, A. J., *J. Chem. Phys.*, **1978**, *68*, 5405.

247. Heeger, A. J.; Kivelson, S.; Schrieffer, J. R., Su, W. P., *Rev. Mod. Phys.*, **1988**, *60*, 782.

248. Bredas, J.L.; Street, G.B. *Acc. Chem. Res.* **1985,** *18*, 309.

249. Su, W. P.; Schrieffer, J. R.; Heeger, A. J., *Phys. Rev. Lett.*, **1979**, *42*, 1698.

250. Kaneto, K., Hayashi, S., Ura, S.; Yoshino, K., *J. Phys. Soc., Jp.*, **1985**, *54*, 1146.

251. Colaneri, N., Nowak, M., Spiegel, D., Hotta, S.; Heeger, A. J., *Phys. Rev. B*, **1987**, *36*, 7964.

252. Harbeke, G.; Meier, E.; Kobel, W.; Egli, M.; Kiess, H.; Tosatti, E. *Solid State Comm.* **1985,** *55*, 419.

253. Conwell, E. M., *Synth. Met.* **1985,** *11*, 21.

254. Chen, J., Heeger, A. J., Wudl, F., *Solid State Commun.*, **1986**, *58*, 251.

255. Nowak, M. J., Spiegel, D., Hotta, S., Heeger, A. J.; Pincus, P. A., Macromolecules, **1989**, *22*, 2917.

256. (a) Tolbert, L. M., *Acc. Chem. Res.* **1992,** *25*, 561., (b) Wegner, G.; Ruhe, J., *Faraday Discuss. Chem. Soc.*, **1989**, *88*, 333.

257. Vardeny, Z.; Ehrenfreund, E.; Brafman, O.; Nowak, M.; Schaffer, H.; Heeger, A. J.; Wudl, F., *Phys. Rev. Lett.*, **1989**,

258. Shacklette,L. W., Chance, R. R., Ivory, D. M., Miller, G. G.; Baughmann, R. H., *Synth. Met.* **1979,** *1*, 307.

259. Ikehata, J., Kauper, T., Woerner, A., Pron, M. A., Druy, A., Sinak, A. J., Heeger, A. J.; MacDiarmid, A. G., *Phys. Rev. Lett.*, **1980**, *45*, 1123.

260. Lopez-Navarrete, J. T.; Zerbi, G., *Chem. Phys. Lett.*, **1990**, *175*, 125.

261. Winokur, M. J.; Wamsley, P.; Moulton, J.; Smith, P.; Heeger, A. J., *Macromolecules*, **1991**, *24*, 3812.

262. Kawai, T.; Nakazono, M.; Yoshino, K., J. Mater. Chem. **1992**, *2*, 903.

263. (a) Morin, A.; Beniere, M.; Beniere, F. *J. Phys. Chem. Solids*, **1989**, *50*, 611, (b) Corish, J., *Philos. Mag. A*, **1991**, *64*, 1073.

264. Pron, A.; Bernier, P.; Billaud, D., Lefrant, S., *Solid state Commun.*, **1983**, *46*, 587.

265. Budrowski, C.; Przyluski, J.; Kucharski, Z.; Suwalski, J., *Synth. Met.* **1990**, *35*, 151.

266. Gill, N. S.; Nyholm, R. S., *J. Chem. Soc.*, **1959**, 3997.

267. Bard, A. J.; Faulkner, L. R., *Electrochemical Methods*, Wiley, USA, 1980.

268. Wieder, H. H., *Laboratory Notes on Electrical and Galvanomagnetic Measurements*, Material Science Monograph, Vol. 2, Elsevier Pub., Amsterdam, 1979.

269. Carlson, T. A., *Photoelectron and Auger Spectroscopy*, Plenum Press, N.Y., 1975.

270. Briggs, D.; Seah, M.P., *Practical Surface Analysis by Auger and X-ray Photoelectron Spectroscopy*, Wiley, N.Y., 1983.

271. Muilenberg, G. E., *Handbook of X-ray Photoelectron Spectroscopy*, Perkin Elmer, USA, 1979.

272. Muilenberg, G. E., *Handbook of Auger electron Spectroscopy*, Perkin Elmer, USA, 1979.

273. (a) Day, P.; Jorgensen, C. K. *J. Chem. Soc.* **1964** 6226, (b) Friedman, H. L. *J. Amer. Chem. Soc.* **1952**, *74*, 5, (c) Swanson, T.B.; Laurie, V.W. *J. Phys. Chem.* **1965,** *69*, 244.

274. (a) Edwards, P.R.; Johnson, C.E. *J. Chem Phys.* **1968,** *49*, 211, (b) Pron, A.; Fatseas, G.A.; Krichene, S.; Lefrant, S.; Maurice, F.; Froyer, G. *Phys. Rev. B*, **1985,** *32*, 1839.

275. (a) Fichou, D.; Horowitz, G.; Garnier, F., *Synth. Met.* **1990** *39*, 125, (b) Fichou, D.; Horowitz, G.; Xu, B.; Garnier, F., *Synth. Met.* **1990** *39*, 243, (c) Fichou, D.; Xu, B.; Horowitz, G.; Garnier, F., *Synth. Met.* **1991** *41-43*, 463.

276. The characteristic Mössbauer resonance signal for iron (II) occurs at d ~0.9±0.1 mm s^{-1}.

277. Comparable light intensities.

278. Dezsi, I.; Vertes, A.; Komor, M., *Inorg. Nucl. Chem. Lett.* **1968,** *4*, 649.

279. In order to clarify that reduction with NH_3 proceeded as a redox reaction only, FTIR spectra were recorded prior to doping, immediately following doping, and following subsequent chemical reduction with ammonia gas. The chemically reduced sample exhibited an identical FTIR spectrum to that of the pristine, neutral polymer with the exception of absorption bands at 3330-3100 and 1485 cm^{-1} due to NH_4^+ . No C-N stretching vibrations (i.e., at ~1075 cm^{-1}) were observed, (Foot, P.; Ritchie, T.; Mohammad, F. *J. Chem. Soc., Chem. Commun.*, **1988**, 1536).

280. Balzani, V.; Carassiti; V. *Photochemistry of Coordination Compounds*; Acadamic: London, **1970**, p.145.

281. (a) Brealey, G.J.; Uri, N. *Nature* **1950**, *166*, 959. (b) Brealey, G.J.; Uri, N. *J. Chem. Phys.* **1952**, *20*, 257,

282. Latimer, W.M.; *The Oxidation State of the Elements and their Potentials in Aqueous Solutions;* 2nd Ed, Prentice-Hall: N.Y., **1952**.

283. (a) Furlani, C.; Cervone, E.; Valenti, V. *J Inorg. Nucl. Chem.* **1963,** *25*, 159, (b) Burbridge, C.D.; Goodgame, D.M.L., *J. Chem. Soc.(A)*, **1968,** 1410.

284. (a) Edwards, P.R.; Johnson, C.E.; Williams, R.J.P., *J. Chem Phys.* **1967,** *47,* 2074., (b) Due to the small size of the polymer sample, long acquisition times (10 days) were necessary to accumulate sufficient data for analysis. As a result iron(II) was partly oxidized to iron(III) (d = 0.24 mm s-1) by atmospheric oxygen. After 20 days only iron(III) was observed confirming the oxidation of iron(II) to iron(III).

285. McCusker, P. A.; Kennard, S. M. S. *J. Amer. Chem. Soc.* **1959**, *81*, 2976.

286. Reaction of $OH^{\bullet}$ with $FeCl_4^{2-}$ is possible but since the latter is believed responsible for reduction of the polymer this it is not expected to be a major pathway until the later stages of photolysis.

287. Nicholls, D.; *Complexes and First-Row Transition Elements*; American Elsevier Pub.: Great.Britain, **1975**, p 177.

288. Scandola, F.; Traverso, O.; Carassiti, V., *Mol. Photochem.*, **1969**, *1*,11.

289. Bard, A. J.; Lund, H., Eds., *The Encyclopedia of the Electrochemistry of the Elements*, Marcel Dekker, N.Y, 1973.

290. Mason, W.R., Gray, H.B., *Inorg. Chem.*, **1968**, *7*, 55.

291. Gangopadhayay, A.K., Chakravorty, A., *J. Chem. Phys.*, **1961**, *35*, 2206.

292. Waddington, T. C., *Non-aqueous Sovent Systems*, Academic Press, N.Y., 1965.

293. Puddephatt, R. J., *The Chemistry of Gold*, Elsevier Pub., Amsterdam, 1978.

294. Rich, R.L., Taube, H., *J. Phys. Chem.*,**1954**, *58*, 6.

295. Mazumder, A.s.; Hart, E. J., *Adv. Chem. Ser.* **1968**, *81*, 193.

296. Kurihara, K.; Kizling, J.; Stenius, P.; Fendler, J. H., *J. Amer. Chem. Soc.*, **1983**, *105*, 2574.

297. Goolsby, A.D., Sawyer, D.T., *Anal. Chem.*, **1968**, *40*, 1978.

298. Roulet, R., Nguyen, Q.L., Mason, W.R., Fenske, Jr., G.P., *Helv. chim. Acta.*, **1973**, *56*, 2405.

299. Sillen, L.G., Martell, A.E., Eds., *Stability Constants of Metal-Ion Complexes*, No. 17, The Chemical Society, London, 1964.

300. Dutton, T., VanWonterghem, B., Saltiel, S., Chestnoy, N.V., Rentzeepis, P.M., Shen., T.P., Rogovin, D., *J. Phys. Chem.*, **1990**, *94*, 1100.

301. Behrisch, R., *Sputtering by Particle Bombardment I*, Sringer-Verlag, Berlin, 1981.

302. Bravo, O., Iwamoto, R.T., *Inorg. Chem. Acta*, **1969**, *3-4*, 663.

303. Moodley, K.G., Nicol, M.J., *J.C.S. Dalton*, **1977**, 993.

304. Laidler, K. J., *Chemical Kinetics*, Harper & Row Pub., N.Y., 3rd Ed., 1987.

305. Jordan, P. C., *Chemical Kinetics and Transport*, Plenum Press, N.Y., 1979.

306. Studzinskii, O.P.; Kartushankii, A.L.; Plachenov, B.T.; *Zh. Obshch. Khim.* (English trans). **1985**, *55*, 673.

307. Horowitz, G., *Adv. Mat.* ***2***, **1990**, 287

308. Bradley, D. D. C., *Polymer International*, ***26***, **1991**, 3.

309. Bredas, J. L.; Silbey, R., Eds., *Conjugated Polymers*, Kluwer Acadamic Pubs., Dordrecht, Netherland, 1991.

310. Kao, K. C.; Hwang, W., *Electrical Transport in Solids*, Pergamon Press, Graet Britain, 1981.

311. Lampert, M. A.; Mark, P., *Current Injection in Solids*, Academic Press, N.Y., 1970.

312. Roth, S.; Bleier, H., *Adv. Phys.*, **1987**, *36*, 385.

313. Kaiser, *Phys. Rev. B*, **1989**, *40*, 2806.

314. Conwell, E. M., *IEEE Trans. Elect. Insul.* **1987**, *EI-22*, 591.

315. Park, Y. W., Park, C., Lee, Y. S., Yoon, C. O., Shirakawa, H., Suezaki, Y.; Akagi, K., *Solid State Commun.* **1988**, *65*, 147.

316. Mott, N. F.; Davis, E. A., *Electronic Processes in Non-crystalline Materials*, Clarendon Press. Oxford, 1971.

317. Gutmann, F., Keyzer, H., Lyons, L. E.; Somoano, R. B., *Organic Semiconductors II*, Robert E. Krieger Pub. Florida, USA, 1983.

318. Punkka, E., Laakso, J., Stubb, H.; Kuivalainen, P., *Phys. Rev. B*, **1990**, *41*, 5914.

319. Punkka, E., Rubbner, M. F., Hettinger, J. D., Brooks, J. S.; Hannahs, S. T., *Phys. Rev. B*, **1991**, *43*, 9076.

320. Many, A.; Goldstein, , Y.; Grover, N. B., *Semiconductor Surfaces*, Wiley, N.Y., 1965.

321. Sze, S. M., *Physics of Semiconductor Devices*, 2nd., Ed., Wiley, N.Y., 1981.

322. Nicollian, E. H.; Brews, J. R., *MOS Physics and Technology*, Wiley, N.Y., 1982.

323. Weimer, P. K., *Proc. I.R.E.*, **1962**, *50*, 1462.

324. Borkan, H.; Weimer, P. K., *RCA Rev.*, **1963**, 153.

325. Weimer, P. K., in *Field Effect Transistors*, Wallmark, J. T.; Johnson, H.; Eds., Prentice-Hall Inc., N.J., 1966, Chap.9.

326. Horowitz, G.; Fichou, D.; Peng, X; Xu, Z.; Garnier, F., *Solid State Comm.* , **1989,** *72*, 381.

327. Garnier, F.; Horowitz, G.; Peng, X.; Fichou, D., *Adv. Mat.* , **1990,** *2*, 592.

328. Tsumura, A.; Koezuka, H.; Ando, T., *Appl. Phys. Lett.*, **1986**, *49*, 1210.

329. Tsumura, A.; Koezuka, H.; Ando, T., *Synth. Met.* **1988**, *25*, 11.

330. Assadi, A.; Svensson, C.; Willander, M.; Inganas, O., *Appl. Phys. Lett.*, **1988**, *53*, 195.

331. Paloheimo, J.; Kuivalainen, P.; Stubb, H.; Vuorimaa, E.; Yli-Lahti, P., *Appl. Phys. Lett.*, **1990**, *56*, 1157.

332. Assadi, A.; Willander, M.; Svensson, C.; Helberg, J., *Synth. Met.* , **1993**, *58*, 187.

333. Dyreklev, P.; Inganas, O.; Paloheimo, J.; Stubb, H., *Synth. Met.*, **1993**, *55-57*, 4139.

334. Paloheimo, J.; Stubb, H.; Yli-Lahti, P.; Kuivalainen, P., *Synth. Met.*, **1991**, *41-43*, 563.

335. Dyreklev, P.; Gustaffsson, G.; Inganas, O.; Stubb, H., *Solid State Comm.*, **1992**, *82*, 317.

336. Taylor, D. M.; Gomes, H. L.; Underhill, A. E.; Edge, S.; Clemenson, P. I., *J. Phys. D: Appl. Phys.*, **1991**, *24*, 2038.

337. Ohmori, Y.; Takahashi, H.; Muro, K.; Uchida, M.; Kawai, T.; Yoshino, K., *J. J. Appl. Phys.*, **1991**, *30*, L610.

338. Ohmori, Y.; Takahashi, H.; Muro, K.; Uchida, M.; Kawai, T.; Yoshino, K., *J. J. Appl. Phys.*, **1991**, *30*, L1247.

339. Ohmori, Y.; Muro, K.; Yoshino, K., *Synth. Met.*, **1993**, *55-57*, 4111.

340. Paloheimo, J.; Franssila, S.; Kuivalainen, P.; Stubb, H., *Thin solid Film*, ,**1993**, *41-43*, 563.

341. Paloheimo, J.; Stubb, H.; Gronberg, L., *Synth. Met.*, **1993**, *55-57*, 4198.

342. Garnier, F; Horowitz, G, *Synth. Met.* **1987**,*18*, 693.

343. Garnier, F; Horowitz, G.; Fichou, D., *Synth. Met.* **1989**, *28*, 705.

344. Fichou, D.; Horowitz, G.; Nishikitani, Y; Garnier, F., *Synth. Met.*, **1989**, *28*, 723.

345. Horowitz, G.; Peng, X.; Fichou, D.; Garnier, F., *J. Appl. Phys.*, **1990**, *67*, 528.

346. Horowitz, G.; Peng, X.; Fichou, D.; Garnier, F., *J.Mol. Elect.*, **1991**, *7*, 85.

347. Garnier, F.; Horowitz, G.; Fichou, D., in *Electronic Properties of Polymers*, Kuzmany, H.; Mehring, M. ; Roth, S., Eds., Springer-Verlag, **1992**, p 458.

348. Delannoy, Ph.; Horowitz, G., in *Electronic Properties of Polymers*, Kuzmany, H.; Mehring, M. ; Roth, S., Eds., Springer-Verlag, **1992**, p 466.

349. Horowitz, G.; Peng, X.; Fichou, D.; Garnier, F., *Synth. Met.*, **1992**, *51*, 419

350. Horowitz, G.; Deloffre, F.; Garnier, F.; Hajlaoui, R.; Hmyene, M.; Yassar, A, *Synth. Met.*, **1993**, *54*, 435.

351. Garnier, F.; Deloffre, F.; Horowitz, G.; Hajlaoui, R., *Synth. Met.*, **1993**, *55-57*, 4747.

352. Garnier, F.; Yassar, A.; Hajlaoui, R.; Horowitz, G.; Deloffre, F.; Servet, B.; Ries, S.; Alnot, P., *J. Amer. Chem. Soc.*, **1993**, *115*, 8716.

353. Akimichi, H.; Waragai, K.; Hotta, S.; Kano, H.; Sakaki, H., *Appl. Phys. Lett.*, **1991**, *58*, 1500.

354. Waragai, K.; Akimichi, H.; Hotta, S.; Kano, H.; Sakaki, H., *Synth. Met.* **1993**, *55-57*, 4053.

355. Ostoji, P.; Guerri, S.; Rossini, S.; Servidori, M.; Taliani, C.; Zamboni, R., *Synth. Met.*, **1993**, *54*, 447.

356. Garnier, F.; Hajlaoui, R.; Yassar, A.; Srivastava, P, *Science*, **1994**, *265*, 1684.

357. Gustafsson, G.; Sundberg, M.; Inganas, O.; Svensson, J., *J. Mol. Elect.* **1990**, *6*, 105.

358. Gustafsson, G.; Inganas, O.; Sundberg, M.; Svensson, J., *Synth. Met.*, **1991**, *41-43*, 499.

359. Burroughes, J. H.; Jones, C. A.; Friend, R. H., *Synth. Met.*, **1989**, *28*, C735.

360. Friend, R. H.; Burroughes, J. H.; *Chem. Soc. Faraday Discuss.*,**1989**, *88*, 213.

361. Burroughes, J. H.; Jones, C. A.; lawrence, R. A.; Friend, R. H., in *Electronic Properties of Conjugated Polymers,* Kuzmany, H.; Mehring, M. ; Roth, S., Eds., Springer-Verlag, **1989**, p 437.

362. Helen, I. P., *Practical Integrated Circuit Fabrication*, ICE staff ed. **1982**.

363. (a) Wertz, J. E. and Bolton, J. R., *Electron Spin Resonance, Elementary Theory and Practical Applications* McGraw-Hill, Inc., **1972.**; (b) Zucharski, Z.; Winkler, H.; Trautwein, A. X.; Budrowski, C.; Butzlaff, C.; Length, M., *HyperfineInteractions,* ***69,*** **1991**, 659.

364. (a) Onoda, M.; Manda, Y.; Morita, S.; Yoshino, K., *Jpn. J. Appl. Phys.* **1992**, *31,* 65.; (b) Inoue, M.; Inoue, M. B.; Castillo-Ortega, M. A. M., *Synth. Met.,* **1989**, *33,* 355. (c) Vardeny, Z., Ehrenfreund, E, Brafman, Nowak, M., Schaffer, H., Heeger, A.J., Wudl, *Phys. Rev. Lett.*, **1986**, *56*, 671. (d) Colaneri, N., Nowak, D., Spiegel, D., Hotta, S, Heeger, A.J., *Phys. Rev. B*, **1987**, *36*, 7964.

365. Wilkinson, D.T.; and Crane, H.R., *Phys. Rev.,* **1963**, *130,* 852.

366. (a) Kaneto, K.; Hayashi, S.; Ura, S.; Yoshino, K., *J. Phys. Soc. Japan*, **1985**, *54,* 146.; (b) .Tanaka, K.; Shichiri, T.; Yoshizawa, K.; Yamabe, T.; Hotta, S.; Shimotsuma, W.; Yamauchi, J.; Deguchi, Y., *Solid State Comm.*, **1984**, *51,* 565.

367. Nalamasu, O., Ed., *Advances in Resist Technology and Processing XI*, SPIE **1994,** *Vol. 2195.*

368. Wang, C.; Benz, M. E.; LeGoff, E.; Schindler, J. L.; Thomas, J. A.; Kannewurf, C. R.; Kanatzidis, M. G., *Chem. Mater.*, **1994**, *6*,401.

369. Ziemelis, K. E.; Hussain, A. T.; Bradley, D. D. C.; Friend, R. H.; Ruhe, J.; Wegner, G., *Phys. Rev. Lett.* **1991**, *66*,2231.

370. Ziemelis, K. E.; Hussain, A. T.; Bradley, D. D. C.; Friend, R. H.; Ruhe, J.; Wegner, G., *Synth. Met.*, **1991**, *41-43*, 1045.

371. Burroughes, J. H.; Friend, R. H., *Reference 309*, p. 617.

372. Horowitz, G.; Delannoy, P., *J. Appl. Phys.*, **1991**, *70*, 469.

373. Mulliken, R.S.; Person, W.B., *Molecular Complexes*, Wiley 1969.

374. Foster, R., *Organic Charge Transfer Complexes,* Academic Press, New York, **1969**.

375. Foster, R. Ed., *Molecular Associations*, Academic Press, New York, **1974.**

376. Weller, A., in *The Exciplex*, Gordon, M., Ware, W.R., Eds., Academic Press, New York, 1975.

377. (a) Rehm, D., Weller, A., *Z. Phys. Chem.*, **1970**, *69*, 183. (b) Rehm, D., *Z. Naturforsch.*,**1970,** *25a*, 1442.

378. (a) Benesi, H.A., Hildebrand, *J. Amer. Chem. Soc.*, **1949**, *71*, 2703. (b) Orgel, L.E., Mulliken, R.S., *J. Amer. Chem. Soc.*, **1957**, *79*, 4839.

379. Tamres, M.; Strong, R. L., *Contact Charge-Transfer Spectra, in Molecular Associations*, Vol. 2, Foster, R. Ed., Academic Press, New York, **1974**, p.331.

380. Foster, R.; Foreman, M. I., *Quinone Complexes, in The Chemistry of the Quinoid Compounds*, part 1, Patai, S., Ed., John Wily, New York, **1974**, p 257.

381. Atkins, P. W., *Physical Chemistry*, 3rd. Ed., Freeman and Company, N.Y., 1986.

382. Lotfi, M.; Roberts, R. M. G., *Tetrahedron*, **1979**, *35*, 2123.

383. Rosenberg, B., *J. Chem. Phys.*, **1961**, *34*, 812.

384. Lakowicz, J. R., *Principles of Fluorescence Spectroscopy*, Plenum Press, N.Y., 1983, Chap.9.

385. Fox, M. A., *Adv. Photochem.*, **1986**, *13*, 237.

386. Andrews, L. J.; Keefer, R. M., *Molecular Complexes in Organic Chemistry*, Holden-Day Inc., Calif., 1964.

387. Barrer, R. M., *Diffusion In and Through Solids*, Cambridge University Press, London, **1951**.

388. Comyn, J., *Polymer Permeability*, Elsevier Applied Science Pub., New York, **1985**.

389. Vieth, W. R., *Diffusion In and Through Polymers*, Hanser Pub., New York, **1991**.

390. Rogers, C. E., in *Physics and Chemistry of Organic Solid State*, Vol. II, Fox, D.; Labes, M. M.; Weissberger, A., Interscience Pub., New York, **1965**, Chap. 12.

391. MacCallum, J. R., Rudkin, A. L., *Eur. Polym. J.*, **1979**, *14*, 655.

392. Povich, M. J., *Anal. Chem.*, **1975**, *47*, 346.

393. Hoffmann, V.; Frohlich, D.; Hellstern, U.; Kohlhange, S.; Nahm, W.; Nussbaumer, K.; Oelkrug, D., J. *Molecular Structure*, **1993**, *293*, 253.

394. Brandt, H.; *Exper. Technik Physik*, **1985**, *33*, 423.

395. Barrer, R. M., *Trans. Faraday Soc.*, **1939**, *35*, 628.

396. van-Amerongen, G. J., *J. Appl. Phys.*, **1946,** *17*,, 972.

397. Meares, P, *J. Amer. Chem. Soc.*, **1954**, *76*, 3415.

398. Lomax, M., *Polym. Testing,* **1980,** *1*, 105 and 211.

399. *Annual Book of ASTM Standards (American Society for Testing and Materials)*, ***D 1434-82***, **1982**.

400. Felder, R. M.; Huvard, G. S., in *Methods of Experi. Phys.*, Vol 16, Fava, R. A. Ed., Academic Press, New York, **1980,** Chapt. 17.

401. Yasuda, H., *J. Appl. Polym. Sci.*, **1975**, *19*, 2529.

402. Beringer, R.; Castle, J.G., *Phys. Rev.*, **1951**, *81*, 82.

403. Kristiansen, M.; Scurlock, R. D.; Iu, K-K.; Ogilby, P. R., *J. Phys. Chem.*, **1991**, *95*, 5190.

404. Scaiano, J. C.; Holdcroft, S., *unpublished results*, **1994**.